Humanized Mouse with a Diverse Polyclonal B Cell Repertoire as a Model for Neutralizing Antibody Responses against EBV and HIV

Crystal B. Chhan

A dissertation

submitted in partial fulfillment of the

requirements for the degree of

Doctor of Philosophy

University of Washington

2025

Reading Committee:

Andrew T. McGuire, Chair

Noah Sather

Cynthia A. Derdeyn

Program Authorized to Offer Degree:

Pathobiology

University of Washington

Abstract

Humanized Mouse with a Diverse Polyclonal B Cell Repertoire as a Model for Neutralizing Antibody Responses against EBV and HIV

Crystal B. Chhan

Chair of the Supervisory Committee:
Andrew T. McGuire
Department of Laboratory Medicine and Pathology

Epstein-Barr virus (EBV) and human immunodeficiency virus (HIV) cause diseases of global health importance. However, it has been historically difficult to model human neutralizing B cell responses to these two viruses using small animals. I leveraged a transgenic mouse model that encodes a genetically human antibody repertoire to generate neutralizing monoclonal antibodies (mAbs) against the EBV gp350 and gp42 glycoproteins, which have been technically difficult to isolate from natural infection. gp42 and gp350 are involved in attachment and fusion into B cells respectively. Thus, these mAbs have great potential as therapeutic agents against EBV-associated malignancies. In a second project, I investigated the utility of these humanized mice as a surrogate to model VRC01-class B cell responses, a rare class of HIV broadly neutralizing antibodies that target the CD4 binding site on HIV envelope. I utilized high-throughput sequencing to identify the presence of these rare potentially protective B cells in humanized mice and evaluated if an anti-idiotypic immunogen, designed to target genetically encoded features of VRC01-class B cells, could selectively target and expand these cells *in vivo.*

TABLE OF CONTENTS

ACKNOWLEDGEMENTS

First, I'd like to thank the members of the McGuire lab for making lab such a fun and supportive environment. I had almost no experience with these assays, so I am very appreciative of everyone's patience. Everyone's caring attitude made me want to come into work every day and, I loved hanging out at lunch every day. In no particular order, Leah, Karina, Natalia, Yu-Hsin, Sam S., Sam H., Holly, Lyndsey, Amelia, Roman, and Nicholas, you're all great people and even better friends. It's been a great environment, and I'll always remember this time fondly.

Next, I truly could not have done this degree without my mentor, Andy McGuire. I came to the lab with zero knowledge in the field, and he took a chance on me that I'll be forever thankful for. There's been many bumps, from project switches to failed mouse experiments, but Andy was patient and supportive through it all. For me, I found that we had the perfect balance and expectations for each other. Even during frustrating times, I always felt cared for as a person and respected as a scientist. He's taught me a lot about science, but even more about being an excellent leader. Beyond the lab, he's also enriched my learning about paddleboarding, razor clam digging, and hockey – all hobbies I will continue to enjoy for the rest of my life. He has great taste in food, music, and movies, and I'm very proud to be able to call him my mentor.

For my friends in the Pathobiology program, I'm so glad we were able to spend these years and experiences together. Particularly to my 6-pack cohort, Lakshmi, Guoyue, Shawn, Nola, and Anthony, for hanging out and checking up on each other despite being at different institutions with our own projects and lives. First year of grad school was maybe one of the most difficult years of my life with moving to a new city, cramming in new information every day, and enduring a global pandemic, but y'all maybe it fun and memorable despite the hardships. Somehow, I ended up being the first one to graduate, but I'll always be here for you all. To my

other friends, Nicole, Austin, Kristina, Nhi, Kristine, Maria, and Prerana, thank you for always dragging me out of my apartment and reminding me there's so much more to life than project deadlines and data analysis. To my friends from my rotations, Alexis, Eva, and Andrew K., thank you for bettering my music taste and going to karaoke with me. You all made sure I got to experience the best that living in the Pacific Northwest has to offer.

To my non-PhD friends, particularly Jene, Aliyah, Vanderly, Camille, Haeun, Amanda, Shanie, Kathleen, Celina, and Tira, y'all always keep me sane and stress-free. Thank you for always flying or driving to see me. It's tough maintaining long distance friendships, but let's always keep going to dinners and festivals.

To my family, it's been hard living far from you all, and I miss you always. To my siblings, Brandon, Randy, and Sandra, thanks for always beating me at board games – it keeps me humble. To my grandparents and my parents, Vuy and King, thank you for your sacrifices. Words are not enough to convey my appreciation. Finally, to my new nieces, Sylvia and Katherine, you're both so cute and easy to love – I promise to make this world a better place for you to live in.

LIST OF FIGURES

Chapter 1 Figures:

Chapter 2 Figures:

Chapter 1. Introduction to Epstein-Barr virus (EBV)

Part of this work is published as "Viral Entry" in Current Topics in Microbiology and Immunology as of May 15, 2025[1]

Authors: Samantha R. Hardy[#], Crystal B. Chhan[#,&], Amelia R. Davis[#], Andrew T. McGuire[#,&]

[#]Vaccine and Infectious Disease Division, Fred Hutchinson Cancer Center, Seattle, WA, USA.
[&]Department of Global Health, University of Washington, Seattle, WA, USA.

1.1 Global burden of EBV and EBV-associated malignancies

1.1.1 The global burden of EBV

EBV is a ubiquitous, human-specific gamma herpesvirus that establishes life-long latency within the host[2, 3]. Over 90% of adults globally have been infected with EBV, typically during the first two decades of life[2-4]. EBV is classified into two types, EBV1 and EBV2, with unique geographical distribution[5]. EBV1 globally distributed and is generally more prevalent than EBV2 across most regions, although they are equally prevalent in Sub-Saharan Africa[5]. Indonesia, Papua New Guinea, and Northern Brazil exhibit a higher circulation of EBV2[5]. The incidence of primary infection varies with age. It peaks in the 5–10-year age group in Sub-Saharan Africa while gradually increasing over time in developed countries[4, 6]. While infection is typically asymptomatic, the main sequela of primary infection is infectious mononucleosis (IM). IM is rare in infants and children but fairly common in adolescents and young adults[2, 3, 6]. IM is typically a self-limiting disease and symptoms include pharyngitis, lymphadenopathy, fever, fatigue, splenomegaly and hepatomegaly that typically lasts 2 to 6 weeks[2].

1.1.2 EBV-associated malignancies and other diseases

EBV was the first human oncogenic virus discovered[2]. It is associated with an array of cancers, typically of B cell and epithelial origin, including: Burkitt lymphoma (BL), Hodgkin's lymphoma (HL), non-Hodgkin's lymphoma, diffuse large B cell lymphoma, nasopharyngeal carcinoma (NPC), and gastric cancers (GC)[2, 4, 7]. Estimations of the global burden of EBV-associated malignancies range from 239,700–357,900 new cases of cancer and 137,900–208,700 deaths annually[4, 7]. BL is primarily a childhood malignancy while other EBV-associated cancers tend to develop later in life. BL, HL, NPC, and GC are more common in males with the highest incidence found in Sub-Saharan Africa for BL and in East Asia for the other three malignancies[4, 7]. The reasons for these phenomena are currently unknown, but genetics and lifestyle risk factors are likely important contributors.

EBV can also be a lethal complication for people with immunodeficiencies, such as X-linked lymphoproliferative disease and persons living with human immunodeficiency virus (HIV), or when individuals undergo immunosuppressive therapy post-transplant, which can result in post-transplant lymphoproliferative disease (PTLD)[2]. The risk of PTLD is up to 10% higher for pediatric patients who are likely to be EBV-naïve before transplantation[8-10]. Additionally, EBV has been implicated in autoimmune disorders including multiple sclerosis[11-17], systemic lupus erythematosus[18, 19], and rheumatoid arthritis[20, 21]. It is also linked to complications of COVID-19 infection[22-24]. MS patients have elevated EBV antibody titers and high positive association with a history of IM[11-17]. A recent longitudinal study included over ten million people serving in

the U.S. military and provided substantial evidence for a causal relationship between EBV and MS, finding that the risk of MS increased over 30-fold after EBV infection[17, 25].

1.2 EBV infection of B cells and epithelial cells

1.2.1 EBV transmission

BV is an orally transmitted virus that typically spreads through saliva to the oropharynx, where it can infect both epithelial cells and infiltrating B cells[2]. The virus first establishes lytic infection[2]. It is thought that high levels of viral replication and shedding occur predominantly in squamous epithelial cells and in some locally infiltrating B cells[2, 3]. Interestingly, alternative replication in B cells and human leukocyte antigen receptor (HLA) class II-negative epithelial cells dictate the tropism of the virus (more details below)[26]. Following infection of B cells, the virus reprograms B cells to continuously proliferate[2, 3]. The infection then spreads through growth-transforming infection of B cells in the oropharyngeal lymphoid tissues[2, 3]. While it is unclear if certain B cell subtypes are preferentially targeted, in general, B cells serve as a site of both lytic replication and long-term persistence of the latent virus[2, 3]. The latent virus can periodically reactivate in response to various factors, such as differentiation to plasma cells and expression of the lytic switch gene BZLF1, to produce lytic virus that can go onto seed new infections in the host and transmit virions between hosts[2, 3]. Lifelong viral persistence can occur through latent infection of memory B cells[2, 3]. Viral entry into epithelial and B cells is a complicated and poorly understood process mediated by several viral glycoproteins that define tropism (see below).

1.2.2 EBV infection of B cells

EBV has long been known to have tropism for B cells as it was first discovered in cells cultured from a Burkitt lymphoma biopsy[27]. The first step of B cell infection involves attachment of the viral glycoproteins to the primary attachment receptor on the B cell surface, complement receptor type 2 (also known as the C3d receptor or CD21)[28-30]. Complement receptor type 1 (also known as CD35) is also an attachment receptor for EBV that is bound by gp350[31].

Attachment is mediated by gp350 and gp220. gp350 is a 907 amino acid type I transmembrane protein with three structurally defined extracellular domains[32, 33]. gp220 is the product of alternative splicing of the BLLF1 transcript, which results in the absence of 249 amino acids outside of the structurally defined domains[32, 33]. gp350 and gp220 are the most abundant glycoproteins expressed on the surface of the EBV virion[34]. gp350 is heavily glycosylated and has 37 putative N-linked glycosylation sites[32]. Despite the extensive glycosylation, there is an obvious glycan-free region[35-37]. Mutation of this exposed region precludes the gp350/CD21 interaction, indicating that this region on gp350 is important for binding to CD21[35-37]. Further comparison of the C3d-CD21 and gp350-CD21 crystal structures revealed key molecular interactions that are common between C3d and gp350 for CD21 recognition[37]. The gp350 interactions with CD21 and CD35 are both inhibited by the mAb 72A1[31, 38]. 72A1 also maps to the nonglycosylated surface on gp350, indicating that gp350 interacts with both complement receptors through the same binding site[35]. Recombinant virus in which the BLLF1 gene has been deleted remains infectious but infectivity is substantially reduced compared to wildtype

virus [39]. This demonstrates that the attachment function of gp350 is important, but not essential, for B cell infection.

Following attachment, subsequent fusion of the viral and B cell membranes is orchestrated by 4 additional viral glycoproteins: gp42, gH, gL, and gB[2, 3]. gp42 acts as a receptor-binding protein that is essential for initiating the fusion process[40]. gp42 binds to the heterodimeric viral complex gH/gL at a 1:1:1 ratio, which is required for viral entry into B cells[41]. The binding gp42 to HLA class II molecules acts as the trigger that induces fusion by activating gH/gL to trigger gB[42, 43 40]. gH/gL acts as a regulator molecule that triggers activation of the fusion protein gB to undergo a conformational change from its pre-fusion state to a post-fusion state, driving viral fusion[44, 45]. These 3 proteins are often referred to as the core fusion machinery. Interestingly, orthologs of gH, gL, and gB exist for all herpesviruses and are essential for infectivity[46].

gp42 is a 223 amino acid type II membrane protein with 4 putative N-linked glycosylation sites. It is comprised of an extended amino-terminal domain (NTD) of ~100 amino acids and of a carboxy-terminal C-type lectin domain (CTLD)[47, 48]. The gp42 CTLD binds to HLA β-chain[42, 43, 48]. HLA-DR, HLA-DP, and HLA-DQ can all act as coreceptors in EBV entry, although it has been reported that some HLA-DQ alleles restrict entry due to the lack of a glutamic acid at residue 46[42, 49].

gH/gL forms an elongated rod-like structure comprised of 4 extracellular domains (Figure 1)[46, 50]. Domain I (DI) is formed by the N-terminus of gH and the entirety of gL, while domains II-IV (DII-DIV) are formed entirely by gH. DII-DIV are tightly packed, while there is a large groove between DI and DII. The gp42 NTD wraps around gH/gL,

making extensive contacts with DII-DIV[51]. This positions the gp42 CTLD on the opposite face of the DI/DII groove with the HLA binding site on gp42 exposed[51].

gH/gL/gp42/HLA complexes adopt several conformations ("open" and "closed") as visualized by electron microscopy, indicating that the orientation of gp42's CTLD relative to gH/gL is flexible[52]. It has been proposed that the "closed" conformation might orient the gH/gL/gp42/HLA complex in a position that is favorable for membrane fusion. Additionally, a hydrophobic pocket on gp42 makes additional contact with DII of gH/gL in the "closed" conformation[51]. The hydrophobic pocket appears to be functionally important for fusion since HLA binding induces structural changes within this pocket, and mutations within it inhibit fusion without affecting the gH/gL or HLA interactions[47,

[48, 53]. This is further supported by the fact that the hydrophobic patch harbors epitopes targeted by neutralizing antibodies[54, 55].

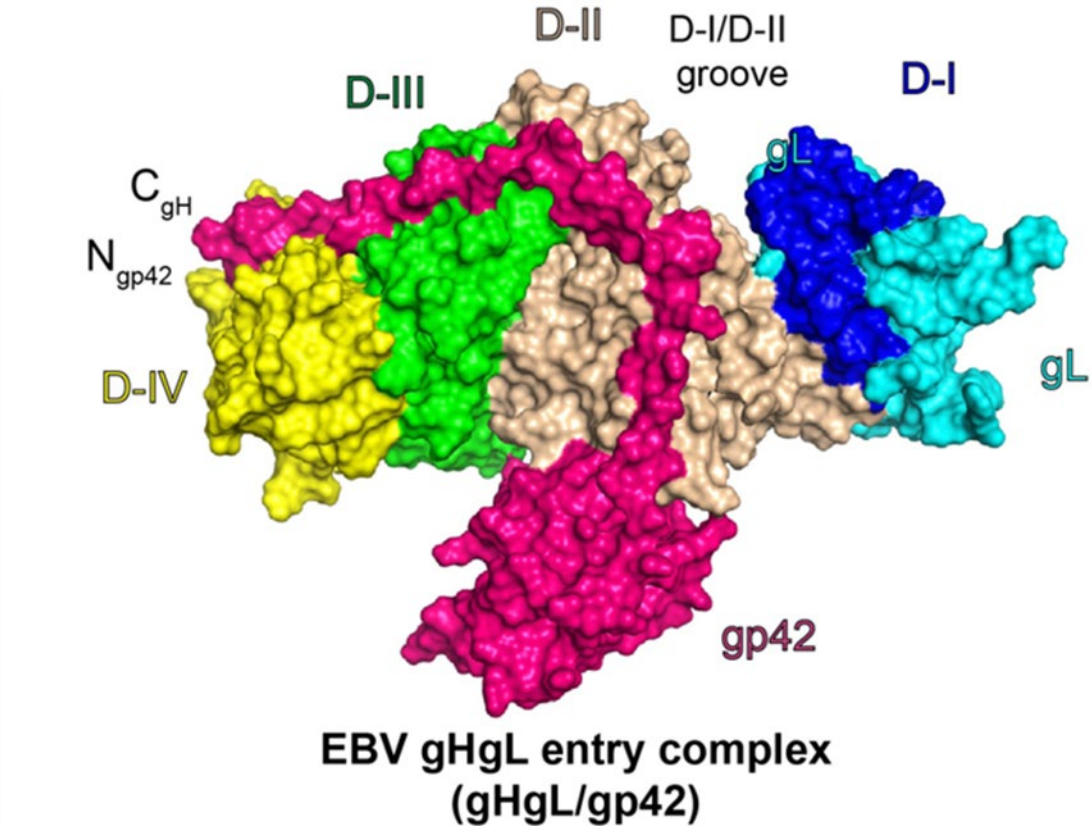

Figure 1. Structure of gp42/gH/gL complex. Image taken from Sathiyamoorthy et. al., 2017[46].

1.2.3 EBV infection of epithelial cells

The process of EBV infection of epithelial cells is not as well defined as that of B cell infection. gp42 is not required for epithelial cell infection. In fact, the presence of soluble gp42 inhibits epithelial cell infection[56, 57]. While epithelial cells are more difficult to infect in vitro with cell-free virus compared to B cells, expression of CD21 can enhance epithelial cell infection[58]. Still, CD21 is dispensable for EBV infection of

epithelial cells since CD21-negative cell lines are susceptible to infection, albeit with reduced efficiency[59-61]. It is unclear whether gp350 plays an important role for epithelial infection *in vivo* or whether CD21 is expressed in epithelial cells of the oral cavity. CD21 mRNA has been detected in tonsil epithelium, but not in epithelial cells from the buccal mucosa, uvula, soft palate, or tongue[62]. Additionally, primary organotypic cultures derived from primary oral tissue, while permissive to EBV infection, also lack detectable CD21 protein[63, 64].

Interestingly, EBV is capable of "transfer infection" in which the virus first attaches to resting B cells, aggregating CD21 and activating adhesion molecules that form a synapse with the basolateral surface of epithelial cells, promoting infection of epithelial cells[64-67]. For cell-free virions, it is thought that binding of gH/gL to cell surface receptors on epithelial cells induces a conformational change required for gB activation and subsequent fusion with the host membrane[51, 60, 68]. After initial infection of epithelial cells, EBV can spread to adjacent epithelial cells directly across lateral membranes[64].

Since gp350 and gp42 are dispensable for epithelial cell infection, the field has sought to identify additional attachment and entry receptors. The viral protein BMRF2, and its integrin-binding motif in particular, plays a key role in viral attachment during the infection process[64, 69, 70]. BMRF2 is also implicated in epithelial cell-to-cell spread of EBV[70].

Ephrin A2 receptor (EphA2), R9AP, DSC2, and αvß5, αvß6, αvß8 integrins have been implicated as gH/gL receptors on epithelial cells[67, 71-76]. Despite the vast number of potential receptors, these studies together implicate the gH/gL DI and DII interface as important for epithelial cell infection. gH has a KGD motif located distally on a

protruding extended loop on DII that appears important for binding to integrins and membrane fusion activity[50, 74]. Incubation of the recombinant gH/gL ectodomain with integrins induces a conformational change with the DI/DII groove on gH/gL[77]. Mutations within the groove negatively affect fusion with epithelial—but not B cell membranes—suggesting that conformational changes within and across this groove are required for activating gB activity during epithelial cell infection[78]. Co-crystal structures of gH/gL in complex with the EphA2 ligand-binding domain revealed a gL-dominated interaction[79]. Additionally, the gH/gL interaction with R9AP is inhibited by the potently neutralizing mAb AMMO1, which binds an epitope that spans DI and DII[76, 80].

A gB interaction with cell surface ligand Neuropilin 1 (NRP1) has also been implicated in epithelial cell infection. NRP1 binds proteins with carboxy-terminal basic sequence (CendR) motifs, leading to endocytosis[81]. The furin site on gB may serve as a CendR motif as cleavage of the furin site improves fusion activity and disruption of the motif abrogates recombinant gB binding to NRP1[75, 82]. gB has also been reported to interact directly with EphA2[73]. Whether the binding site on EphA2 overlaps with that of gH/gL and whether the binding is important for infection remains to be determined.

1.2.4 Tropism Switch

The stoichiometry of the gH/gL/gp42 heterotrimer complex to the gH/gL bipartite complex on a virion influences the use of gH/gL for both viral attachment and entry[56, 57]. As mentioned above, the virus can switch tropism depending on which cell type produces it. B cell-derived virus infects epithelial cells more efficiently than other B cells, and vice versa[26, 56]. This is because HLA class II molecules can sequester gp42 within B cells to the endosome/lysosome for degradation, resulting in less gp42 expression on these

virions. Correspondingly, HLA Class II-negative epithelial cell-derived virions display more surface gH/gL/gp42, allowing for more efficient infection of B cells. Even when HLA class II is available, B cell-derived viruses can continue to use the bipartite gH/gL for viral entry into HLA class II expressing SVKCR2 epithelial cells[56].

1.3 The immune response to EBV infection

In a healthy person, primary EBV infection and spontaneous reactivation from latency to lytic replication are controlled by innate and adaptive immune responses.

1.3.1 Innate immune responses

Since primary infection is often asymptomatic, most of what is known about the initial immune responses to EBV are in the context of IM[2]. Natural killer (NK) cells are rapidly activated and expanded in acute IM and thought to control B cell proliferation and transformation[83, 84]. One study showed that the $CD56^{bright}CD16^{-}$ NK subset prevented or delayed B cell transformation by EBV *in vitro* through IFNγ secretion[85]. It is thought that the reduction of $CD56^{dim}CD16^{-}$ NK cells that occurs through childhood could lead to a reliance on $CD8^{+}$ T cell responses to control EBV infection, resulting in the exaggerated lymphocytosis seen in IM[2]. Evidence of this is seen when NK cells are depleted in a humanized mouse model prior to EBV challenge, resulting in elevated levels of proinflammatory cytokines and increased expansion of both circulating and splenic $CD8^{+}$ T cells[83]. Additionally, increased NK frequencies correlated with improved survival of transplant patients experiencing low-level EBV reactivation[2].

1.3.2 Cellular immune responses

A hallmark of IM is the rapid and massive expansion of $CD8^+$ T cells. Studies of EBV-specific $CD8^+$ T cells show that a significant fraction of those cells (up to 50%) are directed against immediate early or early antigens of the lytic cycle[2, 86]. $CD8^+$ cells specific to late-stage lytic and latent antigens are less frequent and numerically smaller. Infection in asymptomatic children also elicits $CD8^+$ T cell responses, although without the massive expansion seen in IM. Additionally, the skewing of EBV-specific responses to early lytic antigens than to late-stage lytic or latent antigens is also seen in asymptomatic individuals[2, 86]. This is likely driven by direct contact of the $CD8^+$ cells with lytically infected cells. Studies of infection strongly suggest that $CD8^+$ cytotoxic T cells cull infected B cells and that the $CD8^+$ T cell compartment contracts after viral clearance[2, 86, 87]. A virus-specific memory pool of $CD8^+$ T cells persists post-infection to control reactivation of latent infection[2]. Further evidence of the important role of $CD8^+$ T cell mediated control is seen when the cells are immune suppressed such as in post-transplant lymphoproliferative disease (see more below) or in persons living with HIV.

$CD4^+$ T cells also play an important role, particularly contributing to effective antibody responses and $CD8^+$ T cell function[2, 86]. Unlike $CD8^+$ T cells, $CD4^+$ T cells do not massively expand during IM. Still, up to 1% of peripheral $CD4^+$ T cells are EBV-specific[2]. Additionally, these responses are skewed towards latent antigens rather than lytic antigens. A direct antiviral role for EBV-specific $CD4^+$ T cells is not well established. Isolated EBV-specific CD4+ T cell clones have been shown to have direct cytotoxic capacity against HLA-matched LCL targets in vitro[2]. One study has found that adoptive transfer of EBNA1-specific T cell receptor-engineered $CD4^+$ T cells into a NCG

mouse model with xenografted C666-1-EBNA1 tumor cells (derived from nasopharyngeal carcinoma) did inhibit tumor growth and improved survival in all mice[88].

1.3.3. Humoral responses

Studies of serum responses from persons with acute IM show a wide range of antibodies specific to EBV lytic cycle antigens, but the simplest diagnostic criterion uses responses to EBV viral capsid antigen (VCA) and two latent proteins, EBNA1 and EBNA2 (Figure 2)[2, 6]. By onset of acute IM symptoms, patients develop both IgM and IgG antibodies against VCA. IgG antibodies develop against EBV early antigen (EA) and EBNA2, a latent antigen involved in B cell transformation, and then gradually decline. A defining characteristic of acute IM is the absence of EBNA1-specific IgG antibodies (another latent antigen), which develop around 3 to 6 months after infection. This is thought to be attributed to the poor access of the protein to antigen-presenting cells that cross prime $CD4^+$ T cells[89]. Over time, the VCA IgM and EBNA2 IgG responses decrease while the VCA IgG and EBNA1 IgG response stabilizes. Thus, VCA IgM^+, VCA IgG^+, ENBA2 IgG^+, and lack of EBNA1 IgG serves as a serological diagnosis of IM, while a healthy carrier status has VCA IgG^+ and EBNA1 IgG^+ while being negative for VCA IgM and EBNA2 IgG[2, 6].

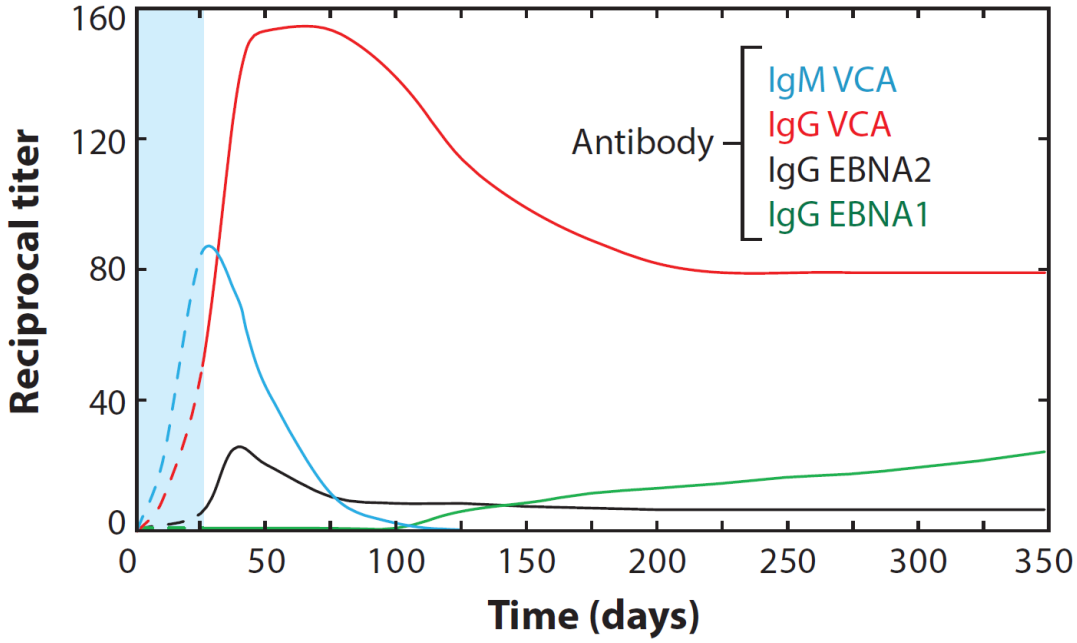

Figure 2: Antibody levels targeting VCA, EBNA1, and EBNA2 during acute IM. Image taken from Taylor et. al., 2015[2].

Neutralizing antibodies targeting viral surface glycoproteins (see below for more details) develop as early as within the first week of IM and persist for at least two years afterwards[90-92]. Although, a high-affinity IgG response develops slowly in IM patients, taking up to about 2 years or more to reach peak levels[2, 6, 90]. Beyond neutralization, EBV-specific antibodies have been shown to promote antibody-dependent cellular cytotoxicity (ADCC)[93-95], antibody-dependent cellular phagocytosis (ADCP)[96], and antibody-dependent neutrophil phagocytosis (ADNP)[94, 97] towards EBV-infected cells. These studies showed that Fc-mediated antibody functions—targeting latent antigens, early-stage antigens, gp350, and VCA—seem to largely appear only after resolution of acute IM patients[93, 96, 98] , which is consistent with the gradual increase of EBV-specific

IgG levels during IM[90]. Further studies of Fc-mediated antibody functions would inform rational vaccine design, especially in the context of impaired T cell function.

1.4 Discovery and development of EBV-specific vaccines and monoclonal antibodies for infectious mononucleosis and EBV-associated cancers

1.4.1 EBV-specific neutralizing monoclonal antibodies (mAbs)

In sera from healthy carriers, most of the antibodies able to neutralize B cell infection bind gp350 while gH/gL-, gB-, and gp42-specific antibodies make smaller contributions[99]. For epithelial cell neutralization, a majority of the neutralizing antibody response targets gH/gL[100]. The isolation and structural characterization of EBV-specific mAbs reveal sites of vulnerability on the various viral glycoproteins involved in infection. This information is valuable for rational vaccine design. Furthermore, mAbs could be utilized as prophylactic therapeutics or treatment, such as in the context of PTLD (see below for more).

Neutralizing mAbs (nAbs) against gp350, gp42, gH/gL, and gB have been elicited in mice, rabbits, and non-human primates by immunization [38, 54, 55, 101-106]. Human neutralizing, EBV-specific mAbs have been difficult to identify, due to their rarity in circulating memory B cells[80]. The anti-gH/gL AMMO1 and anti-gB AMMO2-AMMO5 mAbs were the first EBV-specific human mAbs identified, using antigen-specific sorting of memory B cells from EBV-seropositive donors[80]. Other human gH/gL mAbs have been identified using the same approach[103, 104]. So far, only 13 gH/gL nAbs have been isolated from animals or natural infection; all of which neutralize EBV infection of epithelial cells with a smaller subset capable of potently neutralizing infection of B

cells[60, 80, 101, 103, 104, 107, 108]. AMMO1, 769B10, and 1D8 are the most potent dual-tropic mAbs of human origin[103, 104, 107]. AMMO1 and 769B10 both bind an overlapping epitope on Domain I/II of gH/gL, opposite the 1D8 binding site which binds Domain II. The majority of isolated gB-specific mAbs are non-neutralizing. The small neutralizing subset has variable potency against epithelial cells and/or B cells.

The murine nAb 72A1 is a particularly well characterized mAb against gp350 that potently neutralizes B cell infection[38, 109, 110]. 72A1 is known to inhibit CD21 and CD35 binding[31, 35]. Human mAbs against gp350 and gp42 have only been identified within the past two years. Historically, isolating gp350 and gp42 mAbs with native glycoproteins through antigen-specific sorting has not been possible due their ability to bind with high affinity to complement receptors and HLA class II on the cell surface of B cells, respectively, negating B cell receptor-specific staining[80]. Engineering of a recombinant gp350 variant that disrupts complement receptor binding recently enabled the identification of human memory B cells and their corresponding mAbs through cell sorting[37]. These mAbs map to the CD21-binding site on gp350. Panning of human antibody phage display libraries has enabled isolation of mAbs against gp42[55]. gp42 nAbs from animal immunizations and natural infection have been mapped to the HLA-binding site and hydrophobic pocket[54, 55, 111]. These gp42 and gp350 nAbs neutralize B cell infection, but not epithelial cell infection, which is expected as these glycoproteins are only important for B cell infection.

Passive transfer of EBV-nAbs against gH/gL, gB, gp350, and gp42 into humanized mice prior to EBV challenge can prevent viremia, splenomegaly, EBV-driven lymphoma, and death to varying degrees depending on the experimental model and

individual mAb[54, 55, 101-105]. Similarly, mAbs against gp350 and gH/gL can protect against experimental challenge with rhesus lymphocryptovirus, the EBV ortholog infecting rhesus macaques[107, 110]. At the time of writing, there has only been one clinical trial to test the safety and efficacy of one nAb in humans;72A1[109] (see below, Section 1.5.3).

1.4.2 EBV vaccines

The first EBV vaccine trial in humans tested recombinant vaccinia virus expressing gp350 in both adults and children[112]. While adults had low vaccine-induced immune responses, infants displayed a strong response and neutralizing antibodies were detected in sera of all recipients. However, the vaccine was not preventative as 3 of 9 infants became infected over a period of 16 months post vaccination. Another phase I trial tested recombinant gp350 protein-based vaccine in the context of transplant[113] (see below).

A gp350 subunit vaccine trial conducted in 181 volunteers ages 16-25 in Belgium reduced the incidence of IM by 78%. [114]. Although the correlates of protection were never established, the vaccine elicited antibodies that bind to an epitope known to neutralize EBV infection of B cells[115]. The vaccine had no impact on overall EBV acquisition suggesting that additional or alternative viral proteins could improve on this trial result[114]. To date, several gH/gL-based and multivalent vaccine candidates have been evaluated in various animal models and various platforms including nanoparticles and mRNA[108, 116-122].

Currently, ModernaTX, Inc. has an ongoing Phase I/II clinical trial (NCT05164094, started in December 2021 and set to end in October 2026) to assess the safety and immunogenicity of their multivalent mRNA-based EBV vaccine (mRNA-

1189), which encodes gp42, gp220, gH, and gL, intended to reduce rates of IM. They also have a Phase I trial (NCT05831111, started in April 2023 and set to end in October 2026) to assess mRNA-1195, which included mRNA molecules from mRNA-1189 and additional mRNAs encoding latent antigens EBNA3A and LMP2b, intended to be tested later in transplant patients. The National Institute of Allergy and Infectious Diseases has an ongoing Phase I clinical trial (NCT04645147, started in March 2022 and set to end in July 2026) to assess the safety and immunogenicity of a gp350-ferritin nanoparticle vaccine[123]. Therapeutic vaccines that have been tested in the clinic include an attenuated poxvirus expressing an EBNA1/LMP2 fusion protein[124] that has been shown to boost latent antigens EBNA1- and LMP2-specific T cell responses in NPC patients in remission and autologous dendritic cells pulsed with LMP2 epitope peptides[125] that elicited or boosted epitope-specific $CD8^+$ T cell responses in 9 out of 16 patients.

1.5 EBV and post-transplant lymphoproliferative disease (PTLD)

1.5.1 Overview of EBV's association with post-transplant lymphoproliferative disease

As stated above, growth-transforming B cells during primary EBV infection or reactivation are controlled by EBV-specific cytotoxic T cells in healthy individuals. However, individuals undergoing medically supervised immune suppression in the context of stem cell or organ transplant are at a high-risk for PTLD, a life-threatening lymphoma driven by unchecked proliferation of EBV-infected transformed B cells[2, 8, 10, 126, 127]. PTLD typically occurs within the first 3 years of immune suppression following transplant[8]. PTLD can occur if latent EBV within a patient reactivates during immunosuppression. EBV-seronegative patients, predominantly infants and children,

receiving EBV-positive transplants are at particularly high-risk. The incidence of PTLD is up to 10% higher in EBV-seronegative individuals compared to seropositive individuals, suggesting that pre-existing immunity plays an important role in preventing this lymphoma[10, 126]

1.5.2 Treatments and clinical trials

A first-line of therapy for PTLD is reduction of immunosuppression, however recovery from immunosuppression has a long median time to an effective immune response, host responses are highly variable, and this increases risk of developing allograft rejection or graft-versus-host disease[8, 127].

PTLD is typically treated with rituximab, an anti-CD20 mAb that depletes B cells[2, 8, 10, 126-128]. It has been extremely successful both as a prophylaxis in solid organ transplant and hematopoietic stem cell transplantation and as treatment for PTLD. Nevertheless, there are still patients who fail to respond or relapse following rituximab treatment and are at a high risk of mortality. Rituximab also targets non-infected B cells, further immunosuppressing the already vulnerable patients. Use of rituximab in prophylaxis can lead to emergence of rituximab-refractory CD20-negative malignancies and can cause several side effects like prolonged neutropenia, hypogammaglobinemia, or delayed humoral immune reconstitution[128].

Adoptive cellular immunotherapy is designed to restore the host EBV-specific T cell response[8, 9, 127, 128]. It has proven efficacious and safe as both prophylaxis and treatment even during refractory or relapsed disease, particularly in high-risk hematopoietic stem cell transplant recipients. The T cells can be derived from the patient or from HLA-matched donors. Tabelecleucel is an off-the-shelf, allogeneic, EBV-specific

T cell immunotherapy that has been approved since December 2022 for usage in exceptional circumstances[8, 126, 128]. However, generation of allogenic EBV-specific T cells is time consuming and third-party donors must be carefully selected and matched to avoid complications. Other therapies include designing chimeric antigen receptor cells to target infected B cells, targeting infected cells that express CD30, and lytic induction therapy to make the tumor cells susceptible to antiviral drugs[8, 126, 128].

As for vaccines, a phase I trial showed a recombinant gp350 monomer was safe and tolerable in children with chronic kidney disease awaiting transplantation. The vaccine was immunogenic in all evaluable patients, but only 4 out of 13 patients generated neutralizing antibodies[113]. EBV infection was detected in various patients both before and after transplantation, with one case of EBV-associated PTLD.

Current clinical trials include evaluating rituximab and LMP-specific T Cells in pediatric solid organ recipients (NCT02900976) and additional EBV-specific cytotoxic T cells (NCT03266653), both conducted by at University of California San Francisco.

1.5.3 Potential for EBV-specific monoclonal antibodies as treatment for PTLD

Pre-existing immunity to EBV seems to play a role in reducing the risk of PTLD[8-10]. Thus, it has been speculated that passive transfer of neutralizing antibodies could protect against EBV acquisition in transplant recipients and reduce the risk of PTLD[109]. Additionally, an EBV-specific treatment would not indiscriminately deplete the B cell compartment, and mAbs would be less costly and more accessible than adoptive T cell-based treatments. One clinical study has explored this possibility. Passive delivery of 72A1 was evaluated in four EBV-seronegative liver transplant recipients compared to three controls[109]. The experimental group received 1 mg of 72A1 mAb per kg of body

weight by intravenous infusions immediately before and 6 hours after transplant, then every 2 days for up to 3 weeks. 72A1 appeared to provide short-term protection against EBV acquisition 6-months post-transplant in 3 of the 4 mAb recipients. One mAb recipient remained EBV DNA, EBNA IgG, and VCA IgM and IgG seronegative for 4 years after transplant. However, all participants developed anti-drug antibodies due to the murine origin/composition of the mAb, and one developed a severe, hypersensitivity reaction that required cessation of treatment. This indicated that EBV-specific mAbs have potential to be powerful, off-the-shelf therapeutics against PTLD, but non-reactogenic mAbs are needed. This spurred subsequent efforts to humanize 72A1[106, 129]. Still, humanization of murine mAbs is not guaranteed to remove reactogenicity and could negatively affect potency. Thus, there is an unmet need for the discovery of more non-reactogenic human nAbs.

1.6 Thesis Goals

1.6.1. Isolation and characterization of novel EBV-specific neutralizing monoclonal antibodies

EBV-specific mAbs have potential utility as therapeutics to prevent PTLD, especially in EBV-seronegative transplant patients. As detailed above, human mAbs that prevent B cell infection could overcome reactogenicity seen with the murine mAb 72A1; however, very few human mAbs exist. In Chapter 2 of this thesis, I will detail the isolation and characterization of novel genetically human mAbs against gp350 and gp42 by leveraging a humanized mouse model that has been engineered to express the human gamma and kappa antibody repertoire. I utilized a variety of biochemical and structural assays to define the mechanism of neutralization for both gp350 and gp42 mAbs.

Excitingly, one gp42 mAb was able to protect human $CD34^+$ engrafted mice from EBV challenge and PTLD-like lymphoma formation, while a gp350 mAb provided partial protection. These results demonstrate the utility of this humanized antibody repertoire mouse model to generate protective genetically human mAbs and motivate the continued development of these antibodies as prophylactic agents for the prevention of EBV-driven diseases.

1.6.2 Modeling human immunization in the context of HIV-specific broadly neutralizing antibodies (bNAbs)

In a second project, I wanted to further assess these mice as a surrogate for human B cell responses to VRC01-class germline targeting immunogens. These immunogens are the first step in an immunization scheme to raise bNAbs against HIV. In particular, I was interested in evaluating and optimizing an anti-idiotypic immunogen previously characterized by my lab (iv4/iv9), intended to specifically engage VRC01 precursors, which are rare in the human B cell repertoire[130, 131] . I utilized single cell transcriptomic analysis to ascertain the baseline frequency of B cells with VRC01-class signatures in these mice. By using iv4/iv9 as bait to sort B cells from unimmunized animals, I identified putative VRC01 precursors, indicating these humanized mice may be an appropriate surrogate model. Furthermore, I employed rational design to selectively mutate iv4/iv9 to better select for VRC01 precursors and evaluated if immunization of these mice could selectively expand putative VRC01 precursors *in vivo*.

1.7 Chapter 1 Bibliography

1. Hardy S, Chhan CB, Davis AR, McGuire AT. Viral Entry. Curr Top Microbiol Immunol. 2025. Epub 20250515. doi: 10.1007/82_2025_300. PubMed PMID: 40366394.
2. Taylor GS, Long HM, Brooks JM, Rickinson AB, Hislop AD. The Immunology of Epstein-Barr Virus–Induced Disease. Annual Review of Immunology. 2015;33(1):787-821. doi: 10.1146/annurev-immunol-032414-112326.
3. Cohen JI. Epstein-Barr virus infection. N Engl J Med. 2000;343(7):481-92. doi: 10.1056/NEJM200008173430707. PubMed PMID: 10944566.
4. Khan G, Fitzmaurice C, Naghavi M, Ahmed LA. Global and regional incidence, mortality and disability-adjusted life-years for Epstein-Barr virus-attributable malignancies, 1990–2017. BMJ Open. 2020;10(8):e037505. doi: 10.1136/bmjopen-2020-037505.
5. Blazquez AC, Fellner MD, Lorenzetti MA, Preciado MV. A Comparative Genomic Analysis of Epstein-Barr Virus Strains with a Focus on EBV2 Variability. Int J Mol Sci. 2025;26(6). Epub 20250317. doi: 10.3390/ijms26062708. PubMed PMID: 40141350; PMCID: PMC11943181.
6. Dunmire SK, Hogquist KA, Balfour HH. Infectious Mononucleosis. Curr Top Microbiol Immunol. 2015;390(Pt 1):211-40. doi: 10.1007/978-3-319-22822-8_9. PubMed PMID: 26424648; PMCID: PMC4670567.
7. Wong Y, Meehan MT, Burrows SR, Doolan DL, Miles JJ. Estimating the global burden of Epstein-Barr virus-related cancers. J Cancer Res Clin Oncol. 2022;148(1):31-46. Epub 20211027. doi: 10.1007/s00432-021-03824-y. PubMed PMID: 34705104; PMCID: PMC8752571.
8. Al Hamed R, Bazarbachi AH, Mohty M. Epstein-Barr virus-related post-transplant lymphoproliferative disease (EBV-PTLD) in the setting of allogeneic stem cell transplantation: a comprehensive review from pathogenesis to forthcoming treatment modalities. Bone Marrow Transplantation. 2020;55(1):25-39. doi: 10.1038/s41409-019-0548-7.
9. Allen UD, Preiksaitis JK, Practice tAIDCo. Post-transplant lymphoproliferative disorders, Epstein-Barr virus infection, and disease in solid organ transplantation: Guidelines from the American Society of Transplantation Infectious Diseases Community of Practice. Clinical Transplantation. 2019;33(9):e13652. doi: 10.1111/ctr.13652.
10. Dharnidharka VR, Ruzinova MB, Marks LJ. Post-Transplant Lymphoproliferative Disorders. Seminars in Nephrology. 2024;44(1):151503. doi: 10.1016/j.semnephrol.2024.151503.
11. Levin LI, Munger KL, O'Reilly EJ, Falk KI, Ascherio A. Primary infection with the Epstein-Barr virus and risk of multiple sclerosis. Ann Neurol. 2010;67(6):824-30. Epub 2010/06/03. doi: 10.1002/ana.21978. PubMed PMID: 20517945; PMCID: PMC3089959.
12. Handel AE, Williamson AJ, Disanto G, Handunnetthi L, Giovannoni G, Ramagopalan SV. An updated meta-analysis of risk of multiple sclerosis following infectious mononucleosis. PLoS One. 2010;5(9). Epub 2010/09/09. doi: 10.1371/journal.pone.0012496. PubMed PMID: 20824132; PMCID: PMC2931696.
13. Thacker EL, Mirzaei F, Ascherio A. Infectious mononucleosis and risk for multiple sclerosis: a meta-analysis. Ann Neurol. 2006;59(3):499-503. Epub 2006/02/28. doi: 10.1002/ana.20820. PubMed PMID: 16502434.
14. Munger KL, Levin LI, O'Reilly EJ, Falk KI, Ascherio A. Anti-Epstein-Barr virus antibodies as serological markers of multiple sclerosis: a prospective study among United States military personnel. Mult Scler. 2011;17(10):1185-93. Epub 2011/06/21. doi: 10.1177/1352458511408991. PubMed PMID: 21685232; PMCID: PMC3179777.
15. Nielsen TR, Rostgaard K, Askling J, Steffensen R, Oturai A, Jersild C, Koch-Henriksen N, Sørensen PS, Hjalgrim H. Effects of infectious mononucleosis and HLA-DRB1*15 in multiple sclerosis. Mult Scler. 2009;15(4):431-6. Epub 2009/01/21. doi: 10.1177/1352458508100037. PubMed PMID: 19153174.
16. Ascherio A, Munger KL. Epstein-barr virus infection and multiple sclerosis: a review. J Neuroimmune Pharmacol. 2010;5(3):271-7. Epub 2010/04/07. doi: 10.1007/s11481-010-9201-3. PubMed PMID: 20369303.
17. Bjornevik K, Cortese M, Healy BC, Kuhle J, Mina MJ, Leng Y, Elledge SJ, Niebuhr DW, Scher AI, Munger KL, Ascherio A. Longitudinal analysis reveals high prevalence of Epstein-Barr virus associated with multiple sclerosis. Science. 2022;375(6578):296-301. doi: 10.1126/science.abj8222.
18. Robinson WH, Younis S, Love ZZ, Steinman L, Lanz TV. Epstein-Barr virus as a potentiator of autoimmune diseases. Nat Rev Rheumatol. 2024;20(11):729-40. Epub 20241010. doi: 10.1038/s41584-024-01167-9. PubMed PMID: 39390260.
19. Younis S, Moutusy SI, Rasouli S, Jahanbani S, Pandit M, Wu X, Acharya S, Sharpe O, Wijeratne TU, Harris ML, Yang EY, Chaichian Y, Parsafar S, Baker MC, Harley JB, Meffre E, Steinman L, Marshak-Rothstein A, James JA, Martinez OM, Utz PJ, Orange DE, Lanz TV, Robinson WH. Epstein-Barr virus reprograms autoreactive

B cells as antigen-presenting cells in systemic lupus erythematosus. Sci Transl Med. 2025;17(824):eady0210. Epub 20251112. doi: 10.1126/scitranslmed.ady0210. PubMed PMID: 41223250.
20. Balandraud N, Roudier J. Epstein-Barr virus and rheumatoid arthritis. Joint Bone Spine. 2018;85(2):165-70. Epub 2017/05/14. doi: 10.1016/j.jbspin.2017.04.011. PubMed PMID: 28499895.
21. Fechtner S, Berens H, Bemis E, Johnson RL, Guthridge CJ, Carlson NE, Demoruelle MK, Harley JB, Edison JD, Norris JA, Robinson WH, Deane KD, James JA, Holers VM. Antibody Responses to Epstein-Barr Virus in the Preclinical Period of Rheumatoid Arthritis Suggest the Presence of Increased Viral Reactivation Cycles. Arthritis Rheumatol. 2021. Epub 2021/10/05. doi: 10.1002/art.41994. PubMed PMID: 34605217.
22. Su Y, Yuan D, Chen DG, Ng RH, Wang K, Choi J, Li S, Hong S, Zhang R, Xie J, Kornilov SA, Scherler K, Pavlovitch-Bedzyk AJ, Dong S, Lausted C, Lee I, Fallen S, Dai CL, Baloni P, Smith B, Duvvuri VR, Anderson KG, Li J, Yang F, Duncombe CJ, McCulloch DJ, Rostomily C, Troisch P, Zhou J, Mackay S, DeGottardi Q, May DH, Taniguchi R, Gittelman RM, Klinger M, Snyder TM, Roper R, Wojciechowska G, Murray K, Edmark R, Evans S, Jones L, Zhou Y, Rowen L, Liu R, Chour W, Algren HA, Berrington WR, Wallick JA, Cochran RA, Micikas ME, Wrin T, Petropoulos CJ, Cole HR, Fischer TD, Wei W, Hoon DSB, Price ND, Subramanian N, Hill JA, Hadlock J, Magis AT, Ribas A, Lanier LL, Boyd SD, Bluestone JA, Chu H, Hood L, Gottardo R, Greenberg PD, Davis MM, Goldman JD, Heath JR. Multiple early factors anticipate post-acute COVID-19 sequelae. Cell. 2022;185(5):881-95.e20. Epub 20220125. doi: 10.1016/j.cell.2022.01.014. PubMed PMID: 35216672; PMCID: PMC8786632.
23. Bernal KDE, Whitehurst CB. Incidence of Epstein-Barr virus reactivation is elevated in COVID-19 patients. Virus Res. 2023;334:199157. Epub 20230626. doi: 10.1016/j.virusres.2023.199157. PubMed PMID: 37364815; PMCID: PMC10292739.
24. Chen T, Song J, Liu H, Zheng H, Chen C. Positive Epstein-Barr virus detection in coronavirus disease 2019 (COVID-19) patients. Sci Rep. 2021;11(1):10902. Epub 20210525. doi: 10.1038/s41598-021-90351-y. PubMed PMID: 34035353; PMCID: PMC8149409.
25. Bjornevik K, Münz C, Cohen JI, Ascherio A. Epstein-Barr virus as a leading cause of multiple sclerosis: mechanisms and implications. Nature Reviews Neurology. 2023;19(3):160-71. doi: 10.1038/s41582-023-00775-5.
26. Borza CM, Hutt-Fletcher LM. Alternate replication in B cells and epithelial cells switches tropism of Epstein-Barr virus. Nat Med. 2002;8(6):594-9. doi: 10.1038/nm0602-594. PubMed PMID: 12042810.
27. Epstein MA, Achong BG, Barr YM. Virus Particles in Cultured Lymphoblasts from Burkitt's Lymphoma. Lancet. 1964;1(7335):702-3. doi: 10.1016/s0140-6736(64)91524-7. PubMed PMID: 14107961.
28. Fingeroth JD, Weis JJ, Tedder TF, Strominger JL, Biro PA, Fearon DT. Epstein-Barr virus receptor of human B lymphocytes is the C3d receptor CR2. Proc Natl Acad Sci U S A. 1984;81(14):4510-4. doi: 10.1073/pnas.81.14.4510. PubMed PMID: 6087328; PMCID: PMC345620.
29. Tanner J, Weis J, Fearon D, Whang Y, Kieff E. Epstein-barr virus gp350/220 binding to the B lymphocyte C3d receptor mediates adsorption, capping, and endocytosis. Cell. 1987;50(2):203-13. doi: 10.1016/0092-8674(87)90216-9.
30. Nemerow GR, Mold C, Schwend VK, Tollefson V, Cooper NR. Identification of gp350 as the viral glycoprotein mediating attachment of Epstein-Barr virus (EBV) to the EBV/C3d receptor of B cells: sequence homology of gp350 and C3 complement fragment C3d. J Virol. 1987;61(5):1416-20. doi: 10.1128/JVI.61.5.1416-1420.1987. PubMed PMID: 3033269; PMCID: PMC254117.
31. Ogembo JG, Kannan L, Ghiran I, Nicholson-Weller A, Finberg RW, Tsokos GC, Fingeroth JD. Human Complement Receptor Type 1/CD35 Is an Epstein-Barr Virus Receptor. Cell Reports. 2013;3(2):371-85. doi: 10.1016/j.celrep.2013.01.023.
32. Beisel C, Tanner J, Matsuo T, Thorley-Lawson D, Kezdy F, Kieff E. Two major outer envelope glycoproteins of Epstein-Barr virus are encoded by the same gene. Journal of Virology. 1985;54(3):665-74. doi: 10.1128/jvi.54.3.665-674.1985.
33. Hummel M, Thorley-Lawson D, Kieff E. An Epstein-Barr virus DNA fragment encodes messages for the two major envelope glycoproteins (gp350/300 and gp220/200). Journal of Virology. 1984;49(2):413-7. doi: 10.1128/jvi.49.2.413-417.1984.
34. Johannsen E, Luftig M, Chase MR, Weicksel S, Cahir-McFarland E, Illanes D, Sarracino D, Kieff E. Proteins of purified Epstein-Barr virus. Proceedings of the National Academy of Sciences. 2004;101(46):16286-91. doi: 10.1073/pnas.0407320101.
35. Szakonyi G, Klein MG, Hannan JP, Young KA, Ma RZ, Asokan R, Holers VM, Chen XS. Structure of the Epstein-Barr virus major envelope glycoprotein. Nature Structural & Molecular Biology. 2006;13(11):996-1001. doi: 10.1038/nsmb1161.

36. Sun C, Fang X-Y, Bu G-L, Zhong L-Y, Xie C, Zhao G-X, Sui S-F, Liu Z, Zeng M-S. Structural basis of Epstein-Barr virus gp350 receptor recognition and neutralization. Cell Reports. 2025;44(1):115168. doi: 10.1016/j.celrep.2024.115168.
37. Joyce MG, Bu W, Chen W-H, Gillespie RA, Andrews SF, Wheatley AK, Tsybovsky Y, Jensen JL, Stephens T, Prabhakaran M, Fisher BE, Narpala SR, Bagchi M, McDermott AB, Nabel GJ, Kwong PD, Mascola JR, Cohen JI, Kanekiyo M. Structural basis for complement receptor engagement and virus neutralization through Epstein-Barr virus gp350. Immunity. 2025;58(2):295-308.e5. doi: 10.1016/j.immuni.2025.01.010.
38. Hoffman GJ, Lazarowitz SG, Hayward SD. Monoclonal antibody against a 250,000-dalton glycoprotein of Epstein-Barr virus identifies a membrane antigen and a neutralizing antigen. Proceedings of the National Academy of Sciences. 1980;77(5):2979-83. doi: 10.1073/pnas.77.5.2979.
39. Janz A, Oezel M, Kurzeder C, Mautner J, Pich D, Kost M, Hammerschmidt W, Delecluse HJ. Infectious Epstein-Barr virus lacking major glycoprotein BLLF1 (gp350/220) demonstrates the existence of additional viral ligands. J Virol. 2000;74(21):10142-52. doi: 10.1128/jvi.74.21.10142-10152.2000. PubMed PMID: 11024143; PMCID: PMC102053.
40. Wang X, Hutt-Fletcher LM. Epstein-Barr virus lacking glycoprotein gp42 can bind to B cells but is not able to infect. J Virol. 1998;72(1):158-63. doi: 10.1128/JVI.72.1.158-163.1998. PubMed PMID: 9420211; PMCID: PMC109360.
41. Kirschner AN, Omerovic J, Popov B, Longnecker R, Jardetzky TS. Soluble Epstein-Barr virus glycoproteins gH, gL, and gp42 form a 1:1:1 stable complex that acts like soluble gp42 in B-cell fusion but not in epithelial cell fusion. J Virol. 2006;80(19):9444-54. doi: 10.1128/JVI.00572-06. PubMed PMID: 16973550; PMCID: PMC1617263.
42. Haan KM, Kwok WW, Longnecker R, Speck P. Epstein-Barr virus entry utilizing HLA-DP or HLA-DQ as a coreceptor. J Virol. 2000;74(5):2451-4. doi: 10.1128/jvi.74.5.2451-2454.2000. PubMed PMID: 10666279; PMCID: PMC111730.
43. Spriggs MK, Armitage RJ, Comeau MR, Strockbine L, Farrah T, Macduff B, Ulrich D, Alderson MR, Mullberg J, Cohen JI. The extracellular domain of the Epstein-Barr virus BZLF2 protein binds the HLA-DR beta chain and inhibits antigen presentation. J Virol. 1996;70(8):5557-63. doi: 10.1128/JVI.70.8.5557-5563.1996. PubMed PMID: 8764069; PMCID: PMC190515.
44. Gonzalez-Del Pino GL, Heldwein EE. Well Put Together-A Guide to Accessorizing with the Herpesvirus gH/gL Complexes. Viruses. 2022;14(2). Epub 20220130. doi: 10.3390/v14020296. PubMed PMID: 35215889; PMCID: PMC8874593.
45. Connolly SA, Jardetzky TS, Longnecker R. The structural basis of herpesvirus entry. Nat Rev Microbiol. 2021;19(2):110-21. Epub 20201021. doi: 10.1038/s41579-020-00448-w. PubMed PMID: 33087881; PMCID: PMC8579738.
46. Sathiyamoorthy K, Chen J, Longnecker R, Jardetzky TS. The COMPLEXity in herpesvirus entry. Current Opinion in Virology. 2017;24:97-104. doi: 10.1016/j.coviro.2017.04.006.
47. Kirschner AN, Sorem J, Longnecker R, Jardetzky TS. Structure of Epstein-Barr Virus Glycoprotein 42 Suggests a Mechanism for Triggering Receptor-Activated Virus Entry. Structure. 2009;17(2):223-33. doi: 10.1016/j.str.2008.12.010.
48. Mullen MM, Haan KM, Longnecker R, Jardetzky TS. Structure of the Epstein-Barr Virus gp42 Protein Bound to the MHC Class II Receptor HLA-DR1. Molecular Cell. 2002;9(2):375-85. doi: 10.1016/S1097-2765(02)00465-3.
49. Haan KM, Longnecker R. Coreceptor restriction within the HLA-DQ locus for Epstein-Barr virus infection. Proc Natl Acad Sci U S A. 2000;97(16):9252-7. doi: 10.1073/pnas.160171697. PubMed PMID: 10908662; PMCID: PMC16854.
50. Matsuura H, Kirschner AN, Longnecker R, Jardetzky TS. Crystal structure of the Epstein-Barr virus (EBV) glycoprotein H/glycoprotein L (gH/gL) complex. Proceedings of the National Academy of Sciences. 2010;107(52):22641-6. doi: 10.1073/pnas.1011806108.
51. Sathiyamoorthy K, Hu YX, Möhl BS, Chen J, Longnecker R, Jardetzky TS. Structural basis for Epstein–Barr virus host cell tropism mediated by gp42 and gHgL entry glycoproteins. Nature Communications. 2016;7(1):13557. doi: 10.1038/ncomms13557.
52. Sathiyamoorthy K, Jiang J, Hu YX, Rowe CL, Möhl BS, Chen J, Jiang W, Mellins ED, Longnecker R, Zhou ZH, Jardetzky TS. Assembly and Architecture of the EBV B Cell Entry Triggering Complex. PLOS Pathogens. 2014;10(8):e1004309. doi: 10.1371/journal.ppat.1004309.
53. Silva AL, Omerovic J, Jardetzky TS, Longnecker R. Mutational analyses of Epstein-Barr virus glycoprotein 42 reveal functional domains not involved in receptor binding but required for membrane fusion. J

Virol. 2004;78(11):5946-56. doi: 10.1128/JVI.78.11.5946-5956.2004. PubMed PMID: 15140992; PMCID: PMC415818.
54. Bu W, Kumar A, Board NL, Kim J, Dowdell K, Zhang S, Lei Y, Hostal A, Krogmann T, Wang Y, Pittaluga S, Marcotrigiano J, Cohen JI. Epstein-Barr virus gp42 antibodies reveal sites of vulnerability for receptor binding and fusion to B cells. Immunity. 2024;57(3):559-73.e6. doi: 10.1016/j.immuni.2024.02.008.
55. Zhao G-X, Fang X-Y, Bu G-L, Chen S-J-B, Sun C, Li T, Xie C, Wang Y, Li S-X, Meng N, Feng G-K, Zhong Q, Kong X-W, Liu Z, Zeng M-S. Potent human monoclonal antibodies targeting Epstein-Barr virus gp42 reveal vulnerable sites for virus infection. Cell Reports Medicine. 2024;5(5):101573. doi: 10.1016/j.xcrm.2024.101573.
56. Borza CM, Morgan AJ, Turk SM, Hutt-Fletcher LM. Use of gHgL for attachment of Epstein-Barr virus to epithelial cells compromises infection. J Virol. 2004;78(10):5007-14. doi: 10.1128/jvi.78.10.5007-5014.2004. PubMed PMID: 15113881; PMCID: PMC400351.
57. Wang X, Kenyon WJ, Li Q, Mullberg J, Hutt-Fletcher LM. Epstein-Barr virus uses different complexes of glycoproteins gH and gL to infect B lymphocytes and epithelial cells. J Virol. 1998;72(7):5552-8. doi: 10.1128/JVI.72.7.5552-5558.1998. PubMed PMID: 9621012; PMCID: PMC110204.
58. Li QX, Young LS, Niedobitek G, Dawson CW, Birkenbach M, Wang F, Rickinson AB. Epstein-Barr virus infection and replication in a human epithelial cell system. Nature. 1992;356(6367):347-50. doi: 10.1038/356347a0. PubMed PMID: 1312681.
59. Yoshiyama H, Imai S, Shimizu N, Takada K. Epstein-Barr virus infection of human gastric carcinoma cells: implication of the existence of a new virus receptor different from CD21. J Virol. 1997;71(7):5688-91. doi: 10.1128/JVI.71.7.5688-5691.1997. PubMed PMID: 9188650; PMCID: PMC191818.
60. Molesworth SJ, Lake CM, Borza CM, Turk SM, Hutt-Fletcher LM. Epstein-Barr virus gH is essential for penetration of B cells but also plays a role in attachment of virus to epithelial cells. J Virol. 2000;74(14):6324-32. doi: 10.1128/jvi.74.14.6324-6332.2000. PubMed PMID: 10864642; PMCID: PMC112138.
61. Imai S, Nishikawa J, Takada K. Cell-to-cell contact as an efficient mode of Epstein-Barr virus infection of diverse human epithelial cells. J Virol. 1998;72(5):4371-8. doi: 10.1128/JVI.72.5.4371-4378.1998. PubMed PMID: 9557727; PMCID: PMC109667.
62. Jiang R, Gu X, Nathan CO, Hutt-Fletcher L. Laser-capture microdissection of oropharyngeal epithelium indicates restriction of Epstein-Barr virus receptor/CD21 mRNA to tonsil epithelial cells. J Oral Pathol Med. 2008;37(10):626-33. Epub 20080815. doi: 10.1111/j.1600-0714.2008.00681.x. PubMed PMID: 18710421; PMCID: PMC2584167.
63. Hayman IR, Temple RM, Burgess CK, Ferguson M, Liao J, Meyers C, Sample CE. New insight into Epstein-Barr virus infection using models of stratified epithelium. PLoS Pathog. 2023;19(1):e1011040. Epub 20230111. doi: 10.1371/journal.ppat.1011040. PubMed PMID: 36630458; PMCID: PMC9873185.
64. Tugizov SM, Berline JW, Palefsky JM. Epstein-Barr virus infection of polarized tongue and nasopharyngeal epithelial cells. Nat Med. 2003;9(3):307-14. Epub 20030218. doi: 10.1038/nm830. PubMed PMID: 12592401.
65. Shannon-Lowe C, Rowe M. Epstein-Barr virus infection of polarized epithelial cells via the basolateral surface by memory B cell-mediated transfer infection. PLoS Pathog. 2011;7(5):e1001338. Epub 20110505. doi: 10.1371/journal.ppat.1001338. PubMed PMID: 21573183; PMCID: PMC3088705.
66. Shannon-Lowe CD, Neuhierl B, Baldwin G, Rickinson AB, Delecluse HJ. Resting B cells as a transfer vehicle for Epstein-Barr virus infection of epithelial cells. Proc Natl Acad Sci U S A. 2006;103(18):7065-70. Epub 20060410. doi: 10.1073/pnas.0510512103. PubMed PMID: 16606841; PMCID: PMC1459019.
67. Wang H, Mou Z, Yeo YY, Ge Q, Liu X, Narita Y, Li Z, Wang C, Li W, Zhao KR, Li J, Bu W, Gewurz B, Cohen JI, Teng M, Dai X, Liu X, Jiang S, Zhao B. Epstein-Barr virus exploits desmocollin 2 as the principal epithelial cell entry receptor. Nat Microbiol. 2025;10(11):2781-96. Epub 20250926. doi: 10.1038/s41564-025-02126-0. PubMed PMID: 41006833.
68. Mohl BS, Chen J, Sathiyamoorthy K, Jardetzky TS, Longnecker R. Structural and Mechanistic Insights into the Tropism of Epstein-Barr Virus. Mol Cells. 2016;39(4):286-91. Epub 20160406. doi: 10.14348/molcells.2016.0066. PubMed PMID: 27094060; PMCID: PMC4844934.
69. Xiao J, Palefsky JM, Herrera R, Berline J, Tugizov SM. The Epstein-Barr virus BMRF-2 protein facilitates virus attachment to oral epithelial cells. Virology. 2008;370(2):430-42. Epub 20071022. doi: 10.1016/j.virol.2007.09.012. PubMed PMID: 17945327; PMCID: PMC2268893.
70. Xiao J, Palefsky JM, Herrera R, Berline J, Tugizov SM. EBV BMRF-2 facilitates cell-to-cell spread of virus within polarized oral epithelial cells. Virology. 2009;388(2):335-43. Epub 20090424. doi: 10.1016/j.virol.2009.03.030. PubMed PMID: 19394065; PMCID: PMC2726254.

71. Chen J, Rowe CL, Jardetzky TS, Longnecker R. The KGD motif of Epstein-Barr virus gH/gL is bifunctional, orchestrating infection of B cells and epithelial cells. mBio. 2012;3(1). Epub 20120103. doi: 10.1128/mBio.00290-11. PubMed PMID: 22215569; PMCID: PMC3251506.
72. Chen J, Sathiyamoorthy K, Zhang X, Schaller S, Perez White BE, Jardetzky TS, Longnecker R. Ephrin receptor A2 is a functional entry receptor for Epstein-Barr virus. Nat Microbiol. 2018;3(2):172-80. Epub 20180101. doi: 10.1038/s41564-017-0081-7. PubMed PMID: 29292384; PMCID: PMC5972547.
73. Zhang H, Li Y, Wang HB, Zhang A, Chen ML, Fang ZX, Dong XD, Li SB, Du Y, Xiong D, He JY, Li MZ, Liu YM, Zhou AJ, Zhong Q, Zeng YX, Kieff E, Zhang Z, Gewurz BE, Zhao B, Zeng MS. Ephrin receptor A2 is an epithelial cell receptor for Epstein-Barr virus entry. Nat Microbiol. 2018;3(2):1-8. Epub 20180101. doi: 10.1038/s41564-017-0080-8. PubMed PMID: 29292383.
74. Chesnokova LS, Nishimura SL, Hutt-Fletcher LM. Fusion of epithelial cells by Epstein-Barr virus proteins is triggered by binding of viral glycoproteins gHgL to integrins alphavbeta6 or alphavbeta8. Proc Natl Acad Sci U S A. 2009;106(48):20464-9. Epub 20091117. doi: 10.1073/pnas.0907508106. PubMed PMID: 19920174; PMCID: PMC2787161.
75. Wang HB, Zhang H, Zhang JP, Li Y, Zhao B, Feng GK, Du Y, Xiong D, Zhong Q, Liu WL, Du H, Li MZ, Huang WL, Tsao SW, Hutt-Fletcher L, Zeng YX, Kieff E, Zeng MS. Neuropilin 1 is an entry factor that promotes EBV infection of nasopharyngeal epithelial cells. Nat Commun. 2015;6:6240. Epub 20150211. doi: 10.1038/ncomms7240. PubMed PMID: 25670642; PMCID: PMC4339892.
76. Li Y, Zhang H, Sun C, Dong XD, Xie C, Liu YT, Lin RB, Kong XW, Hu ZL, Ma XY, Dai DL, Zhu QY, Li YC, Li Y, Liu SX, Yuan L, Zhou PH, Gao S, Tang YP, Yang JY, Han P, McGuire AT, Zhao B, Bei JX, Robertson E, Zeng YX, Zhong Q, Zeng MS. R9AP is a common receptor for EBV infection in epithelial cells and B cells. Nature. 2025. Epub 20250618. doi: 10.1038/s41586-025-09166-w. PubMed PMID: 40533557.
77. Chesnokova LS, Hutt-Fletcher LM. Fusion of Epstein-Barr virus with epithelial cells can be triggered by alphavbeta5 in addition to alphavbeta6 and alphavbeta8, and integrin binding triggers a conformational change in glycoproteins gHgL. J Virol. 2011;85(24):13214-23. Epub 20110928. doi: 10.1128/JVI.05580-11. PubMed PMID: 21957301; PMCID: PMC3233123.
78. Chen J, Jardetzky TS, Longnecker R. The large groove found in the gH/gL structure is an important functional domain for Epstein-Barr virus fusion. J Virol. 2013;87(7):3620-7. Epub 20130116. doi: 10.1128/JVI.03245-12. PubMed PMID: 23325693; PMCID: PMC3624213.
79. Su C, Wu L, Chai Y, Qi J, Tan S, Gao GF, Song H, Yan J. Molecular basis of EphA2 recognition by gHgL from gammaherpesviruses. Nat Commun. 2020;11(1):5964. Epub 20201124. doi: 10.1038/s41467-020-19617-9. PubMed PMID: 33235207; PMCID: PMC7687889.
80. Snijder J, Ortego MS, Weidle C, Stuart AB, Gray MD, McElrath MJ, Pancera M, Veesler D, McGuire AT. An antibody targeting the fusion machinery neutralizes dual-tropic infection and defines a site of vulnerability on Epstein-Barr virus. Immunity. 2018;48(4):799-811.e9. doi: 10.1016/j.immuni.2018.03.026.
81. Teesalu T, Sugahara KN, Kotamraju VR, Ruoslahti E. C-end rule peptides mediate neuropilin-1-dependent cell, vascular, and tissue penetration. Proc Natl Acad Sci U S A. 2009;106(38):16157-62. Epub 20090902. doi: 10.1073/pnas.0908201106. PubMed PMID: 19805273; PMCID: PMC2752543.
82. Sorem J, Longnecker R. Cleavage of Epstein-Barr virus glycoprotein B is required for full function in cell-cell fusion with both epithelial and B cells. J Gen Virol. 2009;90(Pt 3):591-5. doi: 10.1099/vir.0.007237-0. PubMed PMID: 19218203; PMCID: PMC2768059.
83. Chijioke O, Muller A, Feederle R, Barros MH, Krieg C, Emmel V, Marcenaro E, Leung CS, Antsiferova O, Landtwing V, Bossart W, Moretta A, Hassan R, Boyman O, Niedobitek G, Delecluse HJ, Capaul R, Munz C. Human natural killer cells prevent infectious mononucleosis features by targeting lytic Epstein-Barr virus infection. Cell Rep. 2013;5(6):1489-98. Epub 20131219. doi: 10.1016/j.celrep.2013.11.041. PubMed PMID: 24360958; PMCID: PMC3895765.
84. Zhang Y, Wallace DL, de Lara CM, Ghattas H, Asquith B, Worth A, Griffin GE, Taylor GP, Tough DF, Beverley PC, Macallan DC. In vivo kinetics of human natural killer cells: the effects of ageing and acute and chronic viral infection. Immunology. 2007;121(2):258-65. Epub 20070307. doi: 10.1111/j.1365-2567.2007.02573.x. PubMed PMID: 17346281; PMCID: PMC2265941.
85. Strowig T, Brilot F, Arrey F, Bougras G, Thomas D, Muller WA, Munz C. Tonsilar NK cells restrict B cell transformation by the Epstein-Barr virus via IFN-gamma. PLoS Pathog. 2008;4(2):e27. doi: 10.1371/journal.ppat.0040027. PubMed PMID: 18266470; PMCID: PMC2233668.
86. Hislop AD, Taylor GS. T-Cell Responses to EBV. Curr Top Microbiol Immunol. 2015;391:325-53. doi: 10.1007/978-3-319-22834-1_11. PubMed PMID: 26428380.

87. Rickinson AB, Long HM, Palendira U, Munz C, Hislop AD. Cellular immune controls over Epstein-Barr virus infection: new lessons from the clinic and the laboratory. Trends Immunol. 2014;35(4):159-69. Epub 20140301. doi: 10.1016/j.it.2014.01.003. PubMed PMID: 24589417.
88. Wang C, Chen J, Li J, Xu Z, Huang L, Zhao Q, Chen L, Liang X, Hu H, Li G, Xiong C, Wu B, You H, Du D, Wang X, Li H, Wang Z, Chen L. An EBV-related CD4 TCR immunotherapy inhibits tumor growth in an HLA-DP5+ nasopharyngeal cancer mouse model. J Clin Invest. 2024;134(8). Epub 20240227. doi: 10.1172/JCI172092. PubMed PMID: 38412034; PMCID: PMC11014665.
89. Leung CS, Haigh TA, Mackay LK, Rickinson AB, Taylor GS. Nuclear location of an endogenously expressed antigen, EBNA1, restricts access to macroautophagy and the range of CD4 epitope display. Proc Natl Acad Sci U S A. 2010;107(5):2165-70. Epub 20100119. doi: 10.1073/pnas.0909448107. PubMed PMID: 20133861; PMCID: PMC2836662.
90. Bu W, Hayes GM, Liu H, Gemmell L, Schmeling DO, Radecki P, Aguilar F, Burbelo PD, Woo J, Balfour HH, Jr., Cohen JI. Kinetics of Epstein-Barr Virus (EBV) Neutralizing and Virus-Specific Antibodies after Primary Infection with EBV. Clin Vaccine Immunol. 2016;23(4):363-9. Epub 20160404. doi: 10.1128/CVI.00674-15. PubMed PMID: 26888186; PMCID: PMC4820504.
91. Hewetson JF, Rocchi G, Henle W, Henle G. Neutralizing antibodies to Epstein-Barr virus in healthy populations and patients with infectious mononucleosis. J Infect Dis. 1973;128(3):283-9. doi: 10.1093/infdis/128.3.283. PubMed PMID: 4353929.
92. Miller G, Niederman JC, Stitt DA. Infectious mononucleosis: appearance of neutralizing antibody to Epstein-Barr virus measured by inhibition of formation of lymphoblastoid cell lines. J Infect Dis. 1972;125(4):403-6. doi: 10.1093/infdis/125.4.403. PubMed PMID: 4336201.
93. Jondal M. Antibody-dependent cellular cytotoxicity (ADCC) against Epstein-Barr virus-determined membrane antigens. I. Reactivity in sera from normal persons and from patients with acute infectious mononucleosis. Clin Exp Immunol. 1976;25(1):1-5. PubMed PMID: 186222; PMCID: PMC1541383.
94. Patarroyo M, Blazar B, Pearson G, Klein E, Klein G. Induction of the EBV cycle in B-lymphocyte-derived lines is accompanied by increased natural killer (NK) sensitivity and the expression of EBV-related antigen(s) detected by the ADCC reaction. Int J Cancer. 1980;26(3):365-71. doi: 10.1002/ijc.2910260317. PubMed PMID: 6270007.
95. Minab R, Bu W, Nguyen H, Wall A, Sholukh AM, Huang ML, Ortego M, Krantz EM, Irvine M, Casper C, Orem J, McGuire AT, Cohen JI, Gantt S. Maternal Epstein-Barr Virus-Specific Antibodies and Risk of Infection in Ugandan Infants. J Infect Dis. 2021;223(11):1897-904. doi: 10.1093/infdis/jiaa654. PubMed PMID: 33095855; PMCID: PMC8176630.
96. Weiss ER, Alter G, Ogembo JG, Henderson JL, Tabak B, Bakis Y, Somasundaran M, Garber M, Selin L, Luzuriaga K. High Epstein-Barr Virus Load and Genomic Diversity Are Associated with Generation of gp350-Specific Neutralizing Antibodies following Acute Infectious Mononucleosis. J Virol. 2017;91(1). Epub 20161216. doi: 10.1128/JVI.01562-16. PubMed PMID: 27733645; PMCID: PMC5165192.
97. Lopez-Montanes M, Alari-Pahissa E, Sintes J, Martinez-Rodriguez JE, Muntasell A, Lopez-Botet M. Antibody-Dependent NK Cell Activation Differentially Targets EBV-Infected Cells in Lytic Cycle and Bystander B Lymphocytes Bound to Viral Antigen-Containing Particles. J Immunol. 2017;199(2):656-65. Epub 20170619. doi: 10.4049/jimmunol.1601574. PubMed PMID: 28630095.
98. Karsten CB, Bartsch YC, Shin SA, Slein MD, Heller HM, Kolandaivelu K, Middeldorp JM, Alter G, Julg B. Evolution of functional antibodies following acute Epstein-Barr virus infection. PLoS Pathog. 2022;18(9):e1010738. Epub 20220906. doi: 10.1371/journal.ppat.1010738. PubMed PMID: 36067220; PMCID: PMC9481173.
99. !!! INVALID CITATION !!! 76-78.
100. Bu W, Joyce MG, Nguyen H, Banh DV, Aguilar F, Tariq Z, Yap ML, Tsujimura Y, Gillespie RA, Tsybovsky Y, Andrews SF, Narpala SR, McDermott AB, Rossmann MG, Yasutomi Y, Nabel GJ, Kanekiyo M, Cohen JI. Immunization with Components of the Viral Fusion Apparatus Elicits Antibodies That Neutralize Epstein-Barr Virus in B Cells and Epithelial Cells. Immunity. 2019;50(5):1305-16.e6. doi: 10.1016/j.immuni.2019.03.010.
101. Hong J, Zhong L, Zheng Q, Wu Q, Zha Z, Wei D, Chen H, Zhang W, Zhang S, Huang Y, Chen K, Chen J, Li S, Zeng MS, Zeng YX, Xia N, Zhang X, Xu M, Chen Y. A Neutralizing Antibody Targeting gH Provides Potent Protection against EBV Challenge In Vivo. J Virol. 2022;96(8):e0007522. Epub 20220329. doi: 10.1128/jvi.00075-22. PubMed PMID: 35348362; PMCID: PMC9044928.
102. Zhang X, Hong J, Zhong L, Wu Q, Zhang S, Zhu Q, Chen H, Wei D, Li R, Zhang W, Zhang X, Wang G, Zhou X, Chen J, Kang Y, Zha Z, Duan X, Huang Y, Sun C, Kong X, Zhou Y, Chen Y, Ye X, Feng Q, Li S, Xiang T, Gao S, Zeng MS, Zheng Q, Chen Y, Zeng YX, Xia N, Xu M. Protective anti-gB neutralizing antibodies targeting

two vulnerable sites for EBV-cell membrane fusion. Proc Natl Acad Sci U S A. 2022;119(32):e2202371119. Epub 20220802. doi: 10.1073/pnas.2202371119. PubMed PMID: 35917353; PMCID: PMC9371650.
103. Zhu QY, Shan S, Yu J, Peng SY, Sun C, Zuo Y, Zhong LY, Yan SM, Zhang X, Yang Z, Peng YJ, Shi X, Cao SM, Wang X, Zeng MS, Zhang L. A potent and protective human neutralizing antibody targeting a novel vulnerable site of Epstein-Barr virus. Nat Commun. 2021;12(1):6624. Epub 20211116. doi: 10.1038/s41467-021-26912-6. PubMed PMID: 34785638; PMCID: PMC8595662.
104. Chen WH, Kim J, Bu W, Board NL, Tsybovsky Y, Wang Y, Hostal A, Andrews SF, Gillespie RA, Choe M, Stephens T, Yang ES, Pegu A, Peterson CE, Fisher BE, Mascola JR, Pittaluga S, McDermott AB, Kanekiyo M, Joyce MG, Cohen JI. Epstein-Barr virus gH/gL has multiple sites of vulnerability for virus neutralization and fusion inhibition. Immunity. 2022;55(11):2135-48 e6. Epub 20221027. doi: 10.1016/j.immuni.2022.10.003. PubMed PMID: 36306784; PMCID: PMC9815946.
105. Hong J, Zhong L, Liu L, Wu Q, Zhang W, Chen K, Wei D, Sun H, Zhou X, Zhang X, Kang YF, Huang Y, Chen J, Wang G, Zhou Y, Chen Y, Feng QS, Yu H, Li S, Zeng MS, Zeng YX, Xu M, Zheng Q, Chen Y, Zhang X, Xia N. Non-overlapping epitopes on the gHgL-gp42 complex for the rational design of a triple-antibody cocktail against EBV infection. Cell Rep Med. 2023;4(11):101296. doi: 10.1016/j.xcrm.2023.101296. PubMed PMID: 37992686; PMCID: PMC10694767.
106. Mutsvunguma LZ, Rodriguez E, Escalante GM, Muniraju M, Williams JC, Warden C, Qin H, Wang J, Wu X, Barasa A, Mulama DH, Mwangi W, Ogembo JG. Identification of multiple potent neutralizing and non-neutralizing antibodies against Epstein-Barr virus gp350 protein with potential for clinical application and as reagents for mapping immunodominant epitopes. Virology. 2019;536:1-15. doi: 10.1016/j.virol.2019.07.026.
107. Singh S, Homad LJ, Akins NR, Stoffers CM, Lackhar S, Malhi H, Wan Y-H, Rawlings DJ, McGuire AT. Neutralizing Antibodies Protect against Oral Transmission of Lymphocryptovirus. Cell Reports Medicine. 2020;1(3):100033. doi: 10.1016/j.xcrm.2020.100033.
108. Escalante GM, Mutsvunguma LZ, Muniraju M, Rodriguez E, Ogembo JG. Four Decades of Prophylactic EBV Vaccine Research: A Systematic Review and Historical Perspective. Frontiers in Immunology. 2022;13. doi: 10.3389/fimmu.2022.867918.
109. Haque T, Johannessen I, Dombagoda D, Sengupta C, Burns DM, Bird P, Hale G, Mieli-Vergani G, Crawford DH. A mouse monoclonal antibody against Epstein-Barr virus envelope glycoprotein 350 prevents infection both in vitro and in vivo. The Journal of Infectious Diseases. 2006;194(5):584-7. doi: 10.1086/505912.
110. Muhe J, Aye PP, Quink C, Eng JY, Engelman K, Reimann KA, Wang F. Neutralizing antibodies against Epstein-Barr virus infection of B cells can protect from oral viral challenge in the rhesus macaque animal model. Cell Rep Med. 2021;2(7):100352. Epub 20210721. doi: 10.1016/j.xcrm.2021.100352. PubMed PMID: 34337567; PMCID: PMC8324488.
111. Wu Q, Zhong L, Wei D, Zhang W, Hong J, Kang Y, Chen K, Huang Y, Zheng Q, Xu M, Zeng MS, Zeng YX, Xia N, Zhao Q, Krummenacher C, Chen Y, Zhang X. Neutralizing antibodies against EBV gp42 show potent in vivo protection and define novel epitopes. Emerg Microbes Infect. 2023;12(2):2245920. doi: 10.1080/22221751.2023.2245920. PubMed PMID: 37542379; PMCID: PMC10443957.
112. Gu SY, Huang TM, Ruan L, Miao YH, Lu H, Chu CM, Motz M, Wolf H. First EBV vaccine trial in humans using recombinant vaccinia virus expressing the major membrane antigen. Dev Biol Stand. 1995;84:171-7. PubMed PMID: 7796951.
113. Rees L, Tizard EJ, Morgan AJ, Cubitt WD, Finerty S, Oyewole-Eletu TA, Owen K, Royed C, Stevens SJ, Shroff RC, Tanday MK, Wilson AD, Middeldorp JM, Amlot PL, Steven NM. A phase I trial of epstein-barr virus gp350 vaccine for children with chronic kidney disease awaiting transplantation. Transplantation. 2009;88(8):1025-9. doi: 10.1097/TP.0b013e3181b9d918. PubMed PMID: 19855249.
114. Sokal EM, Hoppenbrouwers K, Vandermeulen C, Moutschen M, Léonard P, Moreels A, Haumont M, Bollen A, Smets F, Denis M. Recombinant gp350 Vaccine for Infectious Mononucleosis: A Phase 2, Randomized, Double- Blind, Placebo-Controlled Trial to Evaluate the Safety, Immunogenicity, and Efficacy of an Epstein- Barr Virus Vaccine in Healthy Young Adults. The Journal of Infectious Diseases. 2007;196(12):1749-53. doi: 10.1086/523813.
115. Moutschen M, Léonard P, Sokal EM, Smets F, Haumont M, Mazzu P, Bollen A, Denamur F, Peeters P, Dubin G, Denis M. Phase I/II studies to evaluate safety and immunogenicity of a recombinant gp350 Epstein–Barr virus vaccine in healthy adults. Vaccine. 2007;25(24):4697-705. doi: 10.1016/j.vaccine.2007.04.008.
116. Malhi H, Homad LJ, Wan Y-H, Poudel B, Fiala B, Borst AJ, Wang JY, Walkey C, Price J, Wall A, Singh S, Moodie Z, Carter L, Handa S, Correnti CE, Stoddard BL, Veesler D, Pancera M, Olson J, King NP, McGuire AT. Immunization with a self-assembling nanoparticle vaccine displaying EBV gH/gL protects humanized mice against lethal viral challenge. Cell Reports Medicine. 2022;3(6):100658. doi: 10.1016/j.xcrm.2022.100658.

117. Edwards KR, Malhi H, Schmidt K, Davis AR, Homad LJ, Warner NL, Chhan CB, Scharffenberger SC, Gaffney K, Hinkley T, Potchen NB, Wang JY, Price J, McElrath MJ, Olson J, King NP, Lund JM, Moodie Z, Erasmus JH, McGuire AT. A gH/gL-encoding replicon vaccine elicits neutralizing antibodies that protect humanized mice against EBV challenge. npj Vaccines. 2024;9(1):120. doi: 10.1038/s41541-024-00907-y.
118. Edwards KR, Schmidt K, Homad LJ, Kher GM, Xu G, Rodrigues KA, Ben-Akiva E, Abbott J, Prlic M, Newell EW, De Rosa SC, Irvine DJ, Pancera M, McGuire AT. Vaccination with nanoparticles displaying gH/gL from Epstein-Barr virus elicits limited cross-protection against rhesus lymphocryptovirus. Cell Reports Medicine. 2024:101587. doi: 10.1016/j.xcrm.2024.101587.
119. Cui X, Cao Z, Ishikawa Y, Cui S, Imadome KI, Snapper CM. Immunization with Epstein-Barr Virus Core Fusion Machinery Envelope Proteins Elicit High Titers of Neutralizing Activities and Protect Humanized Mice from Lethal Dose EBV Challenge. Vaccines (Basel). 2021;9(3). Epub 20210319. doi: 10.3390/vaccines9030285. PubMed PMID: 33808755; PMCID: PMC8003492.
120. Wei C-J, Bu W, Nguyen LA, Batchelor JD, Kim J, Pittaluga S, Fuller JR, Nguyen H, Chou T-H, Cohen JI, Nabel GJ. A bivalent Epstein-Barr virus vaccine induces neutralizing antibodies that block infection and confer immunity in humanized mice. Science Translational Medicine. 2022;14(643):eabf3685. doi: 10.1126/scitranslmed.abf3685.
121. Zhong L, Zhang W, Liu H, Zhang X, Yang Z, Wen Z, Chen L, Chen H, Luo Y, Chen Y, Feng Q, Zeng MS, Zhao Q, Liu L, Krummenacher C, Zeng YX, Chen Y, Xu M, Zhang X. A cocktail nanovaccine targeting key entry glycoproteins elicits high neutralizing antibody levels against EBV infection. Nat Commun. 2024;15(1):5310. Epub 20240621. doi: 10.1038/s41467-024-49546-w. PubMed PMID: 38906867; PMCID: PMC11192767.
122. Sun C, Kang YF, Fang XY, Liu YN, Bu GL, Wang AJ, Li Y, Zhu QY, Zhang H, Xie C, Kong XW, Peng YJ, Lin WJ, Zhou L, Chen XC, Lu ZZ, Xu HQ, Hong DC, Zhang X, Zhong L, Feng GK, Zeng YX, Xu M, Zhong Q, Liu Z, Zeng MS. A gB nanoparticle vaccine elicits a protective neutralizing antibody response against EBV. Cell Host Microbe. 2023;31(11):1882-97 e10. Epub 20231016. doi: 10.1016/j.chom.2023.09.011. PubMed PMID: 37848029.
123. Kanekiyo M, Bu W, Joyce MG, Meng G, Whittle JRR, Baxa U, Yamamoto T, Narpala S, Todd J-P, Rao SS, McDermott AB, Koup RA, Rossmann MG, Mascola JR, Graham BS, Cohen JI, Nabel GJ. Rational Design of an Epstein-Barr Virus Vaccine Targeting the Receptor-Binding Site. Cell. 2015;162(5):1090-100. doi: 10.1016/j.cell.2015.07.043.
124. Taylor GS, Jia H, Harrington K, Lee LW, Turner J, Ladell K, Price DA, Tanday M, Matthews J, Roberts C, Edwards C, McGuigan L, Hartley A, Wilson S, Hui EP, Chan AT, Rickinson AB, Steven NM. A recombinant modified vaccinia ankara vaccine encoding Epstein-Barr Virus (EBV) target antigens: a phase I trial in UK patients with EBV-positive cancer. Clin Cancer Res. 2014;20(19):5009-22. Epub 20140814. doi: 10.1158/1078-0432.CCR-14-1122-T. PubMed PMID: 25124688; PMCID: PMC4340506.
125. Lin CL, Lo WF, Lee TH, Ren Y, Hwang SL, Cheng YF, Chen CL, Chang YS, Lee SP, Rickinson AB, Tam PK. Immunization with Epstein-Barr Virus (EBV) peptide-pulsed dendritic cells induces functional CD8+ T-cell immunity and may lead to tumor regression in patients with EBV-positive nasopharyngeal carcinoma. Cancer Res. 2002;62(23):6952-8. PubMed PMID: 12460912.
126. Law N, Logan C, Taplitz R. EBV Reactivation and Disease in Allogeneic Hematopoietic Stem Cell Transplant (HSCT) Recipients and Its Impact on HSCT Outcomes. Viruses. 2024;16(8):1294. doi: 10.3390/v16081294.
127. Daan D, M. HT. Post-Transplantation Lymphoproliferative Disorders in Adults. New England Journal of Medicine. 2018;378(6):549-62. doi: 10.1056/NEJMra1702693.
128. Pociupany M, Snoeck R, Dierickx D, Andrei G. Treatment of Epstein-Barr Virus infection in immunocompromised patients. Biochemical Pharmacology. 2024;225:116270. doi: 10.1016/j.bcp.2024.116270.
129. Tanner JE, Hu J, Alfieri C. Construction and Characterization of a Humanized Anti-Epstein-Barr Virus gp350 Antibody with Neutralizing Activity in Cell Culture. Cancers (Basel). 2018;10(4). Epub 20180409. doi: 10.3390/cancers10040112. PubMed PMID: 29642526; PMCID: PMC5923367.
130. Havenar-Daughton C, Sarkar A, Kulp DW, Toy L, Hu X, Deresa I, Kalyuzhniy O, Kaushik K, Upadhyay AA, Menis S, Landais E, Cao L, Diedrich JK, Kumar S, Schiffner T, Reiss SM, Seumois G, Yates JR, Paulson JC, Bosinger SE, Wilson IA, Schief WR, Crotty S. The human naive B cell repertoire contains distinct subclasses for a germline-targeting HIV-1 vaccine immunogen. Science translational medicine. 2018;10(448):eaat0381. doi: 10.1126/scitranslmed.aat0381.
131. Jardine JG, Kulp DW, Havenar-Daughton C, Sarkar A, Briney B, Sok D, Sesterhenn F, Ereño-Orbea J, Kalyuzhniy O, Deresa I, Hu X, Spencer S, Jones M, Georgeson E, Adachi Y, Kubitz M, deCamp AC, Julien J-P,

Wilson IA, Burton DR, Crotty S, Schief WR. HIV-1 broadly neutralizing antibody precursor B cells revealed by germline-targeting immunogen. Science. 2016;351(6280):1458-63. doi: 10.1126/science.aad9195.

Chapter 2. Transgenic Mouse-Derived Human Monoclonal Antibodies Targeting EBV gp350 and gp42 Provide Structural and Functional Basis for Therapeutic Development

This work is in press at Cell Reports Medicine as of December 9, 2025

Authors:

Crystal B. Chhan[1,2], Kevin Lang[1], Amelia R. Davis[1], Yu-Hsin Wan[1], Nicholas T. Aldridge[1], Gargi Kher[1], Samuel C. Scharffenberger[1,3], Samantha R. Hardy[1], Roman Iureniev[1], Natalia V. Giltiay[1], Kristina R. Edwards[1,2], Stefan Radtke[4,5], Hans-Peter Kiem[4,5,6], Marie Pancera[1], Andrew T. McGuire[1,2,3,#]

[1]Vaccine and Infectious Disease Division, Fred Hutchinson Cancer Center, Seattle, WA, USA.

[2]Department of Global Health, University of Washington, Seattle, WA, USA.

[3]Department of Laboratory Medicine and Pathology, University of Washington, Seattle, WA, USA.

[4]Stem Cell and Gene Therapy Program, Translational Science and Therapeutics Division, Fred Hutchinson Cancer Center, Seattle, WA, 98109, USA

[5]Department of Medicine, University of Washington School of Medicine, Seattle, WA, 98195, USA

[6]Department of Pathology, University of Washington School of Medicine, Seattle, WA, 98195, USA

[#]Corresponding Author: amcguire@fredhutch.org

2.1 Abstract

Epstein-Barr virus (EBV) causes infectious mononucleosis and is linked to neurodegenerative disorders. It is also associated with several malignancies, especially in immune compromised hosts. Transplant patients are at a high-risk of post-transplant lymphoproliferative disease, a life-threatening lymphoma driven by unchecked proliferation of EBV-infected B cells. There are no

approved EBV-specific vaccines or treatments; however, neutralizing antibodies against EBV glycoproteins may offer utility as therapeutic agents. Several viral proteins are involved in infection of B cells. These include gp350, which promotes viral attachment by binding to complement receptors, and gp42, which binds to HLA class II triggering subsequent membrane fusion. Most previously described monoclonal antibodies (mAbs) against these antigens are not of human origin, which limits their use. Here, we leveraged a transgenic mouse model to develop two gp350 and eight gp42 genetically human neutralizing mAbs that prevent binding to complement receptors and HLA class II, respectively. Structural analyses of the mAbs in complex with gp42 and gp350 define extended sites of vulnerability that are relevant to vaccine development. Passive transfer of a gp42 mAb protected humanized mice from EBV challenge, while a gp350 mAb provided partial protection. These mAbs highlight the utility of transgenic mice to develop novel therapeutics with the promise of preventing EBV-driven disease.

2.2 Introduction

EBV is a ubiquitous gamma herpesvirus[1]. The most common sequelae of EBV infection is infectious mononucleosis (IM), a self-limiting illness that can occur following primary infection with EBV[2, 3]. EBV is also associated with multiple sclerosis[4-10], systemic lupus erythematosus[11], rheumatoid arthritis[12, 13], and complications of COVID-19 infection[14-16]. Importantly, EBV was the first virus shown to be oncogenic in humans, and is associated with approximately 358,000 new cases of cancer, resulting in 209,000 deaths each year[17, 18]. Most EBV cancers originate from epithelial cells and B cells[19], the primary cell types infected by EBV, and the sites of replication and latency, respectively.

EBV relies on several glycoproteins and utilizes distinct entry pathways to infect B cells and epithelial cells[19, 20]. The viral fusion machinery gH, gL, and gB are critical for infection,

irrespective of cell type[21, 22]. gH and gL form a 1:1 heterodimeric complex that acts as a regulator of membrane fusion. Upon binding one or more host cell surface receptors, gH/gL relays a triggering signal to the fusogen gB[22-24]. EBV infection of B cells is initiated by attachment to complement receptors 1 (CD35) and/or 2 (CD21) by the viral glycoprotein gp350 or splice variant gp220[25-27]. B cell infection requires an additional viral protein, gp42, that forms a tripartite complex with gH and gL[28]. The extended N-terminus of gp42 wraps around gH/gL, while the position of the C-terminal domain of gp42 relative to gH/gL is conformationally dynamic and can exist in an "open" or "closed" state[29]. Binding of gp42 to class II human leukocyte antigens (HLA) on the B cell surface leads to triggering of gB-mediated fusion through the gH/gL-gp42 complex[29-31]. A hydrophobic pocket formed by gp42 residues 146, 149, 157–160, 181–188, 194, 196–203, and 206 that is distinct from the HLA-binding site makes contact with domain II (DII) of gH/gL in the "closed" conformation, and binding to HLA class II induces structural changes in this pocket[29, 32]. The pocket is functionally important for fusion, as mutating this region inhibits fusion without affecting the gH/gL or HLA interactions[33-35], and this pocket is the target of neutralizing antibodies[36, 37].

Following primary infection, the virus evades the immune response by establishing a latent state, allowing it to persist in resting memory B cells[19, 38]. Latently infected cells can reactivate expression of lytic genes, but these cells are typically eliminated by cytotoxic lymphocytes[38, 39]. As a result, most infected individuals carry the virus asymptomatically for life[19, 39, 40]. However, immune-compromised hosts have reduced immune surveillance capacity, which results in higher rates of EBV-driven malignancies, such as in the case of HIV-infected individuals compared to the general population[41, 42]. Additionally, individuals undergoing medically-supervised immune suppression in the context of stem cell or organ transplant are at a

high-risk for post-transplant lymphoproliferative disease (PTLD), a life-threatening lymphoma driven by unchecked proliferation of EBV-infected cells[19, 43, 44].

The incidence of PTLD is substantially higher in EBV seronegative individuals compared to seropositive individuals, suggesting that pre-existing immunity plays an important role in preventing this lymphoma[45, 46]. It has been speculated that passive transfer of neutralizing antibodies could protect against EBV acquisition in EBV-seronegative solid-organ transplant recipients and reduce the risk of PTLD[47, 48]. Passive transfer of EBV-neutralizing monoclonal antibodies (mAbs) against gH/gL, gB, gp350, and gp42 into humanized mice prior to EBV challenge can prevent viremia, splenomegaly, EBV-driven lymphoma, and death to varying degrees depending on the experimental model and individual mAb[36, 37, 49-53]. Similarly, mAbs against gp350 and gH/gL can protect against experimental challenge with rhesus lymphocryptovirus, the EBV ortholog infecting rhesus macaques[54, 55]. Combined, these data provide *in vivo* proof-of-concept that antibody-mediated prophylaxis may be an effective intervention.

As for human studies, the mAb 72A1[56], isolated from a murine hybridoma and shown to potently neutralize EBV infection of B cells *in vitro,* was evaluated in a small pilot study of EBV-seronegative liver transplant recipients[48]. 72A1 appeared to provide short-term protection against EBV acquisition; however, all participants developed anti-drug antibodies due to the murine origin/composition of the mAb, and one developed a hypersensitivity reaction, indicating that alternative mAbs with reduced reactogenicity are needed.

This spurred subsequent efforts to humanize 72A1[57, 58]. Humanization of murine mAbs is not guaranteed to remove reactogenicity and can negatively affect potency. Alternatively, mAbs targeting EBV glycoproteins have been isolated from human memory B cells of EBV infected

individuals using phage-display libraries or antigen-specific cell sorting[36, 50, 52, 59]. This latter technique relies on using fluorescently labeled antigens to identify pathogen-specific memory B cells through their cell-surface B cell receptors. Historically, isolating gp350 and gp42 mAbs with native glycoproteins with this approach has not been possible due their ability to bind with high affinity to complement receptors and HLA class II on the cell surface of B cells, respectively, negating B cell receptor-specific staining[59]. Engineering of a recombinant gp350 variant that disrupts complement receptor binding recently enabled the identification of human memory B cells and the corresponding mAbs targeting gp350 through cell sorting[60]. Panning of human antibody phage display libraries has enabled isolation of mAbs against gp42[36]. While these mAbs hold promise as prophylactic agents, they have not been tested in the clinic, and additional diverse mAbs warrant evaluation.

As an alternative to these approaches, we leveraged a rearranging mouse model (ATX-GK) from Alloy Therapeutics[61] where both murine antibody heavy chain variable, diversity, and joining genes, as well as kappa variable and joining genes were replaced with human ones. These mice produce a diverse, genetically human antibody repertoire, allowing for the discovery of genetically human antibodies targeting antigens of interest. To isolate and discover mAbs against EBV proteins, ATX-GK mice were immunized with recombinant gp350 and gp42 to generate hybridomas. Hybridomas were subsequently screened for antigen reactivity and neutralizing activity. Using this approach, we identified two unique gp350 mAbs and eight gp42 mAbs, representing two distinct clonal lineages, which were subsequently produced as recombinant, fully human IgG mAbs. The binding kinetics, neutralizing activities, and inhibition of receptor binding by the mAbs, combined with structural analyses of them in complex with their targets, demonstrate that the gp350 and gp42 mAbs neutralize EBV infectivity of B cells by directly

inhibiting viral glycoprotein interactions with host complement receptors (in the case of gp350), and HLA class II (in the case of gp42). Passive transfer of a gp42 mAb prevented splenomegaly, viremia, and detectable viral DNA in the spleens of humanized mice, while a gp350 mAb showed partial protection. These results motivate the continued development of these antibodies as prophylactic agents for the prevention of EBV-driven diseases.

2.3 Results

2.3.1 Isolation of genetically human anti-EBV monoclonal antibodies (mAbs) from transgenic mice

We sought to isolate genetically human monoclonal antibodies against gp350 and gp42 by immunizing ATX-GK transgenic mice, which have been engineered to express an antibody repertoire encoded by human variable heavy and kappa genes (Fig.1A). Paired sequencing of IgM B cell receptors (BCRs) expressed by B cells collected from naïve mice show diverse VH and VL gene usage (Fig. S1A and B). The CDRH3 lengths followed a Gaussian distribution with an average length of 13 amino acids (Fig. S1C). The CDRL3 lengths were less variable with most being 9 amino acids (Fig. S1D). We observed diverse clonotypes in each mouse with a slight skewing to IGKVD1-39 (Fig.S1D and E), consistent with this being the most highly expressed VK gene (Fig. S1B). We reasoned that ATX-GK mice were therefore an appropriate model to elicit genetically human antibodies.

ATX-GK mice were co-immunized with a truncated recombinant gp350 protein (amino acids 1-470) encompassing the first 3 structural domains and the gp42 ectodomain (amino acids 33-233) and used to generate hybridomas, which were seeded at a density of ~50-100/well and cultured in 384 well plates. Culture supernatants with gp350- or gp42-binding antibodies were identified using a high-throughput, flow-based, antigen-coupled bead assay (Fig. 1B). Wells with

the desired binding activity were re-arrayed in 96-well plates, sub-cultured, and screened for neutralizing activity against EBV infection of Raji B cells (Fig. 1C). Culture supernatants that showed at least a 50% reduction in infectivity were then sub-cloned using a ClonePix colony picker to establish monoclonal cell lines. Supernatants from monoclonal lines were re-screened for B cell neutralization (Fig.1D). Those which exhibited at least 50% neutralizing activity were sequenced and produced as recombinant human IgG1 monoclonal antibodies (mAbs) for further characterization. We identified two gp350 and eight gp42 novel neutralizing antibodies, herein deemed ATX-350 or ATX-42 mAbs. Seven of the eight gp42 mAbs (ATX-42-1.1 to ATX-42-1.7) were determined to be clonal variants based on VH and VL gene usage as well as CDRH3 and CDRL3 sequence similarities (Table S1).

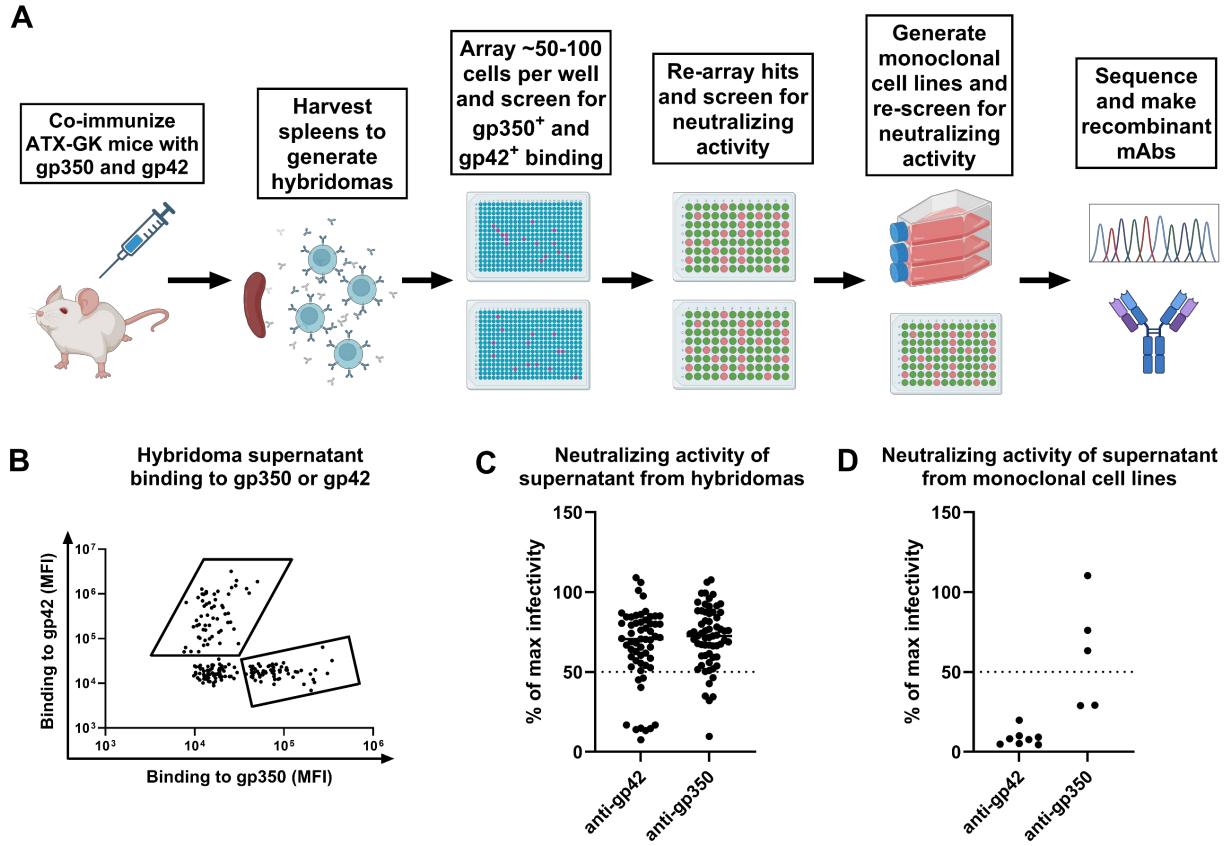

Figure 1. Isolation of anti-EBV antibodies from ATX-GK mice

(**A**) Overview of mAb discovery pipeline. Created with BioRender.com. (**B**) Binding of 190 polyclonal hybridoma culture supernatants to gp42 or gp350 coupled beads. (**C**) Supernatant from hybridoma cultures with gp42 or gp350 binding activity in **B** were evaluated for their ability to neutralize EBV infection of B cells at a 1:1 final dilution. (**D**) Monoclonal cell lines isolated from cultures with neutralizing activity in **C** were re-screened for ability to neutralize EBV infection of B cells. Dashed line represents 50% infectivity in **C** and **D**.

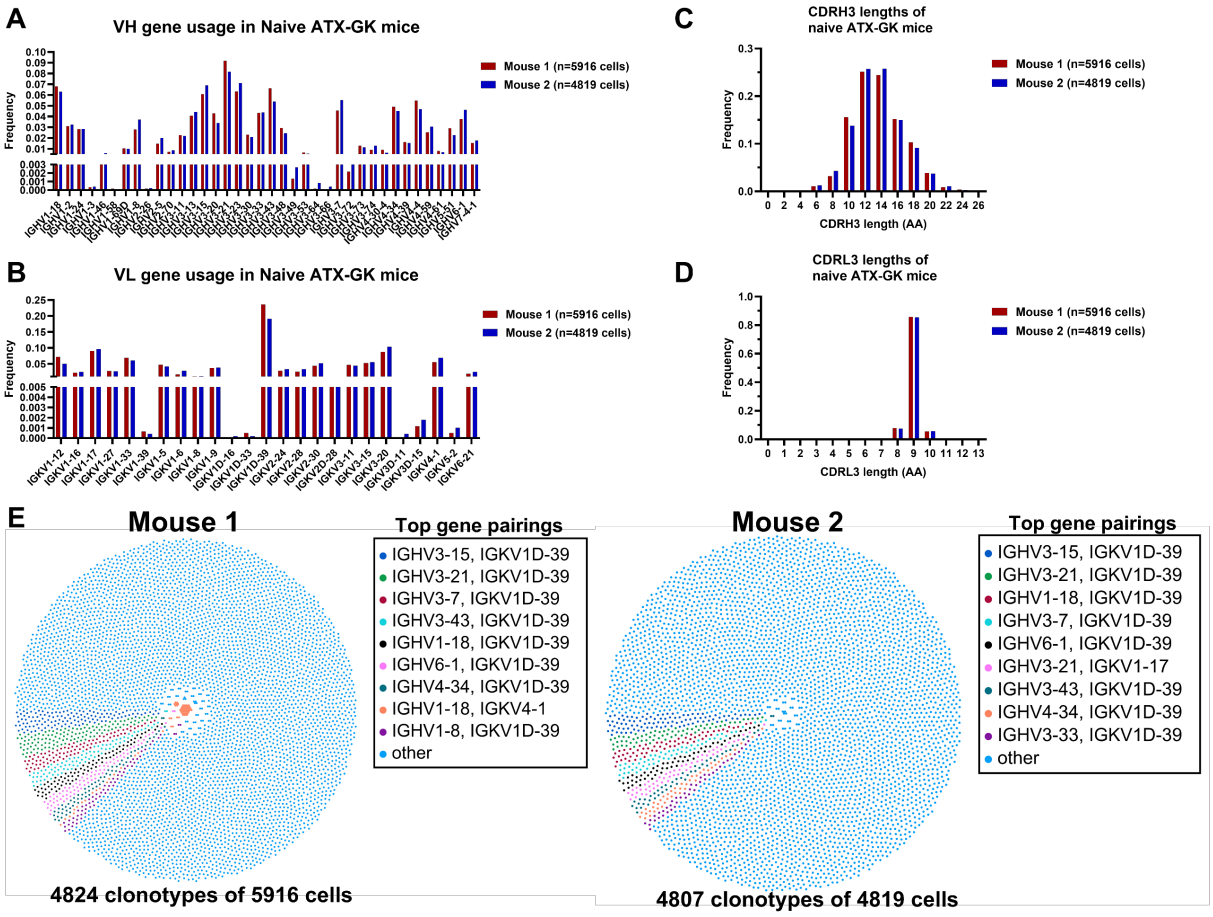

Figure S1. Paired antibody repertoire sequencing of naïve ATX-GK mice. Paired IgM BCR sequencing was performed on 5916 and 4819 splenic B cells from two naïve ATX-GK mice (**A**) Frequency of variable heavy chain (VH) gene usage. (**B**) Frequency of variable light chain (VL) gene usage. (**C**) Frequency of CDRH3 lengths. (**D**) Frequency of CDRL3 lengths. (**E**) Honeycomb plots depicting top 10 gene pairings utilized by IgM B cells from naïve ATX-GK mice. Each dot represents a single cell. Each cluster of dots represent clones of a single clonotype. Single dots represent unique clones.

Table S1. Heavy and light chain CDR sequences of ATX-42 and ATX-350 mAbs. Related to Figure 1.

mAb	V-GENE and allele	CDR3 AA junction	GenBank Accession Number
ATX-350-1	IGHV3-9*01	CAKGRTANTSFDYW	PV837517
	IGKV1-12*01 or IGKV1-12*02 or IGKV1D-12*02	CQQANSFPYTF	PV837527
ATX-350-2	IGHV2-5*01	CAHRYSSRWYWYFDLW	PV837518
	IGKV3-20*01	CQQYGSSHTF	PV837528
ATX-42-1.1	IGHV3-33*01	CARDPGYCSRYTCYGGWFDPW	PV837519
	IGKV1-39*01 or IGKV1D-39*01	CQRSSNSPYTF	PV837529
ATX-42-1.2	IGHV3-33*01	CARDPGYCSRTSCYGGWFDPW	PV837520
	IGKV1-39*01 or IGKV1D-39*01	CQQSDSIPYTF	PV837530
ATX-42-1.3	IGHV3-33*01	CARDPGYCSRTNCYGGWFDPW	PV837521
	IGKV1-39*01 or IGKV1D-39*01	CQKSNNSPYTF	PV837531
ATX-42-1.4	IGHV3-33*01	CARDPGYCSRTNCYGGWFDPW	PV837522
	IGKV1-39*01 or IGKV1D-39*01	CQKSDNSPYTF	PV837532
ATX-42-1.5	IGHV3-33*01	CARDPGYCDRTACYGGWFDPW	PV837523
	IGKV1-39*01 or IGKV1D-39*01	CQQSHNTPYTF	PV837533
ATX-42-1.6	IGHV3-33*01	CARDPGYCSRSNCYGGWFDPW	PV837524
	IGKV1-39*01 or IGKV1D-39*01	CQQSHSFPYTF	PV837534
ATX-42-1.7	IGHV3-33*01	CARDPGYCSRTTCYGGWFDPW	PV837525
	IGKV1-39*01 or IGKV1D-39*01	CQQSDNNLYSF	PV837535
ATX-42-2	IGHV5-51*01	CAREGDYYYGSGTYYKVWFDPW	PV837526
	IGKV3-11*01	CQQRSNWPLTF	PV837536

2.3.2. ATX-350 mAbs bind with high affinity and inhibit EBV infection of B cells

To further characterize the ATX-350 mAbs, we measured the binding affinity of the ATX-350 antigen binding fragments (Fabs) to recombinant gp350 using biolayer interferometry

(BLI). ATX-350-2 had the highest affinity (0.4 nM) which was 2-fold higher than the control 72A1 Fab (0.8 nM, Fig. 2A & Table S2). The affinity of ATX-350-1 (3.4 nM) was ~10 fold lower than ATX-350-2 (Fig. 2A & Table S2).

We next assessed whether the ATX-350 mAbs could neutralize EBV (B95.8/F) infection of Raji B cells. For comparison, we included known gp350 human mAbs, 769A9 and 770E11[60], as well as a version of the 72A1 mAb with a human IgG1 Fc region. The half-maximal inhibitory concentration (IC_{50}) of ATX-350-2 (0.02 μg/mL) was comparable to 72A1 (IC_{50} = 0.03 μg/mL, Fig. 2B & C). ATX-350-1 was significantly less potent (IC_{50} = 9.8 μg/mL) than either ATX-350-2 or 72A1 (Fig. 2B & C). The 50-fold weaker neutralization by ATX-350-1 compared to ATX-350-2 is greater than the 10-fold difference in binding affinity, implying that affinity and neutralization are not strictly correlated. Neither ATX-350-1 or ATX-350-2 were as potent as the recently described 769A9 (IC_{50} = 0.006 μg/mL) and 770E11 (IC_{50} = 0.004 μg/mL) mAbs isolated from humans (Fig. 2B & C).

We next assessed the ability of the ATX-350 mAbs to inhibit EBV (Akata-GFP) infection of SVKCR2 epithelial cells. In this assay, ATX-350-2 was >10-fold more potent than 72A1 and comparable to the gH/gL mAb AMMO1 (Fig. 2D)[59], while ATX-350-1 was non-neutralizing. SVKCR2 cells are engineered to express CD21 to overcome the relatively poor infectivity of cultured epithelial cells[62]. We therefore tested the ability of the mAbs to neutralize EBV infection in a CD21-negative AGS cell line[63, 64]. Here we used the M81 EBV strain, which has an increased propensity to infect epithelial cells and is engineered to express a luciferase reporter gene[63, 65, 66]. In this assay, none of the gp350 mAbs could reduce infectivity by 50%, while the gH/gL mAb AMMO1 retained neutralizing activity (Fig. 2E). 72A1 has shown reduced binding to M81 lymphoblastoid cell lines (LCLs) compared to B95.8 LCLs, potentially due to

gp350 sequence differences between the strains[67]. Therefore, to verify that the lack of neutralization by ATX-350-2 and 72A1 is not due to neutralization resistance by M81, we confirmed that these two mAbs neutralize M81 infectivity in SVKCR2 cells (Fig. S2).

These results indicate that the gp350 mAbs neutralize EBV by inhibiting the gp350-CD21 interaction. To confirm this, we evaluated whether the gp350 mAbs could prevent the gp350-CD21 interaction using BLI. ATX-350-1, ATX-350-2 and 72A1 strongly inhibited soluble recombinant CD21 binding to gp350 immobilized on biosensors, while an isotype control mAb did not (Fig. 2F). CD35 has been identified as another receptor for gp350[27], but we were unable to assess whether the mAbs directly disrupt the gp350-CD35 interaction as we were unable to detect binding of gp350 to the recombinant CD35 ectodomain (Fig. S3). To assess whether the mAbs inhibit binding of gp350 to native CD21 and/or CD35 receptors on B cells, we evaluated whether they could prevent gp350 binding to the surface of Raji B cells. ATX-350-1, ATX-350-2, and 72A1 inhibited APC-conjugated gp350 staining in a dose-dependent manner (Fig. 2G), consistent with their relative potencies in the CD21-positive epithelial cell neutralization assay (Fig. 2D). We further confirmed that high concentrations of these three mAbs could inhibit binding of gp350 to primary B cells as well (Fig. 2H). As expected, the gH/gL AMMO1 mAb did not inhibit APC-gp350 staining of Raji cells (Fig. 2G) or primary B cells (Fig. 2H). Taken together, these data demonstrate that ATX-350-1 and ATX-350-2 mAbs neutralize EBV infection of B cells with differing potencies by inhibiting gp350 from binding to CD21 and presumably CD35.

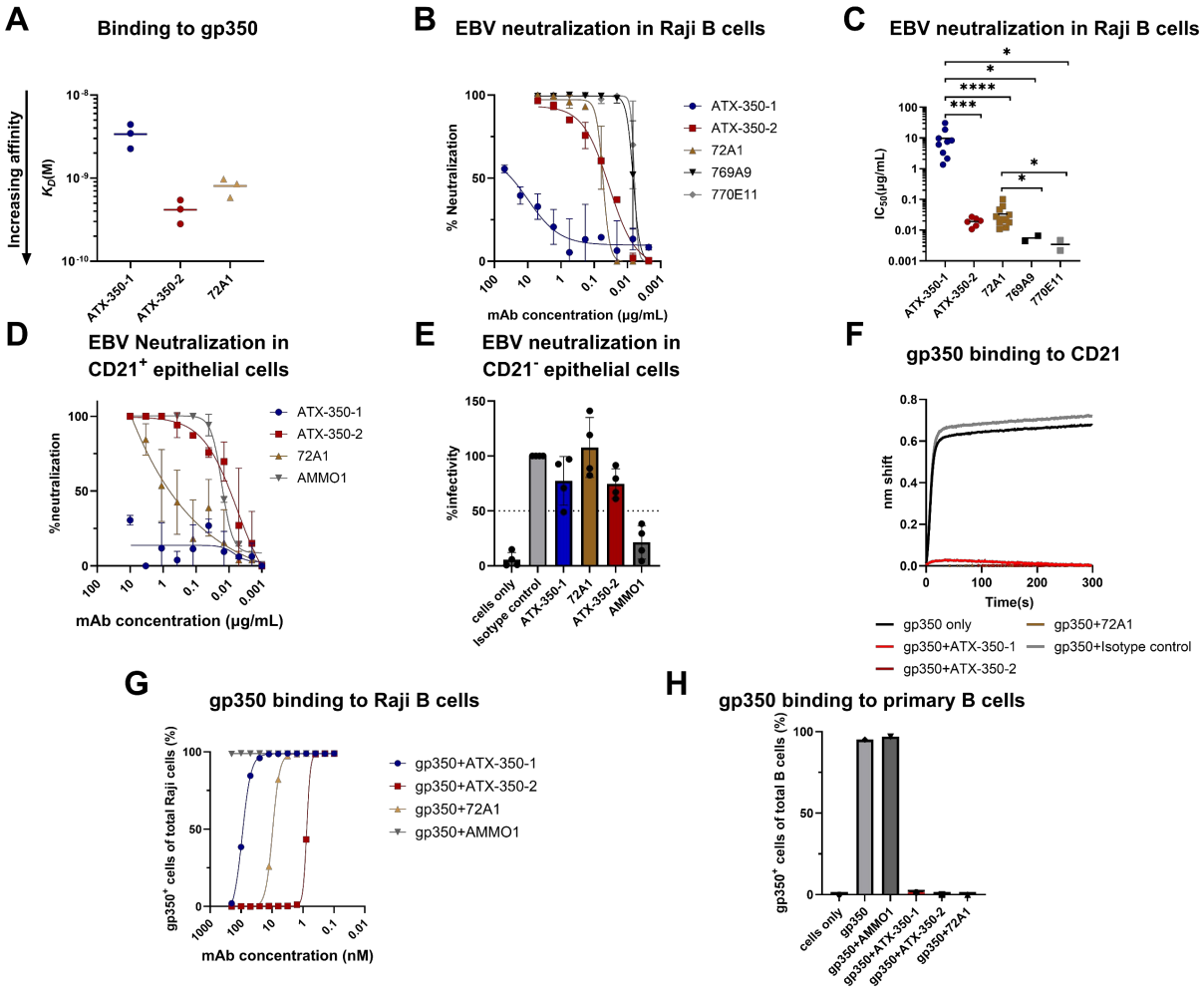

Figure 2. Binding and neutralizing activity of ATX-350 mAbs

(**A**) Binding affinity of the ATX-350 Fabs to recombinant gp350 was measured by biolayer interferometry. Each data point represents the K_D calculated from an independent experiment. (**B**) The indicated mAbs were serially diluted and evaluated for their ability to neutralize EBV (B95.8/F-GFP) infection of Raji cells. Representative curves from one of at least two experimental replicates are shown. (**C**) Half-maximal inhibitory concentration (IC_{50}) for the indicated mAbs was calculated from neutralization dose-response curves. Each datapoint represents an independent experiment measured in duplicate. Asterisks denote a statistically significant difference between two mAbs determined using a Mann-Whitney test where *

indicates $p \leq 0.05$, *** indicates $p \leq 0.0005$, and **** indicates $p \leq 0.0001$. (**D**) The indicated mAbs were serially diluted and evaluated for their ability to neutralize EBV (Akata-GFP) infection of SVKCR2 cells. Each data point represents the mean of two technical replicates, and the error bars represent the standard deviation. Representative curves from one of two experimental replicates are shown. (**E**) The indicated mAbs were evaluated for their ability to neutralize infection of EBV (M81-Luc) in CD21-negative AGS epithelial cells at a concentration of 10 μg/mL. Each data point represents the average infectivity of two technical replicates from an independent experiment. (**F**) The ability of gp350 to bind to soluble CD21 in the presence of the indicated mAbs was determined using biolayer interferometry. (**G**) The indicated mAbs were serially diluted and evaluated for their ability to inhibit binding of APC-conjugated gp350 to Raji cells by flow cytometry. (**H**) The indicated mAbs were incubated with biotinylated gp350 conjugated to SA-APC at a 50:1 molar ratio and then added to primary human B cells. APC-gp350 binding to B cells was quantified by flow cytometry.

Table S2. Kinetics parameters of mAb interactions with gp350, gp42, or gH/gL/gp42 respectively as measured by BLI. Related to Figures 2 and 4.

Ligand	Analyte	K_D (M)	K_{on}(1/Ms)	K_{on} error (1/Ms)	K_{off} (1/s)	K_{off} error (1/s)
gp350	ATX-350-1 Fab	2.26E-09	6.00E+04	9.20E+02	1.36E-04	2.58E-06
gp350	ATX-350-1 Fab	4.42E-09	4.23E+04	6.60E+02	1.87E-04	3.06E-06
gp350	ATX-350-1 Fab	3.46E-09	4.41E+04	7.83E+02	1.53E-04	2.54E-06
gp350	ATX-350-2 Fab	2.81E-10	5.69E+05	1.60E+04	1.60E-04	3.02E-06
gp350	ATX-350-2 Fab	5.44E-10	3.43E+05	9.49E+03	1.86E-04	3.61E-06
gp350	ATX-350-2 Fab	4.22E-10	3.32E+05	7.79E+03	1.40E-04	3.27E-06
gp350	72A1 Fab	9.76E-10	1.55E+05	1.93E+03	1.51E-04	1.75E-06
gp350	72A1 Fab	5.83E-10	2.70E+05	9.76E+03	1.58E-04	2.79E-06
gp350	72A1 Fab	8.52E-10	1.60E+05	2.81E+03	1.37E-04	2.22E-06
ATX-42_1.1 IgG	gp42	3.68E-10	3.93E+05	4.68E+03	1.45E-04	3.14E-06
	gp42/gH/gL complex	2.93E-10	3.92E+05	4.12E+03	1.15E-04	2.81E-06
ATX-42_1.2 IgG	gp42	1.11E-09	1.77E+05	7.44E+02	1.97E-04	2.30E-06
	gp42/gH/gL complex	7.18E-10	2.61E+05	1.73E+03	1.88E-04	2.03E-06
ATX-42_1.3 IgG	gp42	3.59E-10	2.63E+05	4.14E+03	9.44E-05	2.88E-06
	gp42/gH/gL complex	3.25E-10	2.61E+05	3.61E+03	8.47E-05	2.94E-06
ATX-42_1.4 IgG	gp42	7.87E-10	1.91E+05	2.40E+03	1.50E-04	2.81E-06
	gp42/gH/gL complex	4.10E-10	2.67E+05	4.01E+03	1.09E-04	2.82E-06
ATX-42_1.5 IgG	gp42	5.48E-10	1.91E+05	2.38E+03	1.05E-04	2.91E-06
	gp42/gH/gL complex	8.39E-10	1.27E+05	1.77E+03	1.06E-04	2.43E-06
ATX-42_1.6 IgG	gp42	2.45E-09	2.47E+05	2.28E+03	6.04E-04	3.17E-06
	gp42/gH/gL complex	2.21E-09	2.53E+05	3.13E+03	5.58E-04	3.06E-06
ATX-42_1.7 IgG	gp42	6.85E-10	2.59E+05	2.21E+03	1.77E-04	2.65E-06
	gp42/gH/gL complex	9.52E-10	1.92E+05	1.45E+03	1.82E-04	2.19E-06
ATX-42-2 IgG	gp42	1.37E-10	3.83E+05	1.70E+03	5.26E-05	1.81E-06
	gp42/gH/gL complex	1.00E-10	5.52E+05	7.21E+03	5.53E-05	2.27E-06
A10 IgG	gp42	9.81E-11	6.95E+05	2.98E+03	6.82E-05	2.01E-06
	gp42/gH/gL complex	2.42E-10	4.52E+05	2.22E+03	1.09E-04	1.67E-06
4C12 IgG	gp42	2.52E-10	1.19E+06	1.63E+04	3.00E-04	4.30E-06
	gp42/gH/gL complex	4.85E-09	8.48E+04	1.53E+03	4.11E-04	3.83E-06

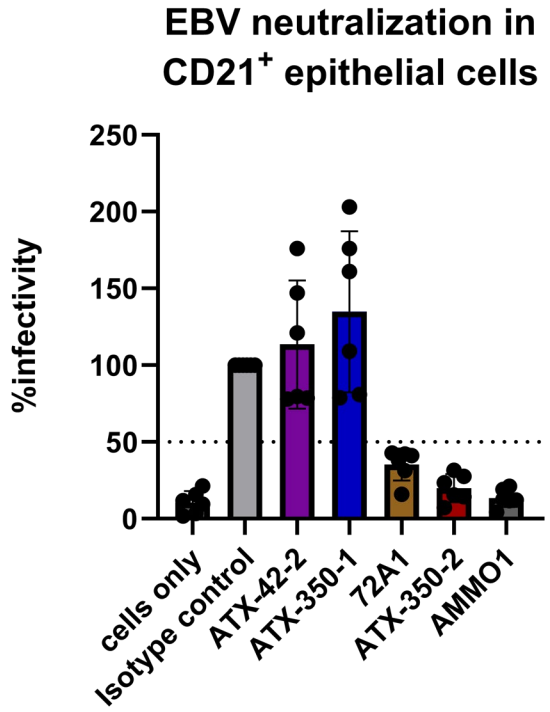

Figure S2. Anti-gp350 mAbs inhibit M81 virus infection of SVKCR2 epithelial cells. Related to Figure 2. The indicated mAbs were incubated with EBV (M81-Luc) to a final concentration of 10 μg/ml. The mAb/virus mixture was added to SVKCR2 cells, and the luciferase activity was read out 3 days later. Each dot represents the average infectivity of an independent experiment conducted in duplicate. Bars represent the mean and error bars represent standard deviation. Data are normalized to the average infectivity in the presence of the isotype control (VRC01). Dashed line demarcates 50% infectivity.

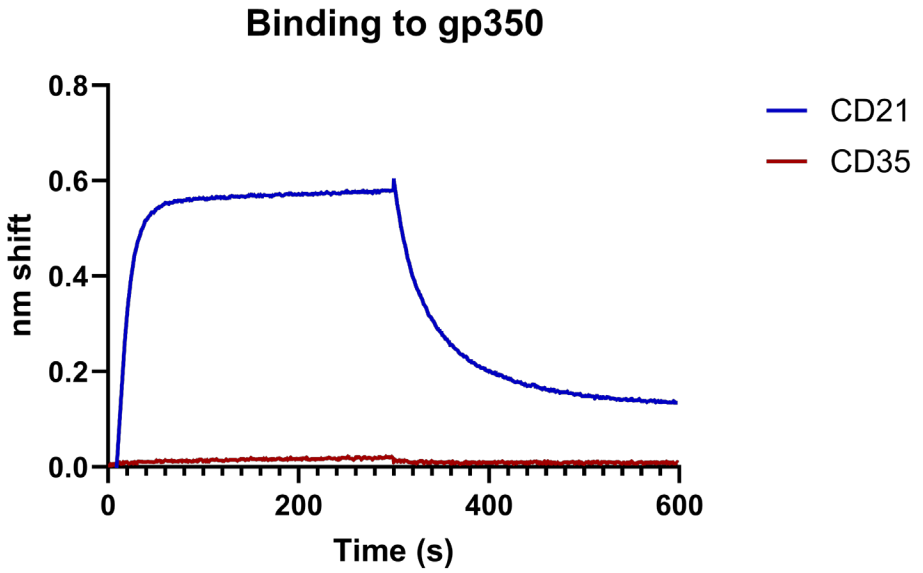

Figure S3. Binding of recombinant gp350 to CD21 and CD35. Related to Figure 2. Biotinylated gp350 was immobilized on streptavidin biosensors then immersed in buffer containing 250nM of either recombinant soluble CD21 or CD35 for 300 s, followed by immersion in buffer alone for 300 s.

2.3.3 ATX-350 mAbs share partially overlapping epitopes on the CD21 binding site of gp350

To understand whether epitope differences between ATX-350-1, ATX-350-2, and 72A1 could explain the differences in their neutralizing potencies, we evaluated whether they compete for binding to recombinant gp350 via BLI. gp350 was immobilized on a biosensor, saturated with a mAb of interest, then immersed in a solution of potentially competing mAb. Inhibition is read out as a reduction in binding of the second mAb relative to its binding in the absence of the first mAb. As expected, all mAbs self-competed for gp350 binding (Fig. 3A). ATX-350-1 and ATX-350-2 strongly competed with each other for gp350 binding. We observed partial

competition between 72A1 and ATX-350-2, while 72A1 and ATX-350-1 did not compete (Fig. 3A). These data suggest that all the mAbs have unique binding footprints on gp350.

Since ATX-350-2 showed the highest neutralizing potency against EBV infection of B cells, we determined the crystal structure of ATX-350-2 Fab in complex with gp350 to a resolution of 3.93 Å (Table S3) to gain a better understanding of the interactions at the molecular level (Fig. 3B, Fig. S4A & B). The structure revealed that the ATX-350-2 epitope is discontinuous (Fig. 3B-C), mainly focused on Domain 1, around residues 147-155 of gp350, an area which accounts for nearly ~59% of the total buried surface area (BSA, Fig. S4E). ATX-350-2 buries ~849 $Å^2$, with ~628 $Å^2$ contributed by the heavy chain and ~221 $Å^2$ from the light chain (Fig. S4E). Similarly, gp350 buries ~847 $Å^2$ on ATX-350-2 surface, with ~618 $Å^2$ on the heavy chain and ~229 $Å^2$ on the light chain (Fig. S4F). All three CDRs are involved in the interaction for the heavy chain, whereas the first and third light chain CDRs are involved in the interaction (Fig. S4F). Interactions are concentrated around residues His17, Leu18, Thr19, Gln147, and Asn148 of gp350 with the light chain (Fig.3C, left). Notably the hydroxyl group of Tyr32 (light chain) forms a hydrogen bond with the carboxyl group of Leu18 of gp350 (Fig. 3C, left). The heavy chain contacts residues Glu21, Asp53, Gln121, Gln122, Asn148, Pro149, Tyr151 and Ile153 of gp350 (Fig. 3C, middle and right). In particular, the guanidinium group of arginines 32, 59 and 102 from the heavy chain make salt bridges with Glu21 and Asp53 of gp350. Additionally, hydrogen bonds are observed between Asp55 and the carboxyl group of Gln121 of gp350, as well as between the carboxyl group of Tyr104 and Asn148 of gp350, and between Asn55 and Gln122 of gp350. A possible CH-π stacking interaction is also observed between Trp103 and Pro149 of gp350 (Fig 3C and S4E). The ATX-350-2 binding site on gp350 overlaps significantly with the CD21-binding footprint (Fig. S4C-D), and many of the contact residues on

gp350 buried in the gp350/CD21 complex are also buried in the gp350/ATX-350-2 complex (Fig. S4E).

To gain a better understanding of the epitopes targeted by ATX-350-1 and 72A1, we used negative stain electron microscopy (nsEM). We obtained 3D reconstructions of gp350 in complex with ATX-350-1 Fab (Fig. 3D), 72A1 Fab (Fig. 3E), and both ATX-350-1 and 72A1 Fabs (Fig. 3F), which confirmed that the mAbs bind to distinct epitopes on gp350. While the 72A1 and ATX-350-1 epitopes do not overlap (Fig. 3F), alignment of the fitted gp350/ATX-350-1 Fab to the gp350/ATX-350-2 Fab and the gp350-CD21 crystal structures[60] reveals that the epitopes of these two mAbs overlap and clash with CD21 (Fig. 3G); although, the clash is more obvious for ATX-350-2 compared to ATX-350-1 (Fig. 3G). Thus, differences in epitopes and affinities of these mAbs for gp350 may explain the difference in neutralizing potency between the two (Fig. 2B). Alignment of the fitted gp350/72A1 Fab to the gp350/ATX-350-2 Fab and the gp350-CD21 crystal structures[60] demonstrates that the two mAbs bind adjacent epitopes on gp350 (Fig. 3H). This suggests that the partial competition measured between ATX-350-2 and 72A1 by BLI (Fig. 3A) may be due to steric inhibition rather than direct epitope overlap.

Finally, we compared the structure of the gp350/ATX-350-2 complex with those of previously described neutralizing mAbs[60]. ATX-350-2 and another genetically human mAb, 769A9, partially overlap (Fig. 3I) and both make contacts with Glu21 on gp350, but their epitope specificities are otherwise distinct (Fig. S4E). These epitope differences may account for the difference in potency of the two mAbs (Fig. 2C). ATX-350-2 also shows partial overlap with the simian mAbs Cy137C02 (Fig. 3J) and CY651H02 (Fig. 3K), emphasizing the discovery of an extended site of vulnerability that overlaps with CD21 binding site.

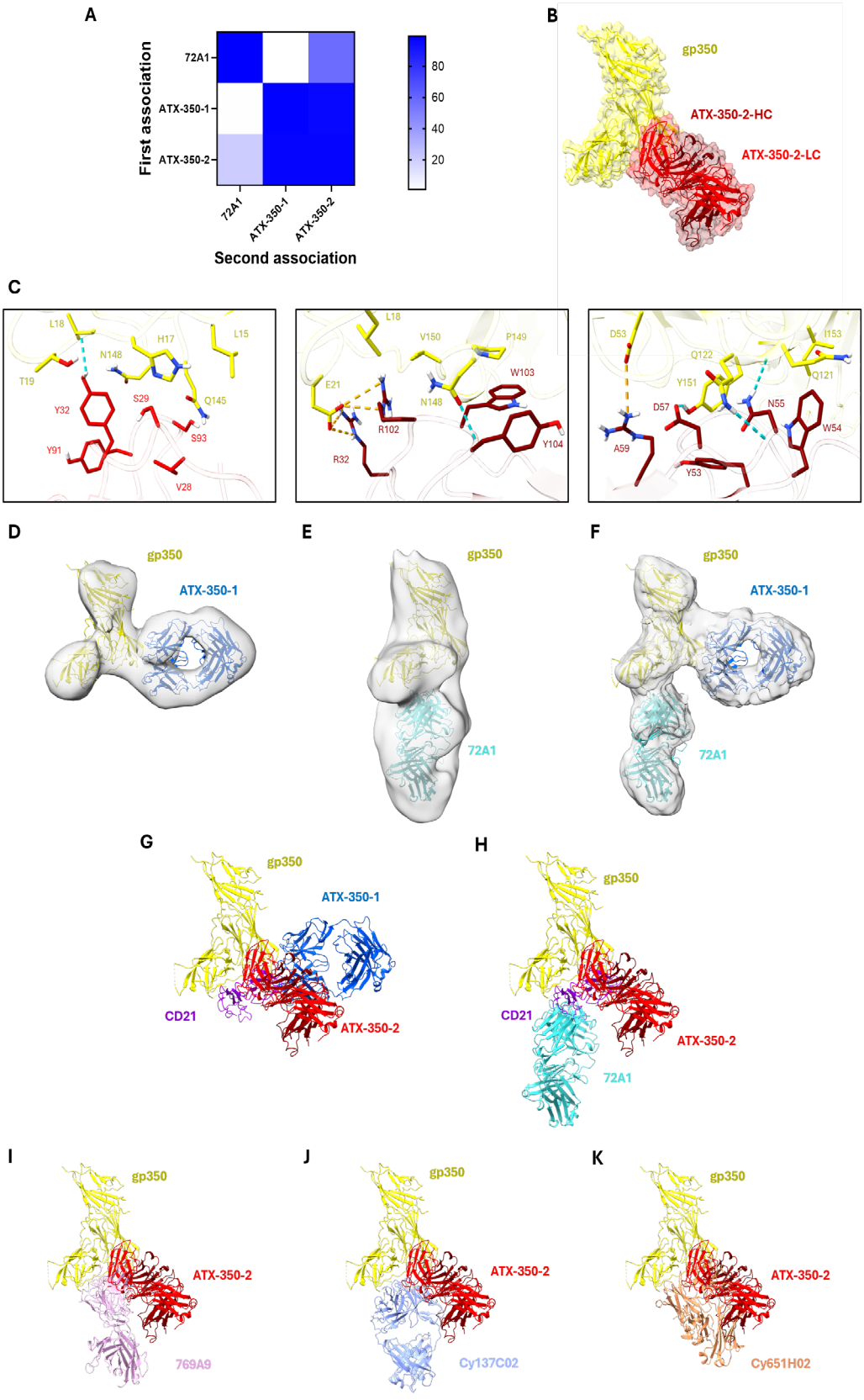
A
First association
72A1
ATX-350-1
ATX-350-2
80
60
40
20
72A1
ATX-350-1
ATX-350-2
Second association
B
gp350
ATX-350-2-HC
ATX-350-2-LC
C
L18
H17
L15
N148
T19
S29
Q145
Y32
S93
Y91
V28
L18
V150
P149
W103
E21
N148
R102
Y104
R32
D53
I153
Q122
Q121
Y151
D57
N55
W54
A59
Y53
D
gp350
ATX-350-1
E
gp350
72A1
F
gp350
ATX-350-1
72A1
G
gp350
ATX-350-1
CD21
ATX-350-2
H
gp350
CD21
ATX-350-2
72A1
I
gp350
ATX-350-2
769A9
J
gp350
ATX-350-2
Cy137C02
K
gp350
ATX-350-2
Cy651H02

Figure 3. ATX-350 mAbs share partially overlapping epitopes on CD21-binding site of gp350

(**A**) mAb competition for binding to gp350 was assessed via BLI. (**B**) X-ray crystal structure of gp350/ATX-350-2 Fab complex. (**C**) Zoom in of the binding interactions of ATX-350-2 with gp350. Hydrogen bonds are indicated by the cyan dashed lines, salt bridges by the orange dashed lines, and residues are labeled and shown in sticks. The first panel shows interactions with the light chain. The central and right panels show interactions with the heavy chain. (**D-F**) ns-EM 3D reconstruction of the gp350/ATX-350-1 Fab (**D**), gp350/72A1 Fab (**E**), and gp350/ATX-350-1 Fab/72A1 Fab complexes (**F**). Coordinates of gp350 (yellow, PDB ID:8SM0) and AlphaFold 3 predictions of the different mAbs (ATX-350-1, blue; 72A1 cyan) were fitted in the 3D map. (**G)** Alignment of the gp350/ATX-350-1 model with structures of gp350/ATX-350-2 (this paper) and gp350/CD21-SRI-II (Sushi repeat I and II subunit, purple, PDB ID:8SM0). (**H**) Alignment of the gp350/72A1 model with the gp350/ATX-350-2 structure (this paper) and gp350/CD21-SRI-II (purple).(**I-K**) Structural comparison of gp350-ATX-350-2 structure (this paper) with other mAbs, gp350 in yellow, ATX-350-2 in red, 769A9 in pink (PDB ID: 8SM1) (**I**), Cy137C02 in light blue (PDB ID: 8SIC) (**J**), Cy651H02 in orange (PDB ID: 8SGN) (**K**).

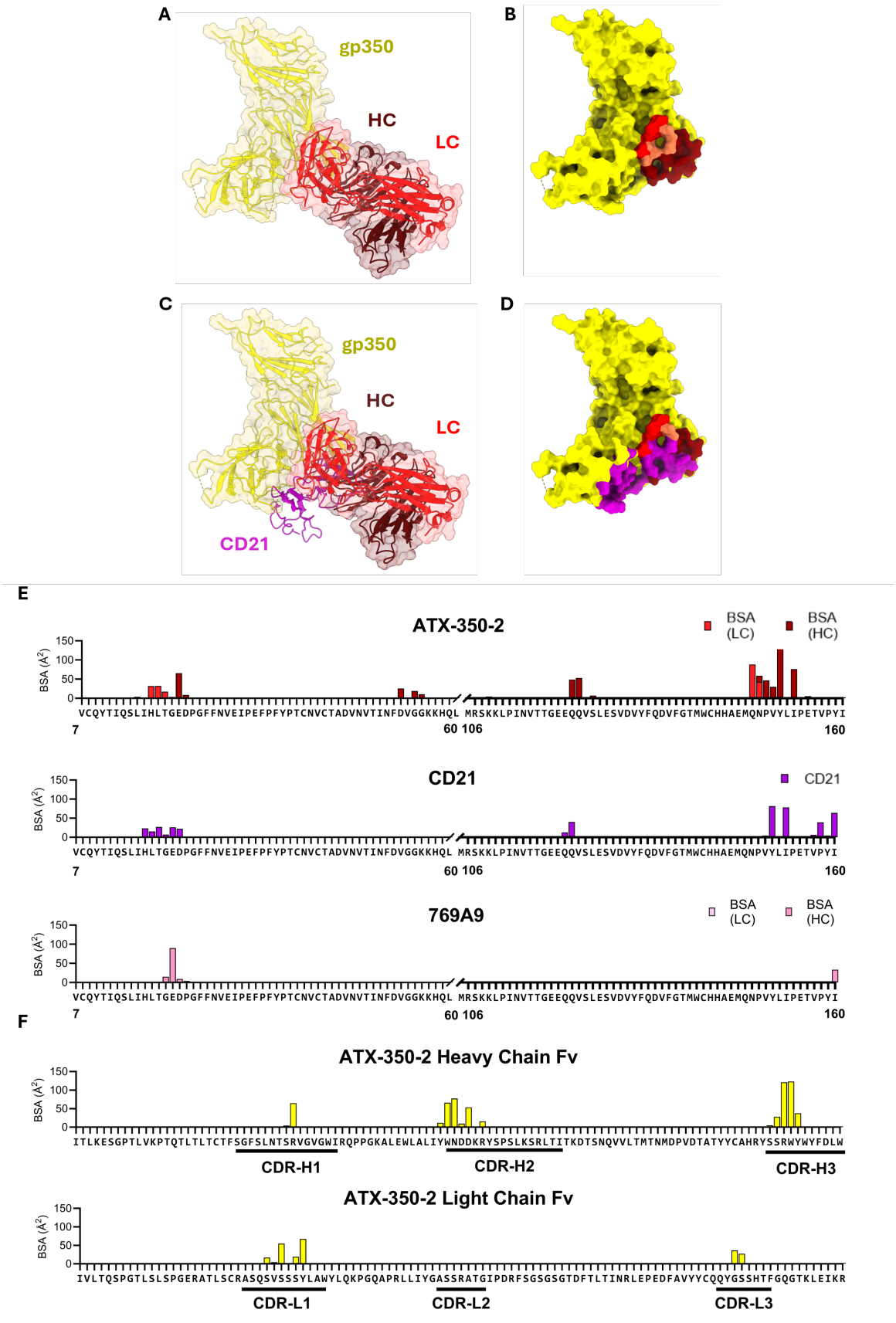
A
gp350
HC
LC
B
C
gp350
HC
LC
CD21
D
E
ATX-350-2
BSA (LC)
BSA (HC)
BSA (Å²)
150
100
50
0
VCQYTIQSLIHLTGEDPGFFNVEIPEFPFYPTCNVCTADVNVTINFDVGGKKHQL MRSKKLPINVTTGEEQQVSLESVDVYFQDVFGTMWCHHAEMQNPVYLIPETVPYI
7
60 106
160
CD21
CD21
769A9
F
ATX-350-2 Heavy Chain Fv
ITLKESGPTLVKPTQTLTLTCTFSGFSLNTSRVGVGWIRQPPGKALEWLALIYWNDDKRYSPSLKSRLTITKDTSNQVVLTMTNMDPVDTATYYCAHRYSSRWYWYFDLW
CDR-H1
CDR-H2
CDR-H3
ATX-350-2 Light Chain Fv
IVLTQSPGTLSLSPGERATLSCRASQSVSSSYLAWYLQKPGQAPRLLIYGASSRATGIPDRFSGSGSGTDFTLTINRLEPEDFAVYYCQQYGSSHTFGQGTKLEIKR
CDR-L1
CDR-L2
CDR-L3

Figure S4. X-ray crystal structure of ATX-350-2 bound to gp350 and binding site comparison (**A**) The overall X-ray crystal structure of ATX-350-2 Fab (dark red for the heavy chain and red for the light chain) bound to gp350 (yellow) is shown in ribbon and transparent surface representation. (**B**) Surface representation of gp350 with the ATX-350-2 epitope footprint (within 5Å of the Fab) outlined in dark red for the heavy chain, red for the light chain and salmon for the residues interacting with both chains. (**C**) The structure of the gp350/ATX-350-2 complex is superimposed on the structure of gp350 bound to CD21 (shown in purple) (PDBI ID: 8SM0). (**D**) Surface representation of gp350 with ATX-350-2 footprint shown as in panel B and the footprint of CD21 in purple. (**E**) BSA plots of gp350 residues involved in the binding of ATX-350-2 (top panel, light chain in red, heavy chain in dark red), CD21 (second panel, purple), and 769A9 (third panel, light chain in light pink, heavy chain in pink). (**F**) BSA plots of ATX-350-2 heavy chain residues involved in gp350 binding (top panel) and ATX-350-2 light chain residues involved in gp350 binding (bottom panel) the CDRs are indicated.

Table S3. Data collection and refinement statistics for crystal structure. Related to Figure 3.

Supplementary Table 3. Data collection and refinement statistics for crystal structures

	gp350-ATX-350-2
Data collection	
Space group	$P4_32_12$
Cell dimensions	
a, *b*, *c* (Å)	116.675, 116.675, 200.03
α, *β*, *γ* (°)	90, 90, 90
Resolution (Å)	46.26 - 3.928 (4.32 - 3.93)
R_{merge}	0.328 (1.695)
<I/σ(I)>	9.7 (1.8)
$CC_{1/2}$	0.996 (0.689)
Completeness	99.85 (99.68)
Redundancy	12.7 (12.5)
Refinement	
Resolution (Å)	46.26 - 3.928 (4.32 - 3.93)
No. unique reflections	12867 (3131)
R_{work}[b]/R_{free}[c]	24.16/28.19 (27.65/32.45)
No. atoms	6504
Protein	6456
Water	6
Ligand	42
B-factors (Å^2)	154.86
Protein	154.18
Water	129.26
Ligand	263.74
RMS bond length (Å)	0.002
RMS bond angle (°)	0.59
Ramachadran Plot Statistics[d]	
Residues	
Most Favored region	93.16
Allowed Region	6.84
Disallowed Region	0.0
Clashscore	1.64
PDB ID	**9PF9**

$R_{merge} = [\sum_h\sum_i|I_h - I_{hi}|/\sum_h\sum_i I_{hi}]$ where I_h is the mean of I_{hi} observations of reflection *h*. Numbers in parenthesis represent highest resolution shell. [b] R_{factor} and [c] $R_{free} = \sum||F_{obs}| - |F_{calc}|| / \sum|F_{obs}| \times 100$ for 95% of recorded data (R_{factor}) or 5% data (R_{free}). [d] Determined using MolProbity (10.1002/pro.3330)

2.3.4 ATX-42 mAbs bind with high affinity and inhibit EBV infection of B cells

Next, we characterized the gp42 mAbs isolated from ATX-GK mice. We first measured the binding affinity of the ATX-42 mAbs to recombinant gp42 and to the recombinant gH/gL/gp42 heterotrimer complex (Fig. S5). We included the A10 mAb isolated from an immunized non-human primate, which binds to the HLA binding site on gp42, and the murine mAb 4C12 which binds to the hydrophobic patch on gp42[37]. All ATX-42-1 clones bound both gp42 alone and gp42 in complex with gH/gL (K_D = 0.29 - 2.5 nM) with no stark differences in affinity between the two (Fig. 4A & Table S2). Relative to the ATX-42-1 clones, ATX-42-2 bound to gp42 with higher affinity (0.14 nM and 0.10 nM for gp42 monomer and gH/gL/gp42, respectively), similar to the affinity of A10 (Fig. 4A & Table S2). In contrast, 4C12 showed ~10-fold reduced affinity to the gH/gL/gp42 complex, consistent with steric occlusion of the hydrophobic patch on gp42 by gH/gL[37] (Fig. 4A).

We next assessed the ability of the ATX-42 mAbs to neutralize EBV infection of B cells. All ATX-42 mAbs neutralized EBV infection of Raji B cells comparably (IC_{50} = 0.1 - 0.3 μg/mL) with ATX-42-2 being the most potent (Fig. 4B-C). The ATX-42 mAbs were more potent than 4C12 and murine mAb F-2-1,[68] but only approximately half as potent as A10 (IC_{50} = 0.06 μg/mL; Fig. 4B & C). None of the gp42 mAbs could neutralize EBV infection of SVKCR2 epithelial cells, while the gH/gL mAb AMMO1 showed potent activity (Fig. 4D).

Neutralizing epitopes on gp42 have been mapped to the HLA binding site, the hydrophobic patch, and an epitope opposite the hydrophobic patch[36, 37, 53, 69]. We evaluated whether the gp42 mAbs could prevent the gp42-HLA-DRβ interaction using BLI. All ATX-42 mAbs, F-2-1, and A10 prevented binding of the soluble gH/gL/gp42 complex (Fig. 4E) and the soluble gp42 monomer (Fig. S6) to immobilized HLA-DR. In contrast, 4C12, which is known to

bind to the hydrophobic pocket of gp42, did not inhibit, but rather enhanced gp42 binding to HLA-DRβ, consistent with an increase in avidity through immune-complex formation (Fig. 4E and S6).

The ATX-42 mAbs, as well as A10, inhibited binding of PE-conjugated gp42 to Raji B cells with comparable potency (Fig. 4F), and they could inhibit gp42 binding to the surface of primary B cells (Fig. 4G), indicating that these mAbs inhibit binding to native HLA class II expressed on the B cell surface. As expected, the gp42 mAb 4C12, which binds the hydrophobic patch, and the gH/gL AMMO1 mAb did not inhibit gp42 binding to Raji or primary B cells (Fig. 4F and G). Taken together, these results demonstrate that eight ATX-42 mAbs belong to two distinct clonal lineages that bind to gp42 with high affinity and neutralize EBV infection of B cells by preventing gp42 from binding to HLA class II.

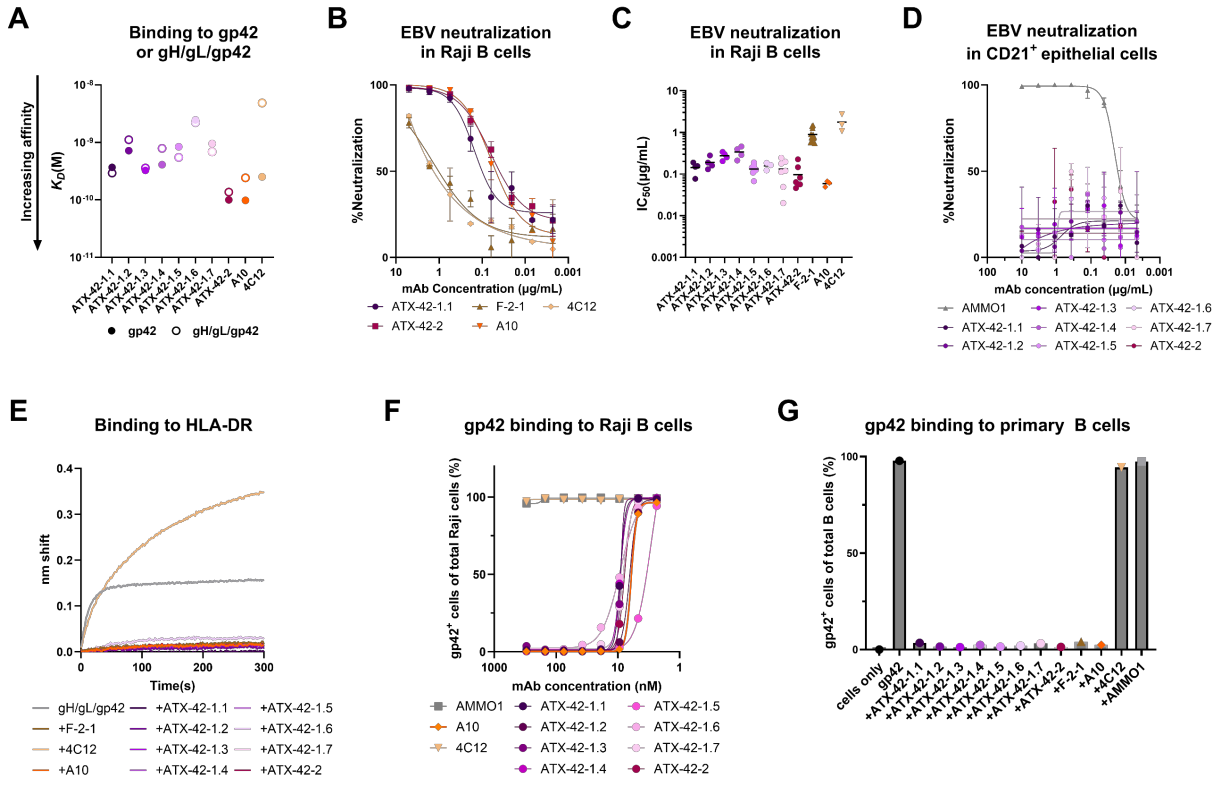

Figure 4. Binding and neutralizing activity of anti-gp42 mAbs

(**A**) Binding affinity of the indicated mAbs to recombinant gp42 (closed circles) or to gp42/gH/gL complex (open circles) was measured by biolayer interferometry. Each data point represents the K_D calculated from one experiment. (**B**) The indicated mAbs were serially diluted and evaluated for their ability to neutralize EBV (B95.8/F-GFP) infection of Raji B cells. Representative curves from one of at least three experimental replicates are shown. (**C**) Half-maximal inhibitory concentration (IC_{50}) for the indicated mAbs calculated from neutralization dose-response curves. Each data point represents an independent experiment measured in duplicate, and bars represent the mean. (**D**) The indicated mAbs were serially diluted and evaluated for their ability to neutralize EBV (AKATA-GFP) infection of SVKCR2 epithelial cells. Each data point represents the mean of two technical replicates, and the error bars represent the standard deviation. Representative curves from one of two experimental replicates are shown.

(**E**) The ability of gH/gL/gp42 to bind to recombinant HLA-DR in the presence of the indicated mAbs was determined using biolayer interferometry. (**F**) The indicated mAbs were serially diluted and evaluated for their ability to inhibit binding of PE-conjugated gp42 to Raji cells by flow cytometry. (**G**) The indicated mAbs were incubated with biotinylated gp42 conjugated to SA-PE at a 3:1 molar ratio and then added to primary human B cells. PE-gp42 binding to B cells was quantified by flow cytometry.

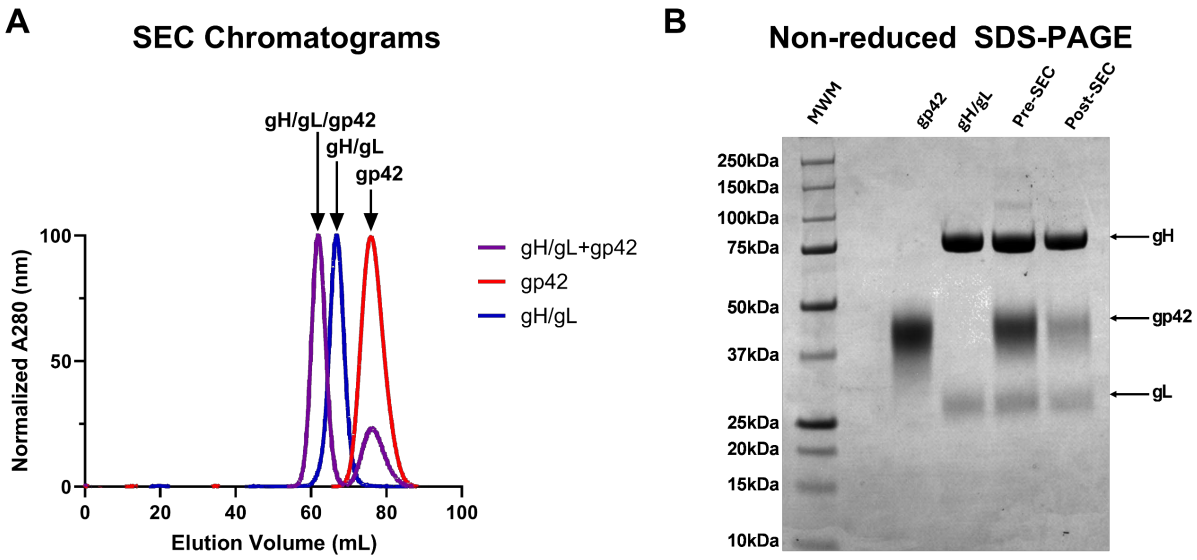

Figure S5. Purification of gH/gL/gp42 complex. Related to Figure 4. (**A**) Chromatograms of gp42, gH/gL, and gH/gL mixed with an excess of gp42 on a Superdex 200 16/600 size exclusion chromatography (SEC) column. Fractions containing the peak corresponding to the gH/gL/gp42 complex were collected and pooled. (**B**) Non-reduced SDS-PAGE gel of gp42, gH/gL, the gH/gL gp42 mix (pre-SEC) and trimer complex post- SEC). MWM = molecular weight marker.

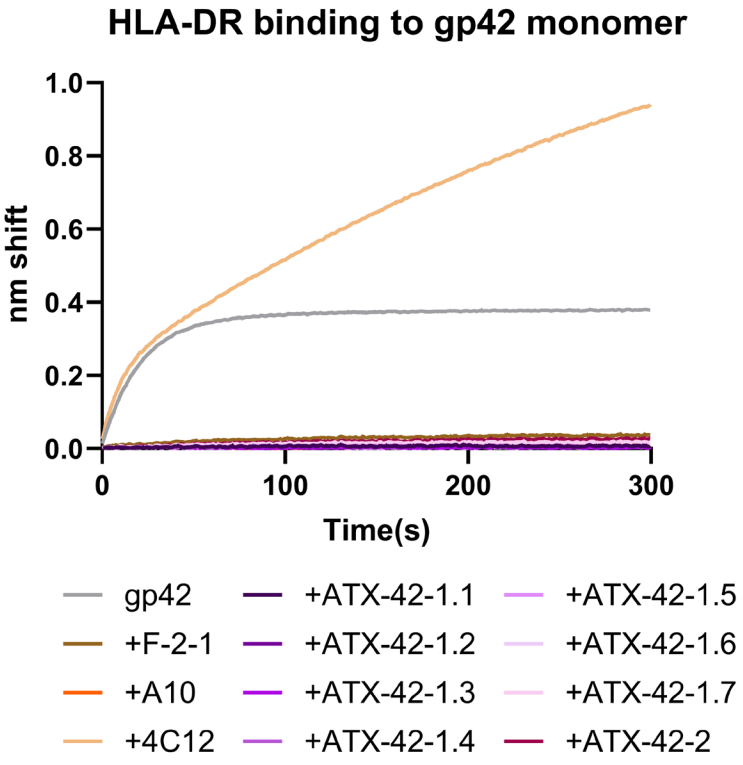

Figure S6. Anti-gp42 mAbs outcompete gp42 monomer for HLA-DR binding. Related to Figure 4. Biosensors loaded with HLA-DRβ were immersed in buffer containing 125 nM of gp42 alone or 125 nM of gp42 pre-incubated with 250 nM of the indicated mAb for 300 s.

2.3.5 ATX-42 mAbs target the HLA-binding site of gp42

To confirm that the ATX-42 mAbs target the HLA binding site on gp42, we carried out epitope competition studies by BLI. The ATX-42-1 clones and ATX-42-2 strongly competed for gp42 binding with each other and with A10 and F-2-1—mAbs that target the HLA binding-site—but not with 4C12 (Fig. 5A and S7). We next sought to structurally characterize the ATX-42-1.1 and ATX-42-2 Fabs in complex with the gH/gL/gp42 heterotrimer using nsEM. We observed different conformations within the 2D class averages relative to gH/gL for each

complex (Fig. 5B). We were able to generate 3D reconstructions of a closed and partially open conformation for the complex with ATX-42-2 (Fig. 5C) and of a partially open and open conformation for the complex with ATX-42-1.1 (Fig. 5D). These conformations were previously observed in the HLA-DQ2–gp42– gH/gL complex and are inherent to gp42 flexibility[29, 32].

We also generated a 3D reconstruction of an HLA-DR1β/gH/gL/gp42 complex in the closed confirmation (Fig. 5E). Despite slight differences in the orientation of gp42, a superimposition of the 3D reconstructions of the ATX-42-2/gH/gL/gp42 and ATX-42-1.1/gH/gL/gp42 complexes in the partially open conformation reveals a clash between both mAbs (Fig. 5F). A superimposition of the 3D reconstructions of the ATX-42-2/gH/gL/gp42 and HLA-DR1β/gH/gL/gp42 in the closed conformation suggests a clash between ATX-42-2 and HLA-DR1β despite slight differences in the orientation of gp42 (Fig. 5G). The collective biochemical (Fig. 4E-G & 5A) and structural analyses (Fig. 5B-G) demonstrate that the ATX-42 mAbs neutralize EBV infection by inhibiting the gp42-HLA class II interaction.

A comparison of the ATX-42-2/gH/gL/gp42 complex (Fig. S8A) with that of previously characterized gp42 antibodies A10[37], 5E3[53] and F-2-1[37] indicates potential epitope overlap with mAbs that block the HLAII-gp42 interaction (Fig. S8 B-D), but not with the non HLA-blocking mAbs 3E8[53], 2C1[36], and 4C12[37] (Fig. S8E-G).

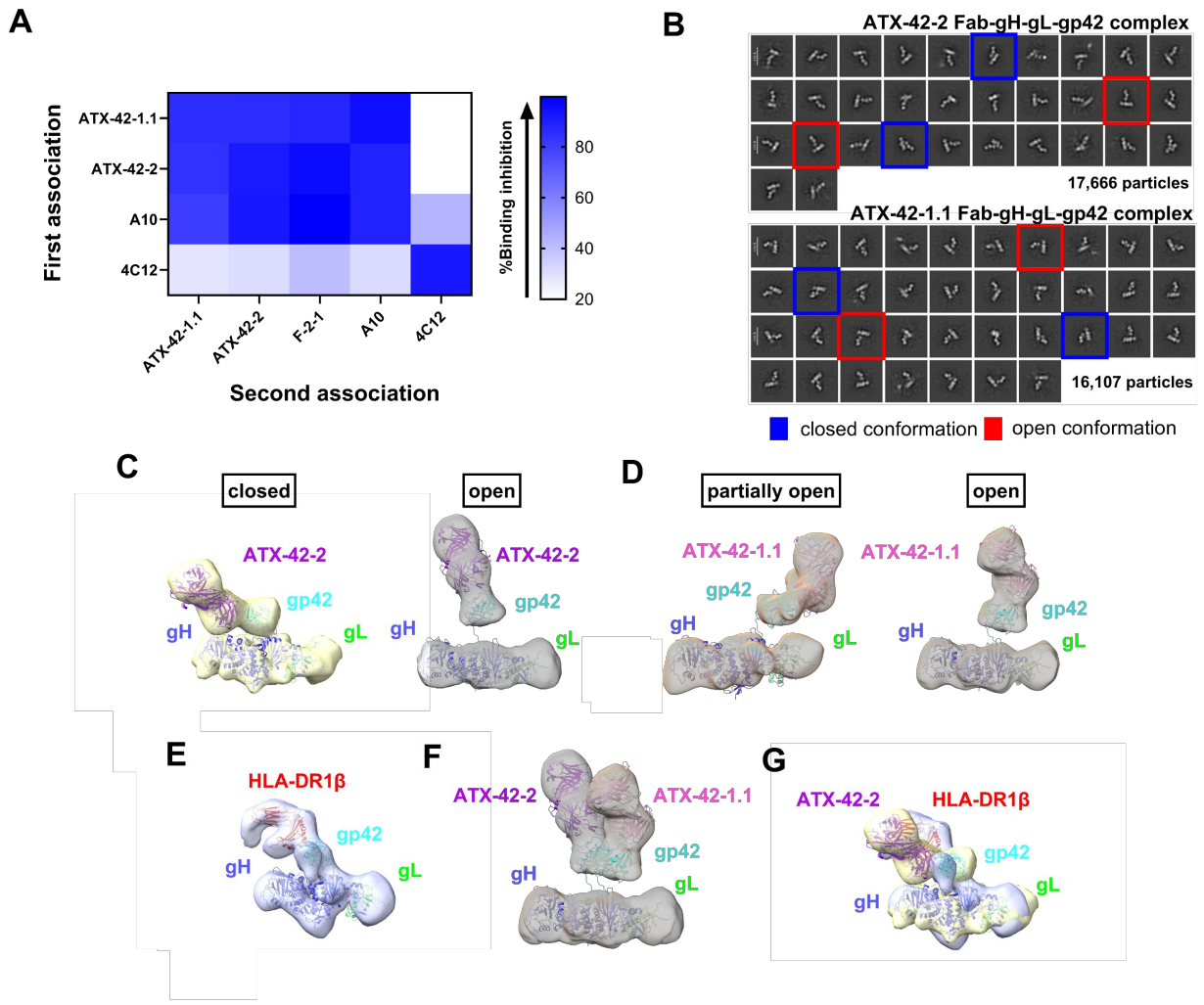

Figure 5. ATX-42 mAbs target the HLA-binding site of gp42

(**A**) mAb competition for binding to gp42 was assessed via BLI. (**B**) Representative reference free 2D class averages of ATX42-2 Fabs and ATX-42-1.1 Fabs bound to gH/gL/gp42 complex. Class averages indicate that ATX-42 mAbs bind to the open and closed conformations of the gH/gL/gp42 complex as indicated by red and blue squares, respectively. (**C-E**) 3D reconstructions of gH/gL/gp42 complex in closed, partially open, and open conformation bound to ATX-42-2 Fab (**C**), ATX-42-1.1 Fab (**D**), and HLA-DR1β (**E**) with coordinates of gH/gL (blue and green, PDB ID 7CZF), gp42 (cyan, PDB ID 1KG0), AF3 models of ATX-42-2 (purple) and ATX-42.1.1 (pink)

and HLA-DR1b (red, PDB ID 1KG0) fitted into the map. (**F**) Superimposition of the gH/gL/gp42/ATX-42-1.1 Fab partially open complex map with the one from gH/gL/gp42/ATX-42-2 Fab open complex. (**G**) Superimposition of the gH/gL/gp42/ATX-42-2 Fab closed complex map with the one from gH/gL/gp42/HLA-DR complex.

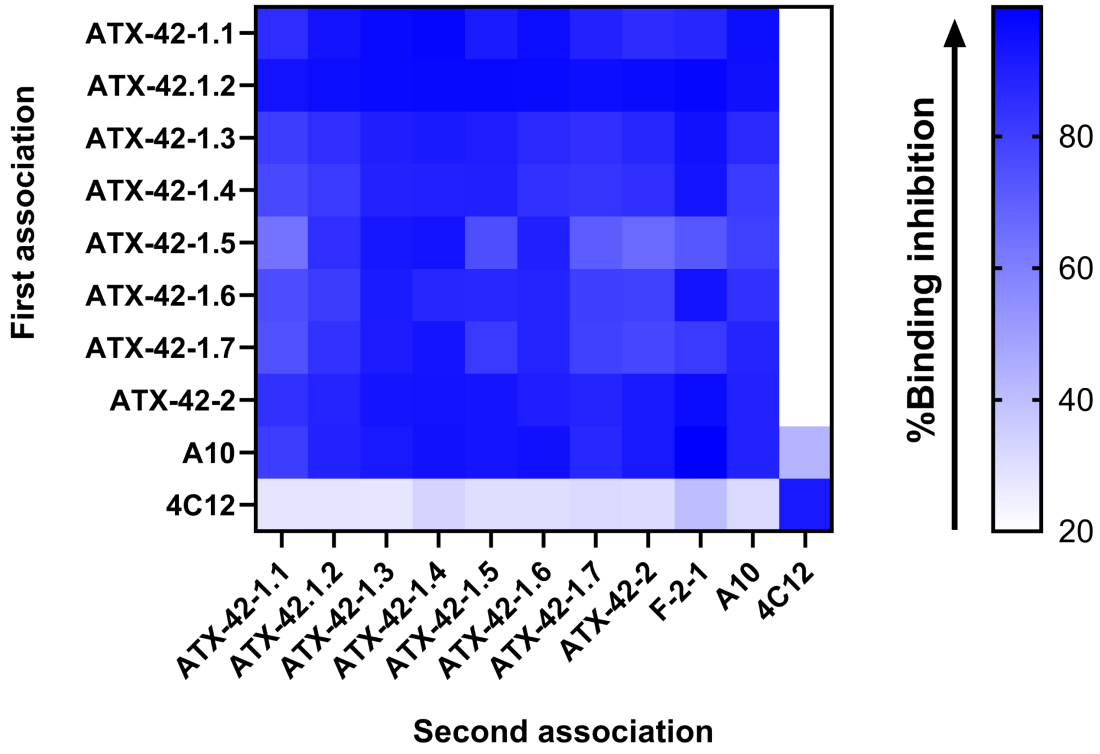

Figure S7. Binding competition between anti-gp42 mAbs. Related to Figure 5. mAb competition was assessed via BLI.

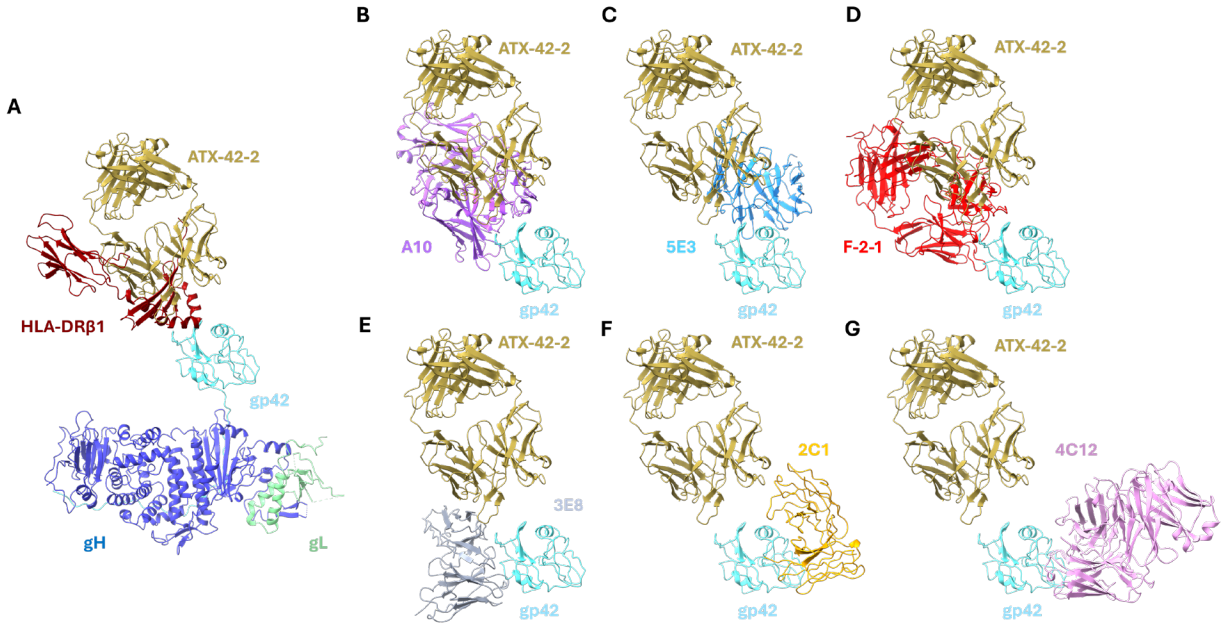

Figure S8. ATX-42-2 mAb shows new epitope compared to previously described gp42 mAbs.

(**A**) Alignment of the gHgL/gp42/ATX-42-2 (respectively in blue, green, cyan and gold) model obtained from ns-EM data fit with the structure of the gp42/HLA-DR1β structure in dark red (PDB ID:1KG0), (**B-G**) Alignment of the gp42/ATX-42-2 model with: the gp42/A10 structure in purple (PDB ID: 8TNN) (**B**), gp42/5E3 structure in light blue (PDB ID: 7YOY) (**C**), the gp42/F2-1 structure in red (PDB ID: 8TNT) (**D**), the gp42/3E8 structure in grey (PDB ID: 7YOY) (**E**),the gp42/2C1 structure in light yellow (PDB ID: 8KHR) (**F**) and the gp42/4C12 structure in pink (PDB ID: 8TOO) (**G**).

2.3.6 Passive transfer of mAbs limit EBV infection in humanized mice

To evaluate whether the mAbs isolated in this study confer protection against EBV challenge *in vivo*, we utilized a humanized NSG mouse model of EBV infection[50, 51, 55, 70-72] (Fig.

6A). 10 weeks following engraftment of human $CD34^+$ cells, we confirmed the reconstitution of the human hematopoietic compartment and presence of human B cells in the mice (Fig. S9). At 16 weeks post engraftment, the mice received an intraperitoneal injection of 500μg of ATX-42-2 (n=5), ATX-350-2 (n=5), 72A1 (n=4), AMMO1 (n=4), or an isotype control (HIV-envelope mAb VRC01[73], n=4), followed by intravenous challenge of EBV B95.8/F equivalent to ~25,000 Raji infectious units 24 hours later. An additional group of uninfected control mice did not receive antibody or virus challenge (n=4). Blood was collected on the day of challenge to confirm the presence of transferred mAbs. Antigen-specific ELISAs indicated that mAbs were successfully transferred to all mice with the exception of mouse 5 in the ATX-350-2 group and mouse 1 in the 72A1 group, which were removed from the study (Fig. 6B & Table S4). Mice were monitored for 11 weeks post challenge for weight loss and survival and bled weekly starting at week 4 to assess viremia (Fig. S10 & Table S4). At the time of euthanasia, spleens were harvested, examined for tumors, weighed, and processed for DNA extraction to quantify viral DNA using qPCR. Spleen sections from representative mice were also submitted for histological staining for CD20 and for EBER1, a non-coding RNA that is abundant in infected cells[74].

2 of 4 challenged mice that received the isotype control mAb had consistently detectable viremia beginning at 4-5 weeks post challenge (Fig. S10B), and all had splenomegaly (Fig. 6C) and viral DNA in splenocytes (Fig. 6D). EBER transcripts were also detected in splenic sections from a mouse in the isotype control group (Fig. 7, mouse 1). Despite all being infected, 2 of 4 mice in the isotype control group survived for 74 days following challenge (Fig. S10A and Table S4). One of four spleens in the isotype control had an obvious tumor group (Fig. S12, mouse 3).

2 of 4 mice that received AMMO1 did not survive until day 74 (Fig. S10A and Table S4), and one exceeded 20% weight loss on day 74 (Fig. S10C). A similar pattern of weight loss and survival was observed in the uninfected control group, indicating that survival in this experimental cohort was independent of EBV infection and likely due to the age of the mice at the time of challenge. None of the animals in the AMMO1 group had splenomegaly (Fig. 6C), viremia (Fig. S10B), detectable viral DNA from splenocytes (Fig. 6D), nor detectable EBER1 RNA (Fig. 7) in the spleen.

ATX-42-2 protected 5 of 5 mice from splenomegaly (Fig. 6C). All mice survived for 74 days after challenge (Fig. S10A & Table S4); however, one mouse reached euthanasia criteria at this point (Fig. S10A & Table S4). One mouse exhibited transient viremia at week 8 (Fig. S10B). Splenocytes from all mice in the ATX-42-2 group lacked detectable viral DNA (Fig. 6D), and EBER transcripts were not observed in a representative mouse from this group (Fig. 7).

2 of 4 mice that received ATX-350-2 survived until day 74 (Fig. S10A & Table S4), and all had normal spleen weights (Fig. 6C) at the time of euthanasia. Although none of the mice in the ATX-350-2 group had viremia (Fig. S10B), viral DNA was detected in the spleen from two of four mice in this group (Fig. 6D). A mouse in the ATX-350-2 group with high viral loads in the spleen (mouse 4) had detectable EBER RNA (Fig. 7), while one absent of viral load (mouse 2) did not (Fig. S13). Two out of three mice that received 72A1 had splenomegaly (Fig. 6C, mouse 3 and 4); one of which (mouse 4) had high levels of viral DNA (Fig. 6D) and EBER transcripts (Fig. 7) in the spleen, and a large tumor (Fig. S12). Mouse 3 did not have a visible splenic tumor (Fig. S12) nor detectable viral DNA in the spleen (Fig. 6D); however, *in situ hybridization* detected EBER1 RNA (Fig. S13).

To confirm these results, we transferred ATX-42-2 (n=5), ATX-350-2 (n=5), AMMO1 (n=4), and the isotype control mAb (n=4) to a separate group of NBSGW mice engrafted with huCD34^{+} cells isolated from cord blood (Fig. S9D & E). We were unable to detect transferred mAb in mouse 2 from the ATX-42-2 group (Fig. 6E), and it was excluded from the study. In the remaining animals, we again observed higher levels of AMMO1 and ATX-42-2, relative to the other mAbs in the serum at the time of challenge (Fig. 6E). One mouse from the ATX-42-2 group (mouse 3), and one from the ATX-350-2 group (mouse 3) required euthanasia 15 days post-challenge (Fig. S10D & Table S4). Two additional mice from the ATX-350-2 group died at days 48 (mouse 1) and 65 (mouse 5) (Fig. S10D & Table S4). Mouse 4 from the isotype control group died at day 68 (Fig. S10D & Table S4). The remaining mice were euthanized at day 83. At the time of euthanasia, spleen weights were comparable in all mice, except for one (mouse 4) in the ATX-42-2 group (Fig. 6F). However, EBV DNA was not detected in the spleens of any mice from the ATX-42-2 group (Fig.6G). In contrast, EBV DNA was present in the spleens from 2 of 5 (mouse 1 and 2) and 3 of 4 (all but mouse 2) mice in the ATX-350-2 and isotype control groups, respectively (Fig. 6G).

In the second experiment, we sought to assess whether the mAbs have different pharmacokinetic profiles. Therefore, we measured the mAb levels in sera over a 3-week period. 1 day post mAb transfer, serum levels were higher for ATX-42-2 and AMMO1 than they were for ATX-350-2 and 72A1 (Fig. 6E & S11A). ATX-350-2 and 72A1 decayed faster than ATX-42-2 and AMMO1 over the first 2 weeks such that only ATX-42-2 and AMMO1 were present above ~0.1 μg/mL in sera at this time point. By week 3, only AMMO1 was present at levels above 0.1 μg/mL. To confirm these results, the same experiment was repeated in NSG mice and comparable results were observed (Fig. S11B-C). Thus, the favorable pharmacokinetic profiles

of AMMO1 and ATX42-2 may have contributed to the superior protection conferred by these two mAbs over ATX-350-2 and 72A1 (Fig. 6C-D & F-G).

Given the favorable kinetic profile of ATX-42-2, we carried out an additional repeat experiment where ATX-42-2 (n=4) or the isotype control (n=4) were administered to another cohort of huCD34^{+} engrafted NSG mice (Fig. S9F & G) and then challenged with EBV. Mouse 1 and mouse 2 from the ATX-42-2 group required euthanasia at days 88 and 82 post-challenge, respectively (Fig. S10E & Table S4). The remaining mice were euthanized 95 days post-challenge. At the time of euthanasia, mice in the isotype control group had larger spleens than mice in the ATX-42-2 group (Fig. 6I). 3 of 4 mice in the isotype control group had detectable viral DNA in the spleen while none in the ATX-42-2 group did (Fig. 6J).

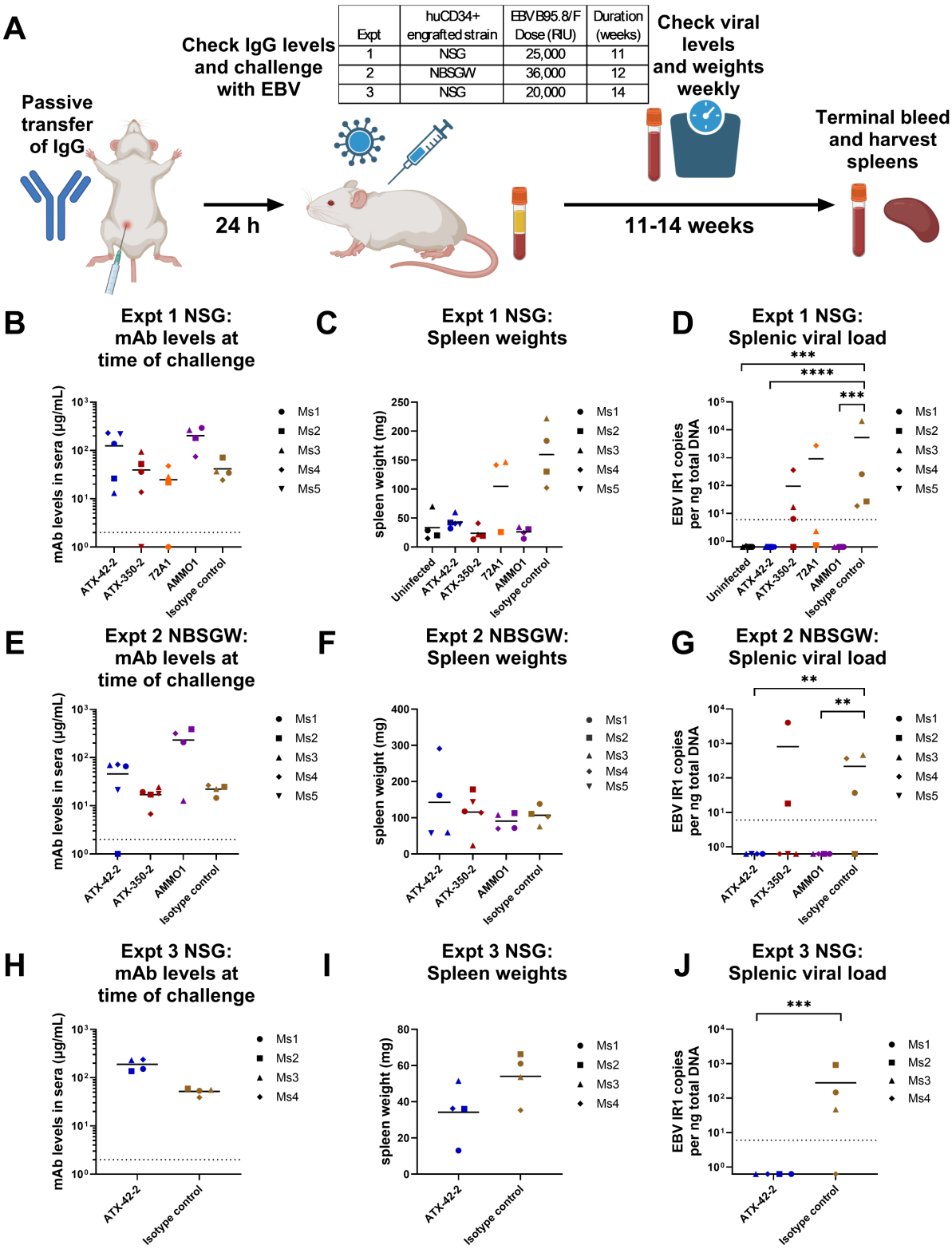

Figure 6. Passive transfer of mAbs limits EBV infection in humanized mice.

(**A**) Schema of experiments: Humanized NSG or NSBGW mice received PBS or 500 µg the indicated mAb via intraperitoneal injection. 24 h later, mice were bled and challenged with EBV via intravenous injection. The inlaid table provides details about three independent experiments which were performed. Mice were weighed weekly and euthanized at the timepoint indicated in the table or earlier if humane endpoints were met. Mice were bled weekly starting at 4 weeks post-challenge to measure viremia (Experiment 1 only). Created using BioRender.com. (**B**) Levels of the indicated mAbs in sera of Experiment 1 were measured at the time of challenge using antigen-specific ELISA. (**C**) Spleen weights from the animals in B at the time of euthanasia. (**D**) Viral IR1 DNA copies were quantified in splenic DNA extracts from the mice in B. (**E**) Levels of the indicated mAbs were measured in sera of Experiment 2 mice at the time of challenge using antigen-specific ELISA. (**F-G**) Spleen weights (**F**) and viral IR1 DNA copies in splenic DNA extracts (**G**) from the mice in E were measured at the time of euthanasia. In **D** and **G**, Asterisks denote a statistically significant difference between the two groups determined using a Kruskal-Wallis test with Dunn's multiple comparisons where ** indicates $p < 0.005$, *** indicates $p < 0.0005$, and **** indicates $p \leq 0.0001$. Only groups with a significant difference are shown. (**H**) Levels of the indicated mAbs in sera of Experiment 3 mice were measured at the time of challenge using antigen-specific ELISA. (**I-J**) Spleen weights (**I**) and viral IR1 DNA copies in splenic DNA extracts (**J**) from the mice in H. Asterisks denote a statistically significant difference between the two groups determined using a Mann-Whitney test where *** indicates $p < 0.0005$. Each symbol represents the average of two technical replicates per individual mouse, bars represent the mean, and the dashed line represents the highest serum dilution tested in **B, E**, and **H**. Serum samples without detectable mAb were plotted at half the highest serum dilution tested. Each symbol represents an individual mouse, and bars represent the mean in **C, F,** and **I**.

Each symbol represents the average of two technical replicates from an individual mouse, bars represent the mean, and dashed lines represents the limit of detection in **D, G,** and **J.**

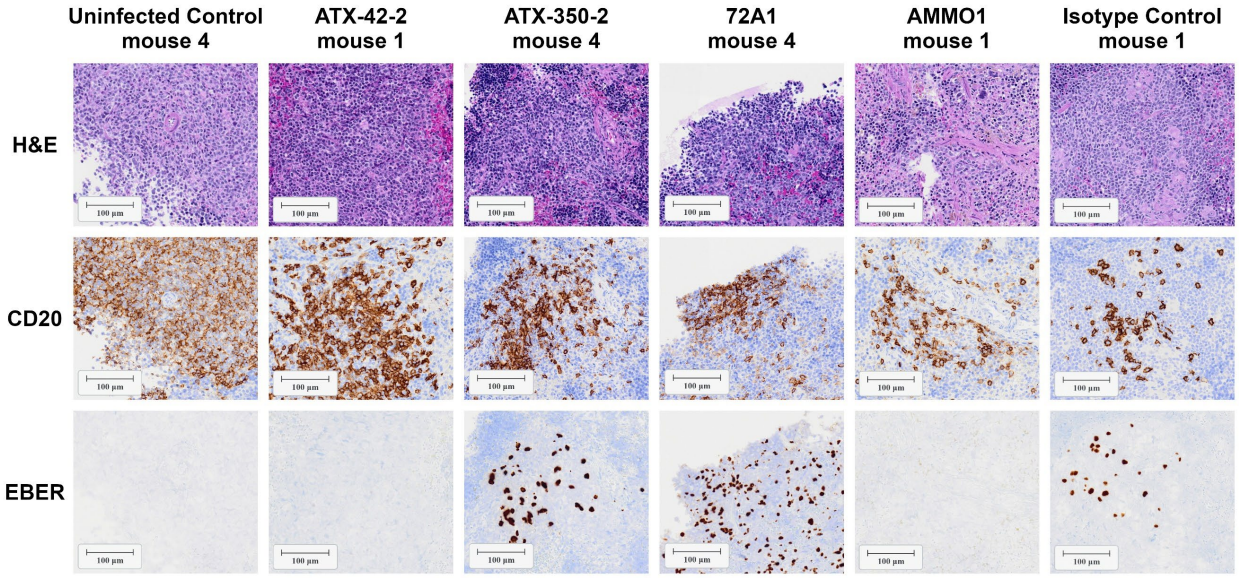

Figure 7. Immunohistochemical analyses of the spleens from EBV-challenged humanized mice.

Splenic sections from representative mice from Experiment 1 (Fig. 6) were stained for hematoxylin and eosin (H&E), human CD20, and EBER1 transcripts at necropsy as indicated. Scale bars represent 100 µm. Each image is from one representative mouse per mAb group.

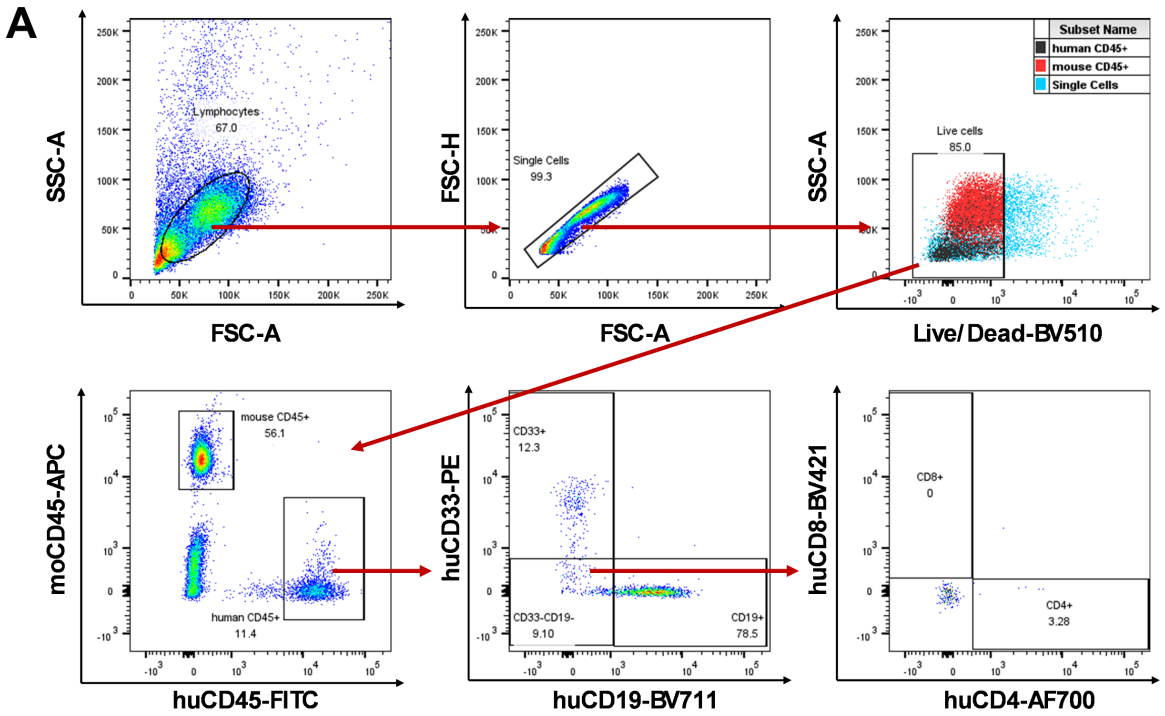
A
SSC-A
FSC-A
Lymphocytes
67.0
FSC-H
FSC-A
Single Cells
99.3
SSC-A
Live/ Dead-BV510
Live cells
85.0
Subset Name
human CD45+
mouse CD45+
Single Cells
moCD45-APC
huCD45-FITC
mouse CD45+
56.1
human CD45+
11.4
huCD33-PE
huCD19-BV711
CD33+
12.3
CD33-CD19-
9.10
CD19+
78.5
huCD8-BV421
huCD4-AF700
CD8+
0
CD4+
3.28

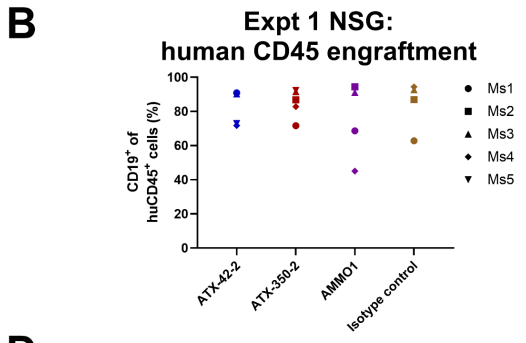
B
Expt 1 NSG:
human CD45 engraftment
CD19+ of huCD45+ cells (%)
Ms1
Ms2
Ms3
Ms4
Ms5
ATX-42-2
ATX-350-2
AMMO1
Isotype control

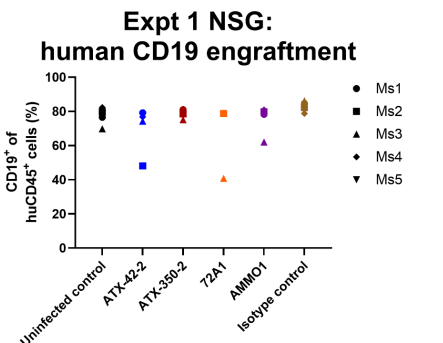
C
Expt 1 NSG:
human CD19 engraftment
CD19+ of huCD45+ cells (%)
Ms1
Ms2
Ms3
Ms4
Ms5
Uninfected control
ATX-42-2
ATX-350-2
72A1
AMMO1
Isotype control

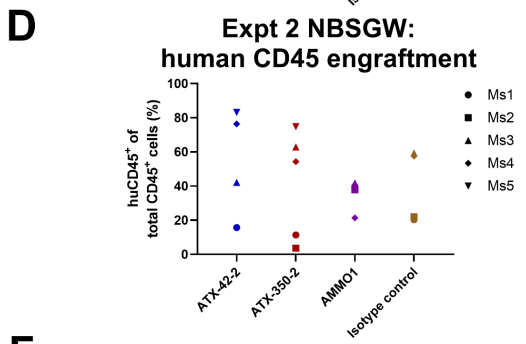
D
Expt 2 NBSGW:
human CD45 engraftment
huCD45+ of total CD45+ cells (%)
Ms1
Ms2
Ms3
Ms4
Ms5
ATX-42-2
ATX-350-2
AMMO1
Isotype control

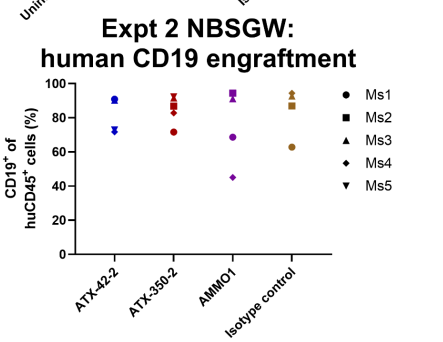
E
Expt 2 NBSGW:
human CD19 engraftment
CD19+ of huCD45+ cells (%)
Ms1
Ms2
Ms3
Ms4
Ms5
ATX-42-2
ATX-350-2
AMMO1
Isotype control

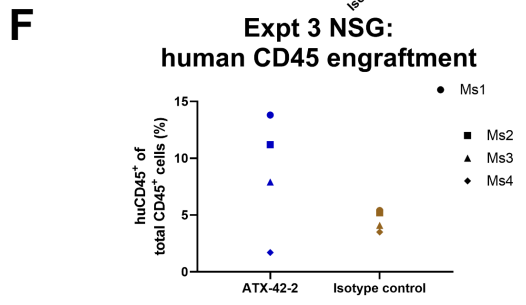
F
Expt 3 NSG:
human CD45 engraftment
huCD45+ of total CD45+ cells (%)
Ms1
Ms2
Ms3
Ms4
ATX-42-2
Isotype control

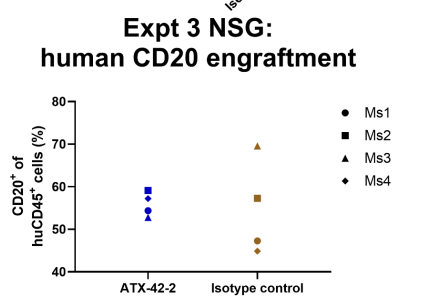
G
Expt 3 NSG:
human CD20 engraftment
CD20+ of huCD45+ cells (%)
Ms1
Ms2
Ms3
Ms4
ATX-42-2
Isotype control

Supplementary Figure 9. Cell engraftment in humanized mice. Related to Figure 6.

(**A**) Gating strategy to determine human lymphocyte populations in peripheral blood of humanized mice. Representative plots from one mouse are shown. (**B-C**) Frequency of human $CD45^+$ lymphocytes and $CD19^+$ B cells in NSG mice assigned to each mAb treatment group in Experiment 1 at 10 weeks post-engraftment of $huCD34^+$ cells. (**D-E**) Frequency of human $CD45^+$ lymphocytes and $CD19^+$ B cells in NBSGW mice assigned to each mAb treatment group in Experiment 2 at 15- or 16-weeks post-engraftment. (**F-G**) Frequency of human $CD45^+$ lymphocytes and $CD20^+$ B cells in NSG mice assigned to each mAb treatment group in Experiment 3 at 10 weeks post-engraftment.

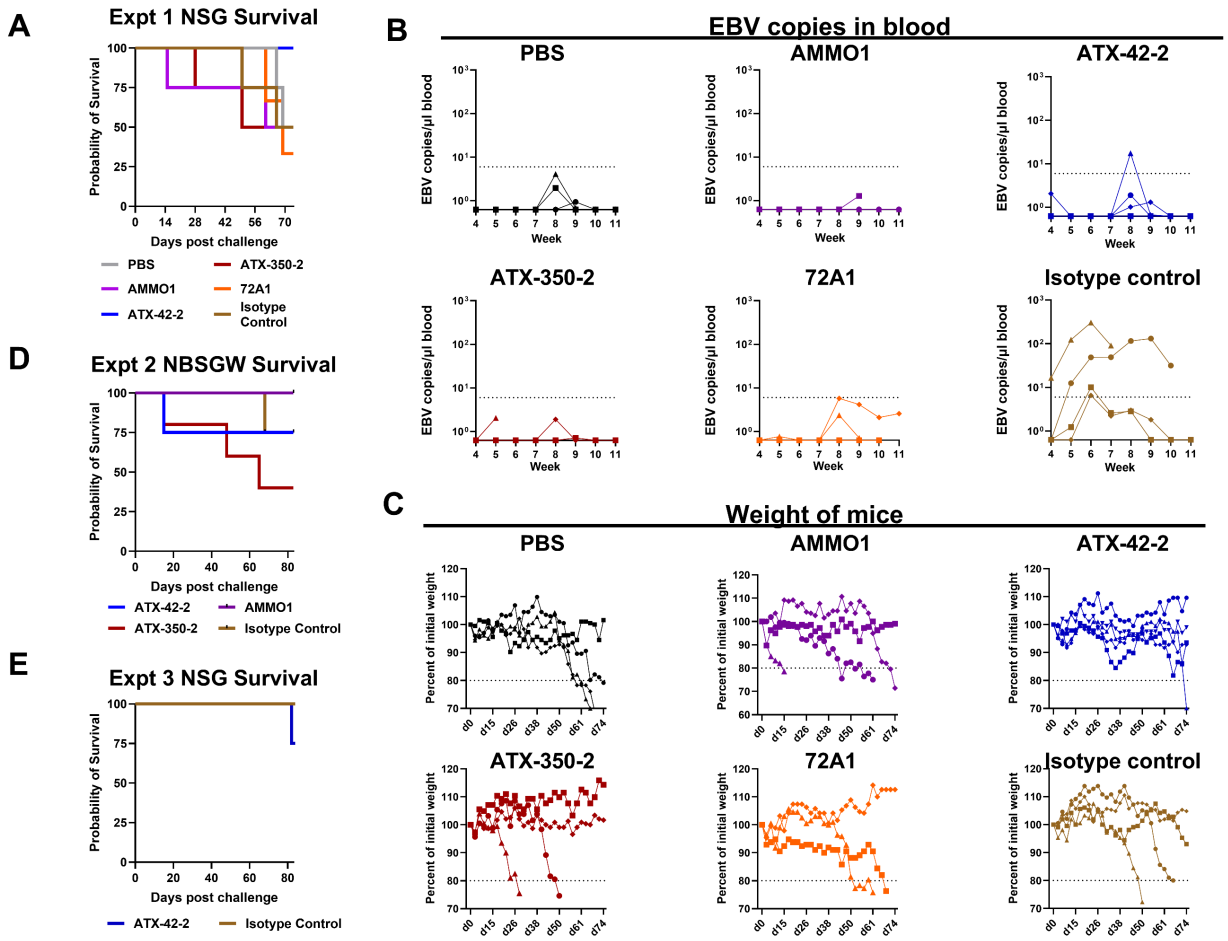

Supplementary Figure 10. Survival, weight, and viremia of humanized mice following EBV challenge. Related to Figure 6. (A) Survival of mice in Experiment 1 after EBV challenge. (**B**) For Experiment 1, EBV copies in blood were measured beginning at week 4 following challenge. Two independent replicates using DNA extracted from the same blood sample were performed per timepoint. Mean viral load per timepoint is graphed. Dashed line indicates limit of detection. (**C**) Weight of individual mice in each mAb treatment group in Experiment following EBV challenge. Dashed line indicates euthanasia criteria (80% of initial weight). (**D**) Survival of mice in Experiment 2 (Fig. 6E-G) following EBV challenge. (**E**) Survival of mice in Experiment 3 (Fig. 6H-J) following EBV challenge.

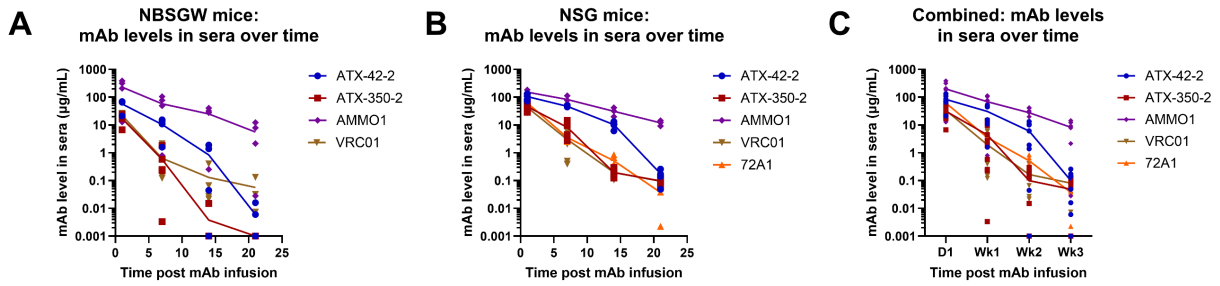

Supplementary Figure 11. Pharmacokinetics of mAbs *in vivo*

Related to Figure 6. (A and B) Intraperitoneal injections of 500µg mAbs were performed in human $CD34^+$ engrafted NBSGW mice from Experiment 2 Fig. 6E-G (**A**) and unchallenged, human $CD34^+$ engrafted NSG mice (**B**). Serum was collected 1 day, 7 days, 14 days, and 21 days later. mAb levels were determined via antigen-specific ELISA. Each dot represents the average of two independent measurements for each sample. When no mAbs were detected, they were assigned a value of 0.001 µg/mL for graphical purposes. (**C**) Average mAb concentration measured across experiments depicted in A and B.

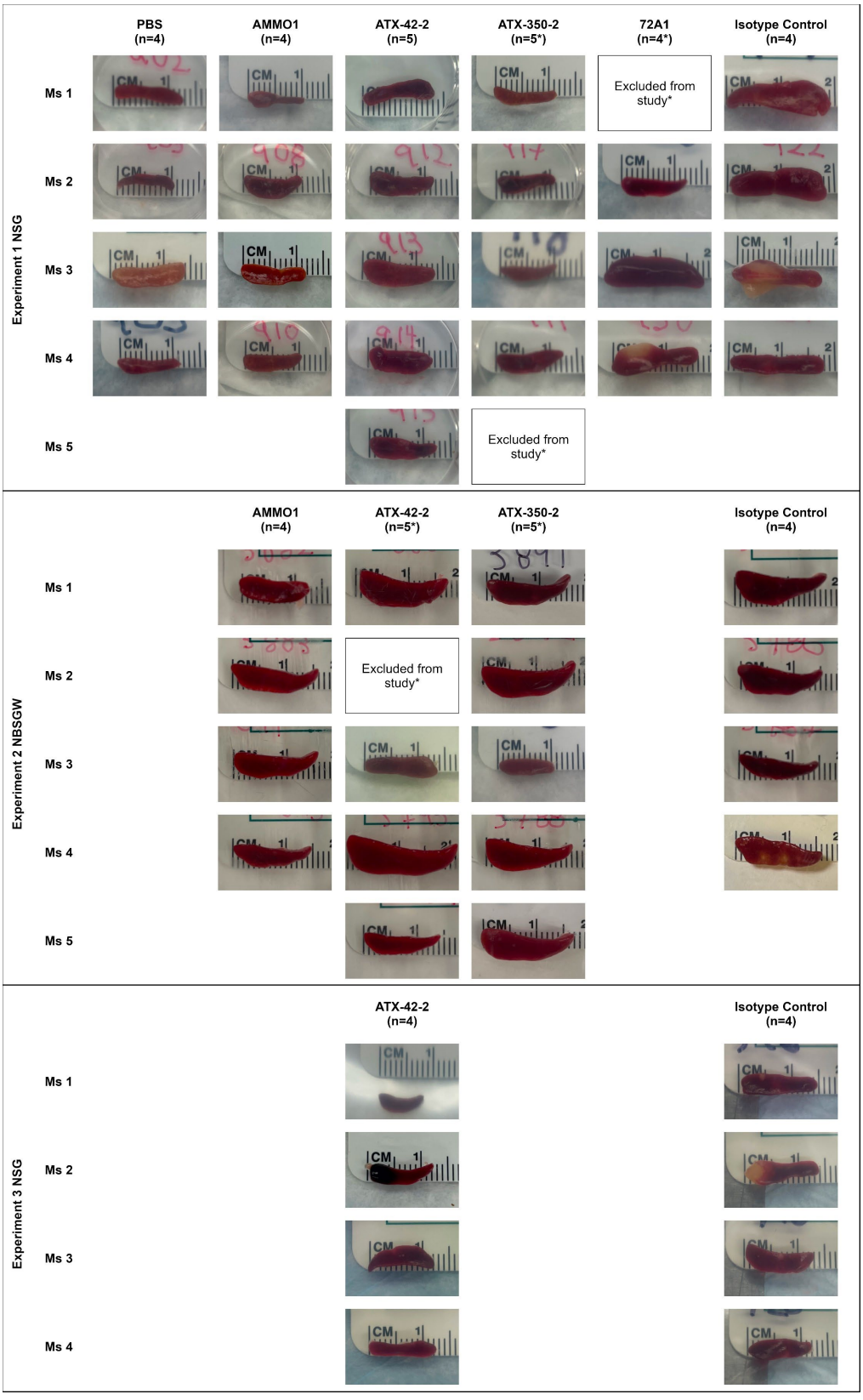

Supplementary Figure 12. Spleens of mice at time of euthanasia. Related to Figure 6.

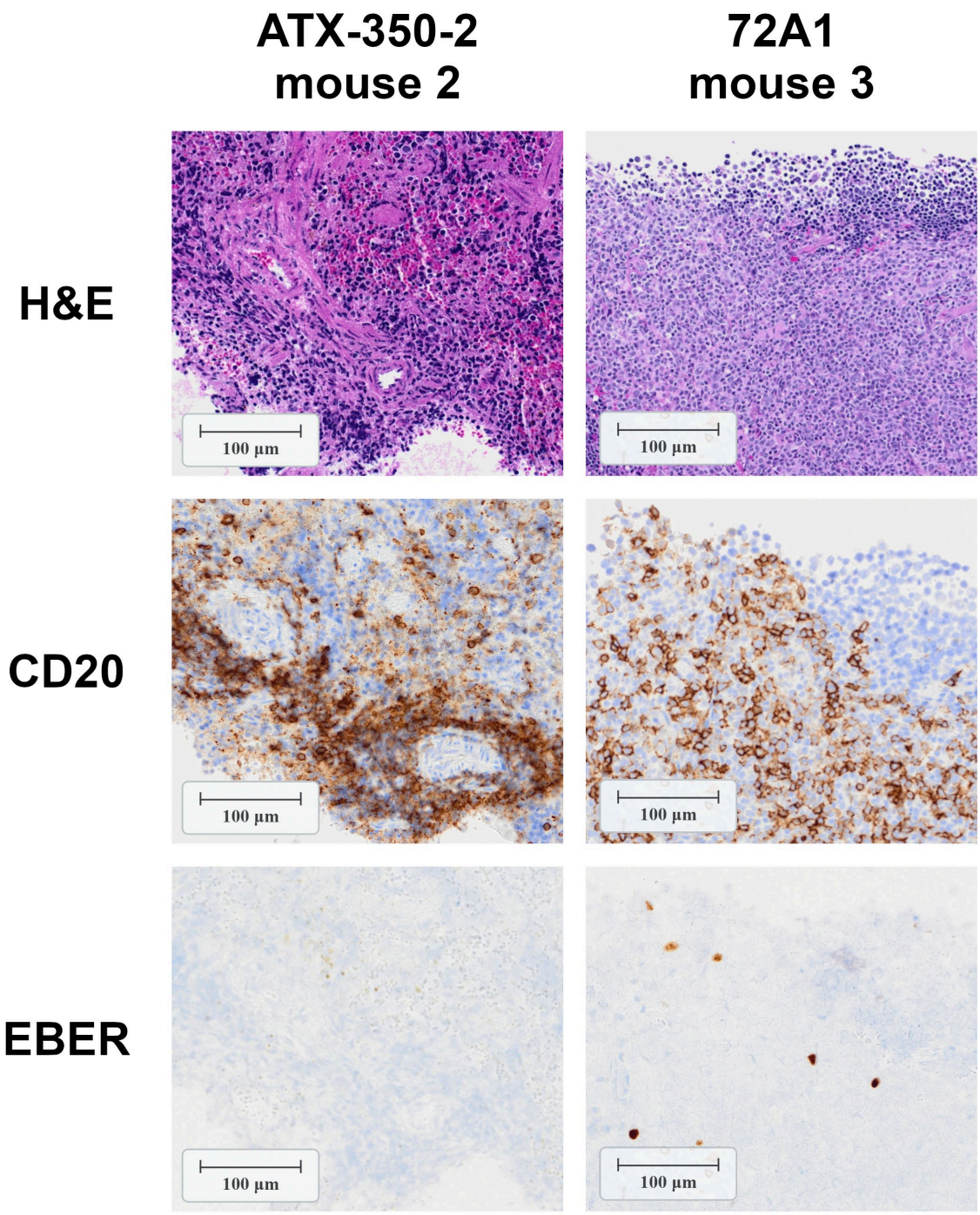

Supplementary Figure 13. Histology of humanized mice from ATX-350-2 and 72A1 group with low viral DNA in spleens. Related to Figures 6 and 7. Splenic sections from the indicated mice in Experiment 1 (Fig. 6B-D) were stained for hematoxylin and eosin (H&E), human CD20,

and EBER1 transcripts at necropsy as indicated. Scale bars represent 100 µm. Each image is from one representative mouse per group.

Table S4. Summary of challenge outcomes in study mice. Related to Figures 6 and 7.

Mouse	Group	Experiment # and Mouse Strain	huCD45+ % of total CD45+ cells at engraftment check	mAb in sera levels on day of infection (ug/mL)	Day of death post infection	Peak viremia in blood (EBV copies/uL) Limit of detection: 6.25	Spleen weight (mg)	Splenic viral copies (EBV copies/ng splenic DNA) Limit of detection: 6.25	Splenic tumor seen? (Yes/No)
1	PBS	Expt 1 NSG	9.3	N/A	74	0.93	28.57	not detected	no
2	PBS	Expt 1 NSG	7.8	N/A	74	1.96	20.02	not detected	no
3	PBS	Expt 1 NSG	30.4	N/A	66	4.09	69.8	not detected	no
4	PBS	Expt 1 NSG	6.1	N/A	69	not detected	14.96	not detected	no
1	ATX-42-2	Expt 1 NSG	17.0	137.3	74	1.90	32.08	not detected	no
2	ATX-42-2	Expt 1 NSG	7.9	26.3	74	not detected	42.16	not detected	no
3	ATX-42-2	Expt 1 NSG	10.6	13.0	74	17.41	60.01	not detected	no
4	ATX-42-2	Expt 1 NSG	15.2	230.4	74	1.31	40.46	not detected	no
5	ATX-42-2	Expt 1 NSG	12.8	218.5	74	not detected	39.38	not detected	no
1	ATX-350-2	Expt 1 NSG	18.2	36.1	50	not detected	13.2	6.36	no
2	ATX-350-2	Expt 1 NSG	16.9	52.6	74	0.71	19.23	not detected	no
3	ATX-350-2	Expt 1 NSG	13.7	94.1	28	2.04	21.85	16.94	no
4	ATX-350-2	Expt 1 NSG	8.0	13.7	74	1.90	40.84	358.48	no
5	ATX-350-2	Expt 1 NSG	excluded from study	not detected	excluded from study	excluded from study	excluded from study	excluded from study	excluded from study
1	72A1	Expt 1 NSG	excluded from study	not detected	excluded from study	excluded from study	excluded from study	excluded from study	excluded from study
2	72A1	Expt 1 NSG	12.1	21.8	69	not detected	25.83	0.72	no
3	72A1	Expt 1 NSG	34.9	28.8	61	2.36	146.49	2.31	no
4	72A1	Expt 1 NSG	16.0	47.6	74	5.73	141.61	2720.54	yes
1	AMMO1	Expt 1 NSG	10.6	292.6	61	1.28	14.34	not detected	no
2	AMMO1	Expt 1 NSG	15.6	180.0	74	not detected	30.71	not detected	no
3	AMMO1	Expt 1 NSG	7.3	264.2	15	not detected	34.5	not detected	no
4	AMMO1	Expt 1 NSG	20.6	74.4	74	not detected	24.69	not detected	no
1	VRC01	Expt 1 NSG	8.0	34.3	66	131.48	183.28	255.83	no
2	VRC01	Expt 1 NSG	11.9	71.0	74	10.03	130.14	26.94	no
3	VRC01	Expt 1 NSG	13.6	36.9	50	303.84	222.08	20781.67	yes
4	VRC01	Expt 1 NSG	19.3	24.4	74	6.53	102.23	18.46	no
1	ATX-42-2	Expt 2 NBSGW	15.7	65.7	83	N/A	161.71	not detected	no
2	ATX-42-2	Expt 2 NBSGW	excluded from study	not detected	excluded from study	N/A	excluded from study	excluded from study	excluded from study
3	ATX-42-2	Expt 2 NBSGW	42.1	69.7	15	N/A	59.6	not detected	no
4	ATX-42-2	Expt 2 NBSGW	76.3	71.6	83	N/A	290.94	not detected	no
5	ATX-42-2	Expt 2 NBSGW	83.1	21.4	83	N/A	57.47	not detected	no
1	ATX-350-2	Expt 2 NBSGW	11.4	19.4	48	N/A	117.4	4021.01	no
2	ATX-350-2	Expt 2 NBSGW	3.6	17.1	83	N/A	178.33	18.18	no
3	ATX-350-2	Expt 2 NBSGW	62.9	24.3	15	N/A	23.5	not detected	no
4	ATX-350-2	Expt 2 NBSGW	54.3	6.7	83	N/A	114.29	not detected	no
5	ATX-350-2	Expt 2 NBSGW	74.8	17.735	65	N/A	143.4	not detected	no
1	AMMO1	Expt 2 NBSGW	39.8	207.1	83	N/A	71.39	not detected	no
2	AMMO1	Expt 2 NBSGW	37.8	388.7	83	N/A	112.82	not detected	no
3	AMMO1	Expt 2 NBSGW	41.9	12.7	83	N/A	107.97	not detected	no
4	AMMO1	Expt 2 NBSGW	21.4	317.9	83	N/A	69.8	not detected	no
1	VRC01	Expt 2 NBSGW	20.3	14.6	83	N/A	138.32	36.86	no
2	VRC01	Expt 2 NBSGW	22.1	24.8	83	N/A	110.54	not detected	no
3	VRC01	Expt 2 NBSGW	59.4	22.3	83	N/A	75.73	464.77	no
4	VRC01	Expt 2 NBSGW	57.5	26.5	68	N/A	103	368.29	yes
1	ATX-42-2	Expt 3 NSG	13.8	151.8	88	N/A	13	not detected	no
2	ATX-42-2	Expt 3 NSG	11.2	137.1	82	N/A	36	not detected	no
3	ATX-42-2	Expt 3 NSG	7.9	232.0	95	N/A	51.5	not detected	no
4	ATX-42-2	Expt 3 NSG	1.7	237.3	95	N/A	36.2	not detected	no
1	VRC01	Expt 3 NSG	5.4	53.5	95	N/A	61	146.22	yes
2	VRC01	Expt 3 NSG	5.2	59.4	95	N/A	66.2	918.17	yes
3	VRC01	Expt 3 NSG	4.1	56.2	95	N/A	53.6	46.99	yes
4	VRC01	Expt 3 NSG	3.5	38.9	95	N/A	35.3	0.63	no

2.4 Discussion

Passive transfer of neutralizing antibodies has been demonstrated to be a safe and effective means of treatment for infectious diseases. In the context of EBV, passive transfer of neutralizing antibodies may be effective in vulnerable patient populations—in particular, organ transplant patients at high risk of PTLD. Proof of concept for antibody-mediated prophylaxis has been demonstrated in animal-infection models; yet, the only study in humans to date evaluated 72A1, a murine antibody against gp350, which may have showed some efficacy but elicited anti-drug antibodies and led to adverse events[48]. Here we leveraged a transgenic mouse model capable of eliciting antibodies with genetically human variable regions to identify gp350 and gp42 mAbs.

The two gp350 mAbs described here neutralized EBV infection of B cells and $CD21^+$ epithelial cells with differing potency. Like all other gp350-neutralizing mAbs, of murine or human origin, they block the interaction between gp350 and CD21[58, 60]. We propose that the differences of affinity of the two mAbs for gp350 and the position of the epitopes relative to the CD21 binding site on gp350 account for the differences in neutralizing potency. The ATX-350-2 mAb exhibited comparable neutralizing potency to 72A1 and would be appropriate for a follow-on study to Haque et al[48].

Out of 63 hybridoma cultures that showed gp350 binding activity, we identified 2 mAbs that were neutralizing. This suggests that the majority of gp350 mAbs elicited by immunization in ATX-GK mice were non-neutralizing. However, we acknowledge that our neutralization screen may have missed neutralizing antibodies if they were present at low levels in the culture supernatants. The finding that neutralizing antibodies are the minority is consistent with another study which found only 4 of 23 gp350 mAbs isolated from wildtype mice immunized with the

gp350 ectodomain were neutralizing[58]. Similarly, most hybridoma cultures with gp42 binding activity were non-neutralizing. These findings suggest that most antibodies directed at gp350 and gp42 in the context of immunization are non-neutralizing. Therefore, neutralizing potency might be improved through epitope-focused vaccine design[75], multimeric display, next-generation vaccine platforms or combinations thereof.

gp42 mAbs have been isolated from immunized mice, non-human primates, rabbits, and from human-derived phage display libraries[36, 37, 53, 68, 69]. To date, the most potent mAb is A10, which binds to the HLA class II binding site and was isolated from a non-human primate. The only other human mAbs against gp42 bind to the hydrophobic patch or an epitope opposite the hydrophobic patch[36]. The ATX-42 mAbs identified here are unique among known gp42 mAbs in that they are genetically human and map to the HLA-DR binding site. They may therefore have utility in a prophylactic or therapeutic setting without any need for humanization. In support of this notion, EBV was undetectable in splenocyte extracts from 13 of 13 mice who received prophylactic treatment with ATX-42-2, in contrast EBV was present in the spleens of 10 of 12 mice who received isotype control across three independent experiments, demonstrating protection against challenge in humanized mice.

In contrast to ATX-42-2 and the gH/gL mAb AMMO1, we observed partial protection with the gp350 mAbs ATX-350-2 and 72A1. This may be related to the fact that gp350 is not essential for EBV infection of B cells[76], while gp42 and gH/gL are. However, we note that it is difficult to draw definitive conclusions about the protective efficacy of the 72A1 and ATX-350-2 mAbs due to small numbers of animals in the groups, the lower average levels of these two mAbs in sera relative to AMMO1 and ATX-42-2 at the time of challenge, and potential

differences in pharmacokinetics. These data are consistent with a lack of protection afforded by 72A1 in one study[55], but contrast with the results of another[48].

Based on previous protection we observed with a single infusion of mAb or polyclonal sera in this challenge model[55, 71, 72], we only provided a single infusion of mAb prior to challenge here. Given that some of the mAbs (72A1 and ATX-350-2) showed more rapid decay, it is likely that protection could be improved with additional infusions of mAbs. An extensive determination of the pharmacokinetic parameters of each mAb would inform an extended dosing regimen for clinical use. It is nevertheless encouraging that most animals treated with EBV neutralizing Abs showed reduced viral loads in spleen, suggesting that prophylactic mAb treatment could lower viral load in transplant patients where high viral loads are a strong indicator of PTLD.

A key limitation of the animal model used here is that only human-origin lymphocytes are susceptible to infection[77, 78]; therefore, we were unable to assess the ability of the ATX-42 and ATX-350 mAbs to prevent infection of epithelial cells *in vivo*. *In vitro,* the ATX-350 mAbs, and 72A1 could neutralize EBV infection of $CD21^+$ but not $CD21^-$ epithelial cells. It is unclear whether CD21 is a relevant receptor on oral epithelial cells. CD21 mRNA has been detected in tonsil epithelium, but not in epithelial cells from the buccal mucosa, uvula, soft palate, or tongue[79]. However, primary polarized cells and primary organotypic cultures derived from primary gingiva and tonsil organotypic cultures which are permissive to EBV infection lack detectable CD21 protein[80, 81]. Unlike gp350 mAbs, the ATX-42 mAbs do not neutralize infection of $CD21^+$ cells. Interestingly, HLA-DR expression has been observed in nasopharyngeal atypical dysplasia and nasopharyngeal carcinoma (NPC) tumor samples[82, 83]. Additionally, it has been suggested that increased gp42 antibodies levels have an inverse association with risk of NPC[83].

Thus, it remains to be determined whether gp350 or gp42 mAbs would inhibit infection of human epithelial cells in a prophylactic or therapeutic setting. Dual tropic neutralizing antibodies that interfere directly with the fusion machinery (i.e., gH/gL and gB) may be more effective in this regard[51, 52, 55]. Alternatively, evaluating whether combinations of neutralizing mAbs targeting different epitopes or antigens show additive or synergistic activity *in vitro* and *in vivo* may overcome potential limitations of mAb monotherapy and compensate for strain diversity and/or selection of escape mutants.

Given the current lack of specific treatment and high mortality rate of PTLD, EBV neutralizing mAbs described here and elsewhere have the potential to fulfill an unmet need. Ultimately, the ability of mAbs to protect against EBV-driven disease, such as PTLD, need to be tested in clinical trials in humans to evaluate efficacy. Genetically human mAbs, such as the ones described herein, will enable these types of studies and potentially avoid adverse events previously observed with the passive transfer of murine mAbs.

2.5 Methods

Human Subjects

PBMC were collected from adults without HIV who were recruited at the Seattle HIV Vaccine Trials Unit (Seattle, Washington, USA) as part of the study "Establishing Immunologic Assays for Determining HIV-1 Prevention and Control", also referred to as Seattle Assay Control (SAC) Cohort. All participants signed informed consent, and the Fred Hutchinson Cancer Center (Seattle, Washington, USA) Institutional Review Board approved the SAC protocol (FHIRB0005567) prior to study initiation. Donors were selected randomly, and no considerations were made for age or sex. De-identified human umbilical cord blood (UCB) was obtained from Bloodworks Northwest after consent was obtained. All UCB work was approved under Fred Hutch's Institutional Review Board Protocol (FHIRB0020199).

Cell Lines

HEK293-EBNA1-6E (RRID:CVCL_HF20) and HEK293S GnTI-/- (RRID:CVCL_A785) cells were cultured in Freestyle 293 expression medium (Thermo Fisher, Cat. # 12338026) and maintained at 37°C and 5% CO_2 with gentle shaking at 130 rpm.

Raji cells (CVCL_0511) were cultured in RPMI-1640 (Corning, Cat #15-040-CV) supplemented with 25 mM L-glutamine, 10% heat-inactivated fetal bovine serum, 200 U/mL Penicillin-Streptomycin (cRMPI), and maintained at 37°C and 5% CO_2.

SVKCR2 cells (RRID:CVCL_YD67) were cultured in DMEM (Corning, Cat #15-013-CV) supplemented with 25 mM L-glutamine, 10% heat-inactivated fetal bovine serum, 200 U/mL

Penicillin-Streptomycin, 10 ng/mL cholera toxin, 400 μg/mL G418[84], and maintained at 37°C and 5% CO_2.

AGS cells (RRID:CVCL_0139) were cultured in Ham's F-21 medium (Thermo Fisher, Cat. #11765062) supplemented with 10% heat-inactivated fetal bovine serum, 200 U/mL Penicillin-Streptomycin and maintained at 37°C and 5% CO_2.

293–2089 cells were cultured in cRPMI containing 100 μg/mL hygromycin.

293 cells harboring a bacterial artificial chromosome encoding the M81 strain with GFP and luciferase reporter genes were cultured in cRPMI containing 100 μg/mL hygromycin[63, 65].

AKATA B cells harboring EBV in which the thymidine kinase gene has been replaced with a neomycin and GFP cassette virus (AKATA-GFP) were grown in cRPMI containing 350 μg/ml G418[84].

Mice

ATX-GK mice were purchased from Alloy Therapeutics[61] and shipped from Charles River Laboratories (Wilmington, MA). Hu-CD34+-engrafted NSG mice were purchased from the Fred Hutchinson Cancer Center Comparative Medicine Facility. NBSGW (NOD.Cg-KitW-41J Tyr + Prkdcscid Il2rgtm1Wjl/ThomJ; strain 026622)[85] breeding pairs were purchased from Jackson Labs and bred in house. All mice used in our studies were housed with free access to food and water with a 12:12 light:dark cycle. The animal facilities are accredited by the Association for Assessment and Accreditation of Laboratory Animal Care. Mice were handled in accordance

with the NIH Guide for the Care and Use of Laboratory Animals, and experiments were approved by the Fred Hutch Cancer Center Institutional Animal Care and Use Committee and Institutional Review Boards (Protocols 000051095, 202000018 and 202000029). Immunizations and retro-orbital bleeds were carried out under anesthesia, which was induced by administering isoflurane, set at 1–5% for 1–2 min in an induction chamber with the flow rate of O_2 set at 1.0 L/min. Animals under anesthesia were then transferred to a nose cone and continued to receive 1-5% isoflurane at an O_2 set to 1.0 L/min during injections and retro-orbital bleeds. Mice were euthanized by administering 100% CO_2 in an induction chamber with a flow rate of 3.0 L/min to allow for 50% of the air in the chamber to be replaced per minute for at least 5 minutes, followed by cervical dislocation.

Paired BCR analysis of Naïve ATX-GK mice

B cells were enriched from splenocytes of two ATX-GK mice independently (StemCell, Cat. #19854). Paired BCR sequencing of B cells was performed using the Chromium Next GEM Single Cell 5' Kit v2 (10x Genomics, Cat #. PN-1000265). For each mouse, 16500 B cells were inputted to generate gel bead-in-emulsions (GEMs). Custom primers for IgM and IgK chains were utilized to amplify VH and VL sequences following manufacturer's instructions. Universal forward primer: 5' GATCTACACTCTTTCCCTACACGACGC 3', IgM first round reverse primer: 5' CACCAAATTCTCATCAGACAGGG 3', IgM second round reverse primer: 5' GAAGACAGTTGGGGAGGACTG 3',IgK first round reverse primer: 5' CAGTTGGTGCAGCATCAGCCC 3' and IgK second round: reverse primer: 5' AGGCACCTCCAGTTGCTAAC 3'. Library sequencing was performed on a Miseq (Illumina) by the Fred Hutch Cancer Center Genomics and Bioinformatics Core Facility

(RRID:SCR_022606) resulting in a depth of 5000 reads per cell. The BCR libraries were then mapped to a human VDJ reference using Cell Ranger (10x Genomics). Each paired BCR's V, D, and J genes for both heavy chain and light chains were determined utilizing Enclone (10x Genomics). Raw sequence data can be found in NCBI Sequence Read Archive under BioProject ID: PRJNA1347123.

Plasmids

Codon-optimized plasmids of neutralizing antibodies were ordered from BioIntron Biological Inc (Metuchen, New Jersey). Plasmids were transformed into DH5Alpha cells (NEB, Cat. #C2987H) and plated on agar plates containing ampicillin and grown overnight at 37°C. Colonies were used to seed 4 mL LB broth cultures containing ampicillin. Glycerol stocks of 500 µL of the overnight culture to 500 µL of 50% *glycerol* were stored at -80°C.

Recombinant Protein Expression

Plasmids encoding EBV proteins[59], pTT3-gp350-HIS-AVI, pTT3-gp42-HIS-AVI, pTT3-gH-HIS-AVI, pTT3-gL as well as a pTT3-gp350 (AA 1-470) construct without any tags for structural studies, were transfected into either HEK293-EBNA1-6E or HEK293S GnTI-/- cells using PEI MAX (Polysciences, Cat. #24765) at a 3:1 mass ratio in 1X PBS, incubated for 20 min at room temperature before dropwise addition to cells cultured at $1x10^6$ cells/mL in Freestyle media. The transfected cultures were incubated at 37°C shaking at 130 rpm with 5% CO_2 for six days. On day six, the culture was centrifuged at 4000 X *g* for 10 min at 4°C. The supernatant was collected and adjusted to 500 mM NaCl, 10 mM Imidazole, 0.02% Azide and then clarified through a 0.22 µm filter (Corning, Cat. #431097). The clarified supernatant was then passed over

Ni-NTA resin (Gold Biotechnology, Cat. #H-350-100) pre-equilibrated with Ni-NTA binding buffer (500 mM NaCl, 10 mM Tris, 10 mM imidazole, 0.02% Azide, pH 7.1), followed by extensive washing with Ni-NTA binding buffer, and then eluted with Ni-NTA elution buffer (10 mM Tris, 500 mM NaCl, 500 mM imidazole, 0.02% Azide, pH 8.0), or purified using Galanthus Nivalis Lectin (GNL) agarose resin (Vector Laboratories) equilibrated with GNA-A buffer (20 mM Tris, 100 mM NaCl, 1 mM EDTA, pH 7.4), the collected supernatant was adjusted with GNA-A buffer, followed by extensive washing with GNA-A buffer, and eluted with GNA-B buffer (20 mM Tris, 100 mM NaCl, 1 mM EDTA, 1 M Methyl-α-D-Mannopyranoside, pH 7.4). Ni-NTA and GNL captured proteins were concentrated using 30 kDa centrifugal filter (Millipore, Cat. #UFC9030) and purified by size exclusion chromatography (SEC) using a HiLoad 16/600 Superdex 200 pg column (Cytiva Lifesciences, Cat. #28989335) preequilibrated in 1X PBS or 1X HEPES running buffer, respectively. gp350 was further treated with Endoglycosidase H (Endo H, New England Biolabs, Cat. #P0702S) at 1:50 EndoH/protein ratio for 1 h at room temperature and used directly for complex formation or stored at -80°C.

Hybridoma Generation

Four ATX-GK mice were injected three times at two-week intervals with of a cocktail of 15 µg recombinant EBV gp350-HisAvi, 15 µg gp42-HisAvi, and 15 µg gH/gL-HisAvi with Adjuplex (Empirion LLC). 7 weeks later, a final immunization was administered 3 days prior to endpoint. Spleens were harvested and used to generate hybridomas at the Fred Hutchinson Cancer Center Antibody Technology Shared Resource, which were seeded at a density of ~50-100/well and cultured in 384 well plates. Hybridoma supernatants were initially screened against gp350, gp42, and gH/gL, using a fluidics-based high-throughput antigen-coupled bead array on an iQue

instrument (Sartorius) to identify wells containing antibodies against gp350, gp42, or gH/gL. Supernatants from positive wells were diluted 1:1 to screen for their ability to neutralize EBV infection of Raji B cells (see below for assay details). Wells containing hybridomas that displayed at least 50% neutralizing activity were sub-cloned using the ClonePix (Molecular Devices) and re-screened for binding and neutralization. Data for gH/gL mAbs will be reported in a separate manuscript in preparation.

Antibody Production

To produce recombinant mAbs, RNA was extracted from 1×10^6 hybridoma cells using the Monarch Total RNA Miniprep Kit, and cDNA encoding the heavy and light chain variable regions of the murine hybridomas were by reverse transcribed and amplified using the procedures outlined in Meyer et al[86]. Amplicons were Sanger sequenced directly or TOPO cloned (Thermo Fisher, Cat. #450245) and then sequenced. Plasmids encoding antibody heavy and light chains were co-transfected into HEK293-EBNA1-6E with PEI Max at a 3:1 ratio in PBS and incubated at 37°C, shaking at 130 rpm with 5% CO_2 for six days. On day six, the cultures were centrifuged at 4000 X *g*. The supernatant was passed through a 0.22 μm filter (Corning, Cat. #431097), and then passed over protein A agarose resin (Gold Biotechnology, Cat. #P-400) pre-equilibrated with 1X PBS followed by washing with 5 column volumes of 1X PBS and eluted using with IgG elution buffer (Pierce, Cat. #21004). Elution fractions were captured in tubes containing a 1:10 ratio of 1 M Tris pH 8.0 to elution volume. The mAbs were then dialyzed overnight (Thermo Fisher, Cat. #66030) into PBS and stored at 4°C for short-term use, or at -80°C for long term use. Fabs were generated from full-length IgG antibodies by incubating antibodies with endoproteinase LysC (NEB, Cat. #P8109S) at a 10:1 ratio by mass at

37°C, rotating at 13 rpm for 16 h. The antibodies were then passed over protein A agarose resin pre-equilibrated in PBS to remove undigested full-length antibody and Fc regions. Fabs were further purified by size exclusion chromatography (SEC) using an Enrich 650 (BioRad, #7801650) equilibrated into PBS to remove LysC and any remaining Fc or undigested IgG.

Biotinylation of EBV Proteins

Recombinant gp42 and recombinant gp350 were biotinylated using either BirA (Avidity LLC, Cat. #BirA500) or EZ-Link NHS-PEG4 biotin (Thermo Fisher, Cat. #A39259) at a theoretical 1:1 biotin to protein ratio. Excess biotin was removed using Zeba spin desalting columns (Thermo Fisher, Cat. #87766). Biotinylated proteins were flash frozen and stored at -80ºC until use.

Generation of gH/gL/gp42 Complex

Recombinant gp42 was incubated with recombinant gH/gL at a 1.5:1 molar ratio at 4°C, with gentle rotation for 16 h. The gH/gL/gp42 complex was purified by size exclusion chromatography using a HiLoad 16/600 Superdex 200 pg column (Cytiva Lifesciences, Cat. #28989335) pre-equilibrated in 1X PBS.

Fluorescently Labeled Streptavidin Tetramer Production

Biotinylated gp42 or gp350 were incubated with either streptavidin-R-phycoerythrin (SA-PE, Agilent, Cat. #PJRS301-1) or streptavidin allophycocyanin (SA-APC, Agilent, Cat. #PJ27S-1) at a 4:1 molar ratio. Proteins and SA conjugates were incubated in the dark at RT for 5 min

followed by an addition of 25 nmol D-biotin (Invitrogen, Cat. #B20656) to quench unoccupied binding sites on SA.

Measuring Glycoprotein Binding to Raji B cells

To measure inhibition of gp350 binding, a 2-fold dilution series of mAbs starting at 800 nM in 20 µL PBS was incubated with 20 µL of 4 nM gp350 conjugated to SA-APC at 37°C for 1 h. To measure inhibition of gp42 binding, a 2-fold dilution series of mAbs starting at 1200 nM in 20 µL PBS was incubated with 20 µL of 125 nM gp42 conjugated to SA-PE in 20 µL PBS at 37°C for 1hr. Then, 50,000 Raji cells in 40 µL cRPMI were added to the antigen-mAb mixture to stain for 30 mins at 4°C. Cells were washed twice with FACS buffer (1X PBS + 2% FBS+ 1 mM EDTA), then fixed with 10% formalin for 15 mins at RT. The percentage of tetramer-positive Raji B cells was measured on a BD FACSCelesta flow cytometer and analyzed using FlowJo software.

Measuring Glycoprotein Binding to Primary B cells

B cells were enriched from human PBMC using EasySep Human B cell Enrichment Kit (Stemcell, Cat #19054). To measure inhibition of gp350 binding, 20 µL of PBS containing 200 nM of each mAb was incubated with 20 µL of 4 nM gp350 conjugated to SA-APC at 37°C for 1 h. To measure inhibition of gp42 binding, 20 µL of PBS containing 400 nM of each mAb was incubated with 20 µL of 125 nM gp42 conjugated to SA-PE at 37°C for 1hr. 2 nM gp350 conjugated to SA-APC and 62.5 nM gp42 conjugated to SA-PE were incubated without mAb as controls. Then, 40,000 enriched B cells in 40 µL of FACS buffer were added to the antigen-mAb mixture for 30 mins at 4°C. Cells were washed twice with FACS buffer, then fixed with 10%

formalin for 15 mins at RT. The percentage of tetramer-positive B cells were measured on a BD FACSCelesta flow cytometer and analyzed using FlowJo software.

Biolayer Interferometry (BLI)

All experiments were carried out on an Octet RED96e at 30°C with 1000 rpm shaking.

Recombinant CD21 and CD35 Binding Screen

Biotinylated gp350 was immobilized on streptavidin biosensors (Sartorius, Cat. #18-5020) for 150 s. Sensors were immersed in KB for 30 s to collect a baseline measurement. Sensors were then immersed in wells containing 250 nM of recombinant soluble CD21 (SinoBiological, Cat #10811-H08H) or recombinant soluble CD35 (Bio-Techne, Cat #5748-CD) in 1X KB buffer. Then the association was measured for 300 s, followed by immersion in 1X KB for 300 s to measure disassociation.

Kinetic Measurements

Biotinylated gp350 monomers were immobilized on streptavidin biosensors (Sartorius, Cat. #18-5020) for 150 s. Sensors were immersed in KB for 30 s to collect a baseline measurement. Sensors were then immersed in wells containing two-fold serial dilutions of Fabs in 1X KB buffer and the association was measured for 300 s, followed by immersion in 1X KB for 600 s to measure dissociation. Anti-gp42 mAbs were immobilized on anti-human IgG Fc Capture (AHC) biosensors (Sartorius, Cat. #18-5063) for 150 s. Sensors were then immersed in KB for 30 s to collect a baseline measurement. Sensors were then immersed in wells containing two-fold serial dilutions of gp42 or a gH/gL/gp42 complex in 1X KB buffer and the association was measured for 300 s. The sensors were then immersed in 1X KB for 600 s to measure dissociation. Empty

reference sensors were used to measure the background signal from each analyte-containing well. Additionally, each ligand-coupled sensor was associated in wells containing only buffer as a reference. Double reference subtraction was performed for each corresponding ligand-coupled sensor at each time-point. Curve fitting was performed using a 1:1 binding model in Octet BLI Analysis 12.2 software. Mean k_{dis} (1/s) and k_{on} (1/Ms) values were determined by averaging all binding curves that matched the theoretical fit with an R^2 value of ≥ 0.99. The K_D value was calculated by taking the mean k_{dis} value divided by the mean k_{on} value.

Epitope Binning

mAb competition was assessed via biolayer interferometry. Biotinylated gp350 or gp42 was loaded onto streptavidin sensors, immersed in buffer containing 500 nM of the first mAb to achieve saturable binding, and then immersed in buffer alone or buffer containing 250 nM of a second mAb for 300 s. The % binding inhibition was calculated as the binding signal measured for the second mAb divided by the binding signal in the absence of any competing mAb × 100%.

CD21-gp350 Binding Competition

Biotinylated gp350 was immobilized on SA biosensors for 150 s. The sensors were immersed in KB buffer containing 500 nM of mAb to achieve saturable binding for 300 s and then immersed in KB buffer containing 250 nM of recombinant human CD21 for 300 s.

HLA-DR-gp42 Competition

Biotinylated HLA-DRβ1*0101 monomer loaded with CLIP peptide (Fred Hutch Immune Monitoring Core) was immobilized on streptavidin sensors for 150 s, and then immersed in wells

containing KB to measure a baseline. Biosensors were then immersed in cells containing 125 nM gp42 or 125 nM of the gH/gL/gp42 complex that had, or had not been, pre-incubated with 250 nM of mAbs for 1h at 37°C for 300 s.

Preparation of EBV Reporter Viruses

To produce B-cell tropic GFP reporter viruses (B95-8/F), 5×10^6 293–2089 cells were seeded on a 100 mm tissue culture dish. 48 h later the cells were washed with PBS, the media was replaced with cRPMI without hygromycin, and cells were transfected with 6 μg each of p509[87] and p2670[88], expressing BZLF1 and BALF4, respectively, using GeneJuice transfection reagent (SigmaAldrich, Cat. #70967). 72 h post transfection, the cell supernatant was collected and centrifuged at 500 × *g* for 3 min to pellet any cell debris and passed through a 0.45 μm filter. Virions were concentrated 25-50-fold by centrifugation at 25,000 × *g* for 2 h and re-suspended in cRPMI. Virus was stored at -80°C and thawed immediately before use.

EBV M81-Luc, expressing GFP and luciferase reporter genes[63, 65], was induced by co-transfection of p509 and p2670 following the steps described to produce B95-8/F virus. Virus was stored at -80°C and thawed immediately before use.

Epithelial cell tropic virus was produced from Akata-GFP EBV cells suspended at 4×10^6 cells/mL in RPMI containing 1% FBS by adding goat anti-human IgG (Southern Biotech, Cat. #2040-01) to a final concentration of 100 μg/mL, and the culture was incubated at 37°C for 4 h. Cells were then diluted to 2×10^6 cells/mL in RPMI containing 1% FBS and cultured for 72 h. Cultures were centrifuged at 300 × *g* for 10 min to pellet cells and supernatant was passed

through a 0.8 μm filter. Bacitracin was added to a final concentration of 100 μg/mL. Virions were concentrated 25× by centrifugation at 25,000 × *g* for 2 h and re-suspended in RPMI containing 100 μg/mL bacitracin. Virus was stored at -80°C and thawed immediately before use.

EBV Neutralization Assay in B cells

B cell neutralization assays were carried out in Raji cells as described by Sashihara et al.[89]. Either 25 μl of supernatant from hybridoma cultures or serially diluted monoclonal antibodies in cRPMI were plated in duplicate wells of 96-well round-bottom plates. 12.5 μl of B95-8/F virus (diluted to achieve an infection frequency of 1-5% at the final dilution) was added and incubated at 37°C for 1 hour. 12.5 μl of cRMPI containing 4×10^6 Raji cells/mL was added to each well and incubated for another hour at 37°C. The cells were then pelleted, washed once with cRPMI, and re-suspended in cRPMI. Antibody concentration is reported relative to the final infection volume (50 μl). After 3 days at 37°C, cells were fixed in 10% formalin. The percentage of GFP^+ Raji cells as determined on a BD FACSCelesta cytometer. To account for any false positive cells due to auto-fluorescence in the GFP channel, the $\%GFP^+$ cells in negative control wells (no virus, n=4) was subtracted from each well. % neutralization in each well was defined as: [$\%GFP^+$ cells in the positive control wells containing virus alone (n=5 wells) – $\%GFP^+$ cells in the antibody containing well] / $\%GFP^+$ cells in the positive control wells × 100. The % neutralization for each well was plotted as a function of the $\log_{10}$ of the mAb concentration. The neutralization curve was fit using the log(inhibitor) vs response- variable slope (four parameters) analysis in Graphpad Prism 10 software.

M81 EBV Neutralization Assay in AGS or SVKCR2 Epithelial Cells

5×10^4 AGS cells or SVKCR2 cells per well were seeded into a 96-well flat-bottom tissue culture plate. The following day, 30 µl of 10µg/mL mAbs in media was incubated with 30 µl of M81-Luc virus for 15 min at 37°C in duplicate. Culture media was aspirated from the cells and replaced with 50 µl of the antibody-virus mixture. Plates were incubated at 37°C for 72 h. Then 50 µl of Steady-Glo reagent (Promega, #PRE2520) was added to each well and incubated at RT for 5 mins. Luminescence was read using a Promega GloMax Plate Reader. % neutralization is reported as the luminescence signal obtained in the presence of the indicated mAb divided by the average signal obtained in the presence of an isotype control × 100%.

Akata-EBV Neutralization Assay in SVKCR2 Epithelial Cells

1.5×10^4 SVKCR2 cells per well were seeded into a 96-well flat-bottom tissue culture plate. The following day, antibodies were serially diluted in duplicate wells containing 20 µl of media in a 96-well round-bottom plate, followed by the addition of 20 µl Akata-GFP virus and incubated for 15 min at 37°C. Media was aspirated from the SVKCR2 cells and replaced with the antibody-virus mixture. Plates were incubated at 37°C. 48 hours later, the number of GFP^+ cells were determined on a Sartorius Incucyte S3 Live-Cell Analysis Instrument. Four images per well were taken at 20x objective in the phase and green channels using the adherent cell-by-cell setting. GFP^+ cells were determined by the machine's basic analyzer software using green segmentation surface fit with area range of $8\mu m^2$ to 1000 μm^2 and intensity minimum of 0.49, and the number of positive cells was averaged across the four images for each well. To account for any false positive cells due to auto-fluorescence in the GFP channel, the average number of GFP^+ cells detected by the software in negative control wells (no virus, n=8) was subtracted from each experimental well. % neutralization in each well was defined as: [number of GFP^+ cells in the

positive control wells containing virus alone (n=8 wells) – number of GFP^+ cells in the antibody containing well] / number of GFP^+ cells in the positive control wells × 100%. The % neutralization for each well was plotted as a function of the log_{10} of the mAb concentration. The neutralization curve was fit using the log(inhibitor) vs response-variable slope (four parameters) analysis in Graphpad Prism 10 software.

Protein Complex Formation for nsEM Analysis

ATX-350-2 Fab and ATX-350-1 Fab complex formation with gp350

Purified EndoH-treated gp350 was incubated with ATX-350-2 or ATX-350-1 Fabs at a 1:1.5 gp350:Fab molar ratio for 30 min at room temperature before purification over a Superdex 200 16/600 (Cytiva, Cat. #45-002-490) size exclusion chromatography (SEC) column, pre-equilibrated in TBS (10 mM Tris HCl, 150 mM NaCl, pH 7.5). Fractions corresponding to the complex peak were pooled, concentrated, run on SDS-PAGE and immediately stained on grids at 0.02 mg/mL in 1x TBS.

gp350/72A1 Fab and gp350/ ATX-350-1/72A1 Fab complex formation

Purified gp350-EndoH treated was incubated with a 1:1.5 gp350:Fab72A1 molar ratio. and 1:1.5:1.5 gp350:ATX-350-1:72A1 molar ratio for 1 h at room temperature before purification over a Superdex 200 16/600 SEC column. Fractions corresponding to the complex peak were pooled, concentrated, validated by SDS-PAGE and immediately stained on grids at 0.02 mg/mL and 0.03 mg/mL, respectively, in 1x TBS.

ATX-42-1.1 Fab/gp42/gHgL complex formation

Purified gp42/gH/gL complex was incubated with a 1:1.5 gH/gL/gp42:Fab molar ratio, then incubated with a 1:1.3 Complex:ATX-42-1.1 molar ratio and 1:2 Complex:ATX-42-2 for 30 min at room temperature. Afterwards, the complex was immediately stained at 0.03 mg/mL with 1x TBS.

ATX-42-2 Fab/gp42/gHgL complex formation

Purified gp42/gHgL complex was incubated with a 1:1.5 gH/gL/gp42:ATX-42-2 molar ratio, then incubated with a 1:2 Complex:ATX-42-1.1 molar ratio for 30 min at room temperature. Afterwards, the complex was immediately stained at 0.04 mg/mL with 1x TBS.

HLA-DR1β/gp42/gHgL complex formation

Purified gp42/gHgL complex was incubated with a 1:2 gHgL/gp42: HLA-DR1β molar ratio. The complex was mixed for 1 h at room temperature and then was immediately stained on grids at 0.01 mg/mL in 1xTBS.

Negative stain electron microscopy grid preparation, acquisition and data analysis

Complexed proteins were deposited onto Formvar, stabilized with Carbon-coated 400-mesh copper grids, hole size: 42 μm (Ted Pella). Proteins were incubated for 30 s on grids before being washed twice with water and once with 2% (w/v) Uranyl -Formate with blotting against filter paper between each step. The grids were then stained with 2% (w/v) uranyl-formate for 30 s followed by blotting on a filter paper and air drying for 3 min. Grids were then imaged at 120 keV on a Talos L120C G2 (Thermo Fisher Scientific) using a 4K × 4K Thermo Scientific Ceta CMOS Camera at 92,000× magnification, -2 μm defocus, total dose of 40 e-/Å^2 and a pixel size

of 1.58 Å. Micrographs were collected using Leginon[90] and the images were transferred to CryoSPARC V4[91] for processing. Particle stacks were generated with particles picked using a Gaussian signal. Particle stacks were then submitted to multiple rounds of 2D classification followed by generation of initial 3D models directly from particle with an ab-initio reconstruction job. Selected 3D classes were refined using homogeneous structure refinement and used to make figures with UCSF Chimera[92]. Micrographs were collected using Leginon[90] and the images were transferred to CryoSPARC V4[91] for processing. Particle stacks were generated with particles picked using a Gaussian signal. Particle stacks were then submitted to multiple rounds of 2D classification followed by generation of initial 3D models directly from particle with an ab-initio reconstruction job. Selected 3D classes were refined using homogeneous structure refinement and used to make figures with UCSF Chimera[92]. Published gp350 (PDB ID: 8SGN chain C)[60], gHgL/gp42 (PDB: 5T1D CHAIN A, B, C)[32] and gp350-CD21 (PDB ID: 8SM0 chain A)[60] structures were used and Alphafold 3[93] predictions of the different Fabs were fit in the nsEM 3D reconstructions for our structural analysis.

Crystal Screening and Structure Determination for gp350/ATX-350-2 Fab Complex

The gp350/ATX-350-2 Fab complex was formed as described above. Initial crystal screening was performed by sitting-drop vapor-diffusion in the MCSG Crystallization Suite (Anatrace) using a NT8 drop setter (Formulatrix) at a complex concentration of 30 mg/mL. Crystals grew in MCSG3 E5 (0.1 M Sodium Citrate:HCl pH 5, 3.15 M Ammonium Sulfate) and diffracting crystals were harvested directly from the 96-well screen and cryoprotected using 20% glycerol. Diffraction data was collected at Advanced Light Source beamline 5.0.2 at 12.7 keV. Data were processed using XDS[94] and data reduction was performed using AIMLESS in CCP4[95] to a

resolution of 3.93Å. Initial phases were solved by molecular replacement (MR) using Phaser in CCP4 with a search model of gp350 (PDBid: 8SM0) and ATX-350-2 fab Alphafold 3 prediction divided into Fv and CH1/CL domains. Model building was completed using Coot[96] and refinement was performed in Phenix[97]. The crystal belonged to space group $P4_32_12$, with one complex in the asymmetric unit. The structure was solved by molecular replacement, yielding R_{work} and R_{free} of 0.2413 and 0.2800, respectively. The data collection and refinement statistics are summarized in Table S3. Structural figures were made in ChimeraX[98]. BSA data was determined using the PDBePISA server[99].

EBV Challenge in Humanized Mice

6-week old, female NSG mice were irradiated (275R of total body irradiation) prior to receiving $1x10^6$ $CD34^+$ granulocyte colony-stimulating factor-immobilized huPBSC (purchased from Cooperative Center of Excellence in Hematology at the Fred Hutchinson Cancer Center) in 200 µL PBS via intravenous (i.v.) injection. Ten weeks later, successful human cell engraftment was confirmed by the presence of human $CD45^+$ lymphocytes in peripheral blood by flow cytometry. Using 50 µL blood, RBCs were lysed and cells were stained using a BV510 viability dye (eBioscience, Cat. #65-0866-14) at 1:200 dilution, and the following antibodies at a 1:100 dilution unless otherwise noted: hCD45 FITC (eBioscience, Cat. #11-9459-42), mCD45 APC (eBioscience, Cat. #17-0451-82; 1:200 dilution), hCD33 PE (BD Bioscience Cat. #555450), hCD19 BV711 (Biolegend, Cat. #302246) or hCD20 BV786 (BD, Cat. #743611; 1:200 dilution), hCD4 AF700 (eBioscience, Cat. #56-0048-82; 1:250 dilution), and hCD8 BV421 (BD Bioscience, Cat. #562429). Cells were stained for 30 min on ice, washed twice in FACS buffer, fixed in 200 µL of 10% formalin for 15 min on ice, washed, and resuspended in 200 µL FACS

buffer for acquisition and analysis on a BDFACS Celesta. Frequency of human $CD45^+$ lymphocytes was calculated from the total of mouse $CD45^+$ plus human $CD45^+$ cell populations. Frequency of human CD19 was calculated from total human $CD45^+$ cell population.

16 weeks post-engraftment, 500 µg of control or experimental mAbs were injected per humanized NSG mouse (n=4 or 5 mice per mAb group) via intraperitoneal injection. 24 h later, blood was collected via retro-orbital (RO) bleed behind the left eye and then challenged with a dose of EBV B95.8/F equivalent to 20,000 or 25,000 Raji infectious units (RIU) via RO injection behind the right eye. Each group of mice receiving the same mAb were housed together. Following viral challenge, mice were weighed three times weekly. Beginning at four weeks post-challenge, RO blood samples were collected weekly to measure the presence of EBV DNA in whole blood. Mice were euthanized 12 to 14 weeks post-challenge, or until mice lost 20% of their starting weight. Terminal bleeds were collected via cardiac puncture. Spleens were photographed, weighted, and sectioned for DNA extraction utilizing the DNeasy Blood & Tissue Kit (QIAGEN) according to manufacturer's instructions or fixed in 10% formalin overnight and embedded in paraffin for histological staining by the Fred Hutchinson Cancer Center Experimental Histopathology shared resource (see below for assay details).

Xenotransplantation and EBV challenge in NBSGW mice

UCB-derived $CD34^+$ cells were isolated using Magnetic Assisted Cell sorting (MACS) from Miltenyi Biotech. NBSGW neonates aged 1-3 days were intrahepatically injected with 30,000-50,000 UCB-derived $CD34^+$ hematopoietic stem and progenitor cells per animal in 30 mL of injection media (filtered RPMI, 1 mM EDTA) as previously described[100-102]. Starting at 8 weeks

after injection, human chimerism was measured as the percentage of human CD45+ cells among the mouse and human CD45+ in the PB. Blood analysis was performed every other week.
Male and female mice were used. All mice were ear tagged and assigned to experimental and control groups to evenly distribute the percentage of human CD45+ and human CD19+ cells. 15 to 16 weeks post-engraftment of UCB-derived $CD34^+$ cells, 500 μg of mAbs were transferred via IP injection. 1 day later, mice were bled then challenged with 36,000 RIU of EBV via RO injection. RO blood samples were also collected at week 1, 2, and 3 post challenge to measure mAb levels in sera as described above. Twelve weeks post-challenge, or until mice lost 20% of their starting weight, mice were euthanized. Endpoints were collected and measured as described above.

Pharmacokinetics of mAbs in Humanized Mice

A second cohort of humanized NSG mice received 500 μg of control or experimental mAbs per humanized NSG mouse (n=4 or 5 mice per mAb group) via intraperitoneal injection at 11 weeks post engraftment. Blood was collected via RO bleed at 1 day, 1 week, 2 weeks, and 3 weeks post injection. Serum was heat-inactivated at 56°C for 10 minutes, then kept at 4°C. Sera from all four time points were assessed for mAb levels compared to each group's respective mAb standard via antigen-specific ELISA (see below for assay details).

Measurement of Passive Transferred IgG in huCD34$^+$ Engrafted Mice

384-well microplates were coated with 190 ng/well of gp350, or with 60 ng/well gp42, gH/gL, or HIV Env 426c.TM4ΔV1-3 in 0.1 M $NaHCO_3$ pH 9.4–9.6 (ELISA coating buffer) at RT overnight at 30 μL/well. The next day, plates were washed 4 times with 1x PBS and 0.02%

Tween 20 (ELISA wash buffer) prior to blocking for 1 h with 100 µl/well of PBS containing 10% non-fat milk and 0.02% Tween 20 (ELISA blocking buffer) at 37ºC. After blocking, serial dilutions of serum or serially diluted mAb standards (2 µg/mL- 0.14 pg/mL) in ELISA blocking buffer was added and incubated for 1 h at 37˚C. 32 control wells were included that contained only blocking buffer without sera or mAb standard. Plates were incubated for 1 h at 37ºC. After washing, a 1:4000 dilution of goat anti-human IgG-HRP (Jackson ImmunoResearch, Cat. #109-035-088) in ELISA blocking buffer was added to each well and incubated 1h at 37ºC. After four washes, 30 µl/well of SureBlue Reserve TMB Microwell Peroxidase substrate (SeraCare, Cat.#5120-0081) was added. After 5 min at room temperature, 30 µl/well of 1 N sulfuric acid was added and the A_{450} of each well was read on a Molecular Devices SpectraMax M2 plate reader. The average A_{450} values of buffer only control wells were subtracted from each serum containing well and plotted in GraphPad Prism 10. A_{450} values were plotted as a function of the $\log_{10}$ of the serum dilution. A binding curve of the mAb standard was fit using the sigmoidal, 4PL, X is log(concentration) least squares fit function. The mAb concentration in the serum was determined by interpolating the concentration of each dilution from the standard curve, multiplying by the dilution factor, and calculating the mean.

Quantitative PCR Analysis EBV DNA in huCD34 Engrafted Mice

A primer-probe mix specific for the EBV IR1 gene[103] was used to quantify EBV in DNA extracted from splenocytes collected from huCD34$^+$ engrafted NSG or NBSGW mice. For DNA extracted from blood, a primer-probe mix specific the EBV BALF5 gene[104] was used. Each 25 µl qPCR reaction contained 12.5 µl QuantiTect Probe PCR Master Mix (QIAGEN), 600 nM of each primer and 300 nM of FAM-labeled probe (IDT), 1.25 µl of a TaqMan VIC-labeled RNase-

P primer probe mix (Fisher Sci, Cat. #4316844). For analysis of splenocytes, reactions contained 1 µg DNA extracted from splenocytes as template. To analyze EBV in peripheral blood, DNA was extracted from 50 µl of blood collected via cardiac puncture or retro-orbital bleed using the DNeasy Blood and Tissue Kit (QIAGEN) and eluted in 50 µl of Buffer AE (QIAGEN). 10 µl of extracted DNA was used as template in qPCR. Reactions were heated to 95ºC for 15 minutes to activate DNA polymerase followed by 50 cycles of 95ºC for 15 s 60ºC for 60 s, on an Applied Biosystems QuantStudio 7 Flex Real Time PCR System. Synthetic DNA fragments containing either the IR1 or BALF5 target gene as well as flanking genomic regions were synthesized as double-stranded DNA gBlocks (IDT) and were used to generate a standard curve with known gene copy numbers ranging from 10^6-10^0 copies/µl. The viral copy number was determined by interpolating from the standard curve. Serial dilutions of reference standard were used to experimentally determine a limit of detection of 6.25 copies, which corresponds to the amount of template that can be detected in > 95% of reactions. For graphical purposes, samples with no amplification or those yielding values below the limit of detection were assigned a value of 0.625 copies.

Immunohistochemistry and in situ Hybridization

Formalin-fixed paraffin-embedded tissues were sectioned at 4 µm onto positively charged slides and incubated for 60 minutes at 60°C. The slides were then dewaxed and stained on a Leica BOND RX autostainer (Leica, Buffalo Grove, IL) using Leica Bond reagents for deparaffinization (Bond Dewax Solution, AR9222).

For immunohistochemistry (IHC), antigen retrieval was conducted at 100°C for 20 minutes with Bond Epitope Retrieval Solution 2 (Leica, AR9640). Endogenous peroxidase was blocked using 3% H_2O_2 (5 minutes), followed by protein blocking with TCT buffer (0.05M Tris, 0.15M NaCl, 0.25% Casein, 0.1% Tween 20, 0.05% ProClin300, pH 7.6) for 10 minutes. Anti-CD20 (mouse polyclonal, Dako clone L26 at a dilution of 1:4000) was applied to slides for 60 minutes at room temperature. For detection, slides were then incubated with Refine Rabbit Polymer HRP (Leica DS9800), or PowerVision Mouse Polymer (Leica PV6114) for 12 minutes, mixed Refine DAB (Leica DS9800) for 10 minutes, followed by counterstaining with Refine Hematoxylin (Leica DS9800) for 4 minutes. Slides were then dehydrated, cleared, and coverslipped with permanent mounting media.

For in situ hybridization (ISH), antigen retrieval was conducted with Epitope Retrieval Solution 2 for 15 minutes at 95°C, protease digestion at 40°C for 15 minutes and rinses after each step (Bond Wash Solution). All other steps were performed at ambient temperature. Staining was performed with RNAscope 2.5 LS Reagent Kit – BROWN (ACD Bio Techne, Cat. #322100). RNAscope 2.5 LS Positive Control Probe Human PPIB (ACD Bio Techne, Cat. #313908), Negative Control probe dapB (ACD Bio Techne, Cat. #312038), and EBV RNAscope 2.5 LS Probe-V-EBER1 probe (ACD Bio Techne, Cat. #310278) was applied and incubated at 42°C for 120 minutes. Chromogenic staining was performed using BOND Polymer Refine Detection (Leica DS9800). Slides were then dehydrated, cleared, and coverslipped with permanent mounting media and imaged on Evident VS200.

Statistical analysis

GraphPad Prism (version 10) was used to perform Mann-Whitney and Kruskal-Wallis tests. P values < 0.05 were regarded as significant and displayed.

Declaration of generative AI and AI-assisted technologies in the writing process

During the preparation of this work the author(s) used Microsoft Copilot in order to generate suggested titles for the manuscript. After using this tool/service, the author(s) reviewed and edited the content as needed and take(s) full responsibility for the content of the publication.

Data and code availability

X-ray coordinates and structure factors are deposited in the RCSB PDB under accession code PDB: 9PF9. Negative-staining EM maps are deposited in the EMDB with accession codes: EMD-71585 (Negative stain EM map of EBV glycoprotein gH/gL in complex with glycoprotein gp42 and Fab ATX-42-1.1 open conformation), EMD-71586 (Negative stain EM map of EBV glycoprotein gH/gL in complex with glycoprotein gp42 and Fab ATX-42-2 Open conformation), EMD-71587 (Negative stain EM map of EBV glycoprotein gH/gL in complex with glycoprotein gp42 and Fab ATX-42-1.1 partially open conformation), EMD-71588 (Negative stain EM map of EBV glycoprotein gH/gL in complex with glycoprotein gp42 and Fab ATX-42-2 closed conformation), EMD-71589 (Negative stain EM map of EBV glycoprotein gH/gL in complex with glycoprotein gp42 and HLA-DR1 Beta chain), EMD-71590 (Negative Stain EM map of EBV glycoprotein gp350 in complex with ATX-350-1 Fab and 72A1 Fab), EMD-71592 (Negative Stain EM map of EBV glycoprotein gp350 in complex with ATX-350-2 Fab), EMD-71593 (Negative Stain EM map of EBV glycoprotein gp350 in complex with ATX-350-1 Fab), EMD-71594 (Negative Stain EM map of EBV glycoprotein gp350 in complex with 72A1 Fab).

2.6 Acknowledgments

This research was supported by NIAID R01AI147846 and NCI R01CA285227 (to ATM.) NLHBI R01HL136135 (to HPK) and by NIH P30 CA015704 to the Fred Hutch/University of Washington/Seattle Children's Cancer Consortium, which includes the Flow Cytometry Shared Resource, RRID:SCR_022613, the Antibody Technology Shared Resource, RRID:SCR_022608, the Comparative Medicine Shared Resource, RRID:SCR_022610, the Electron Microscopy Shared Resource, RRID:SCR_022611, the Cellular Imaging Shared Resource, RRID:SCR_022609, the Immune Monitoring Shared Resource, RRID:SCR_022615, the Genomics and Bioinformatics Shared Resource, RRID:SCR_022606, and the Experimental Histopathology Shared Resource, RRID:SCR_022612. A portion of this research was supported by the NIH S10 instrumentation grant 1S10OD028581-01. X-ray diffraction data was collected at the Berkeley Center for Structural Biology. The Berkeley Center for Structural Biology is supported by the Howard Hughes Medical Institute, Participating Research Team members, and the National Institutes of Health, National Institute of General Medical Sciences, ALS-ENABLE grant P30 GM124169. The Advanced Light Source is a Department of Energy Office of Science User Facility under Contract No. DE-AC02-05CH11231. The content is solely the responsibility of the authors and does not necessarily represent the official views of the National Institutes of Health. The Experimental Histopathology Shared Resource equipment is supported by a grant from the M.J. Murdock Charitable Trust grant SR-202221337. This work was also supported by the Evergreen fund from The Fred Hutchinson Cancer Center. Further funding has been received from the José Carreras/E. Donnall Thomas Endowed Chair for Cancer Research, the Stephanus Family Endowed Chair for Cell and Gene Therapy, as Markey Molecular Medicine Investigator.

We thank the J. B. Pendleton Charitable Trust for its generous support of Formulatrix robotic instruments. We thank Masaru Kanekiyo for the kind gift of the 769A9 and 770E11 mAbs.

2.7 Declarations of Interests

ATM and CBC are listed as inventors on a patent application (63/771,474) related to the monoclonal antibodies described herein.

2.8 Author Contributions

Conceptualization: ATM and CBC

Investigation: CBC, KL, ARD, Y-HW, NTA, GK, SCS, SRH, KRE, NVG, SR

Formal analysis: CBC, KL, ARD, Y-HW, NTA, GK, SCS, SRH, KRE, MP, ATM, SR

Visualization: CBC, KL, GK, ARD, RI

Resources: MP, HPK, SR, ATM

Writing- original draft: ATM and CBC

Review and editing: all

Funding acquisition: ATM, MP, HPK

2.9 Chapter 2 Bibliography

1. Cohen JI. Epstein-Barr virus infection. N Engl J Med. 2000;343(7):481-92. doi: 10.1056/NEJM200008173430707. PubMed PMID: 10944566.
2. Henle G, Henle W, Diehl V. Relation of Burkitt's tumor-associated herpes-ytpe virus to infectious mononucleosis. Proceedings of the National Academy of Sciences. 1968;59(1):94-101. doi: 10.1073/pnas.59.1.94.
3. Dunmire SK, Hogquist KA, Balfour HH. Infectious Mononucleosis. Curr Top Microbiol Immunol. 2015;390(Pt 1):211-40. doi: 10.1007/978-3-319-22822-8_9. PubMed PMID: 26424648; PMCID: PMC4670567.
4. Levin LI, Munger KL, O'Reilly EJ, Falk KI, Ascherio A. Primary infection with the Epstein-Barr virus and risk of multiple sclerosis. Ann Neurol. 2010;67(6):824-30. Epub 2010/06/03. doi: 10.1002/ana.21978. PubMed PMID: 20517945; PMCID: PMC3089959.
5. Handel AE, Williamson AJ, Disanto G, Handunnetthi L, Giovannoni G, Ramagopalan SV. An updated meta-analysis of risk of multiple sclerosis following infectious mononucleosis. PLoS One. 2010;5(9). Epub 2010/09/09. doi: 10.1371/journal.pone.0012496. PubMed PMID: 20824132; PMCID: PMC2931696.
6. Thacker EL, Mirzaei F, Ascherio A. Infectious mononucleosis and risk for multiple sclerosis: a meta-analysis. Ann Neurol. 2006;59(3):499-503. Epub 2006/02/28. doi: 10.1002/ana.20820. PubMed PMID: 16502434.
7. Munger KL, Levin LI, O'Reilly EJ, Falk KI, Ascherio A. Anti-Epstein-Barr virus antibodies as serological markers of multiple sclerosis: a prospective study among United States military personnel. Mult Scler. 2011;17(10):1185-93. Epub 2011/06/21. doi: 10.1177/1352458511408991. PubMed PMID: 21685232; PMCID: PMC3179777.
8. Nielsen TR, Rostgaard K, Askling J, Steffensen R, Oturai A, Jersild C, Koch-Henriksen N, Sørensen PS, Hjalgrim H. Effects of infectious mononucleosis and HLA-DRB1*15 in multiple sclerosis. Mult Scler. 2009;15(4):431-6. Epub 2009/01/21. doi: 10.1177/1352458508100037. PubMed PMID: 19153174.
9. Ascherio A, Munger KL. Epstein-barr virus infection and multiple sclerosis: a review. J Neuroimmune Pharmacol. 2010;5(3):271-7. Epub 2010/04/07. doi: 10.1007/s11481-010-9201-3. PubMed PMID: 20369303.
10. Bjornevik K, Cortese M, Healy BC, Kuhle J, Mina MJ, Leng Y, Elledge SJ, Niebuhr DW, Scher AI, Munger KL, Ascherio A. Longitudinal analysis reveals high prevalence of Epstein-Barr virus associated with multiple sclerosis. Science. 2022;375(6578):296-301. Epub 20220113. doi: 10.1126/science.abj8222. PubMed PMID: 35025605.
11. Robinson WH, Younis S, Love ZZ, Steinman L, Lanz TV. Epstein-Barr virus as a potentiator of autoimmune diseases. Nat Rev Rheumatol. 2024;20(11):729-40. Epub 20241010. doi: 10.1038/s41584-024-01167-9. PubMed PMID: 39390260.
12. Balandraud N, Roudier J. Epstein-Barr virus and rheumatoid arthritis. Joint Bone Spine. 2018;85(2):165-70. Epub 2017/05/14. doi: 10.1016/j.jbspin.2017.04.011. PubMed PMID: 28499895.
13. Fechtner S, Berens H, Bemis E, Johnson RL, Guthridge CJ, Carlson NE, Demoruelle MK, Harley JB, Edison JD, Norris JA, Robinson WH, Deane KD, James JA, Holers VM. Antibody Responses to Epstein-Barr Virus in the Preclinical Period of Rheumatoid Arthritis Suggest the Presence of Increased Viral Reactivation Cycles. Arthritis Rheumatol. 2021. Epub 2021/10/05. doi: 10.1002/art.41994. PubMed PMID: 34605217.
14. Su Y, Yuan D, Chen DG, Ng RH, Wang K, Choi J, Li S, Hong S, Zhang R, Xie J, Kornilov SA, Scherler K, Pavlovitch-Bedzyk AJ, Dong S, Lausted C, Lee I, Fallen S, Dai CL, Baloni P, Smith B, Duvvuri VR, Anderson KG, Li J, Yang F, Duncombe CJ, McCulloch DJ, Rostomily C, Troisch P, Zhou J, Mackay S, DeGottardi Q, May DH, Taniguchi R, Gittelman RM, Klinger M, Snyder TM, Roper R, Wojciechowska G, Murray K, Edmark R, Evans S, Jones L, Zhou Y, Rowen L, Liu R, Chour W, Algren HA, Berrington WR, Wallick JA, Cochran RA, Micikas ME, Wrin T, Petropoulos CJ, Cole HR, Fischer TD, Wei W, Hoon DSB, Price ND, Subramanian N, Hill JA, Hadlock J, Magis AT, Ribas A, Lanier LL, Boyd SD, Bluestone JA, Chu H, Hood L, Gottardo R, Greenberg PD, Davis MM, Goldman JD, Heath JR. Multiple early factors anticipate post-acute COVID-19 sequelae. Cell. 2022;185(5):881-95.e20. Epub 20220125. doi: 10.1016/j.cell.2022.01.014. PubMed PMID: 35216672; PMCID: PMC8786632.
15. Bernal KDE, Whitehurst CB. Incidence of Epstein-Barr virus reactivation is elevated in COVID-19 patients. Virus Res. 2023;334:199157. Epub 20230626. doi: 10.1016/j.virusres.2023.199157. PubMed PMID: 37364815; PMCID: PMC10292739.
16. Chen T, Song J, Liu H, Zheng H, Chen C. Positive Epstein-Barr virus detection in coronavirus disease 2019 (COVID-19) patients. Sci Rep. 2021;11(1):10902. Epub 20210525. doi: 10.1038/s41598-021-90351-y. PubMed PMID: 34035353; PMCID: PMC8149409.

17. Wong Y, Meehan MT, Burrows SR, Doolan DL, Miles JJ. Estimating the global burden of Epstein-Barr virus-related cancers. J Cancer Res Clin Oncol. 2022;148(1):31-46. Epub 20211027. doi: 10.1007/s00432-021-03824-y. PubMed PMID: 34705104; PMCID: PMC8752571.
18. Khan G, Fitzmaurice C, Naghavi M, Ahmed LA. Global and regional incidence, mortality and disability-adjusted life-years for Epstein-Barr virus-attributable malignancies, 1990–2017. BMJ Open. 2020;10(8):e037505. doi: 10.1136/bmjopen-2020-037505.
19. Taylor GS, Long HM, Brooks JM, Rickinson AB, Hislop AD. The Immunology of Epstein-Barr Virus–Induced Disease. Annual Review of Immunology. 2015;33(1):787-821. doi: 10.1146/annurev-immunol-032414-112326.
20. Escalante GM, Mutsvunguma LZ, Muniraju M, Rodriguez E, Ogembo JG. Four Decades of Prophylactic EBV Vaccine Research: A Systematic Review and Historical Perspective. Frontiers in Immunology. 2022;13. doi: 10.3389/fimmu.2022.867918.
21. Bu G-L, Xie C, Kang Y-F, Zeng M-S, Sun C. How EBV Infects: The Tropism and Underlying Molecular Mechanism for Viral Infection. Viruses. 2022;14(11):2372. doi: 10.3390/v14112372.
22. Connolly SA, Jardetzky TS, Longnecker R. The structural basis of herpesvirus entry. Nat Rev Microbiol. 2021;19(2):110-21. Epub 20201021. doi: 10.1038/s41579-020-00448-w. PubMed PMID: 33087881; PMCID: PMC8579738.
23. Gonzalez-Del Pino GL, Heldwein EE. Well Put Together-A Guide to Accessorizing with the Herpesvirus gH/gL Complexes. Viruses. 2022;14(2). Epub 20220130. doi: 10.3390/v14020296. PubMed PMID: 35215889; PMCID: PMC8874593.
24. Li Y, Zhang H, Sun C, Dong XD, Xie C, Liu YT, Lin RB, Kong XW, Hu ZL, Ma XY, Dai DL, Zhu QY, Li YC, Li Y, Liu SX, Yuan L, Zhou PH, Gao S, Tang YP, Yang JY, Han P, McGuire AT, Zhao B, Bei JX, Robertson E, Zeng YX, Zhong Q, Zeng MS. R9AP is a common receptor for EBV infection in epithelial cells and B cells. Nature. 2025. Epub 20250618. doi: 10.1038/s41586-025-09166-w. PubMed PMID: 40533557.
25. Fingeroth JD, Weis JJ, Tedder TF, Strominger JL, Biro PA, Fearon DT. Epstein-Barr virus receptor of human B lymphocytes is the C3d receptor CR2. Proc Natl Acad Sci U S A. 1984;81(14):4510-4. doi: 10.1073/pnas.81.14.4510. PubMed PMID: 6087328; PMCID: PMC345620.
26. Tanner J, Weis J, Fearon D, Whang Y, Kieff E. Epstein-barr virus gp350/220 binding to the B lymphocyte C3d receptor mediates adsorption, capping, and endocytosis. Cell. 1987;50(2):203-13. doi: 10.1016/0092-8674(87)90216-9.
27. Ogembo JG, Kannan L, Ghiran I, Nicholson-Weller A, Finberg RW, Tsokos GC, Fingeroth JD. Human Complement Receptor Type 1/CD35 Is an Epstein-Barr Virus Receptor. Cell Reports. 2013;3(2):371-85. doi: 10.1016/j.celrep.2013.01.023.
28. Kirschner AN, Omerovic J, Popov B, Longnecker R, Jardetzky TS. Soluble Epstein-Barr virus glycoproteins gH, gL, and gp42 form a 1:1:1 stable complex that acts like soluble gp42 in B-cell fusion but not in epithelial cell fusion. J Virol. 2006;80(19):9444-54. doi: 10.1128/JVI.00572-06. PubMed PMID: 16973550; PMCID: PMC1617263.
29. Sathiyamoorthy K, Jiang J, Hu YX, Rowe CL, Möhl BS, Chen J, Jiang W, Mellins ED, Longnecker R, Zhou ZH, Jardetzky TS. Assembly and Architecture of the EBV B Cell Entry Triggering Complex. PLOS Pathogens. 2014;10(8):e1004309. doi: 10.1371/journal.ppat.1004309.
30. Haan KM, Kwok WW, Longnecker R, Speck P. Epstein-Barr virus entry utilizing HLA-DP or HLA-DQ as a coreceptor. J Virol. 2000;74(5):2451-4. doi: 10.1128/jvi.74.5.2451-2454.2000. PubMed PMID: 10666279; PMCID: PMC111730.
31. Spriggs MK, Armitage RJ, Comeau MR, Strockbine L, Farrah T, Macduff B, Ulrich D, Alderson MR, Mullberg J, Cohen JI. The extracellular domain of the Epstein-Barr virus BZLF2 protein binds the HLA-DR beta chain and inhibits antigen presentation. J Virol. 1996;70(8):5557-63. doi: 10.1128/JVI.70.8.5557-5563.1996. PubMed PMID: 8764069; PMCID: PMC190515.
32. Sathiyamoorthy K, Hu YX, Möhl BS, Chen J, Longnecker R, Jardetzky TS. Structural basis for Epstein–Barr virus host cell tropism mediated by gp42 and gHgL entry glycoproteins. Nature Communications. 2016;7(1):13557. doi: 10.1038/ncomms13557.
33. Silva AL, Omerovic J, Jardetzky TS, Longnecker R. Mutational analyses of Epstein-Barr virus glycoprotein 42 reveal functional domains not involved in receptor binding but required for membrane fusion. J Virol. 2004;78(11):5946-56. doi: 10.1128/JVI.78.11.5946-5956.2004. PubMed PMID: 15140992; PMCID: PMC415818.

34. Kirschner AN, Sorem J, Longnecker R, Jardetzky TS. Structure of Epstein-Barr Virus Glycoprotein 42 Suggests a Mechanism for Triggering Receptor-Activated Virus Entry. Structure. 2009;17(2):223-33. doi: 10.1016/j.str.2008.12.010.
35. Mullen MM, Haan KM, Longnecker R, Jardetzky TS. Structure of the Epstein-Barr Virus gp42 Protein Bound to the MHC Class II Receptor HLA-DR1. Molecular Cell. 2002;9(2):375-85. doi: 10.1016/S1097-2765(02)00465-3.
36. Zhao G-X, Fang X-Y, Bu G-L, Chen S-J-B, Sun C, Li T, Xie C, Wang Y, Li S-X, Meng N, Feng G-K, Zhong Q, Kong X-W, Liu Z, Zeng M-S. Potent human monoclonal antibodies targeting Epstein-Barr virus gp42 reveal vulnerable sites for virus infection. Cell Reports Medicine. 2024;5(5):101573. doi: 10.1016/j.xcrm.2024.101573.
37. Bu W, Kumar A, Board NL, Kim J, Dowdell K, Zhang S, Lei Y, Hostal A, Krogmann T, Wang Y, Pittaluga S, Marcotrigiano J, Cohen JI. Epstein-Barr virus gp42 antibodies reveal sites of vulnerability for receptor binding and fusion to B cells. Immunity. 2024;57(3):559-73.e6. doi: 10.1016/j.immuni.2024.02.008. PubMed PMID: 38479361; PMCID: PMC11000673.
38. Hislop AD, Taylor GS, Sauce D, Rickinson AB. Cellular Responses to Viral Infection in Humans: Lessons from Epstein-Barr Virus. Annual Review of Immunology. 2007;25(1):587-617. doi: 10.1146/annurev.immunol.25.022106.141553.
39. Rickinson AB, Long HM, Palendira U, Munz C, Hislop AD. Cellular immune controls over Epstein-Barr virus infection: new lessons from the clinic and the laboratory. Trends Immunol. 2014;35(4):159-69. Epub 20140301. doi: 10.1016/j.it.2014.01.003. PubMed PMID: 24589417.
40. Thorley-Lawson DA, Duca KA, Shapiro M. Epstein-Barr virus: a paradigm for persistent infection - for real and in virtual reality. Trends Immunol. 2008;29(4):195-201. Epub 2008/03/11. doi: 10.1016/j.it.2008.01.006. PubMed PMID: 18328785.
41. da Silva SR, de Oliveira DE. HIV, EBV and KSHV: viral cooperation in the pathogenesis of human malignancies. Cancer letters. 2011;305(2):175-85. Epub 2011/03/16. doi: 10.1016/j.canlet.2011.02.007. PubMed PMID: 21402436.
42. Grulich AE, van Leeuwen MT, Falster MO, Vajdic CM. Incidence of cancers in people with HIV/AIDS compared with immunosuppressed transplant recipients: a meta-analysis. Lancet. 2007;370(9581):59-67. Epub 2007/07/10. doi: 10.1016/s0140-6736(07)61050-2. PubMed PMID: 17617273.
43. Law N, Logan C, Taplitz R. EBV Reactivation and Disease in Allogeneic Hematopoietic Stem Cell Transplant (HSCT) Recipients and Its Impact on HSCT Outcomes. Viruses. 2024;16(8). Epub 20240814. doi: 10.3390/v16081294. PubMed PMID: 39205268; PMCID: PMC11359191.
44. Dharnidharka VR, Ruzinova MB, Marks LJ. Post-Transplant Lymphoproliferative Disorders. Semin Nephrol. 2024;44(1):151503. Epub 20240322. doi: 10.1016/j.semnephrol.2024.151503. PubMed PMID: 38519279; PMCID: PMC11213680.
45. Cockfield SM. Identifying the patient at risk for post-transplant lymphoproliferative disorder. Transpl Infect Dis. 2001;3(2):70-8. doi: 10.1034/j.1399-3062.2001.003002070.x. PubMed PMID: 11395972.
46. Walker RC, Marshall WF, Strickler JG, Wiesner RH, Velosa JA, Habermann TM, McGregor CG, Paya CV. Pretransplantation assessment of the risk of lymphoproliferative disorder. Clin Infect Dis. 1995;20(5):1346-53. doi: 10.1093/clinids/20.5.1346. PubMed PMID: 7620022.
47. Glotz D, Chapman JR, Dharnidharka VR, Hanto DW, Castro MC, Hirsch HH, Leblond V, Mehta AK, Moulin B, Pagliuca A, Pascual J, Rickinson AB, Russo FP, Trappe RU, Webster AC, Zuckermann AO, Gross TG. The Seville expert workshop for progress in post-transplant lymphoproliferative disorders. Transplantation. 2012;94(8):784-93. doi: 10.1097/TP.0b013e318269e64f. PubMed PMID: 22992767.
48. Haque T, Johannessen I, Dombagoda D, Sengupta C, Burns DM, Bird P, Hale G, Mieli-Vergani G, Crawford DH. A mouse monoclonal antibody against Epstein-Barr virus envelope glycoprotein 350 prevents infection both in vitro and in vivo. The Journal of Infectious Diseases. 2006;194(5):584-7. doi: 10.1086/505912.
49. Hong J, Zhong L, Zheng Q, Wu Q, Zha Z, Wei D, Chen H, Zhang W, Zhang S, Huang Y, Chen K, Chen J, Li S, Zeng MS, Zeng YX, Xia N, Zhang X, Xu M, Chen Y. A Neutralizing Antibody Targeting gH Provides Potent Protection against EBV Challenge In Vivo. J Virol. 2022;96(8):e0007522. Epub 20220329. doi: 10.1128/jvi.00075-22. PubMed PMID: 35348362; PMCID: PMC9044928.
50. Zhu QY, Shan S, Yu J, Peng SY, Sun C, Zuo Y, Zhong LY, Yan SM, Zhang X, Yang Z, Peng YJ, Shi X, Cao SM, Wang X, Zeng MS, Zhang L. A potent and protective human neutralizing antibody targeting a novel vulnerable site of Epstein-Barr virus. Nat Commun. 2021;12(1):6624. Epub 20211116. doi: 10.1038/s41467-021-26912-6. PubMed PMID: 34785638; PMCID: PMC8595662.

51. Chen WH, Kim J, Bu W, Board NL, Tsybovsky Y, Wang Y, Hostal A, Andrews SF, Gillespie RA, Choe M, Stephens T, Yang ES, Pegu A, Peterson CE, Fisher BE, Mascola JR, Pittaluga S, McDermott AB, Kanekiyo M, Joyce MG, Cohen JI. Epstein-Barr virus gH/gL has multiple sites of vulnerability for virus neutralization and fusion inhibition. Immunity. 2022;55(11):2135-48 e6. Epub 20221027. doi: 10.1016/j.immuni.2022.10.003. PubMed PMID: 36306784; PMCID: PMC9815946.
52. Zhang X, Hong J, Zhong L, Wu Q, Zhang S, Zhu Q, Chen H, Wei D, Li R, Zhang W, Zhang X, Wang G, Zhou X, Chen J, Kang Y, Zha Z, Duan X, Huang Y, Sun C, Kong X, Zhou Y, Chen Y, Ye X, Feng Q, Li S, Xiang T, Gao S, Zeng MS, Zheng Q, Chen Y, Zeng YX, Xia N, Xu M. Protective anti-gB neutralizing antibodies targeting two vulnerable sites for EBV-cell membrane fusion. Proc Natl Acad Sci U S A. 2022;119(32):e2202371119. Epub 20220802. doi: 10.1073/pnas.2202371119. PubMed PMID: 35917353; PMCID: PMC9371650.
53. Hong J, Zhong L, Liu L, Wu Q, Zhang W, Chen K, Wei D, Sun H, Zhou X, Zhang X, Kang YF, Huang Y, Chen J, Wang G, Zhou Y, Chen Y, Feng QS, Yu H, Li S, Zeng MS, Zeng YX, Xu M, Zheng Q, Chen Y, Zhang X, Xia N. Non-overlapping epitopes on the gHgL-gp42 complex for the rational design of a triple-antibody cocktail against EBV infection. Cell Rep Med. 2023;4(11):101296. doi: 10.1016/j.xcrm.2023.101296. PubMed PMID: 37992686; PMCID: PMC10694767.
54. Muhe J, Aye PP, Quink C, Eng JY, Engelman K, Reimann KA, Wang F. Neutralizing antibodies against Epstein-Barr virus infection of B cells can protect from oral viral challenge in the rhesus macaque animal model. Cell Rep Med. 2021;2(7):100352. Epub 20210721. doi: 10.1016/j.xcrm.2021.100352. PubMed PMID: 34337567; PMCID: PMC8324488.
55. Singh S, Homad LJ, Akins NR, Stoffers CM, Lackhar S, Malhi H, Wan Y-H, Rawlings DJ, McGuire AT. Neutralizing Antibodies Protect against Oral Transmission of Lymphocryptovirus. Cell Reports Medicine. 2020;1(3):100033. doi: 10.1016/j.xcrm.2020.100033.
56. Hoffman GJ, Lazarowitz SG, Hayward SD. Monoclonal antibody against a 250,000-dalton glycoprotein of Epstein-Barr virus identifies a membrane antigen and a neutralizing antigen. Proceedings of the National Academy of Sciences. 1980;77(5):2979-83. doi: 10.1073/pnas.77.5.2979.
57. Tanner JE, Hu J, Alfieri C. Construction and Characterization of a Humanized Anti-Epstein-Barr Virus gp350 Antibody with Neutralizing Activity in Cell Culture. Cancers (Basel). 2018;10(4). Epub 20180409. doi: 10.3390/cancers10040112. PubMed PMID: 29642526; PMCID: PMC5923367.
58. Mutsvunguma LZ, Rodriguez E, Escalante GM, Muniraju M, Williams JC, Warden C, Qin H, Wang J, Wu X, Barasa A, Mulama DH, Mwangi W, Ogembo JG. Identification of multiple potent neutralizing and non-neutralizing antibodies against Epstein-Barr virus gp350 protein with potential for clinical application and as reagents for mapping immunodominant epitopes. Virology. 2019;536:1-15. doi: 10.1016/j.virol.2019.07.026.
59. Snijder J, Ortego MS, Weidle C, Stuart AB, Gray MD, McElrath MJ, Pancera M, Veesler D, McGuire AT. An antibody targeting the fusion machinery neutralizes dual-tropic infection and defines a site of vulnerability on Epstein-Barr virus. Immunity. 2018;48(4):799-811.e9. doi: 10.1016/j.immuni.2018.03.026.
60. Joyce MG, Bu W, Chen W-H, Gillespie RA, Andrews SF, Wheatley AK, Tsybovsky Y, Jensen JL, Stephens T, Prabhakaran M, Fisher BE, Narpala SR, Bagchi M, McDermott AB, Nabel GJ, Kwong PD, Mascola JR, Cohen JI, Kanekiyo M. Structural basis for complement receptor engagement and virus neutralization through Epstein-Barr virus gp350. Immunity. 2025;58(2):295-308.e5. doi: 10.1016/j.immuni.2025.01.010.
61. Alloy Therapeutics Inc. Alloy Therapeutics 2025 [June 26, 2025]. Available from: https://alloytx.com/.
62. Li QX, Young LS, Niedobitek G, Dawson CW, Birkenbach M, Wang F, Rickinson AB. Epstein-Barr virus infection and replication in a human epithelial cell system. Nature. 1992;356(6367):347-50. doi: 10.1038/356347a0. PubMed PMID: 1312681.
63. Tsai MH, Raykova A, Klinke O, Bernhardt K, Gartner K, Leung CS, Geletneky K, Sertel S, Munz C, Feederle R, Delecluse HJ. Spontaneous lytic replication and epitheliotropism define an Epstein-Barr virus strain found in carcinomas. Cell Rep. 2013;5(2):458-70. Epub 20131010. doi: 10.1016/j.celrep.2013.09.012. PubMed PMID: 24120866.
64. Minab R, Bu W, Nguyen H, Wall A, Sholukh AM, Huang ML, Ortego M, Krantz EM, Irvine M, Casper C, Orem J, McGuire AT, Cohen JI, Gantt S. Maternal Epstein-Barr Virus-Specific Antibodies and Risk of Infection in Ugandan Infants. J Infect Dis. 2021;223(11):1897-904. doi: 10.1093/infdis/jiaa654. PubMed PMID: 33095855; PMCID: PMC8176630.
65. Bilger A, Plowshay J, Ma S, Nawandar D, Barlow EA, Romero-Masters JC, Bristol JA, Li Z, Tsai M-H, Delecluse H-J, Kenney SC. Leflunomide/teriflunomide inhibit Epstein-Barr virus (EBV)-induced lymphoproliferative disease and lytic viral replication. Oncotarget. 2017;8(27):44266-80. doi: 10.18632/oncotarget.17863.

66. Delecluse S, Poirey R, Zeier M, Schnitzler P, Behrends U, Tsai M-H, Delecluse H-J. Identification and Cloning of a New Western Epstein-Barr Virus Strain That Efficiently Replicates in Primary B Cells. Journal of Virology. 2020;94(10):10.1128/jvi.01918-19. doi: 10.1128/jvi.01918-19.
67. Slabik C, Kalbarczyk M, Danisch S, Zeidler R, Klawonn F, Volk V, Krönke N, Feuerhake F, Ferreira de Figueiredo C, Blasczyk R, Olbrich H, Theobald SJ, Schneider A, Ganser A, von Kaisenberg C, Lienenklaus S, Bleich A, Hammerschmidt W, Stripecke R. CAR-T Cells Targeting Epstein-Barr Virus gp350 Validated in a Humanized Mouse Model of EBV Infection and Lymphoproliferative Disease. Molecular Therapy - Oncolytics. 2020;18:504-24. doi: 10.1016/j.omto.2020.08.005.
68. Li Q, Turk SM, Hutt-Fletcher LM. The Epstein-Barr virus (EBV) BZLF2 gene product associates with the gH and gL homologs of EBV and carries an epitope critical to infection of B cells but not of epithelial cells. J Virol. 1995;69(7):3987-94. doi: 10.1128/JVI.69.7.3987-3994.1995. PubMed PMID: 7539502; PMCID: PMC189130.
69. Wu Q, Zhong L, Wei D, Zhang W, Hong J, Kang Y, Chen K, Huang Y, Zheng Q, Xu M, Zeng MS, Zeng YX, Xia N, Zhao Q, Krummenacher C, Chen Y, Zhang X. Neutralizing antibodies against EBV gp42 show potent in vivo protection and define novel epitopes. Emerg Microbes Infect. 2023;12(2):2245920. doi: 10.1080/22221751.2023.2245920. PubMed PMID: 37542379; PMCID: PMC10443957.
70. Cui X, Cao Z, Ishikawa Y, Cui S, Imadome KI, Snapper CM. Immunization with Epstein-Barr Virus Core Fusion Machinery Envelope Proteins Elicit High Titers of Neutralizing Activities and Protect Humanized Mice from Lethal Dose EBV Challenge. Vaccines (Basel). 2021;9(3). Epub 20210319. doi: 10.3390/vaccines9030285. PubMed PMID: 33808755; PMCID: PMC8003492.
71. Malhi H, Homad LJ, Wan Y-H, Poudel B, Fiala B, Borst AJ, Wang JY, Walkey C, Price J, Wall A, Singh S, Moodie Z, Carter L, Handa S, Correnti CE, Stoddard BL, Veesler D, Pancera M, Olson J, King NP, McGuire AT. Immunization with a self-assembling nanoparticle vaccine displaying EBV gH/gL protects humanized mice against lethal viral challenge. Cell Reports Medicine. 2022;3(6):100658. doi: 10.1016/j.xcrm.2022.100658.
72. Edwards KR, Malhi H, Schmidt K, Davis AR, Homad LJ, Warner NL, Chhan CB, Scharffenberger SC, Gaffney K, Hinkley T, Potchen NB, Wang JY, Price J, McElrath MJ, Olson J, King NP, Lund JM, Moodie Z, Erasmus JH, McGuire AT. A gH/gL-encoding replicon vaccine elicits neutralizing antibodies that protect humanized mice against EBV challenge. npj Vaccines. 2024;9(1):120. doi: 10.1038/s41541-024-00907-y.
73. Wu X, Yang Z-Y, Li Y, Hogerkorp C-M, Schief WR, Seaman MS, Zhou T, Schmidt SD, Wu L, Xu L, Longo NS, McKee K, O'Dell S, Louder MK, Wycuff DL, Feng Y, Nason M, Doria-Rose N, Connors M, Kwong PD, Roederer M, Wyatt RT, Nabel GJ, Mascola JR. Rational Design of Envelope Identifies Broadly Neutralizing Human Monoclonal Antibodies to HIV-1. Science. 2010;329(5993):856-61. doi: 10.1126/science.1187659.
74. Tierney RJ, Steven N, Young LS, Rickinson AB. Epstein-Barr virus latency in blood mononuclear cells: analysis of viral gene transcription during primary infection and in the carrier state. J Virol. 1994;68(11):7374-85. doi: 10.1128/JVI.68.11.7374-7385.1994. PubMed PMID: 7933121; PMCID: PMC237180.
75. Kanekiyo M, Bu W, Joyce MG, Meng G, Whittle JRR, Baxa U, Yamamoto T, Narpala S, Todd J-P, Rao SS, McDermott AB, Koup RA, Rossmann MG, Mascola JR, Graham BS, Cohen JI, Nabel GJ. Rational Design of an Epstein-Barr Virus Vaccine Targeting the Receptor-Binding Site. Cell. 2015;162(5):1090-100. doi: 10.1016/j.cell.2015.07.043.
76. Janz A, Oezel M, Kurzeder C, Mautner J, Pich D, Kost M, Hammerschmidt W, Delecluse HJ. Infectious Epstein-Barr virus lacking major glycoprotein BLLF1 (gp350/220) demonstrates the existence of additional viral ligands. J Virol. 2000;74(21):10142-52. doi: 10.1128/jvi.74.21.10142-10152.2000. PubMed PMID: 11024143; PMCID: PMC102053.
77. Fujiwara S, Matsuda G, Imadome K. Humanized mouse models of epstein-barr virus infection and associated diseases. Pathogens. 2013;2(1):153-76. Epub 20130314. doi: 10.3390/pathogens2010153. PubMed PMID: 25436886; PMCID: PMC4235711.
78. Fujiwara S, Nakamura H. Animal Models for Gammaherpesvirus Infections: Recent Development in the Analysis of Virus-Induced Pathogenesis. Pathogens. 2020;9(2). Epub 20200212. doi: 10.3390/pathogens9020116. PubMed PMID: 32059472; PMCID: PMC7167833.
79. Jiang R, Gu X, Nathan CO, Hutt-Fletcher L. Laser-capture microdissection of oropharyngeal epithelium indicates restriction of Epstein-Barr virus receptor/CD21 mRNA to tonsil epithelial cells. J Oral Pathol Med. 2008;37(10):626-33. Epub 20080815. doi: 10.1111/j.1600-0714.2008.00681.x. PubMed PMID: 18710421; PMCID: PMC2584167.
80. Hayman IR, Temple RM, Burgess CK, Ferguson M, Liao J, Meyers C, Sample CE. New insight into Epstein-Barr virus infection using models of stratified epithelium. PLoS Pathog. 2023;19(1):e1011040. Epub 20230111. doi: 10.1371/journal.ppat.1011040. PubMed PMID: 36630458; PMCID: PMC9873185.

81. Tugizov SM, Berline JW, Palefsky JM. Epstein-Barr virus infection of polarized tongue and nasopharyngeal epithelial cells. Nat Med. 2003;9(3):307-14. Epub 20030218. doi: 10.1038/nm830. PubMed PMID: 12592401.
82. Jin S, Li R, Chen M-Y, Yu C, Tang L-Q, Liu Y-M, Li J-P, Liu Y-N, Luo Y-L, Zhao Y, Zhang Y, Xia T-L, Liu S-X, Liu Q, Wang G-N, You R, Peng J-Y, Li J, Han F, Wang J, Chen Q-Y, Zhang L, Mai H-Q, Gewurz BE, Zhao B, Young LS, Zhong Q, Bai F, Zeng M-S. Single-cell transcriptomic analysis defines the interplay between tumor cells, viral infection, and the microenvironment in nasopharyngeal carcinoma. Cell Research. 2020;30(11):950-65. doi: 10.1038/s41422-020-00402-8.
83. Kong X-W, Bu G-L, Chen H, Huang Y-H, Liu Z, Kang Y-F, Li Y-C, Yu X, Wu B-H, Li Z-Q, Chen X-C, Xie S-H, Lin D-F, Li T, Yan S-M, Han R-K, Huang N, Wang Q-Y, Li Y, Zhang A, Zhong Q, Huang X-M, Ye W, Ji M-F, Cai Y-L, Cao S-M, Zeng M-S. A large-scale population-based study reveals that gp42-IgG antibody is protective against EBV–associated nasopharyngeal carcinoma. The Journal of Clinical Investigation. 2025;135(4). doi: 10.1172/JCI180216.
84. Molesworth SJ, Lake CM, Borza CM, Turk SM, Hutt-Fletcher LM. Epstein-Barr virus gH is essential for penetration of B cells but also plays a role in attachment of virus to epithelial cells. J Virol. 2000;74(14):6324-32. doi: 10.1128/jvi.74.14.6324-6332.2000. PubMed PMID: 10864642; PMCID: PMC112138.
85. McIntosh BE, Brown ME, Duffin BM, Maufort JP, Vereide DT, Slukvin, II, Thomson JA. Nonirradiated NOD,B6.SCID Il2rγ-/- Kit(W41/W41) (NBSGW) mice support multilineage engraftment of human hematopoietic cells. Stem Cell Reports. 2015;4(2):171-80. Epub 20150115. doi: 10.1016/j.stemcr.2014.12.005. PubMed PMID: 25601207; PMCID: PMC4325197.
86. Meyer L, Lopez T, Espinosa R, Arias CF, Vollmers C, DuBois RM. A simplified workflow for monoclonal antibody sequencing. PLoS One. 2019;14(6):e0218717. Epub 20190624. doi: 10.1371/journal.pone.0218717. PubMed PMID: 31233538; PMCID: PMC6590890.
87. Delecluse HJ, Hilsendegen T, Pich D, Zeidler R, Hammerschmidt W. Propagation and recovery of intact, infectious Epstein-Barr virus from prokaryotic to human cells. Proc Natl Acad Sci U S A. 1998;95(14):8245-50. PubMed PMID: 9653172; PMCID: 20961.
88. Neuhierl B, Feederle R, Hammerschmidt W, Delecluse HJ. Glycoprotein gp110 of Epstein-Barr virus determines viral tropism and efficiency of infection. Proc Natl Acad Sci U S A. 2002;99(23):15036-41. doi: 10.1073/pnas.232381299. PubMed PMID: 12409611; PMCID: 137540.
89. Sashihara J, Burbelo PD, Savoldo B, Pierson TC, Cohen JI. Human antibody titers to Epstein-Barr Virus (EBV) gp350 correlate with neutralization of infectivity better than antibody titers to EBV gp42 using a rapid flow cytometry-based EBV neutralization assay. Virology. 2009;391(2):249-56. doi: 10.1016/j.virol.2009.06.013. PubMed PMID: 19584018; PMCID: 2728425.
90. Suloway C, Pulokas J, Fellmann D, Cheng A, Guerra F, Quispe J, Stagg S, Potter CS, Carragher B. Automated molecular microscopy: the new Leginon system. J Struct Biol. 2005;151(1):41-60. doi: 10.1016/j.jsb.2005.03.010. PubMed PMID: 15890530.
91. Punjani A, Rubinstein JL, Fleet DJ, Brubaker MA. cryoSPARC: algorithms for rapid unsupervised cryo-EM structure determination. Nat Methods. 2017;14(3):290-6. Epub 20170206. doi: 10.1038/nmeth.4169. PubMed PMID: 28165473.
92. Pettersen EF, Goddard TD, Huang CC, Couch GS, Greenblatt DM, Meng EC, Ferrin TE. UCSF Chimera--a visualization system for exploratory research and analysis. J Comput Chem. 2004;25(13):1605-12. doi: 10.1002/jcc.20084. PubMed PMID: 15264254.
93. Abramson J, Adler J, Dunger J, Evans R, Green T, Pritzel A, Ronneberger O, Willmore L, Ballard AJ, Bambrick J, Bodenstein SW, Evans DA, Hung CC, O'Neill M, Reiman D, Tunyasuvunakool K, Wu Z, Zemgulyte A, Arvaniti E, Beattie C, Bertolli O, Bridgland A, Cherepanov A, Congreve M, Cowen-Rivers AI, Cowie A, Figurnov M, Fuchs FB, Gladman H, Jain R, Khan YA, Low CMR, Perlin K, Potapenko A, Savy P, Singh S, Stecula A, Thillaisundaram A, Tong C, Yakneen S, Zhong ED, Zielinski M, Zidek A, Bapst V, Kohli P, Jaderberg M, Hassabis D, Jumper JM. Accurate structure prediction of biomolecular interactions with AlphaFold 3. Nature. 2024;630(8016):493-500. Epub 20240508. doi: 10.1038/s41586-024-07487-w. PubMed PMID: 38718835; PMCID: PMC11168924.
94. Kabsch W. Xds. Acta Crystallogr D Biol Crystallogr. 2010;66(Pt 2):125-32. Epub 20100122. doi: 10.1107/S0907444909047337. PubMed PMID: 20124692; PMCID: PMC2815665.
95. Agirre J, Atanasova M, Bagdonas H, Ballard CB, Basle A, Beilsten-Edmands J, Borges RJ, Brown DG, Burgos-Marmol JJ, Berrisford JM, Bond PS, Caballero I, Catapano L, Chojnowski G, Cook AG, Cowtan KD, Croll TI, Debreczeni JE, Devenish NE, Dodson EJ, Drevon TR, Emsley P, Evans G, Evans PR, Fando M, Foadi J, Fuentes-Montero L, Garman EF, Gerstel M, Gildea RJ, Hatti K, Hekkelman ML, Heuser P, Hoh SW, Hough MA,

Jenkins HT, Jimenez E, Joosten RP, Keegan RM, Keep N, Krissinel EB, Kolenko P, Kovalevskiy O, Lamzin VS, Lawson DM, Lebedev AA, Leslie AGW, Lohkamp B, Long F, Maly M, McCoy AJ, McNicholas SJ, Medina A, Millan C, Murray JW, Murshudov GN, Nicholls RA, Noble MEM, Oeffner R, Pannu NS, Parkhurst JM, Pearce N, Pereira J, Perrakis A, Powell HR, Read RJ, Rigden DJ, Rochira W, Sammito M, Sanchez Rodriguez F, Sheldrick GM, Shelley KL, Simkovic F, Simpkin AJ, Skubak P, Sobolev E, Steiner RA, Stevenson K, Tews I, Thomas JMH, Thorn A, Valls JT, Uski V, Uson I, Vagin A, Velankar S, Vollmar M, Walden H, Waterman D, Wilson KS, Winn MD, Winter G, Wojdyr M, Yamashita K. The CCP4 suite: integrative software for macromolecular crystallography. Acta Crystallogr D Struct Biol. 2023;79(Pt 6):449-61. Epub 20230530. doi: 10.1107/S2059798323003595. PubMed PMID: 37259835; PMCID: PMC10233625.

96. Emsley P, Lohkamp B, Scott WG, Cowtan K. Features and development of Coot. Acta Crystallogr D Biol Crystallogr. 2010;66(Pt 4):486-501. Epub 20100324. doi: 10.1107/S0907444910007493. PubMed PMID: 20383002; PMCID: PMC2852313.

97. Liebschner D, Afonine PV, Baker ML, Bunkoczi G, Chen VB, Croll TI, Hintze B, Hung LW, Jain S, McCoy AJ, Moriarty NW, Oeffner RD, Poon BK, Prisant MG, Read RJ, Richardson JS, Richardson DC, Sammito MD, Sobolev OV, Stockwell DH, Terwilliger TC, Urzhumtsev AG, Videau LL, Williams CJ, Adams PD. Macromolecular structure determination using X-rays, neutrons and electrons: recent developments in Phenix. Acta Crystallogr D Struct Biol. 2019;75(Pt 10):861-77. Epub 20191002. doi: 10.1107/S2059798319011471. PubMed PMID: 31588918; PMCID: PMC6778852.

98. Meng EC, Goddard TD, Pettersen EF, Couch GS, Pearson ZJ, Morris JH, Ferrin TE. UCSF ChimeraX: Tools for structure building and analysis. Protein Sci. 2023;32(11):e4792. doi: 10.1002/pro.4792. PubMed PMID: 37774136; PMCID: PMC10588335.

99. Krissinel E, Henrick K. Inference of macromolecular assemblies from crystalline state. J Mol Biol. 2007;372(3):774-97. Epub 20070513. doi: 10.1016/j.jmb.2007.05.022. PubMed PMID: 17681537.

100. Traggiai E, Chicha L, Mazzucchelli L, Bronz L, Piffaretti JC, Lanzavecchia A, Manz MG. Development of a human adaptive immune system in cord blood cell-transplanted mice. Science. 2004;304(5667):104-7. Epub 2004/04/06. doi: 10.1126/science.1093933. PubMed PMID: 15064419.

101. Choo S, Wolf CB, Mack HM, Egan MJ, Kiem HP, Radtke S. Choosing the right mouse model: comparison of humanized NSG and NBSGW mice for in vivo HSC gene therapy. Blood Adv. 2024;8(4):916-26. doi: 10.1182/bloodadvances.2023011371. PubMed PMID: 38113461; PMCID: PMC10877116.

102. Saito Y, Ellegast JM, Manz MG. Generation of Humanized Mice for Analysis of Human Dendritic Cells. Methods Mol Biol. 2016;1423:309-20. doi: 10.1007/978-1-4939-3606-9_22. PubMed PMID: 27142026.

103. Palser AL, Grayson NE, White RE, Corton C, Correia S, Ba Abdullah MM, Watson SJ, Cotten M, Arrand JR, Murray PG, Allday MJ, Rickinson AB, Young LS, Farrell PJ, Kellam P. Genome diversity of Epstein-Barr virus from multiple tumor types and normal infection. J Virol. 2015;89(10):5222-37. Epub 20150318. doi: 10.1128/JVI.03614-14. PubMed PMID: 25787276; PMCID: PMC4442510.

104. Kimura H, Morita M, Yabuta Y, Kuzushima K, Kato K, Kojima S, Matsuyama T, Morishima T. Quantitative analysis of Epstein-Barr virus load by using a real-time PCR assay. J Clin Microbiol. 1999;37(1):132-6. doi: 10.1128/JCM.37.1.132-136.1999. PubMed PMID: 9854077; PMCID: PMC84187.

Chapter 3. Using a Humanized Mouse Model to Evaluate Activation and Selective Expansion of VRC01-class Broadly Neutralizing Antibodies against HIV

This work is still in progress as of Nov 11, 2025.

Authors:

Crystal B. Chhan[1,2], Yu-Hsin Wan[1], Andrew Wilcox-King[1], Leah J. Homad[1], Nicholas T. Aldridge[1], Leonidas Stamatatos[1], Andrew T. McGuire[1,2#]

[1]Vaccine and Infectious Disease Division, Fred Hutchinson Cancer Center, Seattle, WA, USA.

[2]Department of Global Health, University of Washington, Seattle, WA, USA.

[#]Corresponding Author: amcguire@fredhutch.org

3.1 Abstract

An effective HIV-1 vaccine will likely need to elicit broadly neutralizing antibodies (bNAbs). bNAbs bind relatively conserved regions of the otherwise highly variable envelope (Env) glycoproteins. VRC01-class bNAbs target the CD4-binding site and are among the most broad and potent of all bNAbs. VRC01-class bNAbs have been isolated from multiple HIV-1 infected individuals, and passive transfer of VRC01-class bNAbs in humans showed lower incidence of infection with VRC01-sensitive isolates compared to the placebo group – highlighting their importance for vaccine design. To achieve broad neutralization, naïve VRC01-class antibodies undergo extensive somatic mutation. However, unmutated VRC01-class antibodies do not bind recombinant Env – heralding efforts to design immunogens to engage germline VRC01 precursors andbegin the maturation process (germline-targeting). Our group developed a germline-targeting immunogen, iv4/iv9, derived from anti-idiotypic antibodies that target two

genetic signatures found on all VRC01-class bNAbs: the VH1-2 encoded heavy chain and a light chain containing a rare 5 amino acid long complementarity-determining region 3 (CDRL3). iv4/iv9 preferentially activates VRC01 B cell precursors *in vitro* and in an adoptive transfer model *in vivo*. Here, we seek to utilize a more physiologically representative *in vivo* model. ATX-GK mice have a fully functional immune system with a diverse human-derived gamma and kappa antibody repertoire. Single cell transcriptomic analysis was used to ascertain the frequency of B cells expressing BCRs with VRC01-class signatures in unimmunized animals. This approach identified putative VRC01 precursors, indicating ATX-GK mice may be a potential model to evaluate VRC01-class germline targeting immunogens. We assessed how modulating affinity of an anti-idiotypic, bispecific immunogen (iv4/iv9) impacted selective expansion of VRC01 precursor B cells *in vivo* using the ATX-GK mice.

3.2 Introduction

HIV-1 is the causative agent of acquired immunodeficiency syndrome (AIDS)[1]. HIV-1 predominantly infects $CD4^+$ T cells which play a central role in the adaptive immune system[1]. There are 41 million individuals living with HIV globally with 1.3 million newly acquired infections in 2024 [1]. Even with the availability of antiretroviral therapy, 630,000 people die from HIV-related causes annually[1]. HIV-1 is a rapidly evolving and immunoevasive virus with incredible diversity even within a single infected individual[2, 3]. Despite many ongoing efforts, there is currently no cure or effective vaccine for HIV-1[1]. Since the discovery of broadly neutralizing antibodies (bNAbs) in infected individuals that can neutralize multiple strains of HIV-1, the field has sought to elicit these antibodies prior to viral exposures[2-4].

bNAbs can prevent infection of diverse strains of HIV-1 by binding to conserved regions of the HIV Envelope glycoprotein (Env)[2-4]. Among these, VRC01-class bNAbs target the CD4-

binding site (CD4bs) in a nearly identical manner and are among the most broad and potent of all bNAbs[5-12]. VRC01-class bNAbs can potently neutralize up to 95% of cross-clade isolates[5, 8-14]. Crystal structures of VRC01-class bNAbs complexed with Env have shown that the bNAbs bind conserved regions of the CD4bs in a similar manner, despite up to 50% sequence divergence across different VRC01-class bNAbs[8-11, 15-17]. Encouragingly, passive transfer or genetic expression of VRC01-class bNAbs protected animals from experimental HIV-1 infection[18-22]. Additionally, human clinical trials showed that passive delivery of VRC01-class bNAbs reduced incidence of infection with VRC01-sensitive isolates compared to the placebo group[23, 24]. These studies indicate that eliciting VRC01-class bNAbs could be an important component of an effective vaccine response. Additionally, VRC01-class bNAbs have been isolated from multiple HIV-1 infected individuals, suggesting that they could be reproducibly elicited by vaccination[5, 6, 8-11].

VRC01-class mAbs are highly mutated as a result of extensive somatic hypermutation in response to the chronic antigenic exposure of the rapidly mutating virus[2, 3, 6, 9]. However, recombinant Envs fail to engage unmutated VRC01 B cell receptors (VRC01 BCRs)[25] which has led to the development of germline targeting strategies where immunogens are designed to selectively target VRC01 B cell precursors and begin the process of maturation towards broad neutralization [26-32]. Numerous Env-derived immunogens have been designed to engage VRC01 precursors. Three are currently, or recently completed, testing in phase I human clinical trials: eOD-GT8(NCT05414786)[33, 34], 426c.Mod.Core-C4b (NCT05471076)[27], and BG505 SOSIP.v4.1-GT1.1 (NCT04224701)[35]. However, these immunogens also present epitopes that are recognized by more abundant, non-neutralizing Env-specific B cells that could potentially be recalled and dominate the B cell responses upon subsequent Env immunizations[30, 33, 35-38].

VRC01-class bNAbs can overcome steric hindrance from variable loops and glycans on Env to engage the CD4bs through key features including: residues that are encoded by the VH1-2 heavy chain that make direct contact with Env, an unusually short 5 amino acid long complementarity-determining region 3 in the light chain (5aa CDRL3) to accommodate glycans and variable loops within the CD4bs and either a short or flexible CDRL1 to avoid steric clashing with glycan N276 on Env[6, 12, 14-17, 39]. Our group previously designed and characterized a novel germline-targeting, non-Env-based immunogen, derived from anti-idiotypic mAbs that can simultaneously target two genetic signatures found in all VRC01-class bNAbs[40]. One arm (iv9) targets the VH1-2 heavy chain while the iv4 arm targets light chains harboring a rare 5aa CDRL3. We hypothesize that avid binding by the bispecific immunogen selectively crosslinks and activates B cell receptors (BCRs) of VRC01 precursors.

Since no small animal model naturally encodes a VH1-2 ortholog[26, 34, 36], we previously used an adoptive transfer system[41], transferring B cells from a knock-in mouse model engineered to express the iGL-VRC01 BCR into wildtype mice, to show that iv4/iv9 selectively expands target B cells present at relevant physiological frequencies[40, 42]. A limitation of this model is that all the VRC01-class precursors have a fixed BCR[34, 41, 43]. Another murine model from Kymab can endogenously rearrange human heavy and light chains[36]. However, VRC01 precursors are 150-fold to 900-fold lower in these mice than in humans. Therefore, we investigated whether ATX-GK mice are an appropriate surrogate model to evaluate the ability of our germline-targeting, anti-idiotypic vaccine candidates to elicit VRC01 class antibody responses in a human-like B cell repertoire[44]. ATX-GK mice have been engineered to express a more human-like antibody repertoire that permits endogenous rearrangement of naïve BCRs.

Additionally, it is currently unknown how affinity and selectivity of an anti-idiotypic immunogen affects the fate of its target B cell in the germinal center. Other studies have suggested that binding strength and specificity of a BCR to its cognate immunogen within the germinal center will determine the selective expansion of the desired B cells within a polyclonal repertoire[41, 43, 45]. The iv9 arm has stronger affinity for its target compared to iv4; as a result, bispecific iv4/iv9 strongly selects for VH1-2 encoded B cells, including those with irrelevant light chains that may interfere with the development of VRC01-class bNAbs. We hypothesized that reducing the affinity of iv9 to generate a more selective derivative of iv4/iv9 will better select for VRC01 precursors within a polyclonal B cell system.

We found that immunizing ATX-GK mice with an optimized iv4/iv9 derivative lead to clonal expansion of precursor VRC01 B cells; however, this result was only in one mouse of seven total. Furthermore, we failed to show selective expansion of VRC01 precursors after immunization of ATX-GK mice with eOD-GT8, an Env-based, germline-targeting immunogen that has recently completed human clinical trials[33]. From these results, we conclude that while the ATX-GK can develop precursor VRC01 B cells, their frequency may be too rare to be reliably targeted by immunization in a majority of the mice.

3.3 Results

3.3.1 Assessment of ATX-GK mice as a model for germline VRC01-targeting

Our group had previously characterized a germline-targeting, non-Env-based immunogen, iv4/iv9, derived from anti-idiotypic antibody binding fragments (Fabs) that form a bispecific through SpyTag-Spycatcher technology[40, 46]. iv4/iv9 can simultaneously target two genetic signatures found in all VRC01-class bNAbs[40, 42] (Figure 1). The iv9 arm targets the VH-2

heavy chain while the iv4 arm targets light chains harboring a rare 5 amino acid long complementarity-determining region 3 (5aa CDRL3). We hypothesize that avid binding by the bispecific immunogen selectively crosslinks and activates B cell receptors (BCRs) of VRC01 precursors.

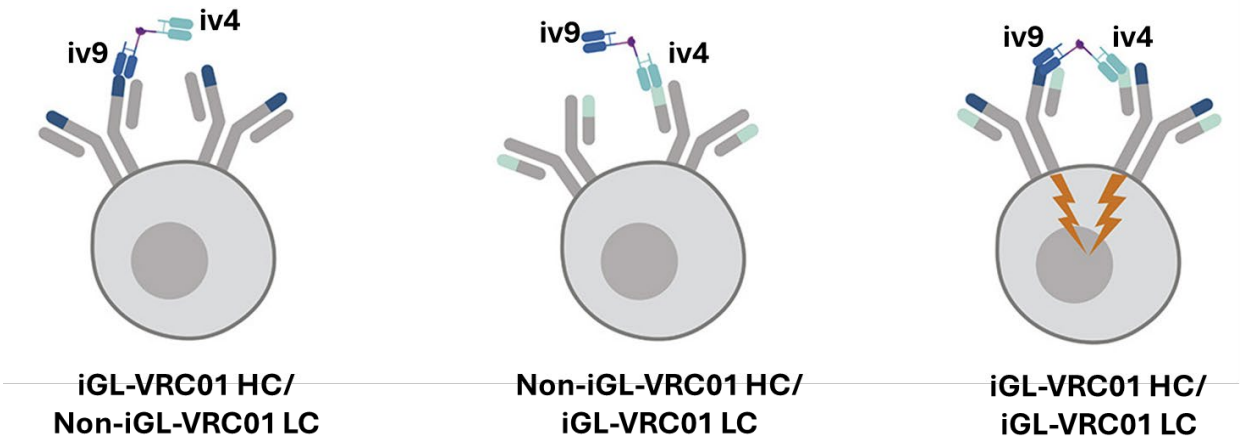

Figure 1. Schematic of bispecific engagement of germline VRC01 B cell receptor (BCR) Our bispecific anti-idiotypic immunogen is composed of iv9 that binds VH1-2 heavy chains and iv4 that preferentially binds light chains with 5 amino acid long CDRL3. We hypothesize that engagement from both arms of the bispecific will preferentially expand germline VRC01 cells by crosslinking the BCRs.

We previously showed that while iv4/iv9 can prime a strong B cell response in an adoptive transfer model where B cells were engineered to expresses the iGL-VRC01 BCR and transferred into wildtype mice at relevant physiological frequencies, the knock-in model lacks competing B cells that could be engaged by the anti-idiotype, such as B cells that encode VH1-2

with irrelevant light chains[40, 42]. Additionally, all the transferred VRC01-class precursors have a fixed BCR. Therefore, we sought to evaluate a more physiologically relevant mouse model that could better recapitulate the human B cell response. ATX-GK mice have been engineered to express a more human-like antibody repertoire that permits endogenous rearrangement of naïve BCRs. Unbiased, single-cell deep-sequencing of splenocytes from two naïve ATX-GK mice revealed that VH1-2 heavy chains (HCs) are present at physiologically relevant frequencies (~3% of B cells) while light chains containing 5 amino acids long complementarity-determining region 3 (5aa CDRL3 LCs) are found in ~0.07% of B cells, which is 7-fold lower than in humans[47] (Fig. 2A). However, we were unable to identify VRC01 precursor cells (defined as B cells encoding both the VH1-2 heavy chain and 5aa CDRL3 light chain). Based on the frequencies of VH1-2 HC and 5aa CDRL3 LCs found, we estimated the expected frequency of VRC01 precursors in an ATX-GK mouse to range from 1 in 50,000 B cells to 1 in 30,000 B cells (Table 1).

We used iv4/iv9 to label and sort splenic B cells from one naïve ATX-GK mouse, hypothesizing that the anti-idiotype should enrich for VRC01 precursors. Single-cell sequencing of iv4/iv9-sorted B cells showed a strong enrichment of B cells encoding VH1-2 HCs (95.6%), comparable to frequencies of iv4/iv9-sorted human B cells from peripheral blood in previous studies[40] (Fig. 2B). We were able to identify one VRC01 precursor from 1508 sequenced B cells (Fig. 2B). The frequency of B cells with 5aa CDRL3 LCs amongst iv4/iv9-sorted B cells was 36-fold lower in the ATX-GK mouse compared to results obtained from comparable single-cell sorting from humans[40] (Fig. 2B). Taken together, we conclude that the ATX-GK mouse can produce VRC01 precursors that could be engaged by our anti-idiotypic immunogen *ex vivo*, although frequency of naïve VRC01 precursors identified through iv4/iv9-sorting is 8-fold lower

in the mouse compared to previous human data. This result indicates that ATX-GK mice might be an appropriate surrogate model to evaluate the ability of our germline-targeting, anti-idiotypic vaccine candidates to elicit VRC01 class antibody responses.

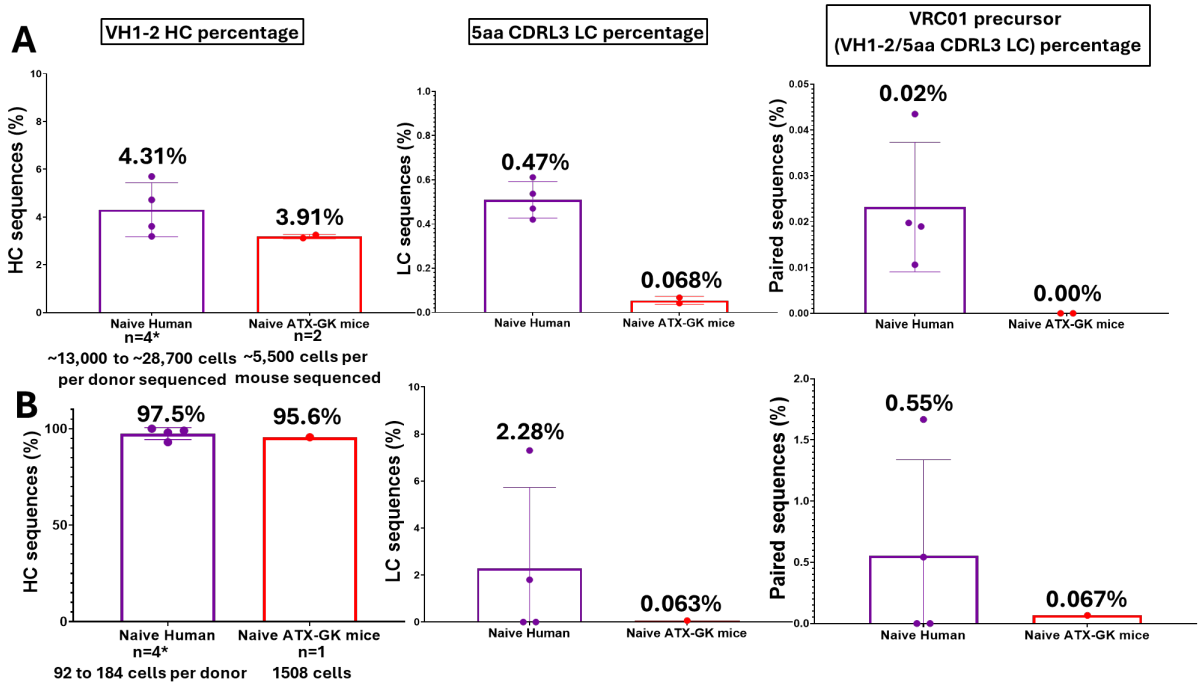

Figure 2. Frequency of VH1-2 heavy chain, 5 amino acid long CDRL3 bearing light chains, and VRC01 precursors in naive ATX-GK mice (A) Frequencies of VH1-2 heavy chains, light chains with 5aa CDRL3 LCs, and VRC01 precursors in naïve B cells from ATX-GK mice identified by unbiased, high-throughput paired sequencing of naïve B cells and compared to published naïve human BCR sequences from circulating B cells[47]. **(B)** iv4/iv9 was used to label and sort B cells from naïve ATX-GK splenocytes. Frequencies of VH1-2 heavy chains, light chains with 5aa CDRL3, and VRC01 precursors were found using high-throughput paired BCR sequencing and compared to published iv4/iv9-sorted naïve human B cell data[40].

Table 1: Expected number of VRC01 precursors in an individual naïve ATX-GK mice

Mouse ID	VH1-2 frequency (%)	5aa CDRL3 frequency (%)	Expected frequency of VRC01 precursors (%)	Expected number of VRC01 precursors at any given time (of ~75 million B cells per mouse)
Naïve Mouse #1	3.25	0.103	0.00335 (1 in 30,000 B cells)	2512
Naïve Mouse #2	3.11	0.067	0.00209 (1 in 50,000 B cells)	1567

3.3.2 Optimization of a germline VRC01-targetting, anti-idiotypic, bispecific immunogen

Previous studies have shown that *ex vivo* sorting of human B cells with antigen predicts which B cells respond upon immunization[33, 36, 43]. When this strategy was applied to ATX-GK mice, we found that 95% of iv4/iv9 sorted B cells expressed VH1-2 heavy chains but only 0.06% of those B cells were VRC01 precursors (Fig. 2B). This indicates that over 90% of B cells that would respond to iv4/iv9 are off-target B cells expressing VH1-2 HCs with undesired light chains, which are substantially more abundant than the VRC01 precursors. Additionally, iv9 has higher affinity for VH1-2 than iv4 does for light chains with 5aa CDRL3s as assessed by biolayer interferometry (BLI)[40] (Fig. 3C). We hypothesized that this affinity difference could bias the bispecific anti-idiotype to select for B cells expressing VH1-2 HCs with undesired light chains. Since it has been demonstrated that antigen affinity is a key determinant of a how well target cells are recruited into and compete in germinal centers[41, 43, 45, 48], we sought to lower the affinity of iv9 in efforts to make the bispecific anti-idiotype more selective for VRC01 precursors.

We reverted all somatic mutations in iv9 to their inferred germline residues (iGL-iv9) and found that binding to iGL-VRC01 was abrogated (Fig. 3B). Using the crystal structure of iv9 in complex with iGL-VRC01 as a guide[40], we selectively reintroduced somatically mutated residues that directly contact the VH1-2 heavy chain with the highest buried surface area: one in the

heavy chain ($D52W_{HC}$) and one in the light chain ($H92E_{LC}$) (Fig. 3A). We produced iGL-iv9 antibodies containing either one or both mutations and tested them for binding to iGL-VRC01 (Fig. 3B). We found that the single mutants had very weak affinity for iGL-VRC01, while iGL-iv9 $D52W_{HC}$ $H92E_{LC}$ (K_D=3.24x10^7M) had modest binding with a faster off-rate compared to parental iv9 (K_D=6.05x10^9M) (Fig. 3B). Then, we conjugated iGL-iv9 $D52W_{HC}$ $H92E_{LC}$ to iv4 and assessed engagement of on-target versus off-target BCRs. We tested binding to iGL-VRC01 IgG or chimeric IgG that contained the iGL-VRC01 heavy chain paired with an irrelevant light chain or vice versa. We found that the mutating the iv9 arm did not affect iv4engagement of the iGL-VRC01 light chain (Fig. 3C). The double mutant bispecific was able to avidly engage iGL-VRC01 comparably to parental iv4/iv9 (Fig. 3C). The double mutant iGL-iv9 arm engaged the iGL-VRC01 HC/irrelevant LC chimeric IgG more weakly with a fast off-rate (Fig. 3C). iv4/iGL-iv9 D52W H92E also activated DG-75 cells transduced to express iGL-VRC01 BCRs in calcium flux assays while iv4 Fab and iGL-iv9 D52W H92E Fab alone could not (Fig. 3D). Altogether, these data indicate that iv4/iGL-iv9 D52W H92E retains the ability to selectively activate VRC01 precursors while limiting activation of off-target B cells.

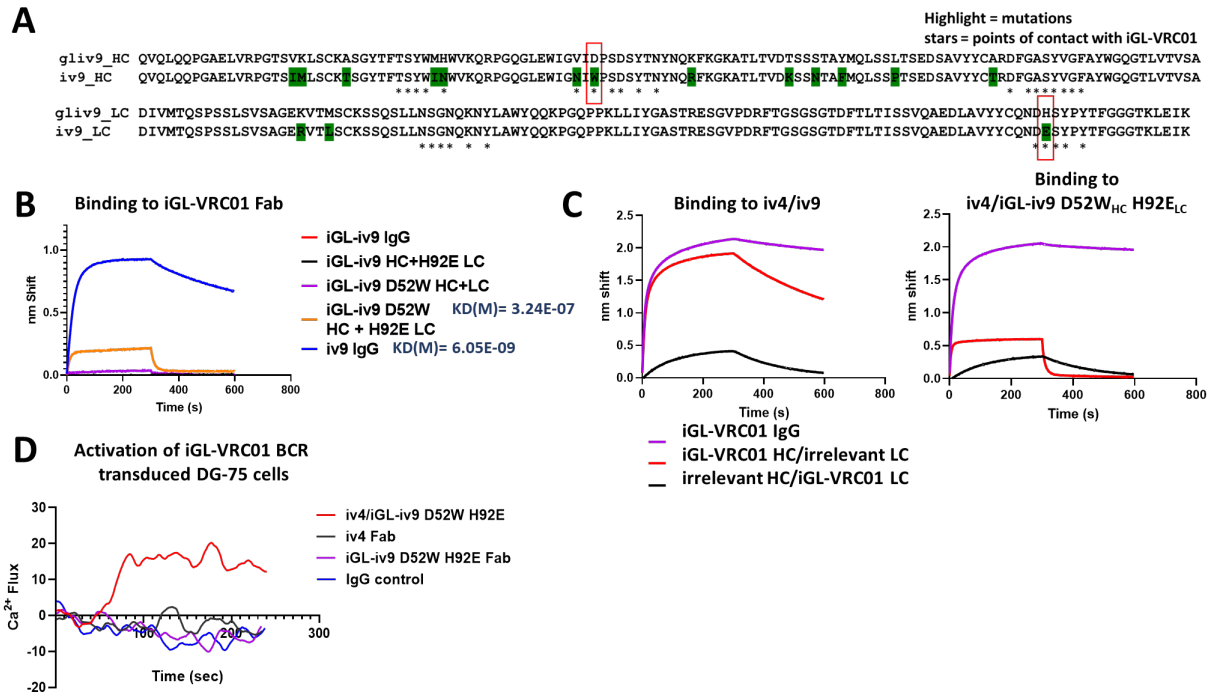

Figure 3. Selective mutation to reduce affinity of iv9 for VH1-2 heavy chains

(A) HC and LC sequences of iv9 aligned to inferred germline sequences. Mutations that arose from somatic hypermutation are highlighted in green while residues that contact iGL-VRC01 are denoted by an asterisk. Trp52$_{HC}$ and Glu92$_{LC}$ (red boxes) were chosen for iGL-iv9 derivatives as they encode contact residues. **(B)** The indicated iv9 derivatives were tested for binding to iGL-VRC01 using biolayer interferometry. **(C)** Binding of iv4/iv9 (left) and iv4/iGL-iv9 D52W H92E to iGL-VRC01, a chimeric mAb with the iGL-VRC01 HC paired with an irrelevant LC, and a mAb with an irrelevant HC paired with theiGL-VRC01 LC by (right) was assessed via biolayer interferometry. **(D)** Calcium flux assay was used to measure activation of DG-75 cells transduced to express iGL-VRC01 BCRs by iv4/iGL-iv9 D52W H92E, iv4 Fab, and iGL iv9 D52W H92E Fab. An irrelevant IgG was used as a negative control.

3.3.3 Immunizing three ATX-GK mice with an anti-idiotypic immunogen leads to clonal expansion of VRC01 precursors in one mouse

To determine if iv4/iGL-iv9 D52W H92E could expand VRC01 precursors *in vivo*, we performed immunizations using the ATX-GK mice. In the first experiment, we pre-primed 3 mice with a peptide (2W1S) known to elicit a strong $CD4^+$ T cell response in C57BL/6 mice [40, 42, 49]. Mice were then immunized (bilateral intramuscular) with iv4/iGL-iv9 D52W H92E fused to the 2W1S peptide with SMNP as an adjuvant[50]. We had previously used this peptide fusion strategy to recruit pre-existing T cell help and improve B cell responses elicited by an anti-idiotypic mAb[42, 49]. In parallel, mice were immunized with the parental iv4/iv9-2W1S as a comparison. 14 days post immunization, we sorted IgG^+ splenic B cells from two immunized mice per group pooled together for high-throughput, single-cell sequencing (Fig. S1). We included a naïve mouse as a control. Both immunized samples had higher IgG^+ frequencies compared to the unimmunized control (Fig. 4A). From the recovered sequences, we found that mice immunized with iv4/iGL-iv9 D52W H92E had a lower frequency of VH1-2 HCs compared to mice immunized with the parental iv4/iv9, indicating that the mutations engineered to reduce the affinity of iv9 appeared to limit class switching of VH1-2 B cells in vivo (Fig. 4B).The iv4/iGL-iv9 D52W H92E group had the highest frequency of 5aa CDRL3 LCs (0.205%) compared to the unimmunized mouse (0.0%) and the iv4/iv9 group (0.093%), indicating that reducing the affinity of iv9 appeared to allow for better engagement of the iv4 arm (Fig. 4C). Encouragingly, we were able to identify two putative VRC01 precursors from the iv4/iGL-iv9 D52W H92E-immunized splenic IgG^+ B cells while none were found from the iv4/iv9 immunized mice or unimmunized controls (Fig. 4D & Table 2). These results indicate that reducing the affinity for VH1-2 heavy chains increases the specificity of the anti-idiotypic

bispecific for VRC01 precursors. However, a large proportion of off-target cells bearing VH1-2 HCs were found in the class switched population following immunization (Fig. 4B).

Next, we performed antigen-specific, single-cell sorting and sequencing of pooled lymph nodes from the three iv4/iGL-iv9 D52W H92E-immunized mice. In line with what we observed among IgG+ B cells in the spleen, we observed an increase in the frequency of IgG^+ B cells among total B cells in immunized mice compared to naïve mice (Fig. 5A). The antigen-specific IgG^+ frequency was 2-fold higher in the immunized sample compared to the naïve sample (~8% versus ~4%, respectively). The frequency of B cells expressing VH1-2 HCs among antigen-specific cells was slightly higher in the immunized sample (~90%) (Fig. 5B). However, a high frequency of B cells expressing VH1-2 HCs were sorted from the naïve mouse (75%) (Fig. 5B). ~9.5% of sorted B cells expressed 5aa CDRL3 LCs in the immunized sample which is 110-fold higher than found from unbiased sequencing of naïve mice (Fig. 5C and Table 1). Additionally, we identified two putative VRC01 precursors from the immunized sample and were unable to identify any from naïve mice (Fig. 5D). Based off CDRH3 and CDRL3 sequences, we inferred that three of the four putative VRC01 precursors isolated from these immunized mice were clonal variants, presumably from mouse #1.2, which was common to both analyses (Fig. 4D, Fig. 5D, Table 2, & Table 3).

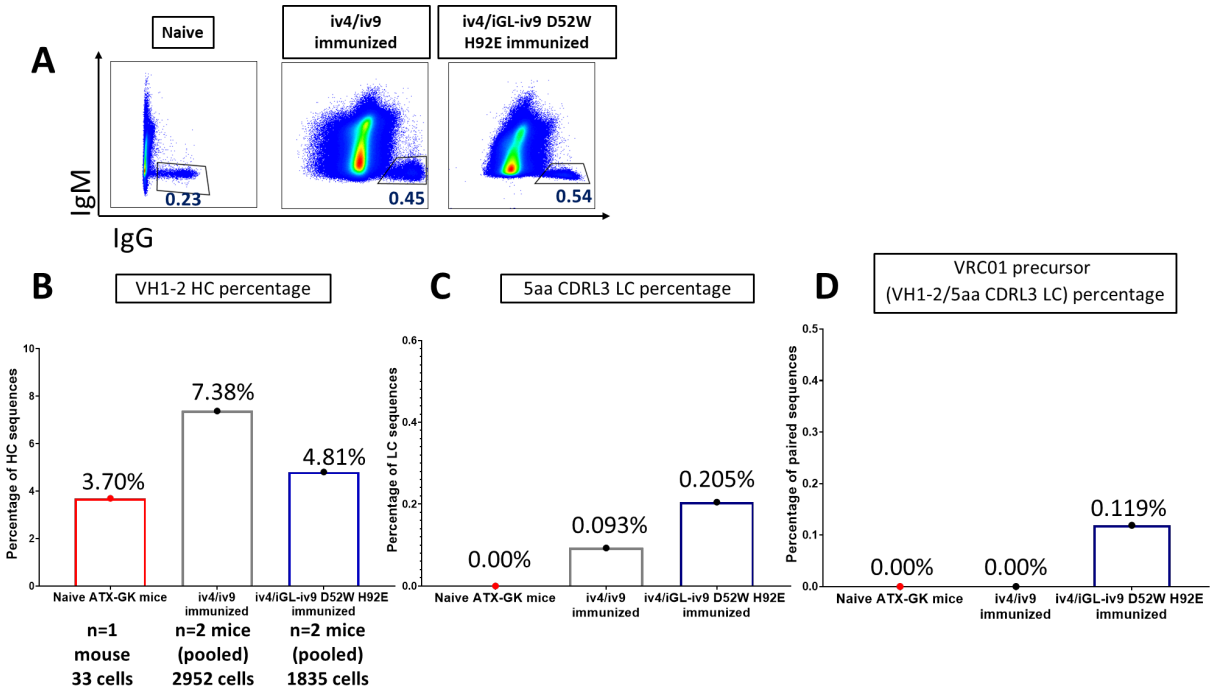

Figure 4. High-throughput sequencing of splenic B cells from ATX-GK mice immunized with anti-idiotypic immunogens (A) Frequency of IgG^+ B cells in splenocytes from unimmunized, iv4/iv9-immunized, and iv4/iGL iv9-D52W H92E-immunized ATX-GK mice. **(B-D)** IgG^+ splenic B cells were sorted from unimmunized (red, left bars), iv4/iv9-immunized (black, middle bars), or iv4/iGL-iv9 D52W H92E-immunized ATX-GK mice (blue, right bars). Immunized mice received 10µg of antigen with SMNP adjuvant. Splenocytes were isolated after 14 days. High throughput paired BCR sequencing was used to determine frequencies of VH1-2 heavy chains (**B**), 5aa CDRL3 LCs (**C**), and VRC01 precursors (**D**).

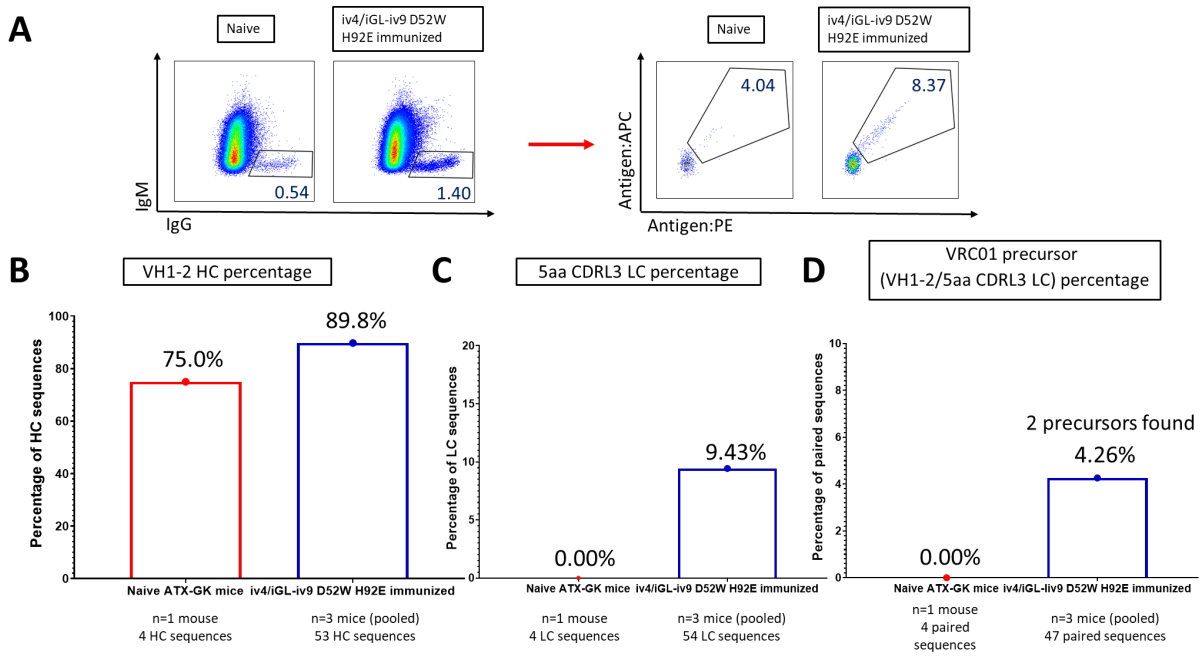

Figure 5. Single-cell sorting and sequencing of B cells from pooled lymph nodes of three ATX-GK mice immunized with optimized anti-idiotypic immunogen (A) Frequency of IgG^+ B cells among total B cells(left) and frequency of antigen-B cells (right) among of total IgG^+ B cells in unimmunized and iv4/iGL-iv9 D52W H92E-immunized ATX-GK mice. **(B)** Single, antigen-specific IgG^+ B cells were sorted from unimmunized (red, left bars) or iv4/iGL-iv9 D52W H92E-immunized ATX-GK mice (blue, right bars). Sanger sequencing was used to determine frequencies of VH1-2 heavy chains (**B**), 5aa CDRL3 LCs (**C**), and VRC01 precursors (**D**).

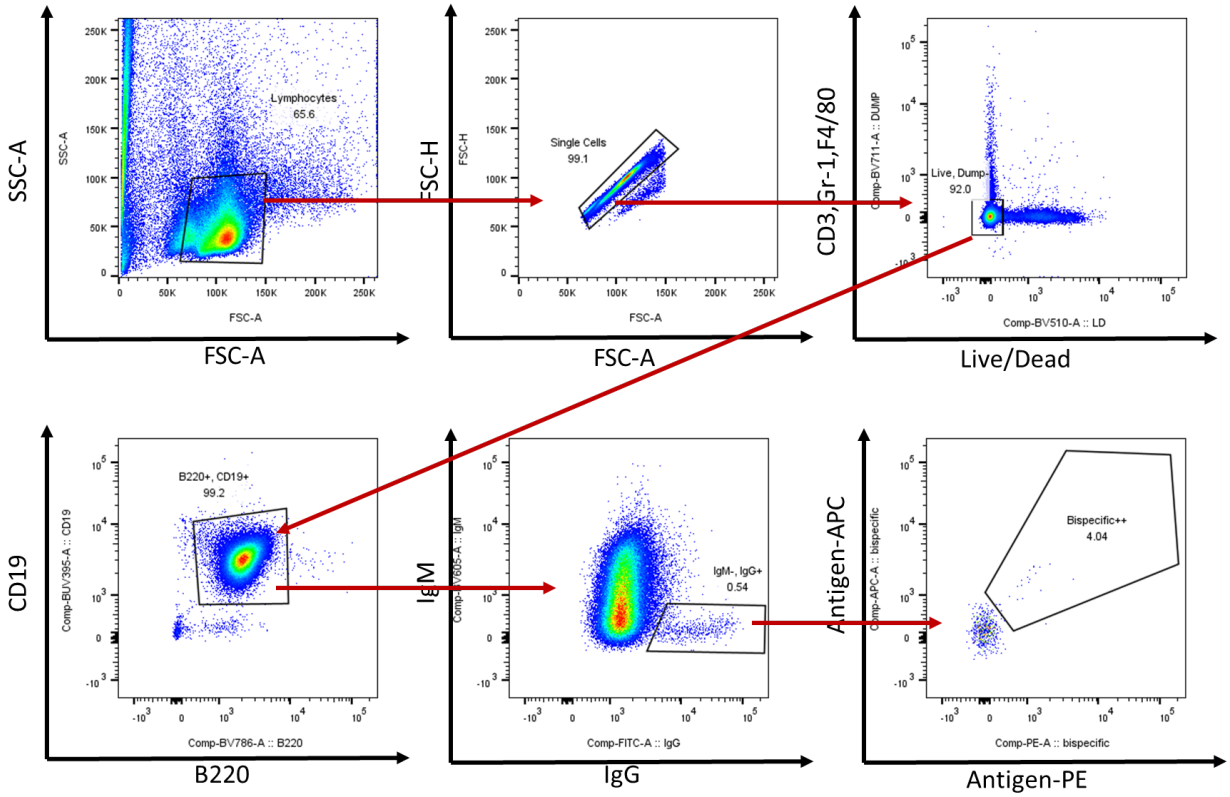

Supplementary Figure 1. Representative gating strategy for single-cell sorting

B cells from spleens or lymph nodes were enriched using a murine B cell isolation kit then sorted based on the following gate strategy: lymphocytes > Single cells > Live cells > $CD19^{+}B220^{+}$ > $IgM^{-}IgG^{+}$. For antigen-specific sorts, IgG^{+} cells were further gated on dual-positive staining with the labeled antigen.

Table 2: Putative VRC01 precursors identified through cell sorting and sequencing of B cells from naïve and iv4/iGL-iv9 D52W H92E-immunized ATX-GK mice

Cell ID	Tissue	Gamma V-Gene	Gamma J-Gene	Gamma D-Gene	CDRH3	Kappa V-Gene	Kappa J-Gene	CDRL3
Naive_10X	Spleen	IGHV1-2	IGHJ3	IGHD6-13	CARGGYRQLVPFDYW	IGK3-20	IGKJ4	CQQYGTF
Immunized 10X_105	Spleen	IGHV1-2	IGHJ6	IGHD3-22	CARDYYDSSGYYSLDYYYYMDVW	IGKV3-15	IGKJ4	CQQYNTF
Immunized 10X_206	Spleen	IGHV1-2	IGHJ6	IGHD1-1	CARAQYNWNDGSYYYYYYMDVW	IGKV1-5	IGKJ1	CQQYNTF
Immunized Plate2_B6	Lymph node	IGHV1-2*02 F	IGHJ6*03 F	IGHD1-1*01 F	CARARYNWHDGSYYYYYHMDVW	IGKV1-5*03 F, or IGKV1-5*04 F	IGKJ1*01 F	CQQYNTF
Immunized Plate1_G6	Lymph node	IGHV1-2*02 F, or IGHV1-2*07 F	IGHJ6*03 F	IGHD1-1*01 F	CARAHYNWNDGSYFYYYYMDVW	IGKV1-5*03 F	IGKJ1*01 F	CQQYNTF

3.3.4 Immunization with an optimized anti-idiotypic immunogen in four additional ATX-GK mice did not lead to identification of VRC01 precursors

To determine if the expansion of VRC01 precursors was reproducible, we repeated the iv4/iGL-iv9 D52W H92E immunization study with four additional ATX-GK mice. Here we sorted splenocytes and lymph nodes from each mouse separately. We performed antigen-specific sorting and Sanger sequencing of B cells from lymph nodes and spleens of both naïve (n=3) and immunized mice (n=4). There was no difference in frequency of IgG^+ splenic B cells in naïve versus immunized mice. However, there was a slightly higher frequency of IgG^+ B cells in the lymph nodes of immunized mice (Fig. 6A). There was an increase of antigen-specific IgG^+ B cells in both the spleen and lymph nodes of immunized mice compared to naïve mice (Fig. 6B).

We were unable to recover any amplicons from antigen-specific B cells sorted from the lymph nodes of one immunized mouse which was excluded from sequencing analysis (Table 3). The frequency of VH1-2 HCs was high in among antigen-specific B cells from both spleen and lymph nodes from either group (Fig. 6C). We were unable to identify any light chain sequences

with 5aa CDRL3 LCs in either group (Fig. 6D). To confirm that mice responded to the immunization, we performed ELISAs to assess the antigen-specific binding of sera pre- and post-immunization. Indeed, we measured higher binding titers 14 days post immunization compared to titers at baseline all mice (Fig. S2). From 86 million total cells collected from both lymph nodes and spleens of three immunized mice and ~4 million B cells analyzed, we were unable to identify any VRC01 precursors (Table 3).

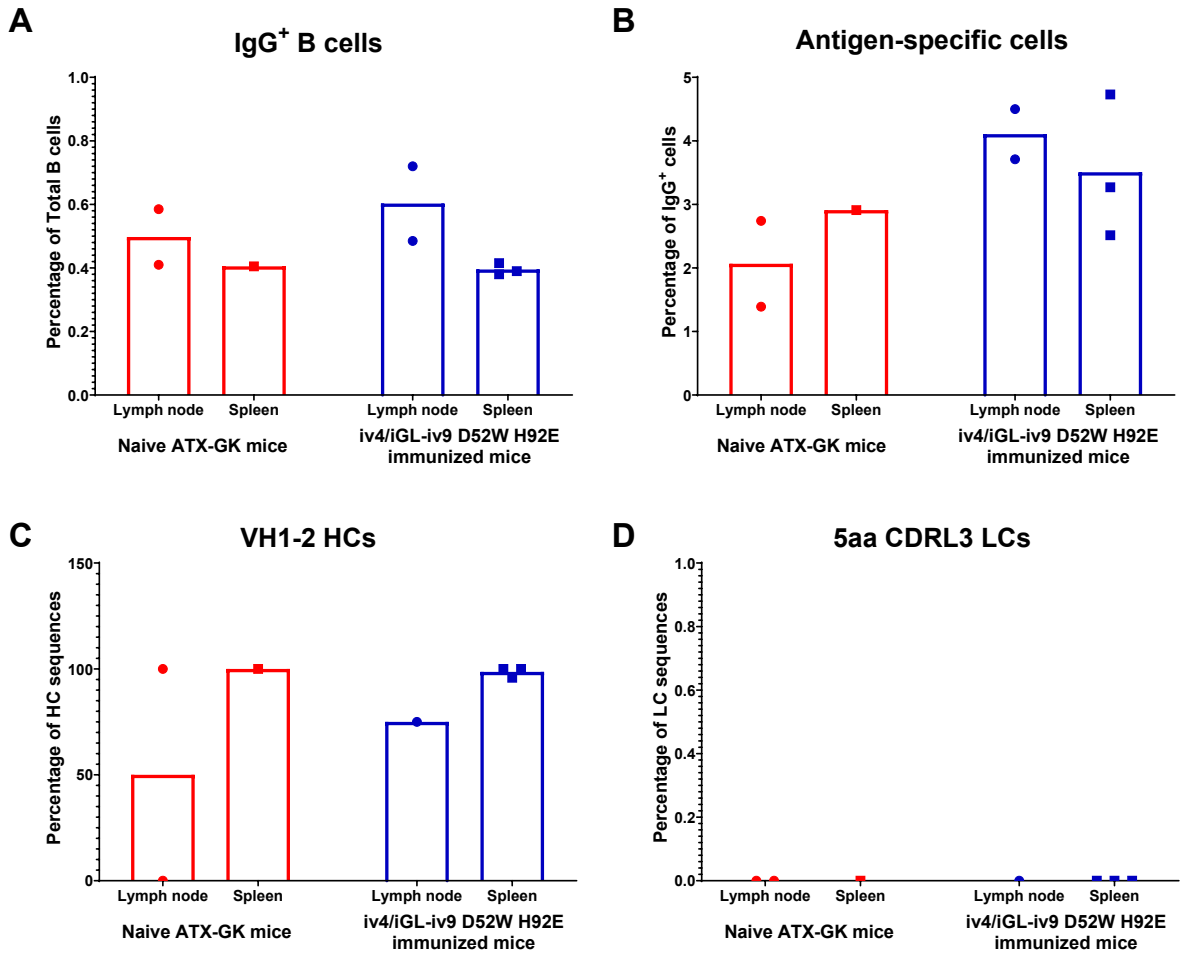

Figure 6. Single-cell sorting and sequencing of B cells from spleens and lymph nodes of ATX-GK mice immunized with optimized anti-idiotypic immunogen (**A**) Percentage of IgG^+

B cells among total B cells in naïve and iv4/iGL iv9 D52W H92E-immunized mice. Each dot represents one mouse. (**B**) Percentage of iv4/iGL-iv9 D52W H92E-specific cells of IgG^+ B cells in naïve and immunized mice. (**C**) Percentage of VH1-2 HCs of total heavy chain sequences recovered from antigen-specific sorted cells from naïve and immunized mice. (**D**) Percentage of light chains with 5aa CDRL3s among total light chain sequences recovered from antigen-specific sorted cells from naïve and immunized mice.

Table 3: Summary of antigen-specific sorting of ATX-GK mice immunized with iv4/iGL-iv9 D52W H92E

Sample	Tissue	Bait	Number of initial cells (M)	Number of B cells	IgG Frequency of Total B cells	Antigen-specific Frequency of IgG cells	Number of sorted cells	Number of IgG amplicons	Number of VH1-2 HCs	Number of IgK amplicons	Number of 5aa CDRL3 LCs	Number of paired sequences	Number of VRC01 precursors
Naïve #1	Lymph node	iv4-gliv9D52WH92E	10	100417	0.54	4.04	8	4	3	4	0	3	0
Naïve #2	Lymph node	iv4-gliv9D52WH92E	5	17847	0.41	2.74	2	1	1	1	0	0	0
Naïve #3	Lymph node	iv4-gliv9D52WH92E	10	24733	0.585	1.39	0	0	0	0	0	0	0
immunized pooled 1.1, 1.2, 1.3	Lymph node	iv4-gliv9D52WH92E	10	179455	1.4	8.37	78	60	53	54	5	47	2
iv4-gliv9D52WH92E immunized ATX-GK 2.1	Lymph node	Have not sorted	N/A	N/A	N/A	N/A	N/A	N/A	N/A	N/A	N/A	N/A	N/A
iv4-gliv9D52WH92E immunized ATX-GK 2.2	Lymph node	Have not sorted	N/A	N/A	N/A	N/A	N/A	N/A	N/A	N/A	N/A	N/A	N/A
iv4-gliv9D52WH92E immunized ATX-GK 2.3	Lymph node	iv4-gliv9D52WH92E	5	116238	0.72	3.71	11	0	0	0	0	0	0
iv4-gliv9D52WH92E immunized ATX-GK 2.4	Lymph node	iv4-gliv9D52WH92E	16	80505	0.485	4.5	5	4	3	2	0	1	0
Naïve #1	Spleen	Have not sorted	N/A	N/A	N/A	N/A	N/A	N/A	N/A	N/A	N/A	N/A	N/A
Naïve #2	Spleen	Have not sorted	N/A	N/A	N/A	N/A	N/A	N/A	N/A	N/A	N/A	N/A	N/A
Naïve #3	Spleen	iv4-gliv9D52WH92E	20	305609	0.405	2.91	13	10	10	8	0	8	0
iv4-gliv9D52WH92E immunized ATX-GK 1.1	Spleen	iv4-gliv9D52WH92E	10	240578	0.43	1.16	7	7	7	3	0	3	0
iv4-gliv9D52WH92E immunized ATX-GK 1.2	Spleen	iv4-gliv9D52WH92E	10	818000	0.62	3.91	82	65	62	51	0	43	0
iv4-gliv9D52WH92E immunized ATX-GK 1.3	Spleen	Have not sorted	N/A	N/A	N/A	N/A	N/A	N/A	N/A	N/A	N/A	N/A	N/A
iv4-gliv9D52WH92E immunized ATX-GK 2.1	Spleen	Have not sorted	N/A	N/A	N/A	N/A	N/A	N/A	N/A	N/A	N/A	N/A	N/A
iv4-gliv9D52WH92E immunized ATX-GK 2.2	Spleen	iv4-gliv9D52WH92E	20	567000	0.39	3.27	21	20	20	18	0	17	0
iv4-gliv9D52WH92E immunized ATX-GK 2.3	Spleen	iv4-gliv9D52WH92E	20	870000	0.38	4.73	53	43	43	42	0	33	0
iv4-gliv9D52WH92E immunized ATX-GK 2.4	Spleen	iv4-gliv9D52WH92E	25	675334	0.415	2.515	25	24	23	22	0	13	0

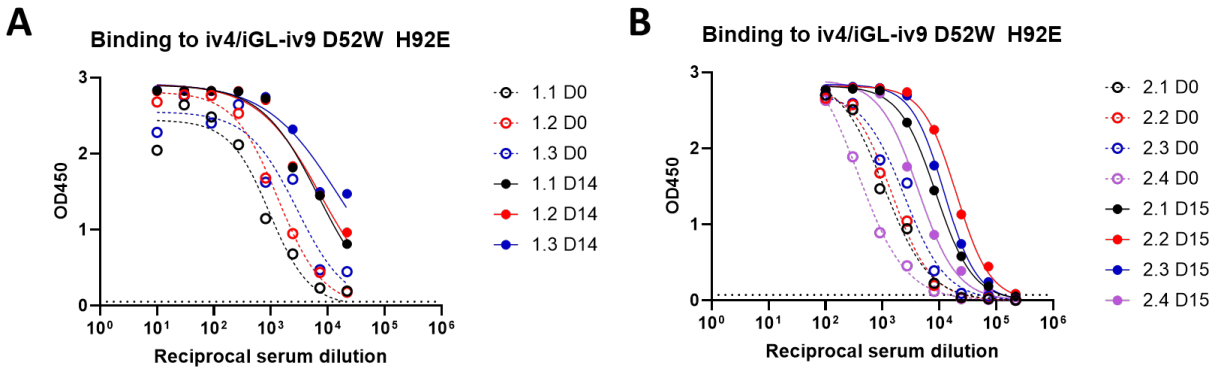

Supplementary Figure 2. **Pre- and post-immunization sera binding to anti-idiotypic immunogen.** Antigen-specific ELISA was performed using sera from the first immunization study (**A**) and repeat study (**B**).

3.3.5 Immunizing ATX-GK mice with an Env-based, germline-targeting immunogen

To determine if VRC01 precursors could be expanded in ATX GK mice using an alternative Env-based, germline-targeting immunogen, we immunized three ATX-GK mice with a 24mer eOD-GT8 ferritin formulated with SMNP. When presented as a 60mer, eOD-GT8 successfully primed VRC01 precursors in Kymab mice[36] and a phase I human clinical trial[33]. Spleens and lymph nodes were collected 14 days post immunization. We sorted antigen-specific IgG^+ from both lymph nodes and spleens. While we saw a large expansion of both total IgG^+ B cells and antigen-specific IgG^+ B cells following immunization, we were unable to identify a high frequency of VH1-2 HCs nor any 5aa CDRL3 LCs (Table 4). Taken together with the minimal number of 5aa CDRL3 LCs found in the naïve mice and anti-idiotype-immunized mice (Table 3), we conclude that the ATX-GK mice do not serve as a reliable model for assessing VRC01 responses due to a low frequency of 5aa CDRL3 LCs.

Table 4: Summary of antigen-specific sorting of ATX-GK mice immunized with eOD-GT8

Sample	Tissue	Bait	Number of initial cells (M)	Number of B cells	IgG Frequency of Total B cells	Antigen-specific Frequency of IgG cells	Number of sorted cells	Number of IgG amplicons	Number of VH1-2 HCs	Number of IgK amplicons	Number of 5aa CDRL3 LCs	Number of paired sequences	Number of VRC01 precursors
eOD-GT8 #1	Lymph node	eOD-GT8	10	92396	7.205	36.65	216	112	3	88	0	67	0
eOD-GT8 #2	Lymph node	Have not sorted	N/A	N/A	N/A	N/A	N/A	N/A	N/A	N/A	N/A	N/A	N/A
eOD-GT8 #3	Lymph node	eOD-GT8	5	18357	4.6	12.7	25	5	0	5	0	2	0
naïve #3	Spleen	eOD-GT8	25	194503	0.438	0.088	0	0	0	0	0	0	0
eOD-GT8 #1	Spleen	Have not sorted	N/A	N/A	N/A	N/A	N/A	N/A	N/A	N/A	N/A	N/A	N/A
eOD-GT8 #2	Spleen	eOD-GT8	10	225100	1.36	2.58	26	12	0	8	0	4	0
eOD-GT8 #3	Spleen	eOD-GT8	5	137292	1.14	4.66	24	4	0	3	0	2	0

3.3.6 Putative VRC01 precursors isolated from ATX-GK mice do not bind to germline-targeting, Env-derived proteins

For successful vaccination, it is believed that the process of extensive maturation towards broad neutralization would begin with priming the VRC01 precursors followed by immunizations with more and more complex Env proteins to "guide" mutations needed to engage wildtype Env on the HIV virions[26-32].

To assess if the VRC01 precursors elicited by the anti-idiotype could be engaged by an Env-derived immunogen, we produced the four putative VRC01 precursors isolated from iv4/iv9 D52W H92E-immunized mice as recombinant IgG1 monoclonal antibodies (mAbs)[51]. We also produced the putative VRC01 precursor isolated from a naïve ATX-GK mouse. We performed biolayer interferometry to assess binding of the mAbs to iv4-2W1S-Spycatcher, iGL-iv9 D52W H92E-Spytag, and two germline-targeting Env-derived proteins: eOD-GT8[33] and 426c.Mod.Core[27]. As expected, all mAbs bound to either the iv4-2W1S-Spycatcher or the iGL-iv9 D52W H92E-Spytag component that forms the bispecific anti-idiotypic immunogen. However, no mAbs bound to either germline-targeting Env-derivatives.

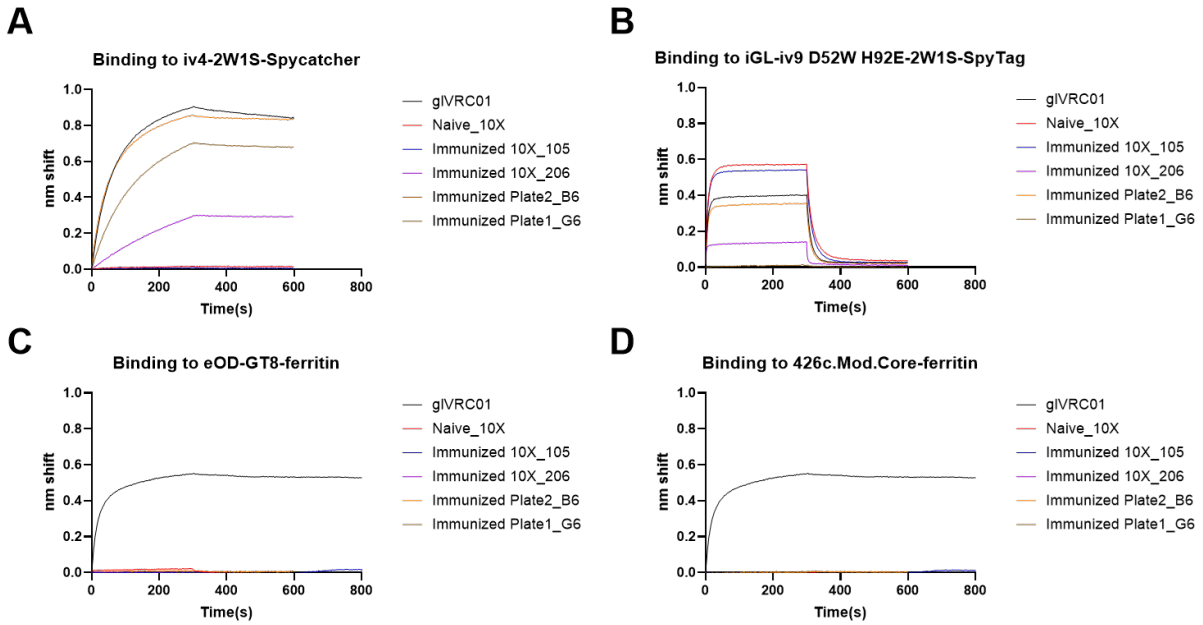

Figure 7. Identified putative VRC01 precursors do not bind to Env-derived immunogens

Biolayer interferometry was used to assess antibody binding to ligands. Antibodies were immobilized on biosensors then immersed in a solution with respective ligands: iv4-2W1S-Spycatcher at 250nM (**A**), iGL-iv9 D52W H92E-2W1S-Spytag at 250nM (**B**), eOD-GT8-ferritin at 1μM (**C**), and 426c.Mod.Core-ferritin at 1μM (**D**). Germline VRC01 IgG was used as a positive control.

3.4 Discussion and Future Directions

We previously showed that the anti-idiotype iv4/iv9 could prime VRC01 precursors in an adoptive transfer model where target B cells are present at physiological frequencies[52]. However, key limitations of the adoptive transfer model include the use of a fixed BCR and competing mouse B cells lack VH1-2 heavy chains. ATX-GK mice from Alloy therapeutics encode 41V, 23D, and 6J human VH as well as 19V and 5J human VK genes. From our deep-sequencing

analysis of splenic B cells from two naïve mice, we found that these mice encode the VH1-2 at near human physiological frequency (~3%). However, these mice express a 5aa CDRL3 light chain at ~7-fold lower frequency than found in humans. As we were only able to expand VRC01 precursors in one of seven mice using an iv4/iv9 derivative designed to better engage VRC01 precursors and unable to identify VRC01 precursors in mice immunized with eOD-GT8-ferritin, we conclude that the ATX-GK mice do not serve as a consistent model for HIV bNAb germline-targeting immunogens.

Since the discovery of VRC01-like bNAbs from multiple HIV-infected individuals that can neutralize up to 95% of cross-clade isolates[5, 8-14], considerable effort has gone into eliciting this class of antibodies through vaccination. However, a major hinderance in these attempts is that recombinant Envs fail to engage unmutated inferred-germline VRC01 BCRs[25]. Additionally, VRC01-class bNAbs are highly mutated in comparison to their germline counterparts, likely arising from multiple rounds of somatic hypermutation as a response to the chronically mutating virus[2, 3, 6, 9].

Thus, it has been proposed to begin a multi-stage vaccination scheme with an immunogen that can target VRC01 precursors (germline-targeting) and then introduce more complex Env derivatives to raise bona fide mature VRC01 bNAbs. Three are currently, or recently completed, testing in phase I human clinical trials: eOD-GT8 (NCT05414786)[33, 34], 426c.Mod.Core-C4b (NCT05471076)[27], and BG505 SOSIP.v4.1-GT1.1 (NCT04224701)[35]., eOD-GT8 and BG505 SOSIP.v4.1-GT1.1 showed acceptable safety and reactogenicity, while results for 426c.Mod.Core are pending. Both immunogens were able to expand VRC01 precursors that were CD4bs-specific. For eOD-GT8, this was successful in all vaccine recipients after the first immunization. Still, VRC01-class BCRs were only a small percentage of the total eOD-GT8-

specific IgG^+ B cells (3.5% to 8%) and VRC01-class BCRs accounted for 16% to 28% of the CD4bs-specific IgG^+ BCRs. Additionally, the homologous boost led to an increase in off-target cells (eOD-GT8-specific cells that were not specific to the CD4bs). For BG505 SOSIP.v4.1-GT1.1, the VRC01 precursors accounted for 4 to 74% of the CD4bs-specific memory B cell repertoire, however, the overall proportion of vaccine receipts with a VRC01-class response was only ~60%. Therefore, we investigated whether these vaccination results could be improved by first expanding the pool of VH1-2/5aa CDRL3 LC bearing B cells through an anti-idiotypic approach.

The most likely explanation is that the VRC01 precursors in these mice are too rare to be reliably targeted in ATX-GK mice. The factor limiting VRC01 precursor frequency in ATX GK mice is the low frequency of 5aa CDRL3s. Compared to humans, murine light chains exhibit more restricted CDRL3 lengths that are typically 9aa long due to the lack of expression of terminal deoxynucleotidyl transferase (TdT) during light chain recombination[53-55]. TdT, a DNA polymerase, increases VDJ junction diversity through non-templated nucleotide additions to the 3' end of DNA as well as suppresses recurrent CDR3s resulting from microhomology-mediated VDJ joining[55-57]. TdT is expressed during light chain VDJ recombinant in postnatal human pre-B cells, however, it is not expressed in postnatal murine pre-B cells[53-55]. Although the ATX-GK mice encode diverse antibody light chain genes, like wildtype mice, they likely do not express TdT during light chain recombination, limiting development of light chains with 5aa CDRL3s. Fredrick Alt's group has engineered two mice strains with VRC01-class rearranging human VH1-2 HCs and human LCs along with the human TdT enzyme (VH1-2/Vk3-20 and VH1-2/Vk1-33 mouse models)[55]. However, the VH1-2 heavy chain exists at 44.8% compared to 3% found in human B cells. Additionally, the human light chain is restricted to Vk1-33 or Vk3-20

and the 5aa CDRL3 is still 5-fold to 8-fold less frequent compared to that in humans. Therefore, our current version of the anti-idiotype may engage the much more predominant off-target B cells that have VH1-2 HCs with undesired LCs.

Of the five VRC01 precursors identified from the ATX-GK mice, none bound to eOD-GT8-ferritin nor to 426c.Mod.Core-ferritin. The absence of binding of the mAbs to these two germline-targeting immunogens is not entirely unexpected. Firstly, these two immunogens are not expected to bind all available VH1-2 HC/5aa CDRL3 LC paired BCRs[43, 58, 59]. Previously, sorting of human B cells with the original iv4/iv9 identified putative VRC01 precursors: one of which bound to eOD-GT8, but none bound to 426c.Mod.Core[40]. Secondly, we found that in the adoptive transfer model of fixed VRC01 precursor naïve B cells that priming and boosting with the original iv4/iv9 could drive mutations away from Env-recognition[42].

Nevertheless, our immunization studies in the ATX-GK mice demonstrated that reducing the affinity of the anti-idiotypic bispecific immunogen for VH1-2 heavy chains could increase the specificity for VRC01 precursors. However, a large proportion of off-target cells with VH1-2 heavy chains but irrelevant light chains were still activated (Fig. 4B), suggesting better optimization could be possible by further modifying the affinity of the iv9 arm. Additionally, the affinity of iv4 for binding to 5aa CDRL3 light chains could be improved such as through deep mutational scanning, yeast display or other machine learning techniques[60]. Alternatively, the discovery of a singular anti-idiotypic molecule that can select for both VRC01-signatures could circumvent the issues faced by this bispecific design.

While we found an increase in antigen specific IgG^+ cells upon immunization in both spleens and lymph nodes, there was only a small difference between the percentage of total IgG^+ cells in the lymph nodes of mice immunized with the anti-idiotype compared to naïve mice; and

no difference of total IgG^+ cells in the spleens of the two groups. In contrast, mice immunized with eOD-GT8-ferritin had a ~3-fold increase of total IgG^+ cells in the spleen and ~20-fold increase in the lymph nodes compared to naïve mice. This could indicate that the anti-idiotype is not as immunogenic as a protein-based immunogen. While multimerization could increase immunogenicity, it could also lead to more engagement of off-target VH1-2 cells with undesired light chains due to the much larger frequency of those cells compared to the desired VRC01 precursors. Direct conjugation of an adjuvant that improves immunogenicity and/or T cell could help to better drive expansion of VRC01 precursors[61, 62]. For example, linking of C3d, a component of the complement pathway, to an HIV antigen demonstrated a more robust germinal center response[63].

Thus, there is potential of an anti-idiotypic approach to beneficially increase the pool of VH1-2/5aa CDRL3 LC paired BCR bearing B cells before boosting with an Env-based immunogen. However, it remains to be seen if the anti-idiotype approach can successfully prime VRC01 precursors amongst a relevant pool of off-target B cells. Additionally, it is unknown if an anti-idiotypic immunogen could lead to undesired mutations away from being bona fide VRC01-class precursors in a more physiologically relevant animal model.

3.5 Methods

Mice

Mice were purchased from Alloy Therapeutics[64] and shipped from Charles River Laboratories (Wilmington, MA). All mice used in our studies were housed with free access to food and water with a 12:12 light:dark cycle. The animal facilities are accredited by the Association for Assessment and Accreditation of Laboratory Animal Care. Mice were handled in accordance with the NIH Guide for the Care and Use of Laboratory Animals, and experiments were approved by the Fred Hutch Cancer Center Institutional Animal Care and Use Committee and Institutional Review Boards. Immunizations and retro-orbital bleeds were carried out under anesthesia, which was induced by administering isoflurane, set at 1–5% for 1–2 min in an induction chamber with the flow rate of O_2 set at 1.0 L/min. Animals under anesthesia were then transferred to a nose cone and continued to receive 1-5% isoflurane at an O_2 set to 1.0 L/min during injections and retro-orbital bleeds. Mice were euthanized by administering 100% CO_2 in an induction chamber with a flow rate of 3.0 L/min to allow for 50% of the air in the chamber to be replaced per minute for at least 5 minutes, followed by cervical dislocation.

Germline reversion and site-directed mutagenesis of iv9

Germline reversion

Germline iv9 HC (IGH1-59*01 V region sequence taken from IMGT[65]) with mature iv9 CDRH3 and mature iv9 J region and of germline iv9 LC (IGKV8-28*01 F V region sequence taken from IMGT) with mature iv9 CDRL3 and mature iv9 J region were ordered as human codon-optimized gBlocks synthetic gene fragments (IDT) with adapters for cloning. The VH/VL

sequences were cloned into full-length pTT3 derived IgG1 and IgK expression vectors containing human constant regions using Gibson assembly[51]. Vectors were transformed into DH5-alpha cells (NEB) and plasmid sequencing was performed (Azenta Life Sciences).

Site-directed mutagenesis

Site-directed mutagenesis to add back $D52W_{HC}$ and $H92E_{LC}$ to germline iv9 was performed using the Agilent QuikChange Primer Design online tool and Agilent QuikChange II Site-Directed Mutagenesis Kit (Agilent, Cat. #200523) according to manufacturer's instructions. Vectors were transformed into DH5-alpha cells (NEB) and plasmid sequencing was performed (Azenta Life Sciences).

$D52W_{HC}$ Forward primer: 5'-aagagtcggagggccatattacaccgatccattccagcccc-3'

$D52W_{HC}$ Reverse primer 5'-ggggctggaatggatcggtgtaatatggccctccgactctt-3'

$H92E_{LC}$ Forward primer: 5'-caaaggtgtatggataggactcatcattctggcaataataaactgcc-3'

$H92E_{LC}$ Reverse primer: 5'-ggcagtttattattgccagaatgatgagtcctatccatacacctttg-3'

Plasmids

The mAb leader sequences and VH regions were also cloned in frame with AA 1-106 of the IgG1 constant region encompassing the C1 fused to AA 24-121 of spycatcher[46], followed by a gly-gly linker and a 6X His tag in pTT3 (pTT3-iv4-Fab-HC-SC).

mAb leader sequences and VH regions were also cloned in frame with AA 1-106 of the IgG1 constant region encompassing the C1 region followed by a gly-ser linker, 6X His tag and spytag[46] (pTT3-iv9-Fab-HC-ST and pTT3-iGL-iv9 D52W H92E-Fab-HC-ST).

The plasmid encoding the pTT3 derived IgG1 heavy chain of iGL-VRC01 was modified to express a 6X His tag and a stop codon downstream of the C1 region using site-directed mutagenesis to create pTT3-iGL-VRC01-HC-Fab.

iGL-VRC01 (VK3-11-derived kappa chain with C98S mutation in the heavy chain) was prepared as previously described[8, 25, 27, 66].

pTT3 plasmid expressing eOD-GT8 has been described previously[34, 49].

SpyCatcher/SpyTag Fab purification

pTT3-iv4-Fab-HC-SC plus pTT3-iv4 LC, or pTT3-iv9-Fab-HC-ST plus pTT3-iv9-LC were transfected into 293E cells at a density of 10^6 cells/mL in Freestyle 293 media using the 293Free transfection reagent according to the manufacturer's instructions. Expression was carried out for 6 days after which cells and cellular debris were removed by centrifugation at 4,000 × g followed by filtration through a 0.22 μm filter. Clarified cell supernatant containing iv4-SC or iv9-ST was passed over Ni-NTA resin, pre-equilibrated with Ni-NTA binding buffer (0.3MNaCl, 20mMTris,10mM imidazole, pH 8.0), followed by extensive washing with Ni-NTA binding buffer, and then eluted with 250 mM imidazole, 0.3 M NaCl, 20 mM Tris, pH 8.0 (Ni-NTA elution buffer). Proteins were further purified by SEC using a Enrich SEC 650 10X300 column equilibrated in PBS. To generate a bispecific iv4/iv9, iv4-Fab-SC was incubated with a 1.5-fold excess of iv9-Fab-ST for 1 hour at room temperature. The complex was then separated from excess iv9-Fab ST using a Enrich SEC 650 10X300 column equilibrated in PBS. iv4SC/iv9ST (referred to iv4/iv9) was either conjugated to DyLight 550-NHS ester or DyLight-650-NHS ester

(Thermofisher) and then flash frozen, or was flash frozen without a fluorescent label and stored at -20°C.

Purification and generation for iv4/iGL-iv9 D52W H92E-SC-ST followed the above methods with the exception of transfection: pTT3-iv4-Fab-HC-SC plus pTT3-iv4 LC, or pTT3-iv9 D52W-Fab-HC-ST plus pTT3-iv9 H92E-LC were transfected into 293E cells at a density of 10^6 cells/mL in Freestyle 293 media using the 293Free transfection reagent according to the manufacturer's instructions.

Recombinant protein expression and purification

All recombinant proteins were produced in 293E cells in Freestyle 293 media using the 293Free transfection reagent according to the manufacturer's instructions. Cells were transfected at a density of 10^6 cells/mL. For IgGs, 250 mg heavy and 250 mg light chain encoding plasmids were co-transfected per liter of suspended culture. For, eOD-GT8-his-avi, 500 mg of DNA was transfected per liter of suspended culture. Expression was carried out for 6 days after which cells and cellular debris were removed by centrifugation at 4,000×g followed by filtration through a 0.22 μm filter. Clarified cell supernatant containing recombinant antibodies was passed over Protein A Agarose resin. Protein A resin was extensively washed with PBS and eluted with IgG elution buffer. Clarified cell supernatant containing eOD-GT8-his-avi was passed over Nickel nitrilotriacetic acid (Ni-NTA) resin pre-equilibrated with Ni-NTA binding buffer (0.3 M NaCl, 20 mM Tris,10mM imidazole, pH 8.0), followed by extensive washing with Ni-NTA binding buffer, and then eluted with 250 mM imidazole, 0.3 M NaCl, 20 mM Tris, pH 8.0 (Ni-NTA elution buffer). All affinity purified proteins were further purified using a using a HiLoad 16/600

Superdex 200 pg column pre-equilibrated PBS. Fractions containing purified proteins were pooled, aliquoted, frozen in liquid nitrogen and stored at -20°C.

Calcium flux assays

Calcium mobilization in B cells stably expressing BCRs upon stimulation with the anti-idiotype was monitored as previously described[25, 27, 40]. Briefly, prior to antigenic challenge, cells were loaded with Fluo-4 Direct calcium indicator, mixed 1:1 with complete RPMI at 37°C for 1 h. Cells were pelleted and stained with PE-conjugated anti-human Fcγ Fab (Jackson ImmunoResearch) (1:100 dilution in 100 µL complete RPMI plus Fluo-4 Direct) for 30 min. The cells were washed with 5 mL of complete RPMI and resuspended at ~2x10^6 cells/mL in complete RPMI and subjected to Ca^{2+} flux analysis at a medium flow rate on a FACSymphony A5 (BD Biosciences) flow cytometer. In all cases, BCR transduced cells were mixed with un-transduced cells as an internal control at a 5:2 ratio. Levels of background fluorescence (Min_{FL}) were determined by averaging the background Fluo-4 absorbance in cells for 30s. After that, activation of B cells expressing exogenous BCRs by the various immunogens was determined by monitoring changes in Fluo-4 fluorescence associated with cells expressing the exogenous BCRs (PE^+ cells) for 210s. The bispecific iv4/iGL-iv9 D52W H92E anti-idiotype, iGL-iv9 D52W H92E-ST Fab, iv4-SC Fab, and control mAb (anti-EBV AMMO1[67]) were added at a final concentration of 100 nM. Ionomycin was added to a final concentration of 150 nM for 60s following the immunogen addition, and maximum Fluo-4 fluorescence (Max_{FL}) was established by averaging the Fluo-4 fluorescence signal recorded during the last 10s. The percent of maximum Fluo-4 fluorescence at each time point *t* was determined using the formula: (Fluorescence at *t*-Min_{FL})/(Max_{FL}-Min_{FL}) × 100. This analysis was performed on both the BCR

positive (anti-Human Fcγ-PE$^+$) and BCR negative cells (anti-Human Fcγ-PE$^-$) simultaneously. The background Fluo-4 fluorescence signal from the BCR negative cells was subtracted from that of the BCR positive population at each time point. All flow analysis was done with FlowJo 10.8.1 software (Tree Star).

Biolayer interferometry (BLI)

BLI assays were performed on the Octet Red 96E Instrument (Sartorious) at 30°C with shaking at 1,000 RPM.

Kinetics analysis

iGL-iv9 D52W H92E IgG was immobilized on Anti-Human IgG Fc capture (AHC) biosensors (Sartorius) for 150 s. Sensors were immersed in KB for 30 s to collect a baseline measurement. Sensors were then immersed in wells containing two-fold serial dilutions of iGL-VRC01 Fabs in 1X KB buffer and the association was measured for 300 s, followed by immersion in 1X KB for 600 s to measure dissociation. Empty reference sensors were used to measure the background signal from each analyte-containing well. Additionally, each ligand-coupled sensor was associated in wells containing only buffer as a reference. Double reference subtraction was performed for each corresponding ligand-coupled sensor at each time-point. Curve fitting was performed using a 1:1 binding model in Octet BLI Analysis 12.2 software. Mean k_{dis} (1/s) and k_{on} (1/Ms) values were determined by averaging all binding curves that matched the theoretical fit with an R^2 value of ≥ 0.99. The K_D value was calculated by taking the mean k_{dis} value divided by the mean k_{on} value.

iv9 mutants binding screen

iv9 IgG and iGL-iv9 IgG mutated derivatives were immobilized on AHC biosensors for 150 s. After loading, the baseline signal was then recorded for 60 s in KB. The sensors were then immersed into wells containing iGL-VRC01 Fab at 250nM for 300 s (association phase), then followed by immersion in KB for an additional 300 s (dissociation phase).

Bispecific anti-idiotype binding screen

iGL-VRC01 IgG and chimeric IgGs comprised of either a VRC01-class IgH paired with a non-VRC01-class IgL, or a non-VRC01-class IgH paired with a VRC01-class IgL were immobilized on AHC biosensors for 150 s. After loading, the baseline signal was then recorded for 60 s in KB. The sensors were then immersed into wells containing iv4/iGL-iv9 D52W H92E at 250nM for 300 s (association phase), then followed by immersion in KB for an additional 300 s (dissociation phase).

Binding screens with putative VRC01 precursors from ATX-GK mice

mAbs were immobilized on AHC biosensors for 150 s. After loading, the baseline signal was then recorded for 60 s in KB. The sensors were then immersed into wells containing various proteins (iv4-2W1S-SC and iGL-iv9 D52W H92E-2W1S-ST at 250nM; eOD-GT8-ferritin and 426c.Mod.Core-ferrtin at 1μM) diluted in KB for 300 s (association phase), then followed by immersion in KB for an additional 300 s (dissociation phase).

Mouse immunization scheme

10 μg of immunogen (iv4/iv9, iv4/iGL-iv9 D52W H92E, or eOD-GT8-ferritin) resuspended in 50 μL PBS was mixed with 50 μL of SMNP[50] adjuvant and injected intramuscularly split between each hind leg. Mice were euthanized 14 days after immunization, where spleens and

lymph nodes (inguinal, axillary, and lumbar) were harvested and whole blood was collected by terminal cardiac bleed. Single cell suspensions were prepared by mechanical disruption of the spleens or lymph nodes through a 70 μm filter and incubating with 2 mL of RBC Lysing Buffer. Cells were quenched with FACS buffer then resuspended in 10% DMSO/90% FBS at 5M or 20M/mL tubes. Cells were frozen Mr. Frosty containers overnight in -80C before transfer to liquid nitrogen storage. Serum was obtained by subsequent centrifugation at 10,000 rpm for 5 min, heat-inactivated at 56°C for 10 mins, then stored at 4°C.

Antigen-specific serum IgG ELISA

384-well microplates were coated with 60 ng/well iv4/iGL-iv9 D52W H92E in 0.1 M NaHCO3 pH 9.4–9.6 (ELISA coating buffer) at RT overnight at 30 μL/well. The next day, plates were washed 4 times with 1x PBS and 0.02% Tween 20 (ELISA wash buffer) prior to blocking for 1 h with 100 μl/well of PBS containing 10% non-fat milk and 0.02% Tween 20 (ELISA blocking buffer) at 37ºC. After blocking, serial dilutions of serum in ELISA blocking buffer was added and incubated for 1 h at 37˚C. 32 control wells were included that contained only blocking buffer without sera or mAb standard. Plates were incubated for 1 h at 37ºC. After washing, a 1:10000 dilution of Peroxidase AffiniPure Goat Anti-Mouse IgG, Fcγ fragment specific (Jackson ImmunoResearch, Cat. #115-035-071) in ELISA blocking buffer was added to each well and incubated 1h at 37ºC. After four washes, 30 μl/well of SureBlue Reserve TMB Microwell Peroxidase substrate (SeraCare, Cat. #5120-0081) was added. After 5 min at room temperature, 30 μl/well of 1 N sulfuric acid was added and the A_{450} of each well was read on a Molecular Devices SpectraMax M2 plate reader. The average A_{450} values of buffer only control wells were subtracted from each serum containing well and plotted in GraphPad Prism 10. A_{450} values were

plotted as a function of the $\log_{10}$ of the serum dilution. A binding curve was fit using the sigmoidal, 4PL, X is log(concentration) least squares fit function.

ATX-GK Mouse B cell sorting

B cells were enriched from either cryopreserved single-cell suspensions from spleens or lymph nodes (StemCell, Cat. #19854). CD16/CD32 Fc block was added at 1:200 dilution for 15 mins at RT. Cells were stained using a BV510 viability dye (eBioscience, Cat. #65-0866-14) at 1:200 dilution, and the following antibodies at a 1:100 dilution unless otherwise noted: CD3 BV711 (Biolegend, Cat. #100349), Gr-1 BV711 (Biolegend, Cat. #127643), F4/80 BV711 (Biolegend, Cat. #123147), CD19 BUV395 (BD, Cat. #563557; 1:200 dilution), B220 BV786 (Biolegend, Cat. #103246; 1:250 dilution), IgM Superbright 600 (eBioscience, Cat. #63-5790-82; 1:200 dilution), IgG FITC (JacksonImmuno, Cat. #115-095-164; 1:200 dilution). Dylight-labeled antigens were added at 0.5µg per sample of cells. Cells were stained for 30 min on ice, washed twice in FACS buffer, and resuspended in 200 µL sorting buffer (PBS + 2% BSA) for sorting and analysis on a BDFACS Symphony S6. Cells were single-cell sorted into 96-well plates.

Paired single-cell BCR sequencing

<u>10x sequencing of naïve ATX-GK mice</u>

B cells were enriched from splenocytes of two naïve ATX-GK mice independently (StemCell, Cat. #19854). Paired BCR sequencing of B cells was performed using the Chromium Next GEM Single Cell 5' Kit v2 (10x Genomics, Cat #. PN-1000265). 16500 B cells were inputted to generate gel beads-in-emulsions (GEMs) for each mouse. Custom primers from Alloy

Therapeutics for IgM and IgK chains were utilized to amplify VH and VL sequences. Library sequencing at a depth of 5000 reads per cell was performed on a NextSeq 2000 (Illumina) by the Fred Hutch Cancer Center Genomics and Bioinformatics Core Facility (RRID:SCR_022606). The BCR libraries were then mapped to a human VDJ reference using Cell Ranger (10x Genomics). Each paired BCR's V, D, and J genes for both heavy chain and light chains were determined utilizing Enclone (10x Genomics).

10x sequencing of IgG^+ B cells from ATX-GK mice

IgG^+ or antigen-specific IgG^+ B cells were sorted from ATX-GK mice (see B cell sorting methods above). Paired BCR sequencing of B cells was performed using the Chromium Next GEM Single Cell 5' Kit v2 (10x Genomics, Cat #. PN-1000265). Sorted B cells were inputted to generate gel beads-in-emulsions (GEMs) for each mouse. Custom primers from Alloy Therapeutics for IgG and IgK chains were utilized to amplify VH and VL sequences. Library sequencing at a depth of 5000 reads per cell was performed on a NextSeq 2000 (Illumina) by the Fred Hutch Cancer Center Genomics and Bioinformatics Core Facility (RRID:SCR_022606). The BCR libraries were then mapped to a human VDJ reference using Cell Ranger (10x Genomics). Each paired BCR's V, D, and J genes for both heavy chain and light chains were determined utilizing Enclone (10x Genomics).

Sanger sequencing of antigen-specific IgG^+ B cells from ATX-GK mice

Antigen-specific IgG^+ B cells were single-cell sorted into 96-well plates. cDNA was generated using SuperScript IV First-Strand Synthesis System (Invitrogen, Cat. #18091050). The VH and VL sequences were recovered using gene specific human forward primers, custom ATX-GK reverse primers, and cycling conditions previously described[51]. VH or VL amplicons were purified using the Monarch PCR & DNA Cleanup Kit (NEB, Cat. #T1030L) and sanger

sequenced (Azenta Life Sciences). The antibody gene usage was assigned using IMGT VQUEST[65].

Generation of putative VRC01 precursor mAbs

Putative precursor VRC01 VDJ sequences identified from sorting and sequencing were ordered as human codon-optimized gBlocks synthetic gene fragments (IDT) with adapters for cloning into pTT3 plasmids. The VH/VL sequences were cloned into full-length pTT3 derived IgG1 and IgK expression vectors containing human constant regions using Gibson assembly[51]. Vectors were transformed into DH5alpha cells (NEB) and plasmid sequencing was performed (Azenta Life Sciences). mAbs were produced from transfections of 293E cells as described above.

3.6 Chapter 3 Bibliography

1. Organization WH. HIV and AIDS 2025 [updated July 15 2025; cited 2025 October 11]. Available from: https://www.who.int/news-room/fact-sheets/detail/hiv-aids.
2. Mascola JR, Haynes BF. HIV-1 neutralizing antibodies: understanding nature's pathways. Immunological Reviews. 2013;254(1):225-44. doi: 10.1111/imr.12075.
3. Burton DR, Hangartner L. Broadly Neutralizing Antibodies to HIV and Their Role in Vaccine Design. Annual Review of Immunology. 2016;34(1):635-59. doi: 10.1146/annurev-immunol-041015-055515.
4. Bonsignori M, Liao H-X, Gao F, Williams WB, Alam SM, Montefiori DC, Haynes BF. Antibody-virus co-evolution in HIV infection: paths for HIV vaccine development. Immunological Reviews. 2017;275(1):145-60. doi: 10.1111/imr.12509.
5. Wu X, Yang Z-Y, Li Y, Hogerkorp C-M, Schief WR, Seaman MS, Zhou T, Schmidt SD, Wu L, Xu L, Longo NS, McKee K, O'Dell S, Louder MK, Wycuff DL, Feng Y, Nason M, Doria-Rose N, Connors M, Kwong PD, Roederer M, Wyatt RT, Nabel GJ, Mascola JR. Rational Design of Envelope Identifies Broadly Neutralizing Human Monoclonal Antibodies to HIV-1. Science. 2010;329(5993):856-61. doi: 10.1126/science.1187659.
6. Wu X, Zhou T, Zhu J, Zhang B, Georgiev I, Wang C, Chen X, Longo NS, Louder M, McKee K, O'Dell S, Perfetto S, Schmidt SD, Shi W, Wu L, Yang Y, Yang Z-Y, Yang Z, Zhang Z, Bonsignori M, Crump JA, Kapiga SH, Sam NE, Haynes BF, Simek M, Burton DR, Koff WC, Doria-Rose NA, Connors M, Program NCS, Mullikin JC, Nabel GJ, Roederer M, Shapiro L, Kwong PD, Mascola JR. Focused Evolution of HIV-1 Neutralizing Antibodies Revealed by Structures and Deep Sequencing. Science. 2011;333(6049):1593-602. doi: 10.1126/science.1207532.
7. Scheid JF, Mouquet H, Feldhahn N, Seaman MS, Velinzon K, Pietzsch J, Ott RG, Anthony RM, Zebroski H, Hurley A, Phogat A, Chakrabarti B, Li Y, Connors M, Pereyra F, Walker BD, Wardemann H, Ho D, Wyatt RT, Mascola JR, Ravetch JV, Nussenzweig MC. Broad diversity of neutralizing antibodies isolated from memory B cells in HIV-infected individuals. Nature. 2009;458(7238):636-40. doi: 10.1038/nature07930.
8. Scheid JF, Mouquet H, Ueberheide B, Diskin R, Klein F, Oliveira TYK, Pietzsch J, Fenyo D, Abadir A, Velinzon K, Hurley A, Myung S, Boulad F, Poignard P, Burton DR, Pereyra F, Ho DD, Walker BD, Seaman MS, Bjorkman PJ, Chait BT, Nussenzweig MC. Sequence and Structural Convergence of Broad and Potent HIV Antibodies That Mimic CD4 Binding. Science. 2011;333(6049):1633-7. doi: 10.1126/science.1207227.
9. Wu X, Zhang Z, Schramm CA, Joyce MG, Do Kwon Y, Zhou T, Sheng Z, Zhang B, O'Dell S, McKee K, Georgiev IS, Chuang G-Y, Longo NS, Lynch RM, Saunders KO, Soto C, Srivatsan S, Yang Y, Bailer RT, Louder MK, Benjamin B, Blakesley R, Bouffard G, Brooks S, Coleman H, Dekhtyar M, Gregory M, Guan X, Gupta J, Han J, Hargrove A, Ho S-l, Legaspi R, Maduro Q, Masiello C, Maskeri B, McDowell J, Montemayor C, Park M, Riebow N, Schandler K, Schmidt B, Sison C, Stantripop M, Thomas J, Thomas P, Vemulapalli M, Young A, Mullikin JC, Connors M, Kwong PD, Mascola JR, Shapiro L. Maturation and Diversity of the VRC01-Antibody Lineage over 15 Years of Chronic HIV-1 Infection. Cell. 2015;161(3):470-85. doi: 10.1016/j.cell.2015.03.004.
10. Huang J, Kang BH, Ishida E, Zhou T, Griesman T, Sheng Z, Wu F, Doria-Rose NA, Zhang B, McKee K, O'Dell S, Chuang G-Y, Druz A, Georgiev IS, Schramm CA, Zheng A, Joyce MG, Asokan M, Ransier A, Darko S, Migueles SA, Bailer RT, Louder MK, Alam SM, Parks R, Kelsoe G, Von Holle T, Haynes BF, Douek DC, Hirsch V, Seaman MS, Shapiro L, Mascola JR, Kwong PD, Connors M. Identification of a CD4-Binding-Site Antibody to HIV that Evolved Near-Pan Neutralization Breadth. Immunity. 2016;45(5):1108-21. doi: 10.1016/j.immuni.2016.10.027.
11. Sajadi MM, Dashti A, Rikhtegaran Tehrani Z, Tolbert WD, Seaman MS, Ouyang X, Gohain N, Pazgier M, Kim D, Cavet G, Yared J, Redfield RR, Lewis GK, DeVico AL. Identification of Near-Pan-neutralizing Antibodies against HIV-1 by Deconvolution of Plasma Humoral Responses. Cell. 2018;173(7):1783-95.e14. doi: 10.1016/j.cell.2018.03.061.
12. Zhou T, Georgiev I, Wu X, Yang Z-Y, Dai K, Finzi A, Kwon YD, Scheid J, Shi W, Xu L, Yang Y, Zhu J, Nussenzweig MC, Sodroski J, Shapiro L, Nabel GJ, Mascola JR, Kwong PD. Structural Basis for Broad and Potent Neutralization of HIV-1 by Antibody VRC01. Science (New York, NY). 2010;329(5993):811-7. doi: 10.1126/science.1192819.
13. Li Y, O'Dell S, Walker LM, Wu X, Guenaga J, Feng Y, Schmidt SD, McKee K, Louder MK, Ledgerwood JE, Graham BS, Haynes BF, Burton DR, Wyatt RT, Mascola JR. Mechanism of Neutralization by the Broadly Neutralizing HIV-1 Monoclonal Antibody VRC01 ▿ . Journal of Virology. 2011;85(17):8954-67. doi: 10.1128/JVI.00754-11.
14. West AP, Diskin R, Nussenzweig MC, Bjorkman PJ. Structural basis for germ-line gene usage of a potent class of antibodies targeting the CD4-binding site of HIV-1 gp120. Proceedings of the National Academy of Sciences of the United States of America. 2012;109(30):E2083-90. doi: 10.1073/pnas.1208984109.

15. Scharf L, West AP, Gao H, Lee T, Scheid JF, Nussenzweig MC, Bjorkman PJ, Diskin R. Structural basis for HIV-1 gp120 recognition by a germ-line version of a broadly neutralizing antibody. Proceedings of the National Academy of Sciences. 2013;110(15):6049-54. doi: 10.1073/pnas.1303682110.
16. Zhou T, Zhu J, Wu X, Moquin S, Zhang B, Acharya P, Georgiev IS, Altae-Tran HR, Chuang G-Y, Joyce MG, Kwon YD, Longo NS, Louder MK, Luongo T, McKee K, Schramm CA, Skinner J, Yang Y, Yang Z, Zhang Z, Zheng A, Bonsignori M, Haynes BF, Scheid JF, Nussenzweig MC, Simek M, Burton DR, Koff WC, Mullikin JC, Connors M, Shapiro L, Nabel GJ, Mascola JR, Kwong PD. Multi-donor Analysis Reveals Structural Elements, Genetic Determinants, and Maturation Pathway for Effective HIV-1 Neutralization by VRCO1-class Antibodies. Immunity. 2013;39(2):245-58. doi: 10.1016/j.immuni.2013.04.012.
17. Zhou T, Lynch RM, Chen L, Acharya P, Wu X, Doria-Rose NA, Joyce MG, Lingwood D, Soto C, Bailer RT, Ernandes MJ, Kong R, Longo NS, Louder MK, McKee K, O'Dell S, Schmidt SD, Tran L, Yang Z, Druz A, Luongo TS, Moquin S, Srivatsan S, Yang Y, Zhang B, Zheng A, Pancera M, Kirys T, Georgiev IS, Gindin T, Peng H-P, Yang A-S, Mullikin JC, Gray MD, Stamatatos L, Burton DR, Koff WC, Cohen MS, Haynes BF, Casazza JP, Connors M, Corti D, Lanzavecchia A, Sattentau QJ, Weiss RA, West AP, Bjorkman PJ, Scheid JF, Nussenzweig MC, Shapiro L, Mascola JR, Kwong PD. Structural Repertoire of HIV-1-Neutralizing Antibodies Targeting the CD4 Supersite in 14 Donors. Cell. 2015;161(6):1280-92. doi: 10.1016/j.cell.2015.05.007.
18. Baba TW, Liska V, Hofmann-Lehmann R, Vlasak J, Xu W, Ayehunie S, Cavacini LA, Posner MR, Katinger H, Stiegler G, Bernacky BJ, Rizvi TA, Schmidt R, Hill LR, Keeling ME, Lu Y, Wright JE, Chou T-C, Ruprecht RM. Human neutralizing monoclonal antibodies of the IgG1 subtype protect against mucosal simian–human immunodeficiency virus infection. Nature Medicine. 2000;6(2):200-6. doi: 10.1038/72309.
19. Parren PWHI, Marx PA, Hessell AJ, Luckay A, Harouse J, Cheng-Mayer C, Moore JP, Burton DR. Antibody Protects Macaques against Vaginal Challenge with a Pathogenic R5 Simian/Human Immunodeficiency Virus at Serum Levels Giving Complete Neutralization In Vitro. Journal of Virology. 2001;75(17):8340-7. doi: 10.1128/jvi.75.17.8340-8347.2001.
20. Balazs AB, Chen J, Hong CM, Rao DS, Yang L, Baltimore D. Antibody-based protection against HIV infection by vectored immunoprophylaxis. Nature. 2011;481(7379):81-4. doi: 10.1038/nature10660.
21. Balazs AB, Ouyang Y, Hong CM, Chen J, Nguyen SM, Rao DS, An DS, Baltimore D. Vectored immunoprophylaxis protects humanized mice from mucosal HIV transmission. Nature Medicine. 2014;20(3):296-300. doi: 10.1038/nm.3471.
22. Saunders KO, Pegu A, Georgiev IS, Zeng M, Joyce MG, Yang Z-Y, Ko S-Y, Chen X, Schmidt SD, Haase AT, Todd J-P, Bao S, Kwong PD, Rao SS, Mascola JR, Nabel GJ. Sustained Delivery of a Broadly Neutralizing Antibody in Nonhuman Primates Confers Long-Term Protection against Simian/Human Immunodeficiency Virus Infection. Journal of Virology. 2015;89(11):5895-903. doi: 10.1128/jvi.00210-15.
23. Corey L, Gilbert PB, Juraska M, Montefiori DC, Morris L, Karuna ST, Edupuganti S, Mgodi NM, deCamp AC, Rudnicki E, Huang Y, Gonzales P, Cabello R, Orrell C, Lama JR, Laher F, Lazarus EM, Sanchez J, Frank I, Hinojosa J, Sobieszczyk ME, Marshall KE, Mukwekwerere PG, Makhema J, Baden LR, Mullins JI, Williamson C, Hural J, McElrath MJ, Bentley C, Takuva S, Gomez Lorenzo MM, Burns DN, Espy N, Randhawa AK, Kochar N, Piwowar-Manning E, Donnell DJ, Sista N, Andrew P, Kublin JG, Gray G, Ledgerwood JE, Mascola JR, Cohen MS, Teams HHaHHS. Two Randomized Trials of Neutralizing Antibodies to Prevent HIV-1 Acquisition. The New England Journal of Medicine. 2021;384(11):1003-14. doi: 10.1056/NEJMoa2031738.
24. Scheid JF, Horwitz JA, Bar-On Y, Kreider EF, Lu C-L, Lorenzi JCC, Feldmann A, Braunschweig M, Nogueira L, Oliveira T, Shimeliovich I, Patel R, Burke L, Cohen YZ, Hadrigan S, Settler A, Witmer-Pack M, West AP, Juelg B, Keler T, Hawthorne T, Zingman B, Gulick RM, Pfeifer N, Learn GH, Seaman MS, Bjorkman PJ, Klein F, Schlesinger SJ, Walker BD, Hahn BH, Nussenzweig MC, Caskey M. HIV-1 antibody 3BNC117 suppresses viral rebound in humans during treatment interruption. Nature. 2016;535(7613):556-60. doi: 10.1038/nature18929.
25. Hoot S, McGuire AT, Cohen KW, Strong RK, Hangartner L, Klein F, Diskin R, Scheid JF, Sather DN, Burton DR, Stamatatos L. Recombinant HIV Envelope Proteins Fail to Engage Germline Versions of Anti-CD4bs bNAbs. PLoS Pathogens. 2013;9(1):e1003106. doi: 10.1371/journal.ppat.1003106.
26. Jardine J, Julien J-P, Menis S, Ota T, Kalyuzhniy O, McGuire A, Sok D, Huang P-S, MacPherson S, Jones M, Nieusma T, Mathison J, Baker D, Ward AB, Burton DR, Stamatatos L, Nemazee D, Wilson IA, Schief WR. Rational HIV Immunogen Design to Target Specific Germline B Cell Receptors. Science. 2013;340(6133):711-6. doi: 10.1126/science.1234150.
27. McGuire AT, Hoot S, Dreyer AM, Lippy A, Stuart A, Cohen KW, Jardine J, Menis S, Scheid JF, West AP, Schief WR, Stamatatos L. Engineering HIV envelope protein to activate germline B cell receptors of broadly neutralizing anti-CD4 binding site antibodies. Journal of Experimental Medicine. 2013;210(4):655-63. doi: 10.1084/jem.20122824.

28. Caniels TG, Medina-Ramírez M, Zhang J, Sarkar A, Kumar S, LaBranche A, Derking R, Allen JD, Snitselaar JL, Capella-Pujol J, Sánchez IdM, Yasmeen A, Diaz M, Aldon Y, Bijl TPL, Venkatayogi S, Beem JSM, Newman A, Jiang C, Lee W-H, Pater M, Burger JA, Breemen MJv, Taeye SWd, Rantalainen K, LaBranche C, Saunders KO, Montefiori D, Ozorowski G, Ward AB, Crispin M, Moore JP, Klasse PJ, Haynes BF, Wilson IA, Wiehe K, Verkoczy L, Sanders RW. Germline-targeting HIV-1 Env vaccination induces VRC01-class antibodies with rare insertions. Cell Reports Medicine. 2023;4(4). doi: 10.1016/j.xcrm.2023.101003.
29. Steichen JM, Kulp DW, Tokatlian T, Escolano A, Dosenovic P, Stanfield RL, McCoy LE, Ozorowski G, Hu X, Kalyuzhniy O, Briney B, Schiffner T, Garces F, Freund NT, Gitlin AD, Menis S, Georgeson E, Kubitz M, Adachi Y, Jones M, Mutafyan AA, Yun DS, Mayer CT, Ward AB, Burton DR, Wilson IA, Irvine DJ, Nussenzweig MC, Schief WR. HIV Vaccine Design to Target Germline Precursors of Glycan-Dependent Broadly Neutralizing Antibodies. Immunity. 2016;45(3):483-96. doi: 10.1016/j.immuni.2016.08.016.
30. Medina-Ramírez M, Garces F, Escolano A, Skog P, de Taeye SW, Del Moral-Sanchez I, McGuire AT, Yasmeen A, Behrens A-J, Ozorowski G, van den Kerkhof TLGM, Freund NT, Dosenovic P, Hua Y, Gitlin AD, Cupo A, van der Woude P, Golabek M, Sliepen K, Blane T, Kootstra N, van Breemen MJ, Pritchard LK, Stanfield RL, Crispin M, Ward AB, Stamatatos L, Klasse PJ, Moore JP, Nemazee D, Nussenzweig MC, Wilson IA, Sanders RW. Design and crystal structure of a native-like HIV-1 envelope trimer that engages multiple broadly neutralizing antibody precursors in vivo. Journal of Experimental Medicine. 2017;214(9):2573-90. doi: 10.1084/jem.20161160.
31. Briney B, Sok D, Jardine JG, Kulp DW, Skog P, Menis S, Jacak R, Kalyuzhniy O, de Val N, Sesterhenn F, Le KM, Ramos A, Jones M, Saye-Francisco KL, Blane TR, Spencer S, Georgeson E, Hu X, Ozorowski G, Adachi Y, Kubitz M, Sarkar A, Wilson IA, Ward AB, Nemazee D, Burton DR, Schief WR. Tailored Immunogens Direct Affinity Maturation toward HIV Neutralizing Antibodies. Cell. 2016;166(6):1459-70.e11. doi: 10.1016/j.cell.2016.08.005.
32. Parks KR, MacCamy AJ, Trichka J, Gray M, Weidle C, Borst AJ, Khechaduri A, Takushi B, Agrawal P, Guenaga J, Wyatt RT, Coler R, Seaman M, LaBranche C, Montefiori DC, Veesler D, Pancera M, McGuire A, Stamatatos L. Overcoming Steric Restrictions of VRC01 HIV-1 Neutralizing Antibodies through Immunization. Cell Reports. 2019;29(10):3060-72.e7. doi: 10.1016/j.celrep.2019.10.071.
33. Leggat DJ, Cohen KW, Willis JR, Fulp WJ, deCamp AC, Kalyuzhniy O, Cottrell CA, Menis S, Finak G, Ballweber-Fleming L, Srikanth A, Plyler JR, Schiffner T, Liguori A, Rahaman F, Lombardo A, Philiponis V, Whaley RE, Seese A, Brand J, Ruppel AM, Hoyland W, Yates NL, Williams LD, Greene K, Gao H, Mahoney CR, Corcoran MM, Cagigi A, Taylor A, Brown DM, Ambrozak DR, Sincomb T, Hu X, Tingle R, Georgeson E, Eskandarzadeh S, Alavi N, Lu D, Mullen T-M, Kubitz M, Groschel B, Maenza J, Kolokythas O, Khati N, Bethony J, Crotty S, Roederer M, Karlsson Hedestam GB, Tomaras GD, Montefiori D, Diemert D, Koup RA, Laufer DS, McElrath MJ, McDermott AB, Schief WR. Vaccination induces HIV broadly neutralizing antibody precursors in humans. Science. 2022;378(6623):eadd6502. doi: 10.1126/science.add6502.
34. Jardine JG, Ota T, Sok D, Pauthner M, Kulp DW, Kalyuzhniy O, Skog PD, Thinnes TC, Bhullar D, Briney B, Menis S, Jones M, Kubitz M, Spencer S, Adachi Y, Burton DR, Schief WR, Nemazee D. Priming a broadly neutralizing antibody response to HIV-1 using a germline-targeting immunogen. Science (New York, NY). 2015;349(6244):156-61. doi: 10.1126/science.aac5894.
35. Caniels TG, Prabhakaran M, Ozorowski G, MacPhee KJ, Wu W, van der Straten K, Agrawal S, Derking R, Reiss EIMM, Millard K, Turroja M, Desrosiers A, Bethony J, Malkin E, Liesdek MH, van der Veen A, Klouwens M, Snitselaar JL, Bouhuijs JH, Bronson R, Jean-Baptiste J, Gajjala S, Rikhtegaran Tehrani Z, Benner A, Ramaswami M, Duff MO, Liu Y-W, Sato AH, Kim JY, Baken IJL, Mendes Silva C, Bijl TPL, van Rijswijk J, Burger JA, Cupo A, Yasmeen A, Phulera S, Lee W-H, Randall KN, Zhang S, Corcoran MM, Regadas I, Sullivan AC, Brown DM, Bohl JA, Greene KM, Gao H, Yates NL, Sawant S, Prins JM, Kootstra NA, Kaminsky SM, Barin B, Rahaman F, Meller M, Philiponis V, Laufer DS, Lombardo A, Mwoga L, Shotorbani S, Holman D, Koup RA, Klasse PJ, Karlsson Hedestam GB, Tomaras GD, van Gils MJ, Montefiori DC, McDermott AB, Hyrien O, Moore JP, Wilson IA, Ward AB, Diemert DJ, de Bree GJ, Andrews SF, Caskey M, Sanders RW. Precise targeting of HIV broadly neutralizing antibody precursors in humans. Science. 2025;0(0):eadv5572. doi: 10.1126/science.adv5572.
36. Sok D, Briney B, Jardine JG, Kulp DW, Menis S, Pauthner M, Wood A, Lee E-C, Le KM, Jones M, Ramos A, Kalyuzhniy O, Adachi Y, Kubitz M, MacPherson S, Bradley A, Friedrich GA, Schief WR, Burton DR. Priming HIV-1 broadly neutralizing antibody precursors in human Ig loci transgenic mice. Science. 2016;353(6307):1557-60. doi: 10.1126/science.aah3945.
37. Dosenovic P, von Boehmer L, Escolano A, Jardine J, Freund NT, Gitlin AD, McGuire AT, Kulp DW, Oliveira T, Scharf L, Pietzsch J, Gray MD, Cupo A, van Gils MJ, Yao K-H, Liu C, Gazumyan A, Seaman MS, Björkman PJ, Sanders RW, Moore JP, Stamatatos L, Schief WR, Nussenzweig MC. Immunization for HIV-1

Broadly Neutralizing Antibodies in Human Ig Knockin Mice. Cell. 2015;161(7):1505-15. doi: 10.1016/j.cell.2015.06.003.
38. McGuire AT, Gray MD, Dosenovic P, Gitlin AD, Freund NT, Petersen J, Correnti C, Johnsen W, Kegel R, Stuart AB, Glenn J, Seaman MS, Schief WR, Strong RK, Nussenzweig MC, Stamatatos L. Specifically modified Env immunogens activate B-cell precursors of broadly neutralizing HIV-1 antibodies in transgenic mice. Nature Communications. 2016;7(1):10618. doi: 10.1038/ncomms10618.
39. Scharf L, West AP, Jr, Sievers SA, Chen C, Jiang S, Gao H, Gray MD, McGuire AT, Scheid JF, Nussenzweig MC, Stamatatos L, Bjorkman PJ. Structural basis for germline antibody recognition of HIV-1 immunogens. eLife. 2016;5:e13783. doi: 10.7554/eLife.13783.
40. Seydoux E, Wan Y-H, Feng J, Wall A, Aljedani S, Homad LJ, MacCamy AJ, Weidle C, Gray MD, Brumage L, Taylor JJ, Pancera M, Stamatatos L, McGuire AT. Development of a VRC01-class germline targeting immunogen derived from anti-idiotypic antibodies. Cell Reports. 2021;35(5):109084. doi: 10.1016/j.celrep.2021.109084.
41. Abbott RK, Lee JH, Menis S, Skog P, Rossi M, Ota T, Kulp DW, Bhullar D, Kalyuzhniy O, Havenar-Daughton C, Schief WR, Nemazee D, Crotty S. Precursor Frequency and Affinity Determine B Cell Competitive Fitness in Germinal Centers, Tested with Germline-Targeting HIV Vaccine Immunogens. Immunity. 2018;48(1):133-46.e6. doi: 10.1016/j.immuni.2017.11.023.
42. Wilcox-King A, Wan YH, Scharffenberger SC, Chhan CB, Davis AR, Homad LJ, Seydoux E, MacPhee KJ, Siddaramaiah LK, Melo M, Dosenovic P, Irvine DJ, Hyrien O, Stamatatos L, McGuire AT. Priming VRC01-precursor B cells with non-envelope immunogens disfavors boosting with HIV-1 envelope. NPJ Vaccines. 2025;10(1):185. Epub 20250805. doi: 10.1038/s41541-025-01235-5. PubMed PMID: 40764319; PMCID: PMC12325944.
43. Havenar-Daughton C, Sarkar A, Kulp DW, Toy L, Hu X, Deresa I, Kalyuzhniy O, Kaushik K, Upadhyay AA, Menis S, Landais E, Cao L, Diedrich JK, Kumar S, Schiffner T, Reiss SM, Seumois G, Yates JR, Paulson JC, Bosinger SE, Wilson IA, Schief WR, Crotty S. The human naive B cell repertoire contains distinct subclasses for a germline-targeting HIV-1 vaccine immunogen. Science translational medicine. 2018;10(448):eaat0381. doi: 10.1126/scitranslmed.aat0381.
44. Alloy Therapeutics [Internet]. [2023-10-19 18:26:34].
45. Dosenovic P, Kara EE, Pettersson A-K, McGuire AT, Gray M, Hartweger H, Thientosapol ES, Stamatatos L, Nussenzweig MC. Anti–HIV-1 B cell responses are dependent on B cell precursor frequency and antigen-binding affinity. Proceedings of the National Academy of Sciences of the United States of America. 2018;115(18):4743-8. doi: 10.1073/pnas.1803457115.
46. Zakeri B, Fierer JO, Celik E, Chittock EC, Schwarz-Linek U, Moy VT, Howarth M. Peptide tag forming a rapid covalent bond to a protein, through engineering a bacterial adhesin. Proceedings of the National Academy of Sciences. 2012;109(12):E690-E7. doi: 10.1073/pnas.1115485109.
47. DeKosky BJ, Kojima T, Rodin A, Charab W, Ippolito GC, Ellington AD, Georgiou G. In-depth determination and analysis of the human paired heavy- and light-chain antibody repertoire. Nature Medicine. 2015;21(1):86-91. doi: 10.1038/nm.3743.
48. Huang D, Abbott RK, Havenar-Daughton C, Skog PD, Al-Kolla R, Groschel B, Blane TR, Menis S, Tran JT, Thinnes TC, Volpi SA, Liguori A, Schiffner T, Villegas SM, Kalyuzhniy O, Pintea M, Voss JE, Phelps N, Tingle R, Rodriguez AR, Martin G, Kupryianov S, deCamp A, Schief WR, Nemazee D, Crotty S. B cells expressing authentic naive human VRC01-class BCRs can be recruited to germinal centers and affinity mature in multiple independent mouse models. Proceedings of the National Academy of Sciences. 2020;117(37):22920-31. doi: 10.1073/pnas.2004489117.
49. Dosenovic P, Pettersson A-K, Wall A, Thientosapol ES, Feng J, Weidle C, Bhullar K, Kara EE, Hartweger H, Pai JA, Gray MD, Parks KR, Taylor JJ, Pancera M, Stamatatos L, Nussenzweig MC, McGuire AT. Anti-idiotypic antibodies elicit anti-HIV-1–specific B cell responses. Journal of Experimental Medicine. 2019;216(10):2316-30. doi: 10.1084/jem.20190446.
50. Silva M, Kato Y, Melo MB, Phung I, Freeman BL, Li Z, Roh K, Van Wijnbergen JW, Watkins H, Enemuo CA, Hartwell BL, Chang JYH, Xiao S, Rodrigues KA, Cirelli KM, Li N, Haupt S, Aung A, Cossette B, Abraham W, Kataria S, Bastidas R, Bhiman J, Linde C, Bloom NI, Groschel B, Georgeson E, Phelps N, Thomas A, Bals J, Carnathan DG, Lingwood D, Burton DR, Alter G, Padera TP, Belcher AM, Schief WR, Silvestri G, Ruprecht RM, Crotty S, Irvine DJ. A particulate saponin/TLR agonist vaccine adjuvant alters lymph flow and modulates adaptive immunity. Science Immunology. 2021;6(66):eabf1152. doi: 10.1126/sciimmunol.abf1152.

51. Tiller T, Meffre E, Yurasov S, Tsuiji M, Nussenzweig MC, Wardemann H. Efficient generation of monoclonal antibodies from single human B cells by single cell RT-PCR and expression vector cloning. Journal of Immunological Methods. 2008;329(1):112-24. doi: 10.1016/j.jim.2007.09.017.
52. !!! INVALID CITATION !!! 42, 48.
53. Li YS, Hayakawa K, Hardy RR. The regulated expression of B lineage associated genes during B cell differentiation in bone marrow and fetal liver. J Exp Med. 1993;178(3):951-60. doi: 10.1084/jem.178.3.951. PubMed PMID: 8350062; PMCID: PMC2191150.
54. Thai TH, Purugganan MM, Roth DB, Kearney JF. Distinct and opposite diversifying activities of terminal transferase splice variants. Nat Immunol. 2002;3(5):457-62. Epub 20020408. doi: 10.1038/ni788. PubMed PMID: 11938351.
55. Luo S, Jing C, Ye AY, Kratochvil S, Cottrell CA, Koo J-H, Chapdelaine Williams A, Francisco LV, Batra H, Lamperti E, Kalyuzhniy O, Zhang Y, Barbieri A, Manis JP, Haynes BF, Schief WR, Batista FD, Tian M, Alt FW. Humanized V(d)j-Rearranging and Tdt-Expressing Mouse Vaccine Models with Physiological Hiv-1 Broadly Neutralizing Antibody Precursors. Proceedings of the National Academy of Sciences. 2023;120(1):e2217883120. doi: 10.1073/pnas.2217883120.
56. Heller M, Owens JD, Mushinski JF, Rudikoff S. Amino acids at the site of V kappa-J kappa recombination not encoded by germline sequences. J Exp Med. 1987;166(3):637-46. doi: 10.1084/jem.166.3.637. PubMed PMID: 3040883; PMCID: PMC2188693.
57. Victor KD, Vu K, Feeney AJ. Limited junctional diversity in kappa light chains. Junctional sequences from CD43+B220+ early B cell progenitors resemble those from peripheral B cells. J Immunol. 1994;152(7):3467-75. PubMed PMID: 7511648.
58. Umotoy J, Bagaya BS, Joyce C, Schiffner T, Menis S, Saye-Francisco KL, Biddle T, Mohan S, Vollbrecht T, Kalyuzhniy O, Madzorera S, Kitchin D, Lambson B, Nonyane M, Kilembe W, Poignard P, Schief WR, Burton DR, Murrell B, Moore PL, Briney B, Sok D, Landais E. Rapid and Focused Maturation of a VRC01-Class HIV Broadly Neutralizing Antibody Lineage Involves Both Binding and Accommodation of the N276-Glycan. Immunity. 2019;51(1):141-54.e6. doi: 10.1016/j.immuni.2019.06.004.
59. Lin Y-R, Parks KR, Weidle C, Naidu AS, Khechaduri A, Riker AO, Takushi B, Chun J-H, Borst AJ, Veesler D, Stuart A, Agrawal P, Gray M, Pancera M, Huang P-S, Stamatatos L. HIV-1 VRC01 Germline-Targeting Immunogens Select Distinct Epitope-Specific B Cell Receptors. Immunity. 2020;53(4):840-51.e6. doi: 10.1016/j.immuni.2020.09.007.
60. Starr TN, Greaney AJ, Hilton SK, Ellis D, Crawford KHD, Dingens AS, Navarro MJ, Bowen JE, Tortorici MA, Walls AC, King NP, Veesler D, Bloom JD. Deep Mutational Scanning of SARS-CoV-2 Receptor Binding Domain Reveals Constraints on Folding and ACE2 Binding. Cell. 2020;182(5):1295-310 e20. Epub 20200811. doi: 10.1016/j.cell.2020.08.012. PubMed PMID: 32841599; PMCID: PMC7418704.
61. Gonzalez SF, Degn SE, Pitcher LA, Woodruff M, Heesters BA, Carroll MC. Trafficking of B cell antigen in lymph nodes. Annu Rev Immunol. 2011;29:215-33. doi: 10.1146/annurev-immunol-031210-101255. PubMed PMID: 21219172.
62. Bode C, Zhao G, Steinhagen F, Kinjo T, Klinman DM. CpG DNA as a vaccine adjuvant. Expert Rev Vaccines. 2011;10(4):499-511. doi: 10.1586/erv.10.174. PubMed PMID: 21506647; PMCID: PMC3108434.
63. Bale S, Yang L, Alirezaei M, Wilson R, Ota T, Doyle ED, Cottrell CA, Guenaga J, Tran K, Li W, Stamatatos L, Nemazee D, Ward AB, Wyatt RT. Fusion of the molecular adjuvant C3d to cleavage-independent native-like HIV-1 Env trimers improves the elicited antibody response. Front Immunol. 2023;14:1180959. Epub 20230522. doi: 10.3389/fimmu.2023.1180959. PubMed PMID: 37283743; PMCID: PMC10239957.
64. Alloy Therapeutics Inc. Alloy Therapeutics 2025 [June 26, 2025]. Available from: https://alloytx.com/.
65. Brochet X, Lefranc M-P, Giudicelli V. IMGT/V-QUEST: the highly customized and integrated system for IG and TR standardized V-J and V-D-J sequence analysis. Nucleic Acids Research. 2008;36(Web Server issue):W503-8. doi: 10.1093/nar/gkn316.
66. Borst AJ, Weidle CE, Gray MD, Frenz B, Snijder J, Joyce MG, Georgiev IS, Stewart-Jones GB, Kwong PD, McGuire AT, DiMaio F, Stamatatos L, Pancera M, Veesler D. Germline VRC01 antibody recognition of a modified clade C HIV-1 envelope trimer and a glycosylated HIV-1 gp120 core. Elife. 2018;7. Epub 20181107. doi: 10.7554/eLife.37688. PubMed PMID: 30403372; PMCID: PMC6237438.
67. Snijder J, Ortego MS, Weidle C, Stuart AB, Gray MD, McElrath MJ, Pancera M, Veesler D, McGuire AT. An antibody targeting the fusion machinery neutralizes dual-tropic infection and defines a site of vulnerability on Epstein-Barr virus. Immunity. 2018;48(4):799-811.e9. doi: 10.1016/j.immuni.2018.03.026.

Chapter 4. Concluding Remarks on the ATX-GK Humanized Mouse Model and EBV-specific Monoclonal Antibodies as Treatment

4.1 Concluding Remarks

Through use of the ATX-GK mouse to model human neutralizing B cell responses, I isolated of two novel EBV gp350 and eight EBV gp42 potently neutralizing mAbs. One gp42 mAb protected human $CD34^{+}$-engrafted mice against EBV challenge and PTLD-like tumor formation, while one gp350 mAb provided partial protection. The ATX-GK mouse model has proven to be a useful tool to rapidly isolate genetically human mAbs against viral proteins, that would otherwise be difficult to isolate from naturally infected donors. This includes the generation of genetically human mAbs that have been historically difficult to isolate either due to rarity or technical restraints including, Ebola virus[1], Rabies virus[2], and henipaviruses[3] for example. They may also be a useful tool to quickly generate nAbs against emerging, highly pathogenic viruses, as a first line of defense like those needed at the start of the COVID-19 pandemic[4]. While another humanized mouse model (the $CAMouse^{HC}$ mice[5]) has been used to generate mAbs against Ebola[6] and Rabies[2], these mice only have 32 human VH genes compared to the ATX-GK's purported 41 human VH genes. Thus, the ATX-GK mice could allow wider discovery. While they encode 41V, 23D, and 6J human VH as well as 19V and 5J human VK genes, we note the human Ig loci is not fully represented in these mice, such as the lack of lambda chains.

We further utilized ten ATX-GK mice to model human B cell responses to HIV VRC01-class germline-targeting immunogens. We were unsuccessful in our attempts to consistently

prime VRC01-class broadly neutralizing B cell precursors with either our anti-idiotypic immunogens or with eOD-GT8, an HIV Env-derived immunogen that has recently completed a Phase I clinical trial,[7]. We believe this is due to the rare frequency of the VRC01-class precursors in these mice, likely due to the restricted CDRL3 lengths. However, not all bNAbs are restricted to these germline features. Thus, it could be useful to determine if the ATX-GK mice could model the generation of other classes of HIV bNAbs (such as VH1-46 lineage or apex-directed bNAbs)[8], as well as bNAbs against other viral pathogens, such as Ebola and Dengue[9].

As stated, the gp42 mAb ATX-42-2 was found to exhibit similar protective efficacy to the gH/gL mAb AMMO1 against EBV-challenge in humanized mice. In contrast, we observed partial protection with the gp350 mAbs ATX-350-2 and 72A1 which showed more rapid decay compared to ATX-42-2 and AMMO1, which may explain their partial protection. The protective capacity of ATX-350-2 and 72A1 could be tested through repeated infusions in a challenge study. Additionally, the partial protection could be related to the fact that gp350 is not essential for EBV infection of B cells[10], while gp42 and gH/gL are[11]. There could still be utility for these gp350 mAbs through extending their half-life for improved potency and inclusion in a cocktail immunization to reduce the chance of viral escape. While gp350 can mutate within a host, the CD21-binding site is relatively conserved[12]. Additionally, EBV mutates relatively slowly, with relatively few variations between gp350 and gp42 across both EBV1 and EBV2 genomes[13]. Still, there are potentially 2 known polymorphisms within the HLA-binding site and 3 known polymorphisms within the CD21-binding site that could impact ATX-42- and ATX-350-2 binding.

In addition to neutralizing antibodies, we elicited an excess of non-neutralizing antibodies with gp42 and gp350 immunizations. It is possible they may offer protection through Fc-

mediated activities, especially since previous studies have found that gp350-antibodies can promote ADCC, ADCP, and ADNP[12, 14, 15]. A human engraftment mouse model that reconstitutes human leukocytes including T cells, B cells, and natural killer (NK) cells was used to determine NK cell control of EBV infection of B cells through depletion experiments[16]. However, EBV-specific non-neutralizing antibody-dependent NK function has not been assessed *in vivo*. It would be interesting to compare a neutralizing but non-ADCC mediating mAb versus a non-neutralizing, ADCC-mediating mAb in an *in vivo* EBV protection study.

While monoclonal antibodies could provide protection during the critical immune suppression period following transplant, PTLD has been known to occur even 3 years post-transplant[17]. Thus, there is a need for other therapeutics, such as EBV-specific vaccines and T cell immunotherapy. A gp350 subunit vaccine reduced the incidence of IM by 78% in a phase II trial, however it could not prevent EBV acquisition[18]. Two vaccines that include gp42 and gH/gL are currently in clinical trials (NCT05164094 and NCT05831111), thus we await to see if they elicit potent neutralizing antibodies and if they prevent EBV acquisition or disease.

Mapping of ATX-350-1 and ATX-350-2 revealed an extended site of vulnerability of the CD21-binding site on gp350. Additional mapping of the non-neutralizing antibodies to gp42 and gp350 could reveal immunodominant epitopes on the glycoproteins that could inform rational vaccine design, such as epitope-masking.

Lastly, EBV-specific chimeric antigen receptor T cells (CAR-T) to target EBV tumor cells have shown promise in an immunodeficient mouse model[19]. Thus, there is potential to utilize the genetically human mAbs as EBV-specific CARs engineered into NK or T cells, further increasing the much needed arsenal of life-saving therapies against PTLD and other EBV-associated malignancies.

Overall, the ATX-GK mice has use as a small animal model to model human B cell responses and to generate genetically human mAbs. We have shown these mice are capable of generating human mAbs against EBV gp42 and gp350, which have been historically technically challenging to isolate. Using a hybridoma technology, potently neutralizing mAbs could be generated in a short timeframe. Still, the human antibody repertoire is very diverse and not entirely represented in these mice. Additionally, there are variations between the human and murine antibody recombination processes beyond encoded genes that impact antibody diversity, such as TdT expression during light chain recombination. Thus, it will be interesting to see how improvements in mouse modeling can better mimic human B cell responses and advance the fields of vaccination and therapeutics development.

4.2 Chapter 4 Bibliography

1. Rijal P, Donnellan FR. A review of broadly protective monoclonal antibodies to treat Ebola virus disease. Curr Opin Virol. 2023;61:101339. Epub 20230629. doi: 10.1016/j.coviro.2023.101339. PubMed PMID: 37392670.
2. Fan L, Zhang L, Li J, Zhu F. Advances in the progress of monoclonal antibodies for rabies. Hum Vaccin Immunother. 2022;18(1):2026713. Epub 20220216. doi: 10.1080/21645515.2022.2026713. PubMed PMID: 35172707; PMCID: PMC8993100.
3. Gomez Roman R, Tornieporth N, Cherian NG, Shurtleff AC, L'Azou Jackson M, Yeskey D, Hacker A, Mungai E, Le TT. Medical countermeasures against henipaviruses: a review and public health perspective. Lancet Infect Dis. 2022;22(1):e13-e27. Epub 20211101. doi: 10.1016/S1473-3099(21)00400-X. PubMed PMID: 34735799; PMCID: PMC8694750.
4. Morales-Nunez JJ, Munoz-Valle JF, Torres-Hernandez PC, Hernandez-Bello J. Overview of Neutralizing Antibodies and Their Potential in COVID-19. Vaccines (Basel). 2021;9(12). Epub 20211123. doi: 10.3390/vaccines9121376. PubMed PMID: 34960121; PMCID: PMC8706198.
5. Yu L, Yang X, Huang N, Wu M, Sun H, He Q, Lang Q, Zou X, Liu Z, Wang J, Ge L. Generation of fully human anti-GPC3 antibodies with high-affinity recognition of GPC3 positive tumors. Invest New Drugs. 2021;39(3):615-26. Epub 20201119. doi: 10.1007/s10637-020-01033-x. PubMed PMID: 33215325.
6. Li W, Yang W, Liu X, Zhou W, Wang S, Wang Z, Zhao Y, Feng N, Wang T, Wu M, Ge L, Xia X, Yan F. Fully human monoclonal antibodies against Ebola virus possess complete protection in a hamster model. Emerg Microbes Infect. 2024;13(1):2392651. Epub 20240826. doi: 10.1080/22221751.2024.2392651. PubMed PMID: 39155772; PMCID: PMC11348817.
7. Leggat DJ, Cohen KW, Willis JR, Fulp WJ, deCamp AC, Kalyuzhniy O, Cottrell CA, Menis S, Finak G, Ballweber-Fleming L, Srikanth A, Plyler JR, Schiffner T, Liguori A, Rahaman F, Lombardo A, Philiponis V, Whaley RE, Seese A, Brand J, Ruppel AM, Hoyland W, Yates NL, Williams LD, Greene K, Gao H, Mahoney CR, Corcoran MM, Cagigi A, Taylor A, Brown DM, Ambrozak DR, Sincomb T, Hu X, Tingle R, Georgeson E, Eskandarzadeh S, Alavi N, Lu D, Mullen T-M, Kubitz M, Groschel B, Maenza J, Kolokythas O, Khati N, Bethony J, Crotty S, Roederer M, Karlsson Hedestam GB, Tomaras GD, Montefiori D, Diemert D, Koup RA, Laufer DS, McElrath MJ, McDermott AB, Schief WR. Vaccination induces HIV broadly neutralizing antibody precursors in humans. Science. 2022;378(6623):eadd6502. doi: 10.1126/science.add6502.
8. Haynes BF, Wiehe K, Borrow P, Saunders KO, Korber B, Wagh K, McMichael AJ, Kelsoe G, Hahn BH, Alt F, Shaw GM. Strategies for HIV-1 vaccines that induce broadly neutralizing antibodies. Nature Reviews Immunology. 2023;23(3):142-58. doi: 10.1038/s41577-022-00753-w.
9. Terzi I, Dimitriadis D, Ntoga M, Petrakis V, Dragoumani I, Markatou F, Rafailidis P. Neutralizing monoclonal antibodies against dengue virus: a scoping review of preclinical and clinical development. Virology. 2025;612:110677. Epub 20250902. doi: 10.1016/j.virol.2025.110677. PubMed PMID: 40916325.
10. Janz A, Oezel M, Kurzeder C, Mautner J, Pich D, Kost M, Hammerschmidt W, Delecluse HJ. Infectious Epstein-Barr virus lacking major glycoprotein BLLF1 (gp350/220) demonstrates the existence of additional viral ligands. J Virol. 2000;74(21):10142-52. doi: 10.1128/jvi.74.21.10142-10152.2000. PubMed PMID: 11024143; PMCID: PMC102053.
11. Cohen JI. Epstein-Barr virus infection. N Engl J Med. 2000;343(7):481-92. doi: 10.1056/NEJM200008173430707. PubMed PMID: 10944566.
12. Weiss ER, Alter G, Ogembo JG, Henderson JL, Tabak B, Bakis Y, Somasundaran M, Garber M, Selin L, Luzuriaga K. High Epstein-Barr Virus Load and Genomic Diversity Are Associated with Generation of gp350-Specific Neutralizing Antibodies following Acute Infectious Mononucleosis. J Virol. 2017;91(1). Epub 20161216. doi: 10.1128/JVI.01562-16. PubMed PMID: 27733645; PMCID: PMC5165192.
13. Blazquez AC, Fellner MD, Lorenzetti MA, Preciado MV. A Comparative Genomic Analysis of Epstein-Barr Virus Strains with a Focus on EBV2 Variability. Int J Mol Sci. 2025;26(6). Epub 20250317. doi: 10.3390/ijms26062708. PubMed PMID: 40141350; PMCID: PMC11943181.
14. Jondal M. Antibody-dependent cellular cytotoxicity (ADCC) against Epstein-Barr virus-determined membrane antigens. I. Reactivity in sera from normal persons and from patients with acute infectious mononucleosis. Clin Exp Immunol. 1976;25(1):1-5. PubMed PMID: 186222; PMCID: PMC1541383.
15. Karsten CB, Bartsch YC, Shin SA, Slein MD, Heller HM, Kolandaivelu K, Middeldorp JM, Alter G, Julg B. Evolution of functional antibodies following acute Epstein-Barr virus infection. PLoS Pathog. 2022;18(9):e1010738. Epub 20220906. doi: 10.1371/journal.ppat.1010738. PubMed PMID: 36067220; PMCID: PMC9481173.

16. Chijioke O, Muller A, Feederle R, Barros MH, Krieg C, Emmel V, Marcenaro E, Leung CS, Antsiferova O, Landtwing V, Bossart W, Moretta A, Hassan R, Boyman O, Niedobitek G, Delecluse HJ, Capaul R, Munz C. Human natural killer cells prevent infectious mononucleosis features by targeting lytic Epstein-Barr virus infection. Cell Rep. 2013;5(6):1489-98. Epub 20131219. doi: 10.1016/j.celrep.2013.11.041. PubMed PMID: 24360958; PMCID: PMC3895765.
17. Al Hamed R, Bazarbachi AH, Mohty M. Epstein-Barr virus-related post-transplant lymphoproliferative disease (EBV-PTLD) in the setting of allogeneic stem cell transplantation: a comprehensive review from pathogenesis to forthcoming treatment modalities. Bone Marrow Transplantation. 2020;55(1):25-39. doi: 10.1038/s41409-019-0548-7.
18. Sokal EM, Hoppenbrouwers K, Vandermeulen C, Moutschen M, Léonard P, Moreels A, Haumont M, Bollen A, Smets F, Denis M. Recombinant gp350 Vaccine for Infectious Mononucleosis: A Phase 2, Randomized, Double- Blind, Placebo-Controlled Trial to Evaluate the Safety, Immunogenicity, and Efficacy of an Epstein- Barr Virus Vaccine in Healthy Young Adults. The Journal of Infectious Diseases. 2007;196(12):1749-53. doi: 10.1086/523813.
19. Slabik C, Kalbarczyk M, Danisch S, Zeidler R, Klawonn F, Volk V, Krönke N, Feuerhake F, Ferreira de Figueiredo C, Blasczyk R, Olbrich H, Theobald SJ, Schneider A, Ganser A, von Kaisenberg C, Lienenklaus S, Bleich A, Hammerschmidt W, Stripecke R. CAR-T Cells Targeting Epstein-Barr Virus gp350 Validated in a Humanized Mouse Model of EBV Infection and Lymphoproliferative Disease. Molecular Therapy - Oncolytics. 2020;18:504-24. doi: 10.1016/j.omto.2020.08.005.